UNIVERSITY OF SOUTHAMPTON

THE LONG-TERM INTERACTIONS OF SATELLITE CONSTELLATIONS WITH THE ORBITAL DEBRIS ENVIRONMENT

by ROGER WALKER (B.Eng)

THESIS SUBMITTED FOR THE DEGREE OF
DOCTOR OF PHILOSOPHY

SCHOOL OF ENGINEERING SCIENCES
AERONAUTICS AND ASTRONAUTICS

February 2000

UNIVERSITY OF SOUTHAMPTON

ABSTRACT

FACULTY OF ENGINEERING AND APPLIED SCIENCE

DEPARTMENT OF AERONAUTICS AND ASTRONAUTICS

Doctor of Philosophy

THE LONG-TERM INTERACTIONS OF SATELLITE CONSTELLATIONS WITH THE ORBITAL DEBRIS ENVIRONMENT

By Roger Walker (B.Eng)

An increasing number of multiple-satellite constellations, providing global telecommunications, will be launched into low Earth orbit (LEO) within the next decade. These systems could be utilised for many years in a growing debris environment that presents a significant long-term collision hazard. The main objective of this PhD is to examine the long-term impact of these systems on the LEO debris environment, and vice versa. The high-resolution simulation of the historical and long-term future evolution of the LEO debris environment, and the detailed long-term prediction of collision risk to any target orbit intersecting LEO, is not trivial to achieve within a single model. The Integrated Debris Evolution Suite (IDES) has been developed as an extremely flexible tool, with a wide scope of state-of-the-art capabilities in all of these areas. A highly novel aspect of the IDES model is the new target-centred approach to the prediction of future collision events. This approach has made an advance over other traditional methods in the area of future collision event prediction and has improved the accuracy of modelling the all-important future collision fragment source within long-term debris evolution models. The IDES simulation software has undergone a rigorous validation programme to assess its accuracy. The historical debris environment simulated by IDES was validated by comparison with reliable measurement data. This validation exercise has greatly improved the confidence in the IDES model for the prediction of the long-term evolution of the debris environment and mission collision risks.

The validated IDES model has been used in a number of comprehensive state-of-the-art applications. The long-term collision interactions of a wide range of different constellation designs with the LEO debris environment have been extensively simulated in a 'business as usual' future traffic scenario, both with and without the implementation of debris mitigation measures. The long-term impact of these different constellation designs on the future collision rate, population levels and collision risks in LEO has been evaluated to determine the sizes and orbits of constellations that the LEO debris environment can tolerate. An overall assessment of the long-term impact of the currently foreseen constellation traffic on the LEO debris environment has been performed. The effectiveness of a package of different routine mitigation measures on stabilising the long-term LEO debris environment has been studied and presented in the thesis. Long-term forecasts of LEO constellation collision risk have been produced by the IDES model. These forecasts are state-of-the-art and should be of considerable interest to constellation mission designers. Estimated debris-induced satellite failure rates were assessed for varying constellation architectures in order to find the sensitivity of the predictions to influential design parameters such as orbit selection, the number of satellites in the system, and satellite cross-sectional area. To put these predictions into context, the estimated debris-induced failure rates were compared to the rates expected from satellite component or sub-system failure.

List of Contents

1 INTRODUCTION 1

1.1 BACKGROUND 1

1.2 OBJECTIVES 3

1.3 MODEL OVERVIEW 3

1.4 THESIS STRUCTURE 7

2 THE ORBITAL DEBRIS ENVIRONMENT IN LOW EARTH ORBIT 10

2.1 OVERVIEW 10

2.2 MEASUREMENTS 13

2.2.1 Object Tracking Data from Space Surveillance Networks 13

2.2.2 Debris Detection Data from Ground-based Sensors 16

2.2.3 Debris Impact Data from Space-based Hardware 19

2.3 MODELS 21

2.3.1 Overview 21

2.3.2 Statistical Particle-In-a-Box Models 23

2.3.3 Deterministic Models 24

2.4 LONG-TERM EVOLUTION 34

2.4.1 Future Traffic 34

2.4.2 Model Predictions 37

2.4.3 Parameter Sensitivity Studies 42

2.4.4 Model Comparisons 43

3 MODEL DEVELOPMENT 44

3.1 INTRODUCTION 44

3.2 MODEL STRUCTURE 44

3.2.1 The Debris Environment Evolution Module 44

3.2.2 Population Representation 47

3.3 ORBITAL DEBRIS SOURCES 48

3.3.1 Launch Traffic 48

3.3.2 Fragmentations 62

3.3.3 Nuclear Reactor Coolant Leakage 70

3.4 Orbital Debris Evolution 75
3.4.1 *Orbit Propagation Techniques* 75
3.4.2 *Long-Term Orbit Perturbations* 75
3.5 Orbital Debris Environment 82
3.5.1 *Debris Flux Determination* 82
3.5.2 *Target-Centred Collision Event Prediction* 86
3.5.3 *Long-Term Collision Risk Prediction* 93
3.6 Operation of the Model 95

4 MODEL VALIDATION 97

4.1 Introduction 97
4.2 Validation of Debris Source and Sink Models 98
4.2.1 *Long-Term Orbit Perturbation Model* 98
4.2.2 *Fragmentation Model* 106
4.3 Validation of the Low Earth Orbit Debris Environment Model 107
4.3.1 *Historical Evolution of the Orbital Debris Environment* 107
4.3.2 *Comparison to Measurements at Decimetre Sizes* 110
4.3.3 *Comparison to Measurements at Centimetre Sizes* 111
4.3.4 *Comparison to Measurements at Sub-millimetre Sizes* 113
4.4 Comparison with Other Debris Models 114
4.5 Summary 116

5 THE EFFECTS OF A LARGE SATELLITE CONSTELLATION ON LONG-TERM DEBRIS EVOLUTION 118

5.1 Introduction 118
5.2 Modelled Future Traffic Scenarios 120
5.3 Constellation Impact 123
5.3.1 *Future Collision Activity* 123
5.3.2 *Future Population Trends* 126
5.4 Summary 130

6 THE EFFECTS OF NEW SATELLITE CONSTELLATION TRAFFIC ON LONG-TERM DEBRIS EVOLUTION 131

6.1 Introduction 131

6.2 MODELLED FUTURE TRAFFIC SCENARIOS 132
6.3 CONSTELLATION IMPACT 136
6.3.1 Future Collision Activity 136
6.3.2 Future Population Trends 138
6.3.3 Future Environment Trends 144
6.4 SUMMARY 150

7 LONG-TERM CONSTELLATION COLLISION RISK ANALYSIS 151

7.1 INTRODUCTION 151
7.2 DIRECTIONAL COLLISION FLUX ANALYSIS FOR A CONSTELLATION SATELLITE 152
7.3 LONG-TERM COLLISION FLUX TRENDS FOR A CONSTELLATION SATELLITE 158
7.4 DEBRIS-INDUCED CONSTELLATION SATELLITE FAILURE RATES 164
7.5 SUMMARY 171

8 CONCLUSIONS 172

8.1 OVERVIEW 172
8.2 MODEL ACCURACY 173
8.3 IMPLICATIONS FOR CONSTELLATION OPERATIONS 174
8.4 MITIGATION MEASURE EFFECTIVENESS 175
8.5 CONSTELLATION RISK ASSESSMENT 175
8.6 FURTHER WORK 176
8.7 SUMMARY 180

BIBLIOGRAPHY 181

APPENDIX A: Examples of the IDES Future Launch Traffic Database Files

APPENDIX B: IDES Historical Fragmentation & Future Explosion Databases

List of Tables

Table 3-1: Description of the future launch traffic data files 57
Table 3-2: Default satellite constellation traffic database 61
Table 5-1: Generic constellation designs modelled in IDES 122
Table 6-1: Description of the new constellation designs modelled in IDES 134
Table 7-1: Data for the directional collision risk analysis of a constellation satellite 153
Table 7-2: Estimated satellite failure probabilities for debris impactors in various logarithmic size ranges of the IDES model 166
Table 7-3 : Constellation failure percentages for different reliability values 170

List of Figures

Figure 1-1: Schematic of the IDES model structure (Sats – satellites, RBs – rocket bodies, MROs – mission-related objects, HI – high intensity, LI – low intensity, LEO – low Earth orbit) 6
Figure 2-1: Sources and sinks of orbital debris 11
Figure 2-2: Historical growth in the catalogued population up to Jan. 1999 13
Figure 2-3: USSPACECOM catalogue spatial density in LEO on 31st March 1998 14
Figure 2-4: Detection limits of the USSPACECOM tracking network 15
Figure 2-5: Haystack detection rate distribution over altitude for different fiscal years of observation 17
Figure 2-6: Size-dependent debris flux measured by the Haystack radar in the 950-1050 km altitude band 18
Figure 2-7: The size dependence of meteoroid and debris measurements 20
Figure 2-8: Comparison of EVOLVE predictions and USSPACECOM catalogue for the 1995 LEO debris environment 27
Figure 2-9: SDM 1997 spatial density distribution in LEO for various size thresholds 30
Figure 2-10: Eccentricity distribution of the 1995 ESA MASTER population for debris size thresholds of 10 cm, 1 cm, 1 mm, and 0.1 mm (in ascending order of magnitude) 32
Figure 2-11: Inclination distribution of the 1995 ESA MASTER population 33
Figure 2-12: Early predictions of the future collision rate 37
Figure 2-13: CHAINEE predictions of mitigation measure effectiveness for different implementation years 40
Figure 2-14: EVOLVE/CHAIN model comparisons for 'Business As Usual' scenario 41
Figure 2-15: SDM model predictions of the >1cm population evolution for various scenarios 42
Figure 3-1: Architectural design of the Debris Environment Evolution Model 45
Figure 3-2: IDES representation of the sub-decimetre debris population (for a given debris mass bin and object type) 47
Figure 3-3: Orbital distributions of payloads launched between 1990 and 1998 52
Figure 3-4: Orbital distributions of payload operational debris launched between 1990 and 1998 53
Figure 3-5: Orbital distributions of rocket bodies launched between 1990 and 1998 54

Figure 3-6: Orbital distributions of rocket body operational debris launched between 1990 and 1998 55
Figure 3-7: Mass distribution of various categories of launch-related objects deposited from 1990 to 1998 56
Figure 3-8: Orbital distributions of all object classes in the future launch traffic model 58
Figure 3-9: Mass spectrum for a low intensity explosion 64
Figure 3-10: Mass Spectrum of a high intensity explosion (1000 kg breakup mass) 65
Figure 3-11: Mass spectrum for a catastrophic collision breakup 66
Figure 3-12: Fragment delta-velocity distribution for a high intensity explosion 67
Figure 3-13: Exponential size spectrum of the total generated population of NaK coolant droplets as predicted by the new source model in IDES 73
Figure 3-14: Cumulative size distribution of the total generated NaK droplet population as predicted by the new source model in IDES 74
Figure 3-15: IDES historical and future solar activity dataset (13-month smoothed solar flux at 10.7 cm wavelength, $F_{10.7}$, in solar flux units, s.f.u.) 78
Figure 3-16: Representation of the debris flux environment in LEO 83
Figure 3-17: Algorithm for the handling of satellite constellations in the IDES long-term debris environment evolution program 92
Figure 3-18: The target-centred moving reference frame for the determination of directional debris impact flux relative to an arbitrary target orbit 94
Figure 3-19: A user's view of IDES in the X-Windows environment 96
Figure 4-1: IDES long-term predictions of semi-major axis for an Ariane 4 stage 3 (1991-050F) in LEO compared to two line element (TLE) data 100
Figure 4-2: IDES long-term predictions of eccentricity for an Ariane 4 stage 3 (1991-050F) in LEO compared to two line element (TLE) data 100
Figure 4-3: IDES long-term predictions of inclination for an Ariane 4 stage 3 (1991-050F) in LEO compared to two line element (TLE) data 101
Figure 4-4: IDES long-term predictions of argument of perigee for an Ariane 4 stage 3 (1991-050F) in LEO compared to two line element (TLE) data 101
Figure 4-5: IDES long-term predictions of semi-major axis for a Molniya stage 4 (1993-002D) in highly-eccentric Molniya-type orbit compared to TLE data 104
Figure 4-6: IDES long-term predictions of eccentricity for a Molniya stage 4 (1993-002D) in highly-eccentric Molniya-type orbit compared to TLE data 104

Figure 4-7: IDES long-term predictions of inclination for a Molniya stage 4 (1993-002D) in highly-eccentric Molniya-type orbit compared to TLE data 105
Figure 4-8: IDES long-term predictions of argument of perigee for a Molniya stage 4 (1993-002D) in highly-eccentric Molniya-type orbit compared to TLE data 105
Figure 4-9: Gabbard diagram for the IDES simulation of the SPOT-1 rocket body fragmentation 106
Figure 4-10: Gabbard diagram of the tracked fragments from the SPOT-1 rocket body fragmentation 106
Figure 4-11: Historical evolution of the >10 cm debris environment in low Earth orbit from 1/10/1957 to 31/3/1998 109
Figure 4-12: Historical evolution of the >1 cm debris environment in low Earth orbit from 1/10/1957 to 31/3/1998 109
Figure 4-13: Comparison of IDES >10cm and USSPACECOM catalogue spatial density distributions on 31st March 1998 110
Figure 4-14: Comparison of IDES predictions and measured detection rates of debris larger than 1 cm in LEO for the US Haystack radar 112
Figure 4-15: Comparison of size-dependent debris impact flux as predicted by IDES and the inferred measurement data from the A11 (52 deg) forward face of the retrieved LDEF spacecraft 113
Figure 4-16: Spatial density distributions for objects >1 cm on 1/1/97 predicted by different space debris models 115
Figure 5-1: Predicted catastrophic collision rates in LEO with and without constellations and mitigation measures 123
Figure 5-2. The average number of catastrophic collisions up to the year 2050 in various altitude bands for different future space flight scenarios 124
Figure 5-3. The average impact of constellations and mitigation measures on the long-term evolution of debris >10 cm in or intersecting LEO 126
Figure 5-4. The average impact of constellations and mitigation measures on the long-term evolution of debris >1 cm in or intersecting LEO 127
Figure 5-5. The average impact of constellations and mitigation measures on the long-term evolution of debris >1 mm in or intersecting LEO 129
Figure 6-1: Predicted LEO catastrophic collisions for the 'Business As Usual' future traffic scenario with and without the new constellation traffic and the mitigation measures. 137

Figure 6-2: Predicted >10 cm LEO population evolution for the 'Business As Usual' future traffic scenario with and without the new constellation traffic and the mitigation measures 138
Figure 6-3: Predicted >1 cm LEO population evolution for the 'Business As Usual' future traffic scenario with and without the new constellation traffic and the mitigation measures 140
Figure 6-4: Predicted >1 mm LEO population evolution for the 'Business As Usual' future traffic scenario with and without the new constellation traffic and the mitigation measures 143
Figure 6-5: Future projection of the >10 cm LEO debris environment for a 'business as usual' future traffic scenario including the new constellation traffic 145
Figure 6-6: Future projection of the >10 cm LEO debris environment for a 'business as usual' future traffic scenario including the new constellation traffic and mitigation measure implementation 146
Figure 6-7: Future projection of the >1 cm LEO debris environment for a 'business as usual' future traffic scenario including the new constellation traffic 147
Figure 6-8: Future projection of the >1 cm LEO debris environment for a 'business as usual' future traffic scenario including the new constellation traffic and mitigation measure implementation 149
Figure 7-1: Average debris flux (>1 cm) encountered by the chosen constellation satellite around its orbit for the BAU scenario (1/1/2020) 154
Figure 7-2: Predicted average impact azimuth angle distribution of the debris flux (>1 cm) encountered by the chosen constellation satellite in the BAU scenario (1/1/2020) 155
Figure 7-3: Predicted average impact elevation angle distribution of the debris flux (>1 cm) encountered by the chosen constellation satellite in the BAU scenario (1/1/2020) 156
Figure 7-4: Predicted average impact velocity distribution of the debris flux (>1 cm) encountered by the chosen constellation satellite in the BAU scenario (1/1/2020) 157
Figure 7-5: Forecast of the average flux of debris larger than 10 cm encountered in the chosen constellation satellite orbit over the next 50 years under four different future traffic scenarios 160
Figure 7-6: Forecast of the average flux of debris larger than 1 cm encountered in the chosen constellation satellite orbit over the next 50 years under four different future traffic scenarios 161

Figure 7-7: Forecast of the average flux of debris larger than 1 mm encountered in the chosen constellation satellite orbit over the next 50 years under four different future traffic scenarios 163
Figure 7-8: Forecast of the average expected number of impacts from debris >1 cm to the 72-sat. constellation system operating at 780 km altitude and 86.4° inclination for different future traffic scenarios 165
Figure 7-9: Forecast of the average expected number of satellite failures due to debris impacts for the 72-sat. constellation system operating at 780 km altitude and 86.4° inclination in two different future traffic scenarios 167
Figure 7-10: Forecast of the average expected number of satellite failures due to debris impacts for the 56-sat. constellation system operating at 1414 km altitude and 52° inclination in two different future traffic scenarios 168
Figure 7-11: Forecast of the average expected number of satellite failures due to debris impacts for the 324-sat. constellation system operating at 1375 km altitude and 85° inclination in two different future traffic scenarios 169

Acknowledgements

The author wishes to recognise his employer, the Defence Evaluation & Research Agency (DERA), in sponsoring his PhD course. The Ministry of Defence Applied Research Programme provided the funding for the development of the IDES debris model at DERA Farnborough.

Many people, from family and friends to colleagues, have provided encouragement and given their kind support to the author in his research. Their support is greatly appreciated. In particular, Sven Hauptmann contributed to the design (including some fast, analytical flux determination techniques) and coded about a third of the IDES simulation software. Jenny Wilkinson is thanked for her significant efforts in running the IDES model and producing many graphs of the IDES predictions included in this thesis. Nicholas Johnson of the NASA Johnson Space Center is thanked for his co-operation in supplying an electronic version of a figure for this thesis. Dr. Richard Crowther, Hedley Stokes and Dr. Graham Swinerd have all provided valuable comments during the technical review of the research and associated publications.

Dr. Graham Swinerd is especially thanked for his supervision and guidance during the full course of the PhD studies. The author wishes to express his gratitude to Prof. Walter Flury and Dr. Heiner Klinkrad of the European Space Agency, for their continued interest in the research.

Last, but certainly not least, the author would like to reserve his greatest appreciation for his wife, Lisa, whose considerable patience and encouragement has made it possible to write the PhD thesis in his spare time.

1 Introduction

1.1 Background

Since the beginning of the space age in 1957, satellite operations in Earth orbit have generated objects serving no useful purpose, in other words *orbital debris*. This unfortunate side effect of space utilisation has grown to such a level that satellite missions are exposed to an increasing risk of colliding with debris, causing significant damage or degradation. There are two main regions of near-Earth space that are used most, Low Earth Orbit (LEO) and Geosynchronous Earth Orbit (GEO). Consequently these regions contain the highest concentrations of man-made debris. In fact, measurements of the current orbital debris environment have revealed that the collision rate between large objects in LEO is about 1 event every 10 to 20 years[1]. The LEO collision rate already exceeds estimates of the rate in the GEO debris environment by almost two orders of magnitude. The collision rate between large objects in GEO is believed to be approximately 1 event every 400 to 700 years, or a collision probability of 0.021 over a 20-year period[2,3]. This is because the LEO regime has been used much more and has become a highly dynamic environment with wide variability in the temporal and spatial dependence of source and sink processes.

The number of objects in the LEO population has grown in the past due to spacecraft, spent rocket bodies, other mission-related objects, nuclear reactor coolant leakages, solid rocket motor burns, surface material degradation, and on-orbit fragmentations. The latter have been the main historic source of debris at larger sizes. The majority of fragmentations have been explosions of the aforementioned discarded payloads and rocket bodies[4]. The events can generate hundreds of large fragments that have contributed to the current debris density. In some regions of LEO, this debris density may have already exceeded a *critical density* where random collisions will start to occur and produce even more fragments[1]. When the rate of fragments being produced by random collisions exceeds the rate at which they are being removed by atmospheric drag, the debris population will start to grow exponentially as collision fragments cause more collisions, and so on. This is a process called *collision cascading*. It is this potential dominance of uncontrollable random collisions over

controllable explosions as the main source of debris that has prompted a growing number of studies into the future evolution of orbital debris.

The future long-term evolution of the orbital debris environment depends upon many different factors. These include the rate of future launch traffic, the rate of explosions, fluctuating solar activity, new space activities, new debris sources, the rate of collisions, and the efforts made by mankind to reduce and control the growth of the population. In order to determine the extent of the population growth in the medium and long-term future by taking account of these factors, simple mathematical models are not sufficient. Instead, complex computer models must be employed to simulate each source and sink in detail, based on estimates of likely or possible future scenarios. Since the discovery that orbital debris may have reached a critical density at some LEO altitudes[1] and that it may *start* to grow in an uncontrollable manner due to a collision chain reaction[5], computer simulation models have become particularly useful in assessing the most effective remedial measures.

Another important use of these long-term evolution models is to determine the impact that new space activities will have on the future debris population growth. The operation of many multiple-satellite constellation systems in LEO for global communications is a good example of a new use of space that might have a such an impact[6,7]. Literally hundreds of commercial constellation satellites are likely to be launched in the next decade and operated to provide the so-called 'globile' satellite phone and high-speed internet/multimedia services. With such a boom in the commercial satellite industry, it is possible that so many extra spacecraft placed in the most crowded orbits of LEO may exacerbate future debris population growth by becoming involved in catastrophic collision interactions with the background debris environment. From a satellite constellation system perspective, long-term exposure of many members of a system to the debris environment may induce extra spacecraft failures due to more frequent, non-catastrophic impact damage. Extra replacement satellites would be needed to ensure that the system's continuous global coverage is maintained. These factors need to be addressed in detail by debris environment models that are specifically tailored to account for constellation-debris interactions.

1.2 Objectives

There is a growing need to develop models that can reliably characterise the current environment and how it will evolve in the future. Analytic models are ideal for making fast, simplified population projections over decades or even centuries, covering a wide range of future traffic scenarios and parameter sensitivities. However, they cannot provide the high resolution required to evolve the debris flux environment for assessing localised variability, or forecasting collision risk to a target satellite in the long-term. Deterministic or semi-deterministic computer models have such a scope and can simulate the dynamics of source and sink mechanisms to a high level of detail. These models can generate debris on a wide range of orbits and down to small sizes, therefore characterising the whole environment and predicting its possible future evolution.

The aims of this PhD were to:

- review the current state-of-the-art research in the area of long-term orbital debris evolution modelling;
- develop a high resolution, semi-deterministic computer simulation model that can predict the LEO debris environment in the past, present and future, and forecast the long-term variation in collision risk for any target mission;
- assess and improve the accuracy in the model predictions by a process of validation, involving comparison with debris measurement data;
- apply the model to study the long-term impact of satellite constellations on the debris environment for various future traffic scenarios (including mitigation measures);
- apply the model to study the potential debris-induced failure rates of satellite constellations.

1.3 Model Overview

In fulfilling the PhD objectives, the Integrated Debris Evolution Suite (IDES) has been developed at the Defence Evaluation & Research Agency in Farnborough, UK. IDES is able to model the historical, current and possible future orbital debris environments in LEO, and can provide directional collision risk assessments for individual orbiting satellites which are

exposed to those environments. IDES has been specially designed to simulate the long-term collision interactions between satellite constellations and the background debris population. Thus, the model can be applied to study the effects of satellite constellations on the future debris environment evolution and the collision fluxes that may be encountered by these systems at various particle sizes. The IDES model has been rigorously developed and tested to ESA PSS-05 Software Engineering Standards[8].

IDES characterises the current debris environment by simulating the debris source and sink processes occurring within fixed time intervals from the beginning of the space age to the present-day. This simulation of historical population evolution includes debris larger than 10 microns in size. Each of the past recorded fragmentation events in space is modelled either as a low intensity explosion, a high intensity explosion, or a catastrophic collision. The resulting fragments are then added to the evolving population. Millimetre and centimetre-sized sodium-potassium (NaK) reactor coolant droplets are added to the evolving population by simulating coolant leakage from each of the past 16 Russian Radar Ocean Reconnaissance Satellite (RORSAT) nuclear reactor core ejection events. This is done using a newly derived mass distribution model. All launch-related objects such as payloads, rocket upper stages, and operational debris catalogued by US Space Command are contained in an historical launch database and are added to the historically evolving population on their recorded launch dates.

IDES also has the ability to model the secondary ejecta and paint flakes resulting from meteoroid/debris impacts on spacecraft/upper stage surfaces. However, their contributions are not currently included in the results, due to the lack of quantitative experimental data on the spallation mechanisms and resulting mass or size distributions. When more experimental data becomes available, new source models will be derived and implemented in future versions of IDES. In the population evolution process, long-term orbit propagation is performed by modelling the major orbit perturbations for debris larger than 10 microns. These include geopotential, atmospheric drag, luni-solar and solar radiation pressure effects.

The debris population predicted by IDES from the historical evolution simulation constitutes the initial condition, which is used along with very detailed future launch and explosion models (derived from the analysis of recent historical activity) for projection of

the debris environment over the next 50 years. A constellation mission model enables any number of different satellite constellation designs to be introduced into the population at any time in the long-term evolution simulation. The size-dependent debris flux environment is efficiently determined at regular time intervals using analytical methods and represented in high resolution, with directionality, whilst retaining low data storage requirements. This enables a novel approach for collision event prediction to make rapid and precise collision risk assessments for large target objects in the population. This, in turn, allows the statistical prediction of collision-induced fragmentations and damaging impacts for specific target objects, such as constellation satellites or larger background debris.

By considering the large objects in the population as candidates for collision-induced breakups, the target-centred approach enables IDES to model future debris environments to a much higher level of detail, compared to the traditional volume-centred approach. This is because the orbital elements and mass of a particular collision-induced breakup event are known, being taken from the specific target object in the population. The volume-centred approach predicts collision events in discrete volumes of space. Therefore, orbit/mass information is not known and must be derived from average values, or randomly sampled from pre-determined distributions. Hence, the target-centred approach allows the correct orbital distribution of collision events, and of the resulting collision fragments to be preserved in the simulation. This is especially the case for the orbital elements of inclination, argument of perigee and right ascension of ascending node, which would be unknown in the volume-centred approach. This preservation of the orbital distribution enables IDES to take snapshots of the future debris flux environment in terms of altitude, declination and right ascension.

The IDES model has an integrated three-stage approach to the complex problem of debris environment modelling. This enables the user to combine the automated debris source event pre-processing with the evolution dynamics simulation and the subsequent post-analysis of results. This approach can be visualised in the top-level model structure, presented in Figure 1-1. All launch, breakup and mitigation events are executed in the simulation at regular fixed points in time. Since there are likely to be many such events occurring during a long-term simulation run, three separate pre-processing programs have been designed, which randomly predict future events from average event rates of pre-determined families of

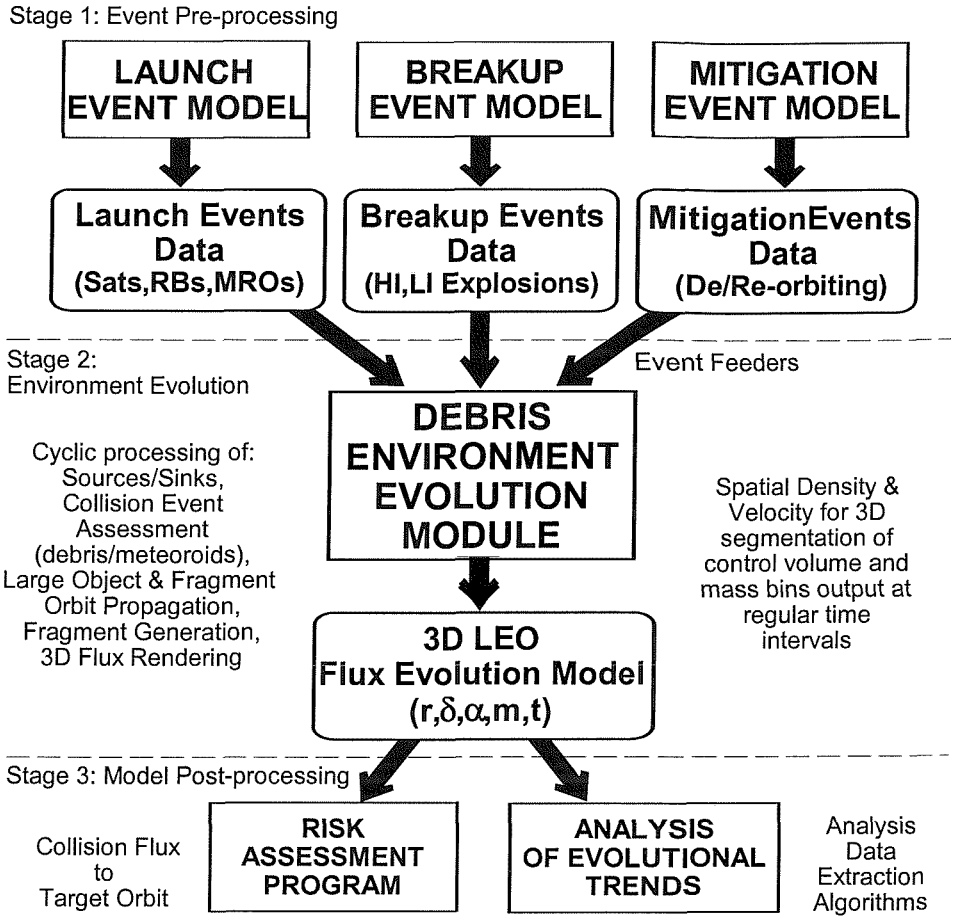

Figure 1-1: Schematic of the IDES model structure (Sats – satellites, RBs – rocket bodies, MROs – mission-related objects, HI – high intensity, LI – low intensity, LEO – low Earth orbit)

objects. This is done by sampling from a discrete Poisson event probability distribution derived from the event rate and time interval. All future event data are stored in the relevant event files, which are subsequently accessed during the execution of the main program. The overall concept of the main program's environment evolution engine is based upon a time increment method[9,10] where all source and sink mechanisms are processed in a cyclic manner over successive timesteps.

The overall function of the main program is to take temporal snapshots of the debris flux environment at regular time intervals. This process renders a flux evolution model for LEO, represented by $F(r,\delta,\alpha,m,t)$, which is dependent upon geocentric radius, r, declination, δ, right ascension, α, mass, m, and time, t. Such a multi-dimensional flux model is then used by the post-processing programs to predict flux relative to a target orbit for various debris

size thresholds and assessment epochs, and to manipulate the large dataset for flexible analyses of parameter distributions and environment evolution trends. Together, the six programs of IDES enable a diverse range of future scenarios to be defined and assessed both for their effects on the entire LEO environment and on any single mission. The results of IDES can also be used as an input to spacecraft system design and mission analysis processes. Due to the randomness of future launch, explosion and collision events, the full IDES simulation of long-term environment evolution must be performed a number of times with each run having different random conditions. This is called the Monte Carlo simulation method, and the model output is averaged over all the runs in order to obtain the likely evolution tendencies of the future environment.

The role of the author in the IDES model design and development was that of chief architectural designer and chief programmer. The author designed most of IDES and wrote approximately two thirds of the source code. The novel target-centred approach to collision event prediction, which has enabled IDES to make advances in long-term evolution modelling, was entirely conceived and developed by the author. The application of IDES to study long-term debris environment evolution was planned and supervised by the author. Another member of the Space Debris group at DERA Farnborough assisted in running the IDES model and processing the results for interpretation (see Acknowledgements section).

1.4 Thesis Structure

The next chapter, Chapter 2, reviews the open literature in order to describe our current knowledge of the orbital debris environment in low Earth orbit across the entire micron to metre object size range from the most significant measurement data and model predictions. Firstly, the sources and sinks of the debris environment are categorised and introduced. Then, our understanding of the environment from the radar/optical tracking of large objects, detection of mid-size debris, and impact statistics of space-returned surfaces/in-situ instruments is examined. Following this, the various environment models available are categorised and reviewed in terms of their different approaches and characterisation of the current debris environment. Finally, the methodologies employed to model future debris sources are presented, and the most important findings from long-term debris evolution modelling are given.

Chapter 3 presents a full and comprehensive description of the IDES model, developed during the course of the PhD programme and applied to study specific long-term environment evolution scenarios for this thesis. The databases, algorithms and mathematical models used or devised to simulate the generation of historical and future debris sources are defined, including objects from launch events, satellite fragmentation events and nuclear reactor coolant leakage events. The techniques and theories employed by IDES to facilitate the evolution process and propagate the orbital states of the debris population due to the major long-term orbit perturbation forces are then given. Finally, the novel approaches developed to determine the debris flux environment, statistically predict future collision events and forecast long-term collision risk variations with respect to any target orbit are discussed.

Chapter 4 summarises the validation process performed in order to evaluate the accuracy of the different components of the IDES model and its overall predictions of the low Earth orbit debris environment for particle sizes down to 10 microns in the past and present. For this purpose, reliable measurement data are used as the benchmark for comparison. This includes the USSPACECOM catalogue of objects for validation of the orbit propagator, fragmentation model, and the >10 cm current environment prediction; the detection rates of the US Haystack radar for validation of the >1 cm environment prediction; and the size-dependent debris impact flux inferred from analysis of the retrieved LDEF spacecraft for validation of the sub-millimetre environment prediction.

Chapter 5 applies the IDES model to make long-term projections of the LEO debris population in order to investigate the long-term effects of operating a large constellation of over 900 satellites in LEO for various future traffic scenarios, including 'business as usual' with and without routine debris mitigation measures implemented. The level of collision interaction of such a large constellation with the background debris population is predicted for these scenarios. The impact of this level of collision interaction on the overall collision rates and population trends is presented.

Chapter 6 employs the IDES model to perform long-term projections of the LEO debris environment in order to more realistically study the long-term implications of operating new

constellation designs similar to those currently being proposed and deployed for commercial communications purposes in the next few years. These designs include a system containing over 300 satellites and several others comprising less than 100 satellites each. The future traffic scenarios modelled are similar to those considered in the previous chapter, except that most of the mitigation measures are delayed by a few years to reflect their more likely timeframe of implementation. The impact of the various constellation-debris collision interactions on the overall collision rates, population trends and environment evolution trends is assessed.

Chapter 7 utilises the long-term LEO debris environment evolution projections produced in the previous chapter in order to conduct collision risk analyses for a selection of the new constellation designs considered. Firstly, the distributions of debris impact flux over impact direction and velocity encountered by one of the satellites in a chosen constellation design are predicted for particular epochs in the future. Then, the long-term temporal variation of mean debris impact flux are computed for the chosen satellite and used to determine the cumulative number of impacts expected from different particle sizes for the chosen constellation design over 50 years. These results are combined with size-dependent estimates of constellation satellite failure probability to ultimately provide forecasts of debris-induced failure rates for the chosen constellation design under the different future traffic scenarios. The same method is then applied to estimate debris-induced failure rates for two other constellation designs.

Chapter 8 discusses the main conclusions and findings of the PhD research, including their scope and significance. The points of discussion include the assessed accuracy of the IDES model and its validity for making long-term environment projections; the implications of the foreseen satellite constellation operations and the constellation designs that may or may not be sustainable from an environmental aspect; the effectiveness of proposed debris mitigation measures in light of constellation deployments; and the implications of debris-induced failure rate forecasts for constellation system availability. Finally, recommendations are made for further research activities that would serve to enhance the accuracy and sophistication of the IDES model for its current purpose, and to extend its scope to study other important issues arising in the space debris research area.

2 The Orbital Debris Environment in Low Earth Orbit

2.1 Overview

Before considering the future evolution of orbital debris, it is important to understand and characterise the present environment as this forms the starting point or initial conditions for the long-term evolution process. This chapter reviews our current understanding of the LEO orbital debris environment from various literature sources. This includes ground-based and space-based measurements of the on-orbit population, and modelling efforts to characterise this population. The most significant predictions of the long-term debris environment evolution by various established models are then reviewed. The LEO debris environment covers orbital altitudes up to 2000 km. It is in this region where most of the satellite constellations will be deployed. The LEO debris environment can be broken down into a number of sources (processes that add objects to the population) and sinks (processes that remove objects from the population), as seen in Figure 2-1.

All debris *sources* can be categorised into three main areas relating to breakups, launches or operations. There are two main types of breakup - explosions and collisions. Explosions vary in intensity and depend upon the cause of the explosion and the class of vehicle. Collisions may be broken down into high energy impacts that cause a *catastrophic* (or destructive) breakup, moderate energy impacts that penetrate the parent object's structure causing *damage* which ejects structural fragments, and finally impacts that do not have enough energy to penetrate the structure but can cause *surface* cratering which deposits paint flakes and other ejecta into the environment. There are three main types of debris that originate from satellite launches: launch-released debris, solid/liquid boost motors, and launch vehicle upper stages. Launch-released debris consists of objects that result from a spacecraft's deployment, for example payload shrouds, spacecraft/upper stage adaptor rings, explosive bolts, lens covers, and protective coverings[11].

Upon the attainment of an initial orbit, the payload and launch vehicle upper stage separate and the spent rocket body is left behind whilst the payload is then boosted to its final orbit.

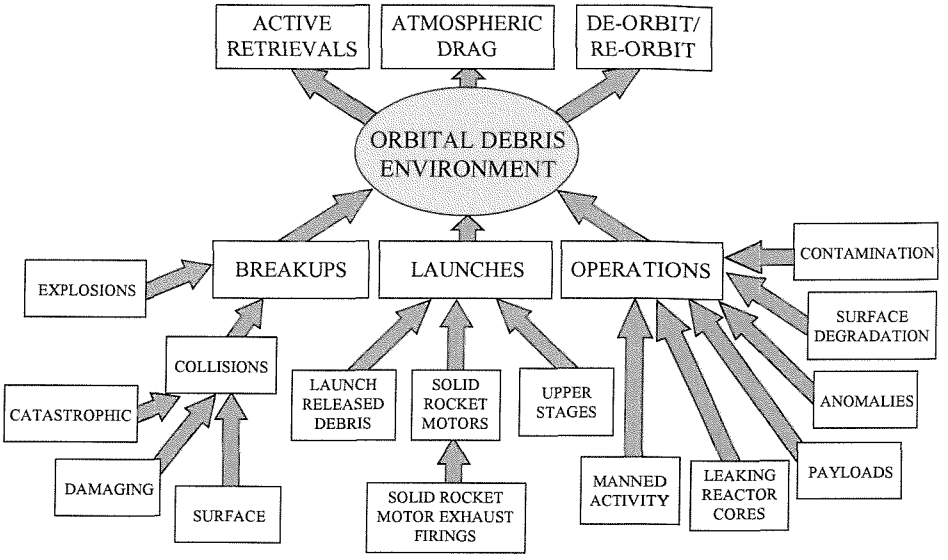

Figure 2-1: Sources and sinks of orbital debris

In the case of a payload destined for GEO, the orbit is attained using a solid or liquid boost motor which is often separated from the payload and left in a Geostationary Transfer Orbit (GTO) or a near-GEO circular orbit. Solid fuel motors are the most common and are known to expel by-products from the exhaust nozzle during and at the end of a burn[12,13,14]. Once the payload has attained its final orbit, the operations phase begins.

During operations of a manned spacecraft, objects such as lost spanners from spacewalks and human waste are left in orbit. At the end of the operational lifetime of an unmanned payload, the payload itself becomes non-functional and is therefore classed as debris, unless it is de-orbited immediately in a controlled atmospheric re-entry. Some unmanned spacecraft are nuclear-powered and have nuclear reactors with fuel cores that are ejected at the end of operational lifetime in a high altitude graveyard orbit. The cooling systems of these reactors are suspected to be leaking liquid metal coolant, forming droplets in specific altitude bands[15,16]. Spacecraft and rocket bodies are exposed to a hostile space environment. Surface materials may degrade with long-term exposure to atomic oxygen, thermal cycling and ultra violet radiation, and may form flakes that float away into space. Specifically, painted surfaces may be particularly susceptible to thermal cycling effects, such as crack

propagation and delamination. These processes may be responsible for depositing many small paint flakes into the orbital environment[17].

The major *sink* of orbital debris in LEO is the atmospheric drag force that causes orbital decay in the upper atmosphere and then the destruction of objects during descent in the lower atmosphere. The natural perturbing forces of atmospheric drag, lunar and solar gravitation, and solar radiation pressure can all work together to reduce the orbital lifetime of debris (given the correct circumstances). In LEO, atmospheric drag is the dominant force that reduces the lifetime of debris. The orbital decay rate of objects due to drag varies according to altitude and time. The lower the altitude, the higher the atmospheric density and the orbital decay rate. During periods of high solar activity at solar maximum, the exospheric temperature of the atmosphere is increased. This heating effect, due to absorption of solar radiation, increases the atmospheric density and leads to the decay of many more debris objects from orbit. In fact, during and near solar maximum the number of objects being removed by drag can exceed the number being generated and hence the population decreases. Conversely, during solar minimum the population grows quite rapidly due to a low rate of atmospheric drag removal, and an undiminished debris source input. It is the fine balance between the future collision debris source and the atmospheric drag sink at specific altitudes that will eventually determine the future stability of the LEO orbital debris environment. In order to retain this balance and ensure environment stability, it has been recognised that operational measures need to be taken to reduce the potential of random collisions between large objects, and hence avoid a collision cascading process.

A large proportion of the total mass and area in LEO is from large objects such as non-functional satellites and spent upper stages. It is these objects that also contain the greatest kinetic energy and therefore there have been proposals to actively remove them from orbit in order to reduce the mass reservoir, which fuels the collision cascading process. However, active retrieval is currently seen as economically unfeasible. A much more acceptable option is for each rocket body and satellite to perform a de-orbit manoeuvre at the end of their useful lives. This would remove or reduce the orbital lifetime of all new satellites and upper stages, and so reduce the potential of random collisions. A number of national agencies, both civil and military, are now producing guidelines/standards that ensure all missions produce less debris and also limit their post-mission orbital lifetimes[18,19,20]. Another option

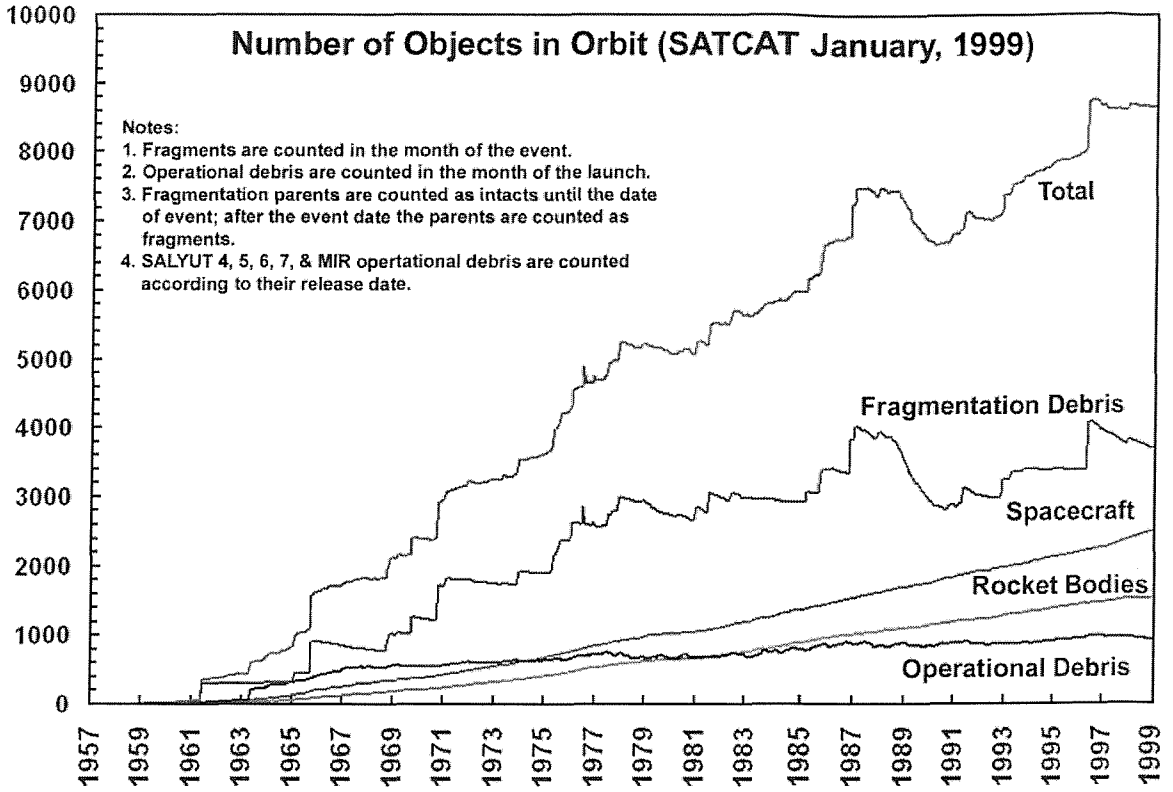

Figure 2-2: Historical growth in the catalogued population up to Jan. 1999[21]

to remove significant amounts of mass from the collision chain is to remove satellites from some of the most crowded orbits up to a storage orbit region situated just above LEO, where there is currently no launch traffic. However, this may be viewed as short-term solution where the storage region could be cleared up when active retrieval becomes technically and economically feasible. If objects are allowed to accumulate in such a storage region, then collision cascading may eventually become an issue there too. The problem could just be shifted to a higher altitude, where there is no atmospheric drag removal. The storage orbit region may be of use in the future and so should be preserved for future missions as much as possible.

2.2 Measurements

2.2.1 Object Tracking Data from Space Surveillance Networks

The most comprehensive method of orbital debris measurement is the tracking and cataloguing of individual orbiting objects. The Unites States Space Command (USSPACECOM) Space Surveillance Network (SSN) performs these functions and

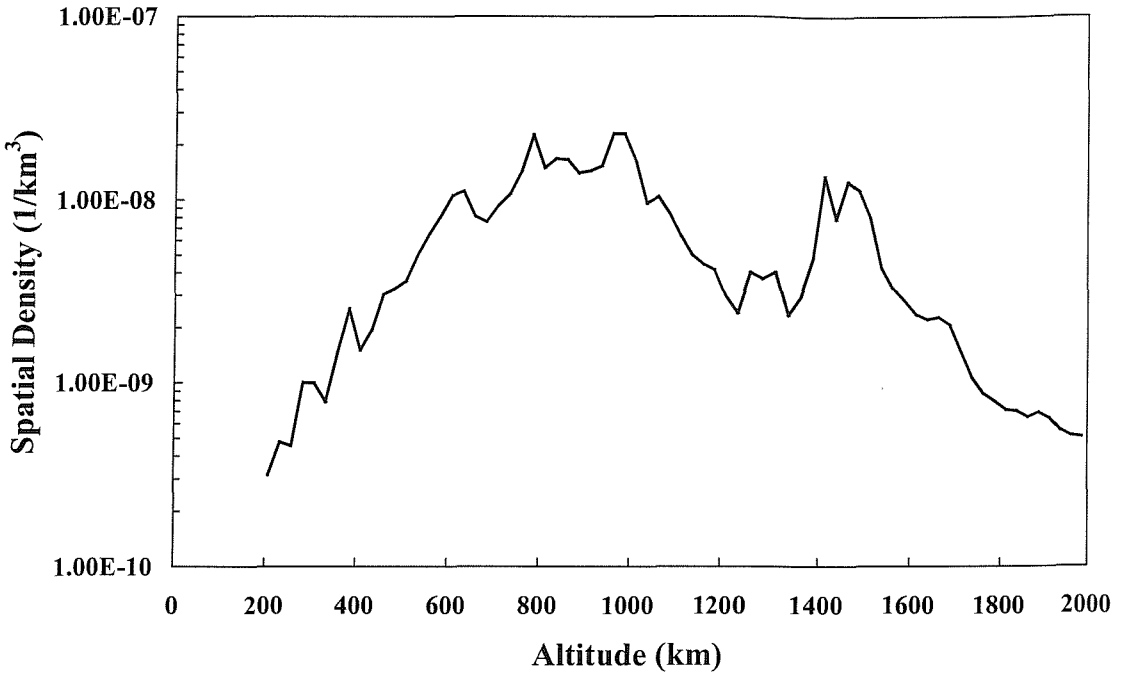

Figure 2-3: USSPACECOM catalogue spatial density in LEO on 31st March 1998

distributes its catalogue to authorised parties on a regular basis. The network consists of ground-based radar and electro-optical stations and can track objects down to the size of 10-20 cm in LEO. USSPACECOM have catalogued over 25,000 objects since 1957, and well over 8,500 are still in orbit. Approximately 45% of objects in the catalogue are breakup fragments, 21% are inactive payloads, 16% are rocket bodies, 12% are mission-related objects (MROs), and only 6% are active payloads (not orbital debris)[22]. Figure 2-2 shows the historical growth of the catalogue up to 1999, broken down by the different object types. The influence of the solar cycle on atmospheric drag decay and therefore the catalogued fragmentation debris population is evident from the fluctuations in the curves. The overall trend in the catalogue over time has been one of linear growth. The majority of catalogued objects have historically been of Russian and U.S. origin (45.5% and 44.9% respectively), since they have been the greatest users of space. A much smaller proportion comes from Europe (3%) and others (6.6%).

The majority of catalogued objects have near-circular orbits with low eccentricities of typically less than 0.1 and semi-major axis values of between 6500 and 8500 km in LEO. There are also a number of objects with semi-major axes of around 25000 km with high

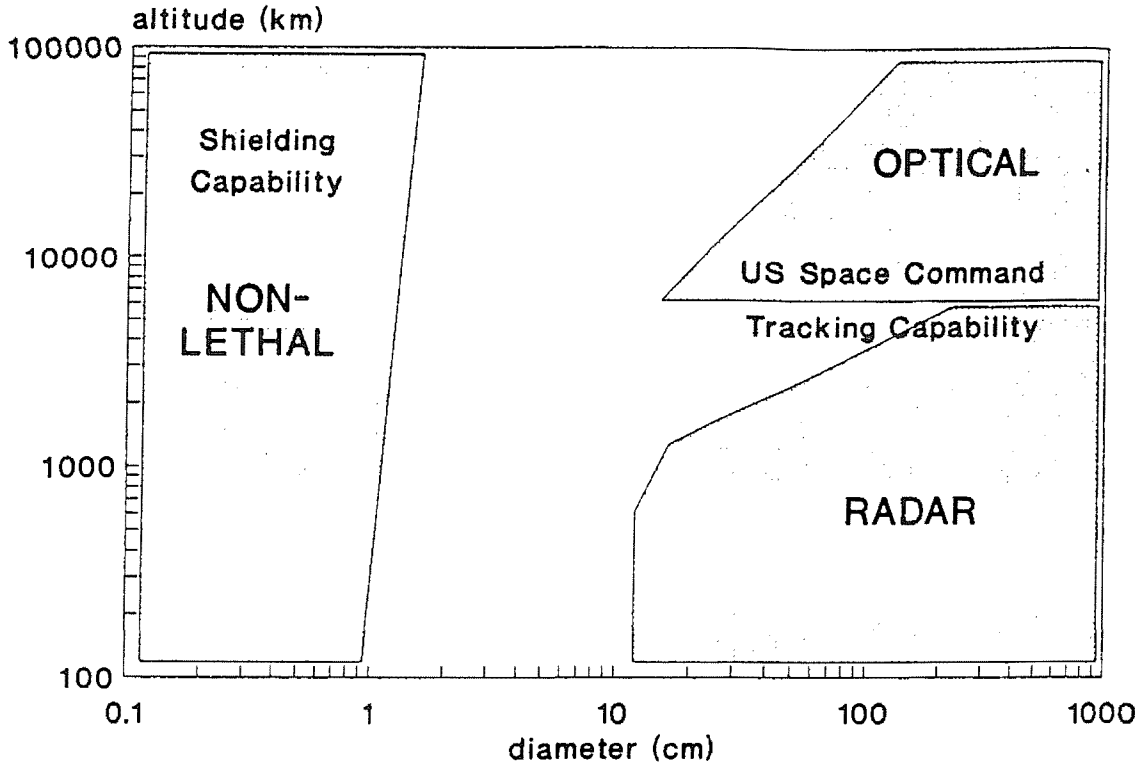

Figure 2-4: Detection limits of the USSPACECOM tracking network[22]

eccentricities between 0.6 and 0.8. These are primarily objects in Geostationary Transfer and Molniya orbits that intersect the LEO regime below 2000 km with higher velocities than those on nominally circular orbits. There are large peaks in the catalogue inclination distribution around 63° and 82° due to launches from Plesetsk, 64° from Molniya-type orbits, 90° from polar weather satellites, and 98° due to sun-synchronous orbits (SSO)[23]. It is these inclinations that are used the most and have the most occurrences of fragmentation events. Figure 2-3 shows the catalogue spatial density distribution over LEO altitudes for 1998. The highest object density regions are well defined at 800 km and 1000 km, with other relatively high density peaks at 1400 km and 1500 km. Below 800 km the spatial density decreases sharply due to the influence of atmospheric drag on the decay and orbital lifetime of debris objects. The spatial densities are averaged over all latitudes, but there are large peaks in the latitude spread at around +/- 82° and +/- 63° respectively.

The minimum sensor detection threshold for the USSPACECOM network is nominally presumed to be approximately 10 cm in LEO and 1 m in GEO. However, the network of radar and optical sensors has a sensitivity that depends upon altitude and it cannot track all objects larger than 10 cm in LEO. As Figure 2-4 shows, the radar sensors have a lower limit

of 10 cm up to about 600 km altitude and above this, the size threshold increases to approximately 20 cm as altitude increases to 2000 km and to 1 m as altitude increases up to 6000 km. Then electro-optical sensors are used, which takes the threshold back down to 10 cm again at this altitude. Sensitivity of the optical sensors decreases towards 1 m as altitude increases towards the GEO regime (~35,800 km).

Debris in particular orbits, such as some Molniya orbits, may be difficult to track because they have stable perigee positions in the southern hemisphere where the network has poor radar sensor coverage and have apogee positions at high altitudes in the northern hemisphere where optical sensors have a reduced sensitivity. Some GTO objects may not be detected due to the high velocities around perigee pass and correspondingly short time intervals spent at lower altitudes. Using USSPACECOM's Ground Electro-Optical Deep Space Sensors (GEODSS), Henize and Stanley[24] performed over 100 hours of observations in LEO to determine the completeness of the catalogue for sizes near the 10 cm radar detection threshold. Only about half of the objects that were observed by GEODSS could be identified from the catalogue. This would suggest that for objects greater than 10 cm in size, the catalogue may be, at worst, only 50% complete.

2.2.2 Debris Detection Data from Ground-based Sensors

In order to measure the untrackable orbital debris population, various methods of sampling the environment, both spatial and temporal have been used. There are essentially two different types of sampling, ground-based and space-based. Ground-based methods have employed higher frequency, shorter wavelength radar (for example NASA's Haystack radar[25] and the German FGAN radar[26]) in a fixed 'beam park' mode for a number of hours, and high magnification optical telescopes (for example the American ETS telescope[27] and GEODSS telescope) in a fixed 'staring' mode. Some of these systems can sample debris with estimated sizes of a few millimetres to a few centimetres in the LEO region.

By concentrating on a particular volume of space in LEO for a particular interval in time, both types of system count the number of debris objects detected in the sensor 'field-of-view'. This has been done with the high powered Haystack radar which operates at X-band frequencies (3 cm wavelength) in various 'beam park' modes, such as vertically (maximum sensitivity) or at 75° and 25° elevation. Haystack, otherwise known as the Long Range

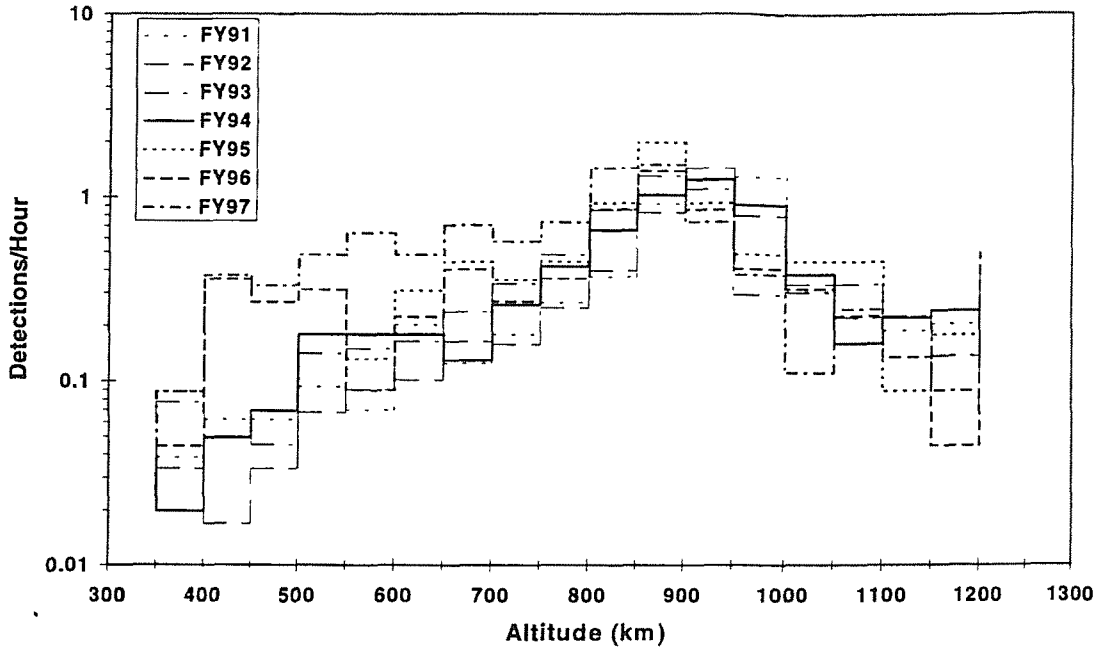

Figure 2-5: Haystack detection rate distribution over altitude for different fiscal years of observation[28]

Imaging Radar (LRIR), has counted debris detections for a total of over 1000 hours since 1990 with a sensitivity of 0.3 cm at 350 km and 0.6 cm at 1400 km. Figure 2-5 shows the LEO altitude distribution of the Haystack detection rate for the different fiscal years of observation. It shows that, particularly for altitudes less than 700 km, the untrackable debris environment is highly dynamic with detection rates varying by up to an order of magnitude. Haystack has also been instrumental in discovering and characterising new sources of orbital debris of millimetre and centimetre dimensions. For example, it was the first to measure the large population of objects with orbits between 800 and 1000 km altitude and inclinations near 65°, which was later recognised to be droplets of liquid metal coolant leaking from Russian RORSAT nuclear reactor systems. Haystack also identified a significant population of centimetre-sized debris on highly eccentric, low inclination orbits now known to be large slag particles ejected as a by-product from solid rocket motor burns.

Measured detection rates are also important to compare with, and validate environment model predictions, providing that the model has the capability to calculate the detection rate for the particular sensor and its detection characteristics[29]. Alternatively, the Haystack data has now been transformed from detection rate into debris flux in the 100 km altitude bins.

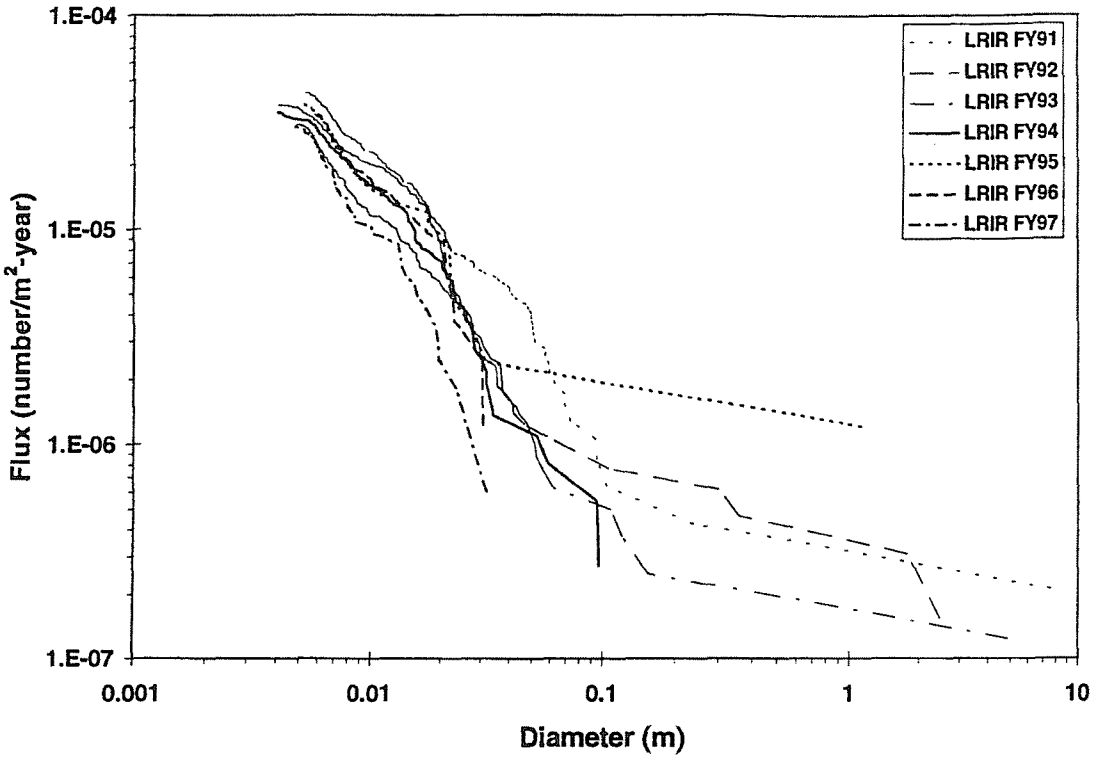

Figure 2-6: Size-dependent debris flux measured by the Haystack radar in the 950-1050 km altitude band[28]

This data is very useful for a direct comparison with model predictions. The measured debris flux is also useful to understand the relative magnitude of the debris population at different particle sizes. Figure 2-6 shows the size-dependent debris flux in the 950-1050 km altitude bin. The measured flux for debris greater than about 3 mm is approximately a factor of 100 higher than the trackable debris flux (debris sizes >10 cm) in this altitude band. For objects of 1 cm and larger, the Haystack measured flux is approximately a factor of 25 greater than the trackable flux. At other altitudes, these factors are smaller. For example, in the 550 km to 650 km altitude band, the factors are 40 and 10 respectively. Based on the number of objects in the USSPACECOM catalogue, these factors can be used to estimate that the >1 cm debris population in LEO may consist of up to 150,000 objects.

The US Goldstone radar[30] has also been available to NASA on a limited basis and has conducted over 108 hours of 'beam park' observation at altitudes up to 3000 km with a total of over 3400 detections between October 1994 and May 1997. Goldstone operates in the X-band and is able to detect a 3 mm conducting sphere at a range of 1000 km, which is more

sensitive than the Haystack radar (6 mm at this range). Goldstone measurements indicate that there may be as many as 500,000 liquid metal coolant droplets larger than 3 mm in orbit with a much wider spread from 1000 km down to 500 km, suggesting that the smaller droplets are now undergoing atmospheric drag decay from orbit.

2.2.3 Debris Impact Data from Space-based Hardware

Space-based methods of sampling the orbital debris environment have so far employed in-situ detectors to measure the spatial and temporal characteristics by counting small-sized (greater than 1 micron) debris impacts as they occur, or by laboratory impact surveys of space-returned hardware. An example of an in-situ detector is the Interplanetary Dust Experiment (IDE)[31] aboard the Long Duration Exposure Facility (LDEF) mission. Space returned surfaces have included the LDEF, the Solar Max, and Eureca spacecraft, and the Hubble Space Telescope (HST) solar array[32]. Due to the decrease in impact frequencies for increasing debris sizes and the durations of exposure, these returned surfaces have received impacts with sizes mainly of the order of microns up to a few tenths of a millimetre. The LDEF mission has provided a good insight into the magnitude and composition of the small-size debris and meteoroid environments experienced at 450 km altitude for the 5.75 years it was in LEO.

LDEF was a gravity gradient stabilised spacecraft with fixed leading and trailing faces, and faces always pointing towards Earth and deep space. Impact analysis of the trailing face showed a much higher flux of debris than was predicted by models. Further analysis by Zhang *et al*[33] could explain this higher flux as belonging to a population of small-sized debris on highly eccentric orbits with an inclination of 28.5°. This was contradictory to the assumption made in the 1989 NASA engineering model that the orbit distribution of smaller debris follows that of the catalogue distribution of mostly circular orbits. Furthermore, this highly eccentric orbit population had to have right ascension of ascending node values close to the ascending node value of LDEF in order to produce the trailing edge flux, thus suggesting that the population was in fact a new debris cloud that had not dispersed fully. This cloud was expected to originate from a new breakup event or from a solid rocket motor firing in GTO. The IDE experiment on LDEF[31] also gave results of discrete peaks in particle flux that were many times the average occurring at the same points around the orbit, thus concluding that LDEF did encounter discrete, undispersed debris clouds.

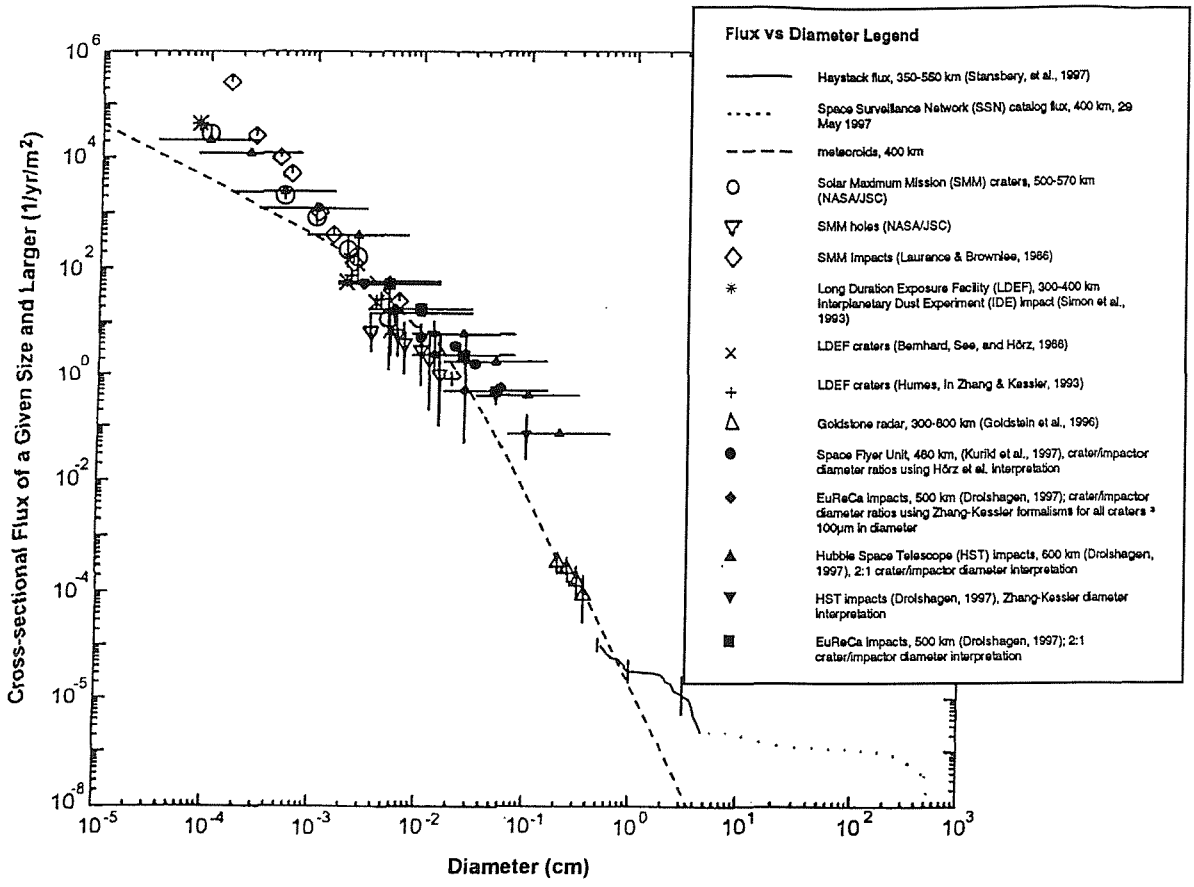

Figure 2-7: The size dependence of meteoroid and debris measurements[37]

Another source of the clouds could be paint flakes being removed from satellite surfaces by thermal cycling or atomic oxygen erosion. Kessler[34] has stated that less than 10 grams of paint is needed to be removed from each orbiting spacecraft per year to explain these results, and only 1 gram per year if the source is highly elliptical. A chemical residue analysis of part of the LDEF spacecraft structure (intercostal F07F02) by the LDEF Meteoroids and Debris Special Investigation Group[35] has shown that a large proportion (43%) of small impact craters were made by paint flakes. Space Shuttle STS-7 Challenger was hit on its outer front window by a 0.2 mm diameter paint flake in 1993. The impact did not seriously damage the window, but it had to be replaced after the orbiter returned to Earth[36]. Many other shuttles have had their windows replaced due to debris impacts.

A good summary of the measurements reviewed in this section and their size dependence compared to the meteoroid environment is given in Figure 2-7. The measurements are spread out over a number of different years and so the population distribution would have

changed, but in general the debris flux levels and therefore the hazard is greater than the equivalent for meteoroids over all sizes, except between 0.03 mm and 1 mm. There is a low debris impact flux and therefore probability of collision between trackable objects, but such collisions are still possible. The first ever recorded collision between trackable objects occurred on 24th July 1996 between the French Cerise defence satellite and a fragment from the November 1986 explosive breakup of an Ariane upper stage. The collision severed the long antenna boom, sending the satellite tumbling rapidly[38]. Note from Figure 2-7 that there are data gaps for some sizes and large gaps in the altitude/orbit coverage for the untrackable debris sizes that have been sampled. It is therefore necessary to develop orbital debris environment models that are able to fill in these data gaps and correlate well with the existing measurement data, thus characterising the whole environment.

2.3 Models

2.3.1 Overview

Before discussing the orbital debris environment that has been predicted by various models, it is necessary to review the different types of model, the functions these models perform, their characteristics and basic attributes. Principally, orbital debris environment models can be placed into two different categories: engineering models and evolutionary models[39].

Engineering models comprise entirely of empirical, analytical relationships that have been derived from a generalisation of measurement datasets and may contain simplifying assumptions or extrapolations about the parts of the environment that are unknown. The simplifying assumptions mainly concern the distribution of the population or the debris flux at untrackable sizes where there are gaps in the measurements, as well as estimates of changes to the distribution in the future. In general use, they allow a simple and quick definition of the current orbital debris environment and its associated collision risks by spacecraft/mission design engineers.

The NASA engineering model[40], first developed in 1985 and enhanced in 1989, is a widely used example of this type of model. It was the recommended design standard for estimation of cumulative debris fluxes relative to spacecraft in LEO. It estimated the flux levels for differing debris sizes by summarising measurements from the USSPACECOM catalogue

(1976-1988), the ETS optical telescope (1984), and impact analyses of Shuttle and Solar Maximum Mission returned surfaces (1984). Data gaps in the size range were interpolated between the measurements. The NASA model assumed that the flux distribution resulting from the USSPACECOM catalogue was complete for sizes down to 10 cm and for objects below 1000 km altitude. At any given size, the variation of impact flux with altitude, inclination, solar activity, velocity and direction was assumed to be the same as the USSPACECOM catalogue variations. This implied that all debris objects are on near-circular orbits. These assumptions have since been proven invalid by more recent measurements in LEO[24,33], although some of these measurements have been used to enhance the model over recent years.

Instead of representing the environment as a simple flux distribution which is scaled by debris size, NASA developed a new engineering model in 1996 called ORDEM96, which includes the distributions of six different types of debris source populations on circular and elliptical orbits and in six different inclination bands[41]. Each inclination band has two families of objects in idealised circular orbits and highly eccentric orbits (with fixed apogee at 20,000 km altitude). These families have functional forms for the estimated variation of object numbers over altitude (circular orbits) or perigee height (highly eccentric orbits) and particle size for the six different source components. These source components include intact objects, large fragments, small fragments, sodium-potassium coolant droplets, paint flakes, and aluminium oxide particles. They each cover particular parts of the size range from 1 micron to >10 cm, where they are known or assumed to contribute to the population. The measurement data from the USSPACECOM catalogue, the Haystack radar, and LDEF returned surfaces, and evolutionary environment model data from NASA's EVOLVE model have been used to define these population distributions. The simplifying assumptions for future debris growth have been improved by a functional variation of each population with time/solar activity levels, although they are still extrapolations of future evolution dynamics. The other aspect to the model is the determination of directional flux incident upon a target satellite orbit from each population, using the theory developed by Kessler[42].

Evolutionary models employ support models to simulate the generation of debris from different sources and evolve the population state with respect to time, either historically to produce a present-day population or into the long-term future (using the pre-determined

present-day population as initial conditions). Examples of the support models include launch traffic models, breakup models, sodium-potassium coolant leakage models, solid rocket motor particle ejection models, orbit perturbation models (e.g. atmospheric drag), and flux environment determination models. There is a wide spectrum of evolutionary models ranging from the simplified, statistical Particle-In-a-Box model to the complex, detailed deterministic model.

2.3.2 Statistical Particle-In-a-Box Models

The statistical Particle-In-a-Box (PIB) model represents the LEO orbital debris environment by the number of objects residing in a limited set of altitude and mass 'bins'. The main use of the PIB model is to make simple and quick projections of the future long-term evolution of orbital debris in LEO. A PIB model computes the interactive collision risk between objects in each of the population bins and employs Monte Carlo methods to predict the number of collisions in each bin. The analytic aspect of these models involves pre-determined functional formulae for the spread of fragment numbers over the altitude and mass bins due to collision-induced breakups, and the decay of object numbers between bins according to size as a result of atmospheric drag perturbations. These analytic expressions tend to be derived from semi-deterministic models, and are designed to greatly reduce the duration of the Monte Carlo computer runs. Additions to the basic population from launch-related debris and explosion fragments are also pre-determined as input rates for each altitude-mass bin.

This type of evolutionary model has given a good insight into the evolution of the LEO debris population in the long-term (the next 100 years) and very long-term (over thousands of years)[43]. A good example of a PIB model is the CHAIN model, developed by Eichler[5]. CHAIN divides the LEO regime into four altitude regions of 0-700 km, 700 to 930 km, 930 to 1100 km, and 1100 to 2000 km. The populations in these altitude bands are further sub-divided into 6 mass ranges to cover objects from 1 mm in size to greater than 1000 kg in mass. The model has 21 different combinations of collisions (e.g. mass bin 2 to mass bin 3 in altitude bin 1 etc.). Collisions in CHAIN are stochastically predicted from collision probabilities dependent upon the scaling of object numbers from the pre-determined reference population and therefore the reference collision probabilities. Results from various Monte Carlo runs are then averaged to obtain the likely tendencies of debris population

growth over time. Another version of CHAIN, called CHAINEE[44] (CHAIN European Extension), was later developed by the Technical University of Braunschweig for the European Space Agency. This model contains more altitude and mass bins and therefore, a higher resolution representation of the LEO debris population. Furthermore, the initial population numbers in these altitude-mass bins are derived from the ESA MASTER model reference population of objects. In addition, the reference interactive collision risks between the CHAINEE altitude-mass bins are computed using the ESA MASTER target orbit impact flux determination tool.

Another example of the statistical type of model for mid- to long-term LEO debris environment forecasting is the Space Debris Prediction and Analysis (SPDA) model developed in Russia by Nazarenko[45]. SDPA accounts for the pollution sources in terms of their mean input rates over altitude and size (down to 1 mm) and the reduction in these pollution sources by atmospheric drag (solar cycle effects included). The future source of debris from collisions and collision cascading is not yet included in the long-term forecast. The initial population distribution is derived from the Russian and US catalogue data for larger (>20 cm) object sizes and also from the US Haystack radar detection measurements for smaller (mm to cm) object sizes. The SDPA model also allows Russian spacecraft design engineers to perform calculations of the directional distribution of collision probability for specific spacecraft with given orbital elements.

PIB models can serve to validate the more complex deterministic models[46] and are ideal for exploring a very wide range of future traffic scenarios and mitigation measures, due to their computational speed. Since they store only the numbers of objects in discrete altitude bands, and not individual objects in the population, PIB models do not tend to experience a rapid exponential increase in computation time and memory requirements as the collision chain reaction is reached. They are also excellent for model sensitivity analyses, but they mostly tend to lack the resolution and precision required to understand the debris environment and its evolution in detail, and also to assess the collision risk to specific spacecraft.

2.3.3 Deterministic Models

Deterministic models are the most detailed, complex evolutionary models and have the most potential for improving our characterisation of the current orbital debris environment and its

evolution in the mid- to long-term future. These models represent the debris population as individual objects or groups of objects with a full set of orbital elements and physical characteristics such as mass and area. All sources and sinks are modelled separately by either simulating the source event characteristics that produce new debris objects with new orbits (such as fragmentation modelling) or predicting the changes of each object's orbit over a period of time (orbit mechanics). This gives a degree of realism to the model and allows the flexibility to implement new source and sink processes as they are discovered. Most of these models use historical data such as launch records and fragmentation event data to generate debris from the modelling of each event. The debris objects are then 'evolved' using an orbit propagator to the present day in order to form a 'snapshot' of the current debris population of objects. Various orbit perturbations such as geopotential, atmospheric drag, luni-solar and solar radiation pressure effects can be considered in this evolution process. Most models can then use their current population of objects as initial conditions for making future environment projections in conjunction with a future traffic model to estimate the future launch and explosion rates for groups of objects of a particular type, mission and orbit.

Representing the population at various sizes with orbital parameters means that most deterministic models are able to calculate the orbital debris environment as spatial densities or particle fluxes through discrete altitude shells of near-Earth space. This enables some deterministic models to compute these fluxes relative to a given target spacecraft orbit and therefore provide an analysis of its collision risk, if the spherical sectors are of sufficiently high resolution and the debris intersection velocities are recorded. Typically, deterministic models utilise their computed spatial density/flux representation of the debris environment to stochastically predict future collision events. This sort of representation also enables analysts to identify the precise regions in space that may become the most hazardous and unstable. Deterministic models offer higher precision and higher resolution than the PIB model, and have the flexibility for many applications. However, the attributes and the level of detail means that these models can be quite computationally slow, when compared to the PIB models, and can have computer memory requirements that increase as the simulated population grows with projection time. Due to these constraints, deterministic models that predict future evolution, nominally perform projections over the next 50 to 200 years. Models of this type that are currently in operation include NASA's EVOLVE[47] (current and

future predictions), the Italian SDM[10] (current and future predictions), and ESA's MASTER[48] (current environment only). The IDES model, developed during this PhD to predict past, present and future environments, also fits into this model category. Therefore, the other deterministic models are reviewed in more detail, in terms of their overall approaches and the knowledge of the LEO debris environment that has been gained from their most significant results.

The NASA EVOLVE model

EVOLVE uses historical databases of launches and breakups in order to simulate the introduction of objects into the LEO environment at the appropriate times in the past. The historical launch database[49] holds information on the launch date, initial orbit, mass, dimensions, type and identifier of each object known to have been injected into orbit. This includes actual catalogued objects and objects generated from mission design data sources to complete the database. Each object is introduced into the EVOLVE historical evolution run at its launch date and then propagated to the reference epoch. Breakup fragments generated by modelling each fragmentation are also propagated to the reference epoch in the same way. EVOLVE also models non-fragmentation sources such as solid rocket motor (SRM) slag particle ejections during firings and RORSAT sodium-potassium coolant droplet leakages, based on support models developed at the NASA Johnson Space Center. The fast, analytic orbit propagator in EVOLVE accounts for geopotential (J_2), air drag, and luni-solar perturbations (for highly eccentric orbits). It is not evident from the literature that solar radiation pressure perturbations are modelled. The minimum debris size considered by the model is 1 mm.

The EVOLVE breakup model has recently been significantly updated[50,51]. Although there appears to be no change to the cumulative number-mass distributions for all types of fragmentation, the new approach taken to derive area-to-mass ratio and delta-velocity of fragments from a breakup event has improved the model's level of detail and accuracy. There are new Gaussian area-to-mass distributions for spacecraft and rocket body breakups, with the latter having 'twin peaks'. They were derived from extensive analysis of catalogued fragment atmospheric decay profiles for a number of different breakup events and from the measured average cross-sectional area and mass of fragments in the Satellite Orbital debris Characterization Impact Test (SOCIT) series. There are new Gaussian delta-velocity

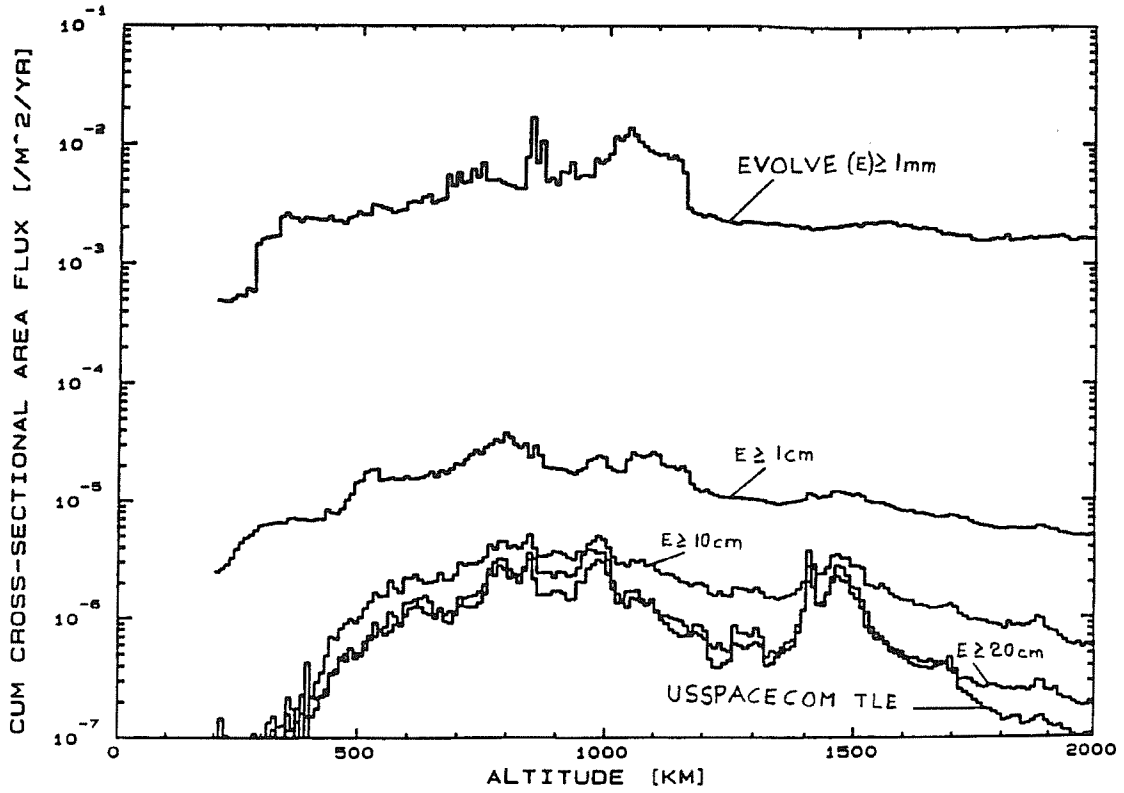

Figure 2-8: Comparison of EVOLVE predictions and USSPACECOM catalogue for the 1995 LEO debris environment[49]

distributions for explosion and collision breakup events, where the distribution shifts according to the fragment area-to-mass ratio. For increasing area-to-mass ratio (and therefore decreasing fragment size), the distribution for collisions exhibits a significant shift to higher delta-velocities, compared to the distribution for explosions. Once implemented, this new breakup model should improve the accuracy of all environment evolution models.

For the current environment, the EVOLVE model has debris fluxes binned into high resolution (approx. 10 km) altitude shells. However, for future environment projections the resolution may be reduced to only 18 (approx. 100 km) altitude shells and 10 size bins covering the LEO regime down to 1 mm sizes. Future collision events are stochastically predicted in a volume-centred approach, based upon computed collision probabilities between different size bin combinations in each altitude shell volume[52]. It does not appear that EVOLVE is currently able to model satellite constellations and their long-term collision interactions with the background debris environment.

In a paper published in 1995 before the recent update was made, EVOLVE predicted around 50,000 objects in LEO greater than 1 cm in size, and nearly 10,000 greater than 10 cm, with a total mass of nearly 1900 tons[46]. In 1996, the implementation of the historical launch database[49] changed the number of objects greater than 10 cm to around 12,800. Figure 2-8 shows the EVOLVE predictions for the 1995 LEO debris environment. The EVOLVE >10 cm flux distribution (E≥10cm line) is double the USSPACECOM catalogue flux distribution over most altitudes. This is consistent with the assumption that the catalogue is only 50% complete for objects >10 cm. In fact, the EVOLVE >20 cm flux distribution (E≥20cm line) has a much better correlation to the catalogue, suggesting that 20 cm is a more realistic estimate of the USSPACECOM tracking threshold in LEO. The contribution of SRM slag particles on high eccentricity, low inclination orbits have been included. They have the effect of 'smoothing' the >1 cm and >1 mm distributions at all altitudes and greatly increasing the fluxes at lower altitudes below 500 km where the perigees of these slag particles are situated. The contribution of RORSAT NaK droplets is not included in Figure 2-8. A comparison between EVOLVE model predictions and some Haystack data[29] in 1995 show a good general agreement for objects greater than 1 cm in size, except in the 800 to 1000 km altitude band, which is the location of the NaK coolant droplets. These droplets are now included in EVOLVE, thus removing this discrepancy with the Haystack data.

The NASA CONSTELL Model

NASA's CONSTELL model[53] has been specifically designed as a flexible tool for the purpose of modelling satellite constellations and their long-term collision interactions with the background debris environment. It utilises the ORDEM96 engineering model to provide the background debris flux environment extrapolated over the next few decades (using assumed population growth rates and solar cycle effects). Then, CONSTELL predicts the explosion and collision-induced breakups of the satellites (and upper stages) associated with a user-defined constellation design. By modelling the spatial density profiles of these breakup fragment clouds over altitude and time, the model is able to estimate the 'constellation-induced' environment and compare it to the background environment over the next few decades. CONSTELL is able to predict the cumulative number of impacts encountered by the constellation over time, due to both background and constellation debris environments. By making assumptions concerning the characteristic size of debris in LEO that may cause constellation satellite failure, the CONSTELL model has made predictions of

the fraction of the constellation that would require replacement after a given amount of time in orbit. The model predicted that a constellation of 1000 spacecraft would require between 8% and 25% of the members to be replaced after 30 years in orbit (assuming the post-mission de-orbiting of constellation satellites), depending upon the operational altitude between 700km and 1000 km altitude. The highest debris-induced failure rates were observed at an operational altitude of 1000 km, where the background debris flux is almost at its peak in the millimetre and centimetre debris size range. There are low atmospheric drag effects and long debris orbital lifetimes at this altitude. It was found that large constellations of 500 satellites or more would start to experience significant increases in their failure rates after 30 years, due to the extra fragments generated by the collision-induced breakups of the constellation.

The Italian SDM Model

The SDM (Semi-Deterministic Model) program has been developed at the CNUCE Institute in Pisa under ESA contract in order to model the future long-term evolution of LEO debris over the next 100 to 200 years[54]. The SDM model represents the LEO debris population larger than 1 mg (~0.9 mm) as individual objects with weighting factors applied at smaller particle sizes. Each object orbit is represented by the orbital elements of semi-major axis, eccentricity and inclination. The 1997 debris population was generated by simulating each of the 140 historical fragmentation events and the 16 RORSAT NaK coolant leakage events. Objects in each debris cloud were generated with a mass, orbital elements, and a weighting factor. Each cloud of fragments was then propagated to the 1st January 1997 reference epoch using the Fast Orbit Propagator (FOP) to accurately consider long-term geopotential, air drag, luni-solar and solar radiation pressure orbit perturbations on each object. After this step, all objects left in orbit were merged with a revised list of USSPACECOM catalogue objects, propagated to the same reference epoch.

SDM spatially represents the debris environment up to GEO altitudes in 50 km altitude shells with 10 logarithmic mass bins covering 1 mg to 10000 kg. The overall spatial density in each altitude-mass bin is stored. In order to predict future collisions, SDM computes these spatial densities from the 'running population' and for each altitude shell, uses them in pairs to predict collision rates between different mass bins. Rather than compute velocity at the same time as the spatial density, SDM uses pre-determined average collision velocities

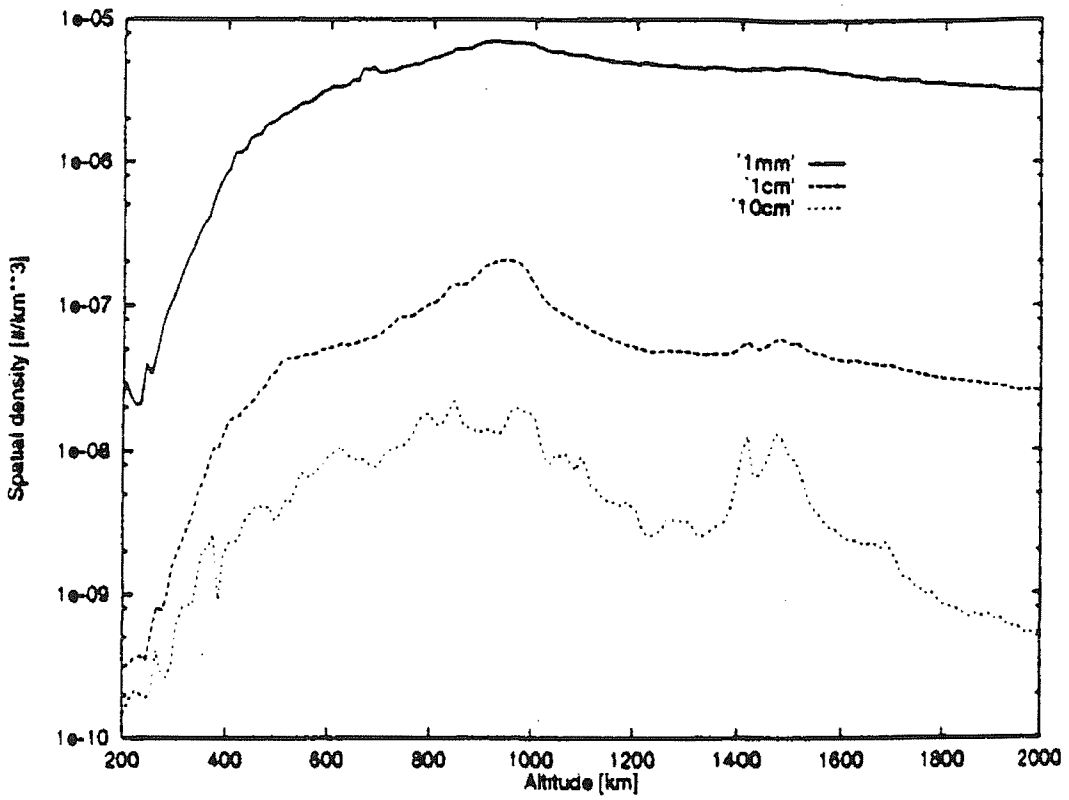

Figure 2-9: SDM 1997 spatial density distribution in LEO for various size thresholds[55]

in each altitude shell as a basis for calculating the collision flux and hence collision rates between different debris sizes (as an approximation). For future evolution runs, SDM employs a much simpler and faster orbit propagator, the Debris Cloud Propagator (DCP), which considers analytic approximations to air drag perturbations only. The future launch traffic model contains a number of different payload classes, each with a representative orbit, mass and percentage share of the overall annual launch rate. Each payload class has an associated rocket body class with orbit and mass information. The traffic model is based on an analysis of routine launch activity of the last few years. Additionally, SDM has a support model, which is able to simulate the launch patterns of future satellite constellations, so that the long-term impact of constellations on the debris environment can be investigated[55]. With a reasonably up-to-date constellation traffic model, including the revised Teledesic design of 324 satellites and some estimation of future architectures, the SDM study found the long-term impact of constellations on the evolution of the debris population to be small.

The SDM model predicted a 1997 LEO debris population of 5 million objects with size greater than 1 mm, around 72,000 objects larger than 1 cm (comprising 14,000 NaK

droplets), and 7,200 objects larger than 10 cm. The distribution of spatial density over altitude predicted by this reference model can be seen in Figure 2-9. The 1997 reference population is then used by SDM as the initial population for performing the long-term evolution projections over 100 to 200 years.

The ESA MASTER Model

MASTER (Meteoroid And Space debris Terrestrial Environment Reference) was developed by Technical University of Braunschweig under another ESA space debris contract[56]. It was designed to provide a high-resolution collision risk analysis tool for the current space debris and meteoroid environments from LEO to GEO. The orbital debris environment model was derived from the output of a previous contract to model the population of small-size debris[57]. The MASTER model is not used to make any predictions of the long-term evolution of the debris environment. The MASTER (release 1) reference debris population reaches down to the minimum size of 0.1 mm, which is an order of magnitude smaller than the 1 mm thresholds of EVOLVE and SDM. The MASTER population consists of individual representative objects with weighting factors at smaller debris sizes. These representative objects have a full set of orbital elements, physical characteristics (mass, size, area-to-mass ratio) and source/origin information. This population is derived from the orbit evolution of modelled fragments from historical breakups and the addition of launch-related objects from the USSPACECOM catalogue. Each fragmentation is classified as either a low intensity explosion, high intensity explosion or collision according to the assessed cause of breakup and class of object. MASTER simulates each historical explosion with a variable intensity in order to fit the mass distribution to the number of tracked fragments at an assumed tracking threshold mass. Each fragment generated has its orbital state propagated to a 1995 reference epoch using the established ESOC FOCUS semi-analytic orbit propagator which accounts for perturbations such as geopotential (J_2-J_5), air drag (with an oblate atmosphere), luni-solar, and solar radiation pressure (with effects of cylindrical Earth shadow).

By employing the theory developed by Klinkrad[58], MASTER (release 1) has a three dimensional spatial representation of the 1995 LEO debris environment with 10 km resolution altitude bins, 2° declination bins and 10° right ascension bins. There are no mass or size bins in this representation because it records the directional flux vector details for the

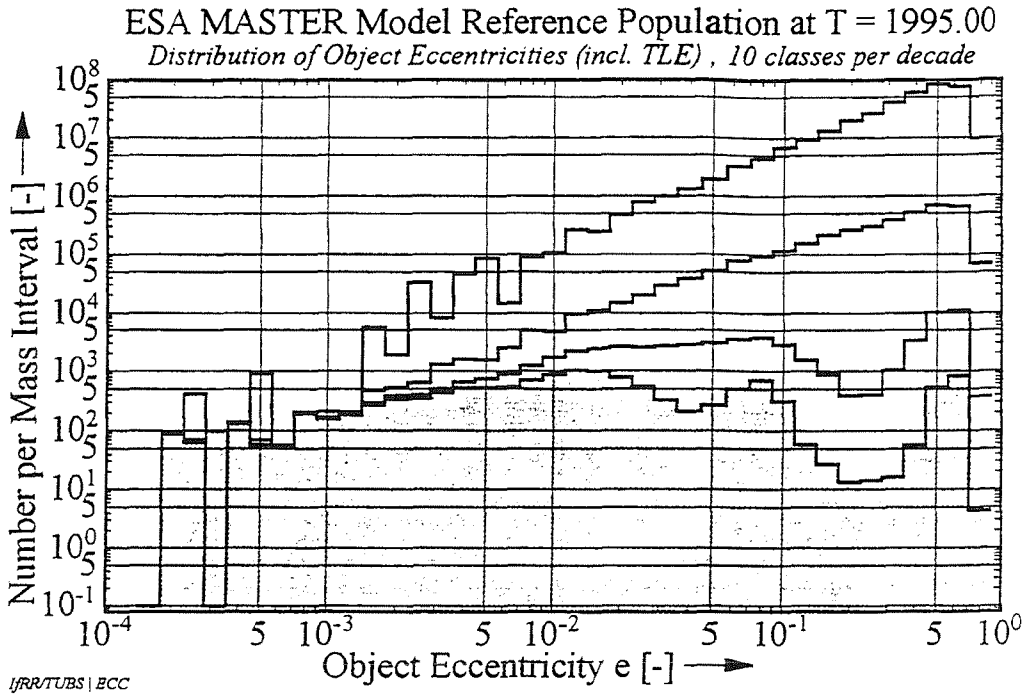

Figure 2-10: Eccentricity distribution of the 1995 ESA MASTER population for debris size thresholds of 10 cm, 1 cm, 1 mm, and 0.1 mm (in ascending order of magnitude)[56]

intersection of each object's orbit with the three-dimensional volume cells in the control volume stretching out to GEO altitudes. For the 250,000 representative objects in the population, this generated around 2 Gigabytes (Gb) of cell passage event data for one snapshot in time. This data has been compressed onto a single CD-ROM and is accessed by MASTER's ANALYST tool, which determines directional flux contributions relative to a user-defined target satellite orbit or ground sensor field-of-view. The approach is extremely detailed and excellent for high precision directional collision risk analysis limited to only a few years beyond the reference epoch (even the origin information on the encountered debris flux is retained). An extrapolation method (considering population growth factors and solar activity effects) is used to scale the collision risk levels for analysis dates beyond the reference epoch.

The MASTER model (release 1) predicts the 1995 object population in Earth orbit to be 12,982 objects larger than 10 cm (9,519 breakup fragments and 3,463 launch-related objects), 67,030 objects greater than 1 cm, over 4 million objects larger than 1 mm, and 415 million objects greater than 0.1 mm in size. The increasing number of objects with decreasing size is due to the power law mass distributions used to model high intensity

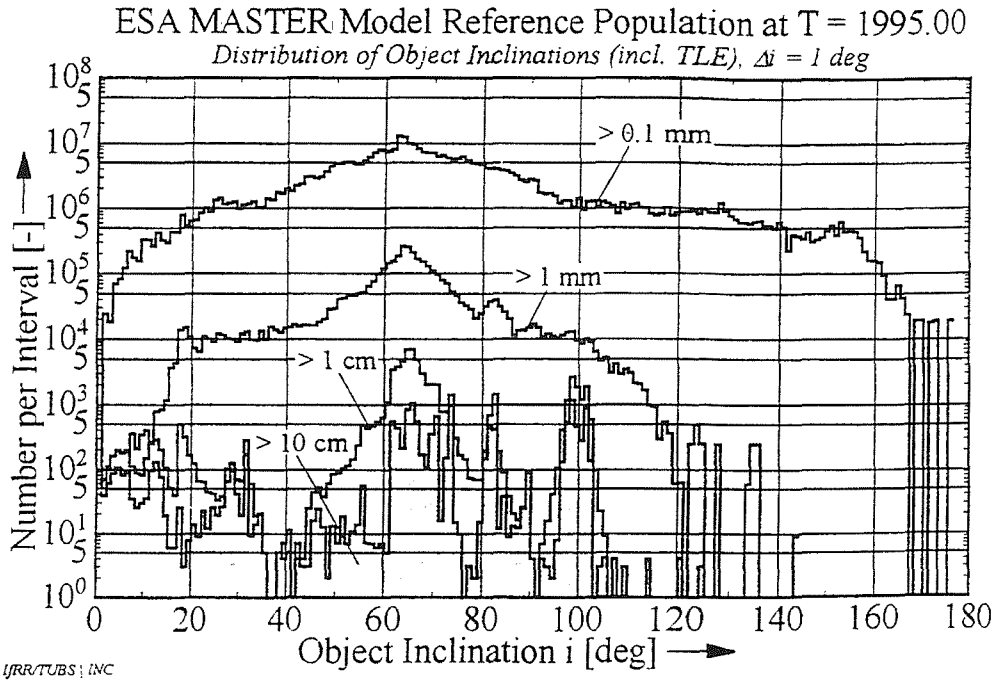

Figure 2-11: Inclination distribution of the 1995 ESA MASTER population[56]

explosions and collisions. The MASTER results have given a good insight into the eccentricity and inclination distributions of the population for the above size thresholds (see Figure 2-10 and Figure 2-11). They show that most large-size debris objects follow low eccentricity, near-circular orbits, with the exception of a sharp peak at around 0.73 due to Geostationary Transfer Orbit (GTO) and Molniya orbits. These objects are also distributed in a number of narrow inclination bands (eg. 28°, 65°, 82°, and 98°), which is confirmed by the USSPACECOM catalogue. For the untrackable population, the average eccentricity increases with decreasing size because smaller breakup fragments are given higher ejection velocities at breakup, compared to larger fragments. At very small sizes such as 0.1 mm, most of the objects have highly eccentric (>0.5) orbits. The MASTER inclination distribution suggests peak numbers of debris at 65° at all sizes below 10 cm. The spreading of small debris about this 65° inclination increases as size decreases, due to the higher breakup ejection velocities in the out-of-plane direction.

In summary, the modelled population smaller than 10 cm is dominated by objects on highly eccentric orbits in the 60° to 70° inclination band. This is a consequence of the considerable number of high intensity explosions that have occurred in both highly eccentric orbits (COSMOS 862 class), and circular LEO orbits (COSMOS 699 class). The MASTER results

compared well with the USSPACECOM catalogue impact flux. The MASTER model (release 1) was compared with other data to validate the untrackable population, such radar detection data and space-returned surface impact fluxes data. From this comparison, MASTER was estimated to under predict the measurement data by a factor of 2 at 1 cm, a factor of 17 at 1 mm, and a factor of 136 at 0.1 mm. Size-dependent scaling factors were universally applied to all flux vectors in order to 'calibrate' the model with the measurements. This large under-prediction was attributed to the limitations of the fragmentation models and non-fragmentation sources not being modelled.

Currently, the MASTER model is undergoing a major upgrade. This involves extension of the minimum particle size down to 1 micron, development of detailed source models for NaK droplet leakage[59], SRM dust/slag particle ejection[60] and a simplistic model for paint flakes. The updated MASTER reference population will probably have a reference epoch in late 1998 or early 1999. These developments should improve the accuracy of MASTER when compared with the debris environment measurement data, especially at untrackable particle sizes where large scaling factors have been applied in release 1 to compensate for the deficiency of non-fragmentation sources in the model.

2.4 Long-Term Evolution

2.4.1 Future Traffic

The number of collisions in the future is strongly dependent upon the number of launches, which could significantly increase the total mass and area in orbit. This would increase the likelihood of catastrophic collision events occurring with larger explosion fragments or with collision fragments themselves (the 'feedback' effect). Furthermore, the increased mass would amplify the feedback effect, and act as a 'fuel' reservoir for the collision cascading process. Therefore, the future traffic model used by the long-term evolution model is critical to the predictive forecasting of future environment trends. Indeed, the simulation of future launch and explosion activity for the next 100 years can be a source of great uncertainty for a long-term evolution model, along with the initial population if it is not validated against measurement data. Usually, a number of different future traffic scenarios are studied in order to account for deviations from the most likely scenario, hence defining the boundaries of the time evolution behaviour. The average explosion rate between 1990 and 1998 was

approximately 5.5 events per year. Explosions can be assumed to continue at this order of magnitude, unless measures are introduced by vehicle manufacturers in order to prevent them. The average launch rate, however, can fluctuate significantly over the period of a few years and is extremely difficult to predict because launches are dictated by political, economic and technology considerations. In the early 1980's the annual launch rate was at a peak of over 120 events per year, but then declined down to under 75 events per year in this decade, due to the reduction in government space spending in the post-Cold War era. There are two different types of future launch traffic model, the steady-state model and the mission model.

The **steady-state model** is based on the assumption that the historical launch activity of the past few years would be typical of future activity and so the average launch rate remains constant into the future. This launch rate can then be scaled up and down year by year to investigate the effects of different launch traffic scenarios. Most long-term evolution models use some sort of steady-state model because it offers stability, flexibility, and uses established information on the orbit and mass distributions of launch-related objects. However, this model does not consider changes in the 'steady-state', such as certain historic activities ceasing and new activities commencing in the future. The steady-state future traffic model employed by the Particle-In-a-Box long-term evolution model tends to simply add the average number of launch-related objects deposited during a single time interval to the population numbers in the various altitude-mass bins, based on the pre-determined historical average deposition rate in each bin. In deterministic long-term evolution models, the steady-state future traffic model usually adds actual launch-related objects to the object population, based on stochastic sampling of launch events from the average launch rate of specific object classes. If taken to a sufficient resolution, this method can preserve the historical orbit and mass distributions of the launch-related object source into the long-term future.

The **mission model** is purely based on estimates of the future uses of space such as new technology over the next 25 years, new space architectures, new launchers, and speculations of civil and military objectives. There were two main mission models[61] that predicted U.S. civil and military activity during the period 1990 to 2010. The Civil Needs Data Base (CNDB) was a NASA-sanctioned analysis of future architectures necessary to meet the U.S.

governmental and scientific needs. There were four options in this CNDB mission model: constrained growth; nominal growth; modest expansion; and aggressive expansion (by a factor of 10) including sub-options for Mars and Lunar Base exploration and exploitation. All four options included the International Space Station construction and support. The U.S. Department of Defense (DoD) mission model consisted of two separate activities: normal classified DoD mission requirements of nominal and constrained growth for meteorology, communications, reconnaissance etc., and Strategic Defense Initiative (SDI) architectures with kinetic-kill vehicles (KKVs) and later, directed-energy weapons (DEWs) support. The SDI architecture would have required a factor of 10 increase in the current U.S. mass-to-orbit rate. European mission scenarios up to the year 2020 were also estimated[62] on the basis of the capability and availability of future European launchers such as Ariane 5, Hermes (manned missions), and the development of an Advanced European Launcher (AEL). If all these launchers were implemented, the study predicted a rise in the ESA launch rate from 8 events per year to 25 events per year by 2020. The impact of various mission models on the future evolution of orbital debris up to 2010 has been studied by Reynolds *et al* using the EVOLVE model[63].

Mission models rely on man's historically poor prediction of the future uses of space. Both civil and military requirements change from year to year. Programmes such as the U.S. SDI architecture and the ESA Hermes project were cancelled at the concept stages. An Advanced European Launcher is not being planned. Other programmes that are still likely to be implemented usually take longer than estimated. For example, the International Space Station was originally planned for construction in 1995, the Ariane 5 launcher has commenced operation a number of years later than anticipated, and missions to settle man on the Moon and Mars are probably over 30 years or more away. Therefore, mission models tend to be over-optimistic and the mission design data (orbits and masses) of most architectures is very sparse. Furthermore, reliable information on the future missions of Russia, historically the biggest user of space, is not known in any great detail. Neither steady-state nor mission model is ideal as a good prediction of future launch traffic. Possibly the best solution for deterministic long-term evolution models is to combine the reliable orbit/mass information and stability of the steady-state model with the more certain future uses of space in the mission model. These could include the operation and support of commercial satellite constellations and International Space Station architectures. The Italian

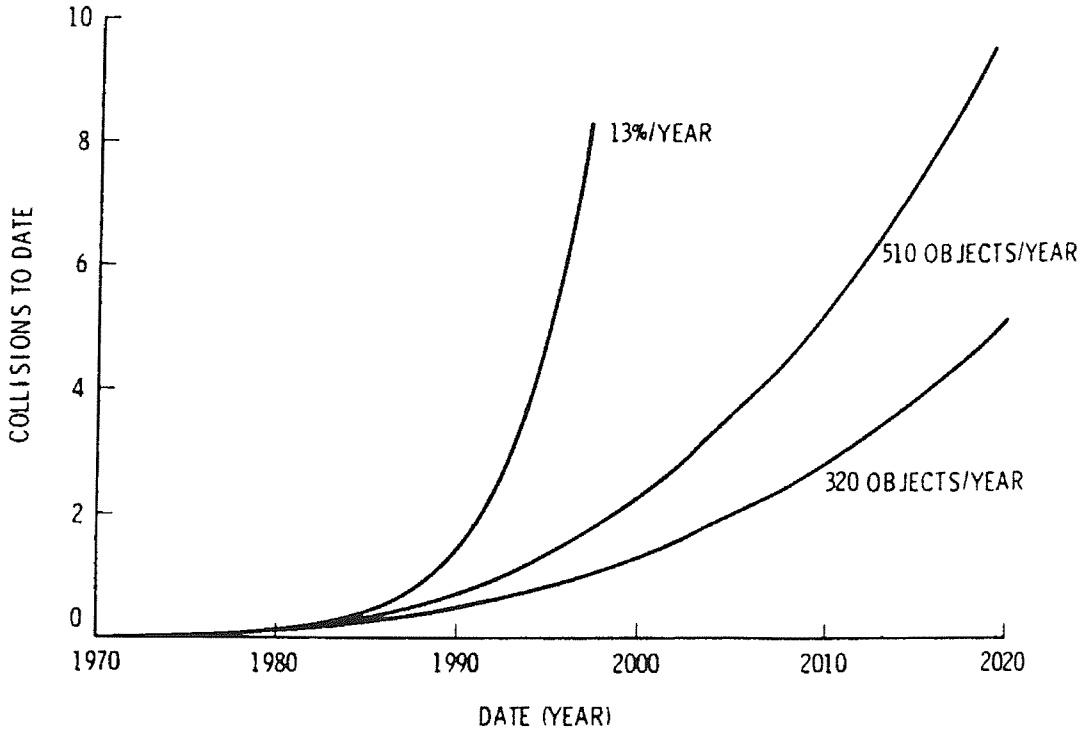

Figure 2-12: Early predictions of the future collision rate[64]

SDM model and the IDES model (see section 3.3.1) use this type of combined traffic model. The NASA EVOLVE model does not currently employ a steady-state future launch traffic model with stochastic prediction of events, but instead repeats the last 8 years of historical launch-related object data in a cyclic manner throughout the 100 year projections.

2.4.2 Model Predictions

The first detailed study of orbital debris long-term evolution was undertaken in 1978 by Kessler and Cour-Palais[64] who predicted an exponentially increasing number of collisions up to the year 2020 and beyond. These predictions used a simple mathematical model and an analysis of the USSPACECOM catalogue and its growth from 1966 to 1978. The study estimated a sampled catalogue spatial density distribution over LEO altitudes, an average collision velocity between catalogue objects of 10 km/s, an average collision cross-sectional area of 4 m^2, and historical catalogue growth rates. These growth rates included a minimum of 320 objects per year (1968-1974), a nominal of 510 objects per year (1975-1978), and a maximum of 13% of the catalogue per year (1966-1978).

As Figure 2-12 shows, Kessler and Cour-Palais statistically predicted that the first collision would occur sometime between 1989 and 1997 in LEO. Indeed, the first recorded collision

occurred on 24th July 1996 between the CERISE spacecraft and a breakup fragment from ESA's SPOT-1 Ariane 4 rocket body[65]. The nominal collision rate projection made by Kessler and Cour-Palais was 2 collisions by the year 2000 and 10 collisions by 2020.

In 1990, Eichler and Rex used the CHAIN particle-in-a-box model to study long-term evolution over the next few hundred years[5]. They predicted that a 'chain reaction' of collisions between objects greater than 1 kg in mass would occur in the next 150 to 200 years, where collision fragments would dominate the population and directly produce more collisions. However, they also predicted that the onset of this collision chain reaction or cascading process would be started in the next 20 to 50 years, if these larger objects increased at a rate of 175 objects per year. A 'critical' population of 200,000 to 300,000 objects larger than 1 cm would be reached at that time, and if the population grew larger than this then it would be too late to prevent the chain reaction.

According to the study, the 930 to 1100 km altitude band is expected to have the most aggressive chain reaction. An analysis of the current population showed that for 35,000 objects between 1 and 10 cm in size, 1750 objects between 10 cm and 1 m, and 1750 objects larger than 1 m, the total collision risk was around 20% per year. The collision risk was found to be only 3.7% per year for catastrophic collisions between large objects. Debris objects larger than 1 kg in LEO have sufficient kinetic energy to cause the complete and catastrophic breakup of a satellite or rocket body. Eichler and Rex found that the collision risk between all objects in LEO rises with the square of the number of objects and is proportional to the collision cross-sectional area, which is low for collisions between small debris and high for collisions involving large objects. The study concluded that reduction and removal of large debris is necessary in the next 10 to 30 years to avoid the onset of the chain reaction altogether, and any delay or slow response would inevitably lead to the onset of the chain reaction.

More recently, Eichler and Reynolds have used CHAIN to perform very long-term evolution projections over thousands of years and have identified four distinct phases of orbital debris evolution[43]. We are currently in the first evolution phase where launches, explosions, and non-fragmentation sources (the background population) are the dominant sources of debris objects. In the second phase, which is deemed to be initiated in the next 30 to 60 years,

collisions amongst objects in the background population start to dominate the population evolution as satellites and rocket bodies collide with each other and with the more common operational debris and explosion fragments. In the third phase in 300 to 600 years time, collisions generated by large background objects impacting with collision fragments will produce collision cascading or the collision chain reaction. Eventually in the fourth phase in about 3500 years from now, there will be no large background objects left because they would be all destroyed by the collisions in the chain reaction. Therefore, the debris population will start to decrease as the collision source is exhausted and the fragments naturally decay due to atmospheric drag. The time-scales for these phases depend upon the mitigation measures taken in the next 10 to 20 years. The study found that in the very long-term, the prevention of explosions is only a short-term measure, and delays these phases by only a few decades. The additional de-orbiting of rocket bodies from 2000 and payloads from 2030 was found to be sufficient to stabilise the collision rate and population growth below 1100 km altitude (where atmospheric drag can remove explosion and collision fragments from orbit). However, the population above 1100 km altitude would still continue to grow over the next few millenia, and so more aggressive mitigation measures would be required to stabilise the growth in this region.

Studies conducted using the ESA/Technical University of Braunschweig CHAINEE particle-in-a-box model for the ESA Space Debris Mitigation Handbook[66] have shown that the year of implementation for mitigation measures is of critical importance to their effectiveness in controlling debris population growth. Predictions of the cumulative number of destructive collisions made by CHAINEE investigating various years of implementation for explosion prevention and de-orbiting (with a 25-year post-mission lifetime limitation) can be seen in Figure 2-13. The reference 'Business As Usual' (BAU) curve is compared to curves of business as usual with: explosion prevention from 2000 and de-orbiting from 2010 (curve A); explosion prevention from 2010 and de-orbiting from 2020 (curve B); explosion prevention from 2020 and de-orbiting from 2030 (curve C); explosion prevention from 2030 and de-orbiting from 2040 (curve D). Significantly, the early implementation of these measures enables the future number of destructive collisions to be reduced by almost a factor of 2. However, the consequences of failing to implement explosion prevention and 25-year post-mission lifetime limitation until the year 2040 would not lead to a significant reduction in the cumulative number of collisions and a still uncontrollable collision rate.

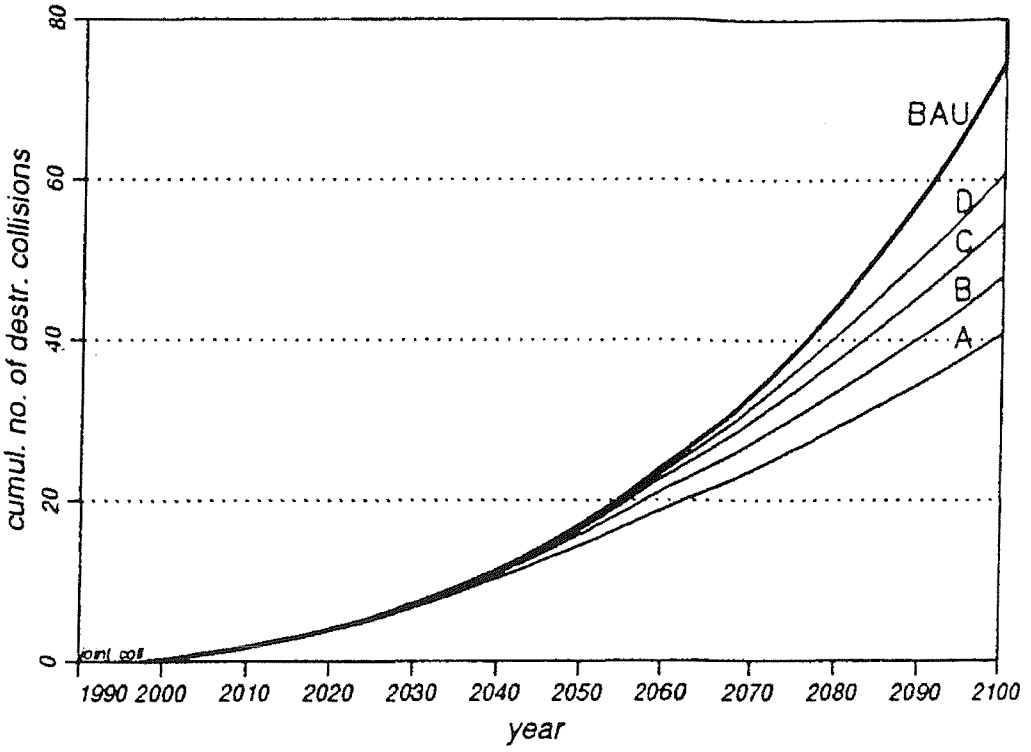

Figure 2-13: CHAINEE predictions of mitigation measure effectiveness for different implementation years[66]

In 1995, the NASA deterministic EVOLVE model and Eichler's particle-in-a-box CHAIN model were extensively compared. Enhancements to both models have been made as a result of this comparison[46]. The model predictions were compared for future projections spanning 100 years and the validated EVOLVE initial conditions were converted for use by CHAIN in order to improve its accuracy with the more detailed EVOLVE projections. EVOLVE has a more detailed future traffic model than CHAIN and this was used to re-define the background population growth rate coefficients in CHAIN. Figure 2-14 shows the comparison of model predictions for the population larger than 1 cm in a 'Business As Usual' scenario. For this case, the original CHAIN projections (CHAIN-STN curve) were a factor of 2 greater than EVOLVE, with an exponential growth from 67,000 objects in 1990 to 600,000 in 2060. EVOLVE predicted an exponential increase from 50,000 objects in 1995 to 300,000 objects in 2060. CHAIN with EVOLVE initial conditions (CHAIN-EIC curve) then started at the same point and resulted in a projection that was very close to EVOLVE. Both predicted 600,000 objects in 2085, which is a factor of 12 increase over the initial population during the 90-year time interval. CHAIN with EVOLVE initial conditions

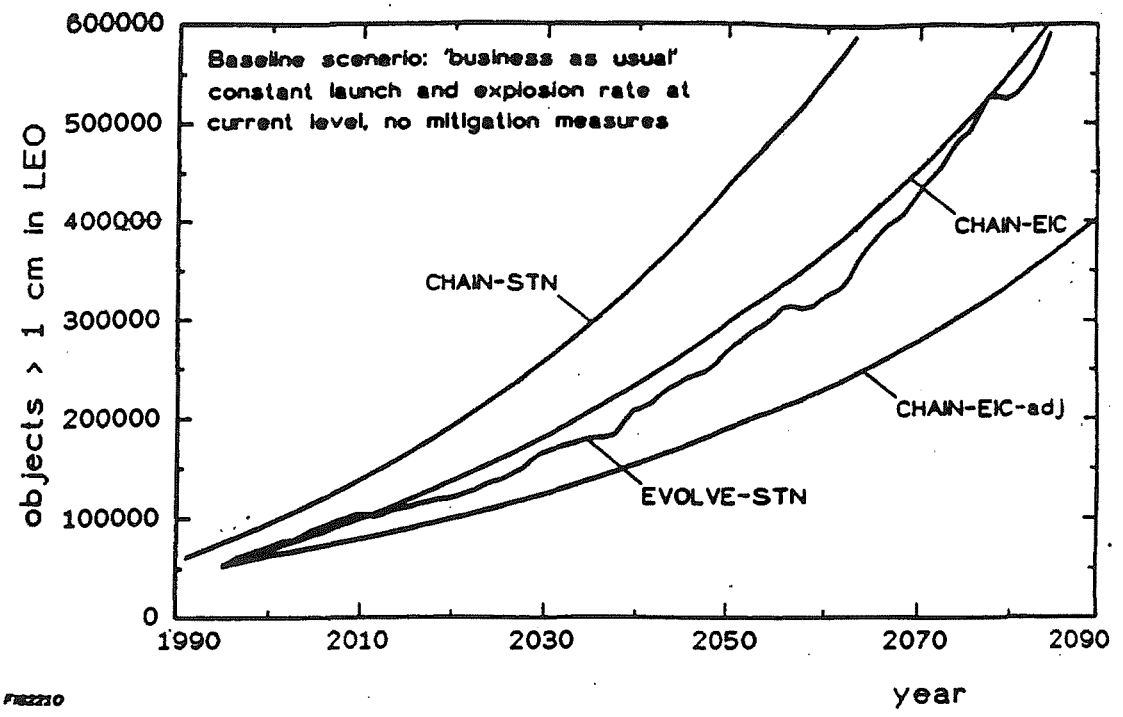

Figure 2-14: EVOLVE/CHAIN model comparisons for 'Business As Usual' scenario[46]

and background population growth rates (CHAIN-EIC-adj curve) resulted in CHAIN under-predicting EVOLVE by nearly a factor of 2 throughout the 100 year projections. This difference must be due to the different collision prediction techniques and collision-induced breakup models employed by the two models. Other EVOLVE results have confirmed that explosion suppression combined with de-orbiting of rocket bodies from 2000 and de-orbiting of payloads from 2030 is the most effective and feasible strategy to control debris population growth and collision cascading over the next 100 years.

SDM has been used extensively to model the long-term evolution of orbital debris for a varying number of scenarios in order to assess the effectiveness of mitigation measures[67]. Figure 2-15 shows the SDM predictions of the >1 cm population over the next 100 years for the 'Business As Usual' scenario (BAU), compared to BAU with explosion suppression from 2010 (NOEX curve); NOEX with de-orbiting of rocket bodies from 2010 (DEOUP curve); DEOUP with de-orbiting of constellation spacecraft (DEORCO curve); and DEORCO with post-mission de-orbiting of all spacecraft from 2030 (DEOALL curve). The BAU scenario increases the population exponentially from 72,000 in 1997 to around 350,000 in 2100, about 30 years after the EVOLVE model projects the same number of objects. The no explosions curve (NOEX) is considerably less than the BAU case at 250,000

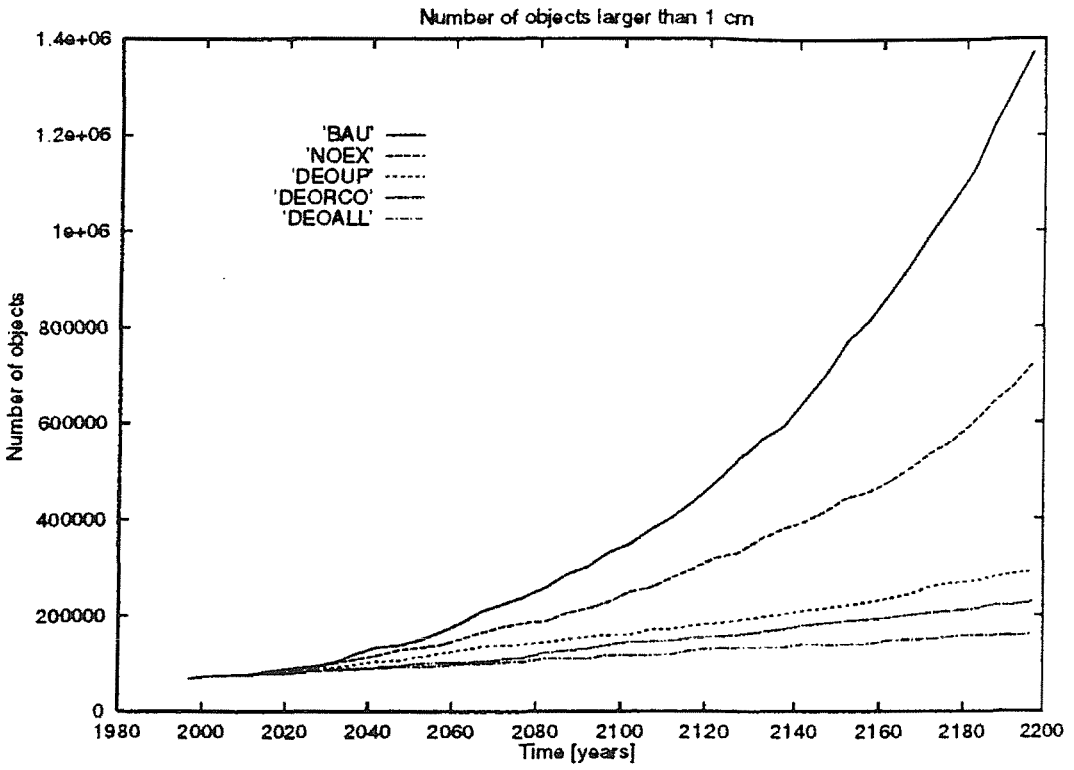

Figure 2-15: SDM model predictions of the >1cm population evolution for various scenarios[67]

objects in LEO in 2100, but the exponential growth due to an increasing number of collisions is still evident. This implies that stopping explosions is only mildly effective in stabilising the environment in the long-term. The DEOUP, DEORCO, and DEOALL curves show that stopping explosions *and* de-orbiting is the most effective strategy to stabilise the exponential population growth over the next 100 years. SDM predicts that stopping explosions and de-orbiting all spacecraft/upper stages (the DEOALL scenario) would limit the population larger than 1 cm to 100,000 objects in 2100, only 28,000 objects more than in the initial 1997 population. This is because spacecraft and upper stage de-orbiting removes significant mass and area from the collision chain. Hence, the collision rate is minimised to remain close to its present-day average of less than 0.1 event per year.

2.4.3 Parameter Sensitivity Studies

Predictions made by long-term evolution models cannot be validated by comparisons to measurement data and the accuracy of these predictions depends upon validation of the initial population and at a lower level, the validation of specific source models such as

breakup models. Breakup models can give rise to significant uncertainties in a long-term evolution model and there have been sensitivity studies to investigate the effect that various breakup model parameters might have on the long-term environment projections. Madler developed the DEEP (Debris Environment Evolution Program) model[68] specifically for this purpose and has shown that there can be order of magnitude differences in the modelled number of current and future objects greater than 0.1 g due to the use of different debris area-to-mass relationships. The area-to-mass ratio directly influences the atmospheric decay rate of objects and therefore the overall number of objects. Large differences in area-to-mass relationships for small-sized debris are due to the poor amount of data on fragmentation objects below 10 cm in size. Madler varied other parameters such as the catastrophic collision threshold and the mass fraction in the power law mass distribution for high intensity explosions, and found that they can alter the debris population composition quite dramatically over time. Rossi *et al* have also used the SDM model for this type of study[54]. They found that there was a factor of 6 difference in object numbers larger than 1 cm when using the highest and lowest published area-to-mass relationships. In an updated study[67], the SDM model predicted that changing the impactor energy-to-target mass ratio threshold from 30,000 J/kg to 60,000 J/kg could reduce the >1 cm debris population by a factor of 2.

2.4.4 Model Comparisons

Quantitatively, the long-term evolution predictions vary widely between different models for any future traffic scenario, in terms of the initial populations used and the extent of population growth over the next 100 years. For the >1 cm population, projections for the 'Business As Usual' scenario may vary by more than a factor of 2 or 3. This is due to the differences in breakup model parameters (mass distribution and area-to-mass ratio) and the future traffic models used (event rates and orbit/mass distributions for launches and explosions). Qualitatively, however, all models tend to produce the same general findings concerning the effectiveness of various debris mitigation measures for the 'Business As Usual' scenario. Namely, that explosion prevention is an effective measure at slowing population growth in the short- to mid-term, but it is not sufficient to significantly control or stabilise the collision rate and hence exponential population growth in the long-term. To achieve this long-term environment stability, immediate de-orbiting of upper stages and then satellites would be required in addition to explosion prevention in the next decade or so.

3 Model Development

3.1 Introduction

In the two previous chapters, the overall top-level design of the model, developed during the course of the PhD programme to simulate the long-term interactions of satellite constellations with the debris environment, was introduced. Also, the other models capable of predicting the current LEO debris environment and/or the long-term evolution of the LEO debris population were reviewed in terms of their most significant findings. The purpose of this chapter is to provide a full and comprehensive description of the IDES model. The databases, algorithms and mathematical models used or devised to simulate the generation of historical and future debris sources are defined, including objects from launch events, satellite fragmentation events and nuclear reactor coolant leakage events. New mass distributions for fragments generated by high intensity explosion events and for liquid metal coolant droplets released by nuclear reactor coolant leakage events are developed. The techniques and theories employed by IDES to facilitate the evolution process and propagate the orbital states of the debris population due to the major long-term orbit perturbation forces are then given. The approaches developed to determine the debris flux environment, statistically predict future collision events and forecast long-term collision risk variations with respect to any target orbit are discussed. Emphasis is given to the approach developed for collision event prediction, given its particularly novel and advanced nature. Finally, the flexible, user-friendly operation of the IDES model via graphical user interface is summarised.

3.2 Model Structure

3.2.1 The Debris Environment Evolution Module

The Debris Environment Evolution Module (DEEM) is the main program in IDES. It acts as the evolution engine that models the long-term dynamics of the debris environment by taking account of the major debris-related processes that occur during each time increment. The architecture, data and control flow of DEEM[69] can be seen in Figure 3-1. The flowchart in Figure 3-1 is similar to that used by Rossi *et al*[10], although the processing order and data structures are different. If a future long-term evolution simulation is to be performed, the

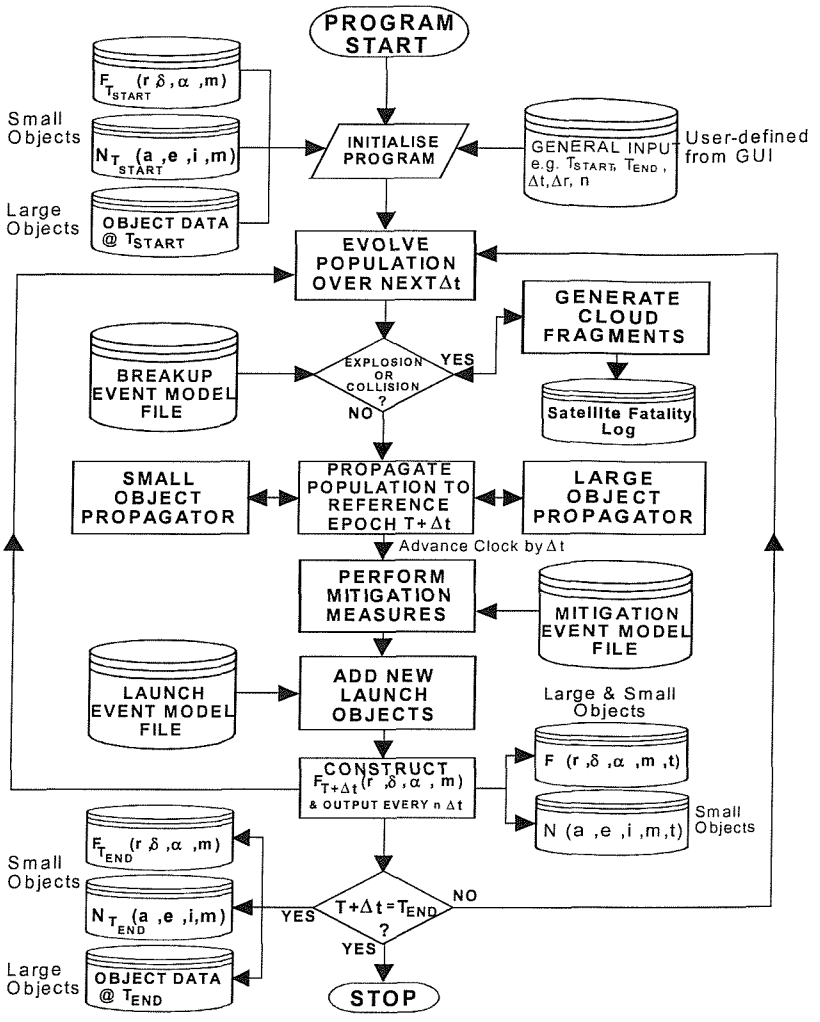

Figure 3-1: Architectural design of the Debris Environment Evolution Model

validated initial conditions are input into DEEM. These include the reference flux model for 31st March 1998 (output by a previous historical evolution run), $F_{1998}(r,\delta,\alpha,m)$, and the debris object population at this reference epoch. Control data concerning the start and end epochs, number of timesteps and other options are also input before starting the time increment process.

On the first timestep cycle, DEEM starts by interrogating the pre-processed breakup event file for any low intensity explosion or high intensity explosion events that are specified to occur in that timestep. If there are breakups to be simulated, then the respective objects are fragmented using the event specific breakup parameters. Fragments are generated according to the relevant breakup model relationships, and then added to the population with their associated derived data, such as initial orbit, mass, size and area.

The collision event prediction algorithm cycles through every large object in the population above a given mass threshold (default of 50 kg), using each such object as a target for rapid collision risk assessment. Here, the reference flux model ($F_{1998}(r,\delta,\alpha,m)$) is used to compute debris flux relative to the target from each debris mass range. This relative flux is utilised (along with the cross-sectional areas of target and debris, and the time interval) to randomly predict the number of collision events to the target over the timestep, according to the collision event probability for a given debris mass bin. The same Poisson distribution sampling method is used as described above for predicting future launch and explosion events. The lethality of each collision event is then assessed. If a catastrophic collision is predicted for a target, then it is fragmented with the event specific parameters. All fragmentation details (for modelled explosion and collision events) are recorded in a Satellite Fatality Log file which can be analysed after a run of DEEM. This information is useful for establishing the frequency and strength of catastrophic collisions in the long-term future, for example. Similarly, the prediction of a non-catastrophic damaging impact to a target is modelled and ejecta fragments added to the population. When impacts from very small debris are predicted for the target, the production of paint chips from painted surfaces on payloads/upper stages can be modelled.

Once collisions/impacts have been processed, DEEM propagates the orbital state of the population forward in time by one time interval, respecting all major orbit perturbations. The simulation clock is then advanced by that time interval. Then, DEEM applies the implementation of the user-defined post-mission mitigation measure scenarios by interrogating the population, to either change the orbital elements of specific members (so simulating de-orbit or re-orbit manoeuvres) or to remove them (modelling complete de-orbits or active retrievals), if appropriate. Similarly, the pre-processed launch event file is scanned in order to introduce any launch-related objects into the evolving population during the timestep.

After the object population has been manipulated by all these source and sink processes, the final computation of the timestep cycle determines the debris flux environment, $F_{t+\Delta t}(r,\delta,\alpha,m)$, for that epoch. The updated object population and its orbital state is taken and utilised to derive debris flux vectors in a matrix of volume cells within a spherical

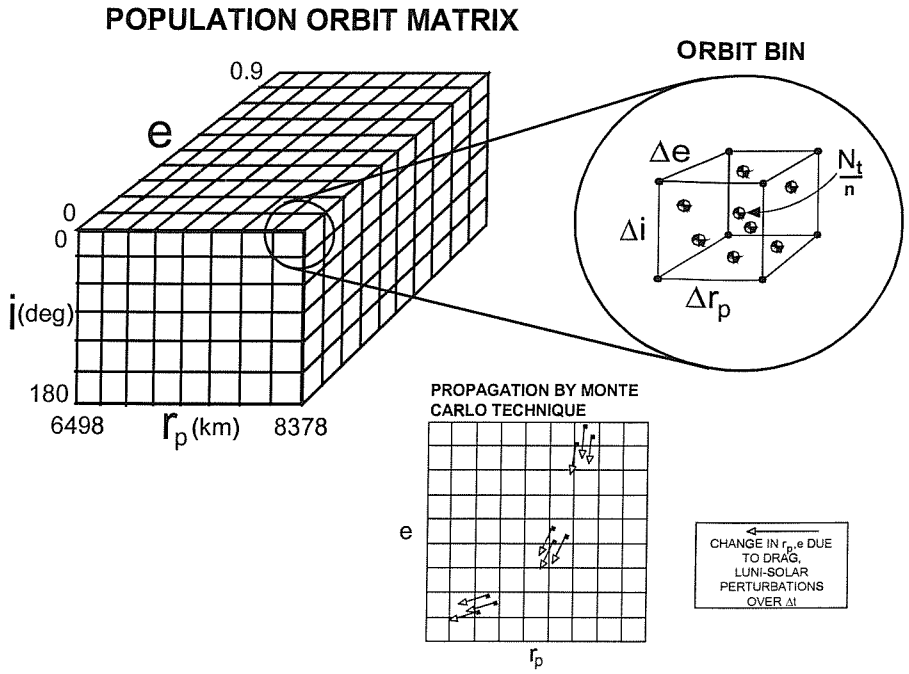

Figure 3-2: IDES representation of the sub-decimetre debris population (for a given debris mass bin and object type)

control volume, which has dimensions of geocentric radius, declination, right ascension and mass. The matrix may be appended as a snapshot to the Flux Evolution Model file, and also utilised in the next cycle during the collision event prediction process. The timestep cycle is then repeated until the final simulation epoch has been reached.

3.2.2 Population Representation

The evolving debris population in IDES has a split representation. Objects greater than 10 cm in size are individually given their own specific attributes, such as an identifier, classification code, orbital elements, mass and area, beginning of life (BOL) epoch, and end of life (EOL) epoch. The small-size debris population is represented by a Population Orbit Matrix, which has the five dimensions of perigee radius, eccentricity, inclination, particle mass, and object type. The matrix contains five-dimensional bins, which are defined by the intervals of the respective dimensions. Each bin stores the number of objects within its particular parameter space. This structure can be seen in Figure 3-2. It has the flexibility to add large numbers of objects as small as 10 microns to the population from discrete breakup events, and more continuous sources such as paint flaking. The representation is similar to

that used by Madler[70], who had mass and size as matrix dimensions, instead of mass and object type. An earlier version of this type of matrix was employed by Rossi *et al*[10] for the SDM/STAT model. The STAT program binned the population by semi-major axis, eccentricity, and mass.

It was necessary to have an object type dimension because the sodium-potassium (NaK) reactor coolant droplet population could not be readily combined with the breakup fragment population in the same Population Orbit Matrix. This is because NaK droplets have a lower material density compared to breakup fragments, and therefore higher area-to-mass ratios, leading to larger atmospheric drag perturbations. Simply adding them to the evolving matrix for the fragment population would have created a false orbital decay profile because the size dependent area-to-mass relationship for breakup fragments would have been applied to the NaK droplet population. By adding an extra object type dimension for the matrix, it becomes possible to separate the breakup fragment population and the NaK droplet population, and therefore apply the correct area-to-mass relationships to each.

3.3 Orbital Debris Sources

3.3.1 Launch Traffic

Historical Launch Event Database

Under contract to DERA, Space Flight Data Applications (SFDA) have supplied a comprehensive historical launch database for use in the IDES model. The database contains data on over 16,000 objects associated with every launch into Earth orbit from Sputnik 1 in 1957 through to 31st March 1998. Each object in the database has the following data: beginning-of-life (BOL) epoch, COSPAR identifier, object classification code, orbital elements at BOL, dry mass, mean cross-sectional area, end-of-life (EOL) epoch, and air drag coefficient. The drag coefficient is set to 0 for operational satellites, simulating the compensation for the effects of air drag, and 2.2 for debris objects, leaving these uncontrolled objects subject to natural orbital decay due to air drag. Each object in the database is classified as belonging to one of 410 different identified families of objects. These object families (or classes) have 9-digit codes, which are constructed from the sub-codes of nationality, orbit type, object type, and family name (or mission type *and* mass range as in the case of payloads). Object types include payloads, launch vehicle upper stages

and final stages, payload mission related objects (e.g. boost motors) and launch vehicle mission related objects (e.g. upper stage shrouds and payload adapter rings). Orbital elements are obtained from the archives of USSPACECOM two-line element (TLE) sets or from the RAE Table of Earth Satellites.

The historical launch event database has enabled the introduction of launch-related objects into the evolving space object population with their correct initial conditions intact. Thus the model can 'predict' the complete LEO debris environment at any date in the past, and it also allows the capability to simulate the build-up of other debris sources that are associated with the launch-related objects in the modelled population. These sources include paint flakes delaminated from the painted surfaces of many payloads and upper stages in orbit by either meteoroid/debris impacts or natural surface degradation (although these sources are not yet included in the model).

In total there are 2522 objects associated with launches between 31/3/1990 and 31/3/1998 in the database. Of these, the database contains orbital data on 863 payloads, 313 payload operational debris objects, 798 rocket bodies, and 445 rocket body operational debris objects. A further 103 operational debris objects in the database have unknown orbital data. The distributions of payloads, payload operational debris, rocket bodies, and rocket body operational debris over semi-major axis versus eccentricity, and eccentricity versus orbital inclination can be seen in Figure 3-3 to Figure 3-6.

In Figure 3-3, there are three discrete clusters of payloads in the semi-major axis range at eccentricities of less than 0.1. These correspond to the near-circular low Earth orbits (LEOs), semi-synchronous medium Earth orbits (MEOs), and geosynchronous Earth orbits (GEOs). There are also some payloads with higher eccentricities (>0.6) which correspond to geosynchronous transfer orbits (GTOs) and the so-called Molniya orbits used by the Commonwealth of Independent States (CIS) and Russia. In the inclination range, there are many clusters of payloads with eccentricities below 0.1. These correspond to launches into geosynchronous Earth orbit (0°), launches from the Kennedy Space Center (28.5°), GPS/GLONASS global navigation satellites in semi-synchronous orbit (55°), mainly low altitude Russian military satellite launches from Plesetsk (63°, 70° and 82°), polar weather satellites (90°), and near-polar remote-sensing satellites (82° and 98°). At higher

eccentricities (0.6 to 0.75), there are clusters corresponding to GTO payloads mainly launched from Kourou (7°) and the Kennedy Space Center (28.5°), and payloads in Molniya orbits near the critical inclination of 63.4°.

For payload operational debris, Figure 3-4 shows a similar orbit distribution to the payloads themselves in terms of the location of clusters of the objects. This is not surprising, considering that most mission-related objects are released with low velocity relative to the spacecraft. Therefore, they would have similar initial values of semi-major axis, eccentricity and inclination. Also, payloads with a beginning-of-life orbit in either semi-synchronous or geosynchronous orbit may release operational debris in their highly eccentric transfer orbits. However, there are orbit regimes where payload operational debris appears to be very sparse. This is evident in the semi-synchronous orbit (~26000 km semi-major axis, eccentricity <0.01), geosynchronous orbit and in the ~63° inclination, high eccentricity Molniya orbit. There may be more payload operational debris (e.g. lens covers, clamp bands) in these orbits, but they are too small at high altitude or in a region of poor coverage to be tracked by the USSPACECOM Space Surveillance Network (SSN). Also, at eccentricities less than 0.1, the inclination distribution is much less populated compared to the payloads themselves. This is probably because not all payloads release objects after separation from the rocket body or during mission operations. In addition, the probable time of release is just after separation from the rocket body, in a low altitude, near-circular parking orbit and not in the higher altitude transfer or operational orbits.

Figure 3-5 shows that the orbital distribution of rocket bodies is very similar to the associated payloads in Figure 3-3. The same characteristics are displayed because the launch vehicles are designed to deliver their payloads as close to the operational or parking orbit as possible, in order to minimise the fuel for operational orbit acquisition. There are many more rocket bodies in highly eccentric orbits than payloads, mainly because these are used as transfer orbits with an apogee close to GEO. Most launchers use transfer stages (e.g. H10 on Ariane 44L), leaving the spacecraft to make a circularising burn. Also, highly eccentric orbits are not popular with spacecraft operators due to the transit through the harsh electron and proton radiation belts.

The operational debris object orbits associated with these rocket bodies are presented in Figure 3-6. The semi-major axis versus eccentricity distribution of this object type is very similar to that of the rocket bodies up to a semi-major axis of 25,000 km. At higher semi-major axis values, the figure shows a distinct lack of rocket body operational debris. This is especially the case in GEO where quite a number of rocket bodies have been abandoned. This is also evident in the eccentricity versus inclination distribution where there is no cluster of objects near 0° inclination, zero eccentricity. This is because these objects are smaller than 1 metre in diameter and therefore below the tracking threshold of the SSN at GEO altitudes. Additionally, there are no rocket body operational debris objects with orbits of around 18 to 28° inclination and an eccentricity of 0.74. However, there are many rocket bodies left in this orbit regime. It is known that the SSN has particular difficulty in tracking smaller (10 to 50 cm diameter) objects in these types of high eccentricity, low inclination orbit. There is a cluster of objects with orbits of 0.72 eccentricity and inclination between 45 and 47° inclination. These are associated with the Proton K rocket launches from Baikonur, Kazakstan. They are Proton K Block DM ullage motors mainly associated with the deployment of the Russian Gorizont communications spacecraft into GEO.

Finally, the mass distributions of the 4 major types of launch-related objects are displayed in Figure 3-7. Payloads are distributed throughout the mass classes up to 10,000 kg. In recent years, with advancing technology, there has been a trend towards smaller spacecraft in LEO and GTO with mass in the sub-100 and 100 to 500 kg mass classes. Indeed, small launch vehicles are being developed to cater for this growing industry. There has also been a trend towards heavier payloads with very large masses of the 5000 to 10,000 kg class. These are communications spacecraft launched into the GEO region. This trend is likely to continue in the future with rising regional demand in the commercial communications sector. Conventional launch vehicles are manufactured in multiple stages, and most upper stages left in orbit are concentrated in the 1500 to 2500 kg and 2500 to 5000 kg mass classes. However, there are a number of rocket bodies with smaller masses and these are mainly transfer stages for payload deployment in GEO and also the final stages of some of the smaller launch vehicles (e.g. Pegasus, Scout and Tsyklon). Payload and rocket body operational debris objects have masses concentrated in the sub-100 kg mass class. This not surprising considering the different operational debris types ranging from solar array latches and explosive bolts to spacecraft adapters, upper stage shrouds, and inter-stage casings.

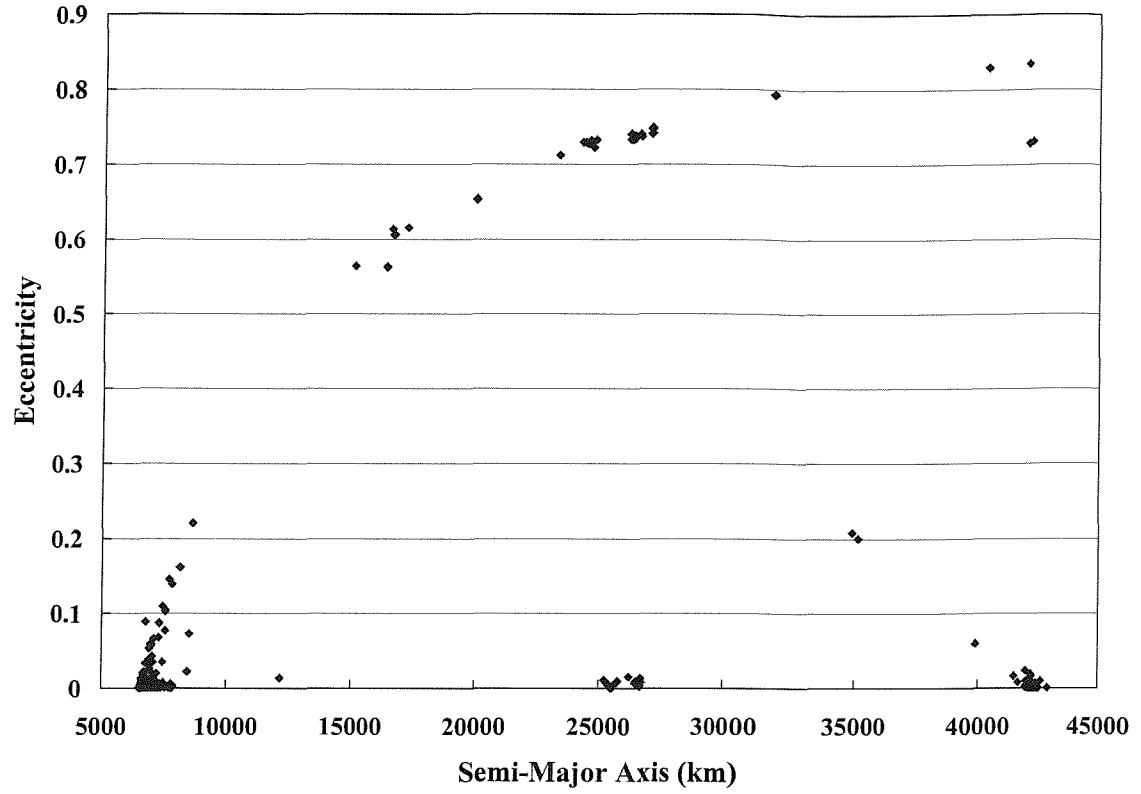

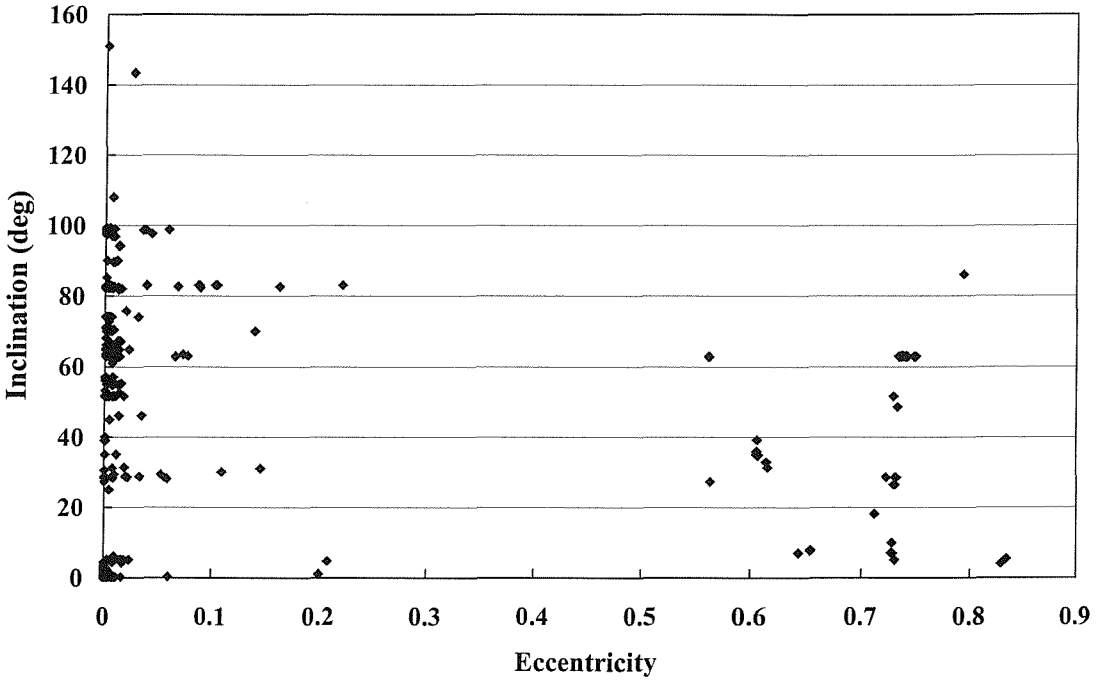

Figure 3-3: Orbital distributions of payloads launched between 1990 and 1998

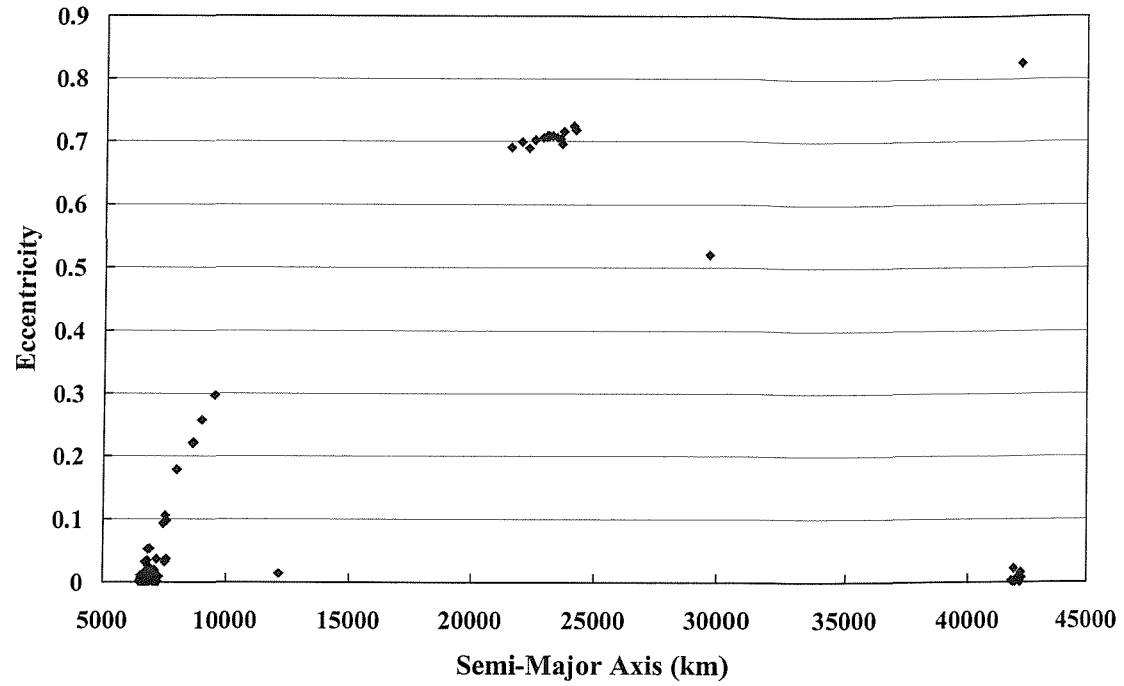

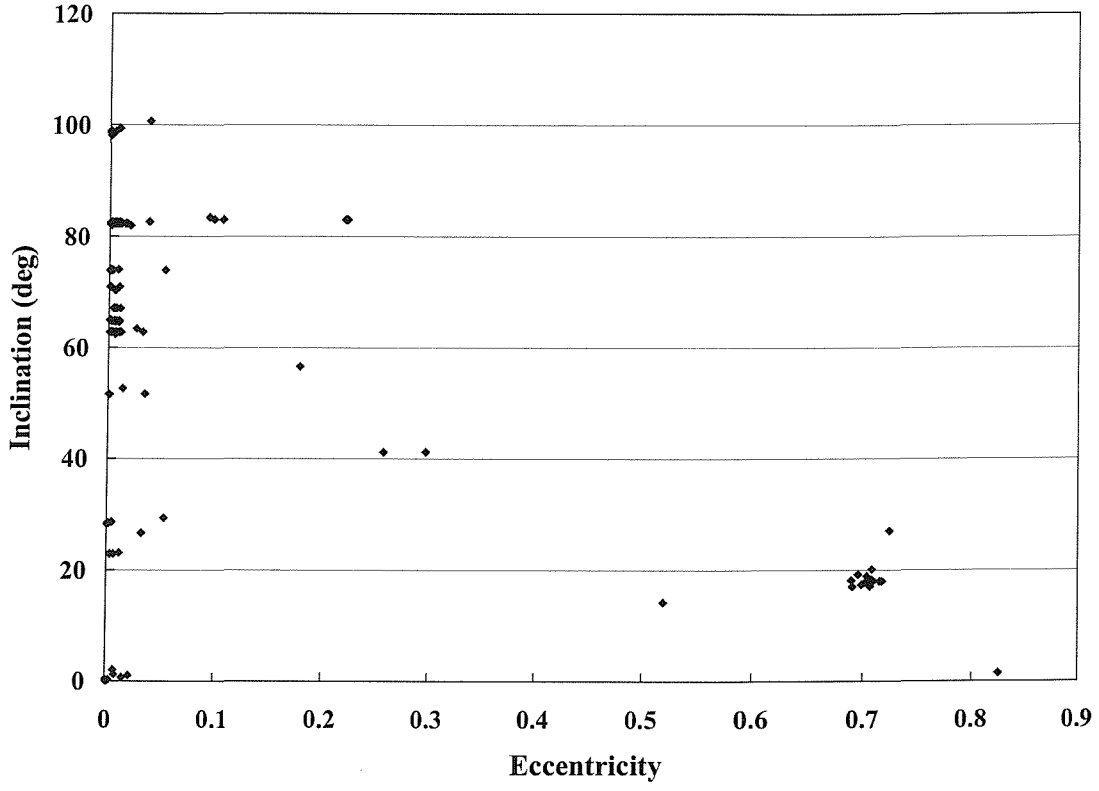

Figure 3-4: Orbital distributions of payload operational debris launched between 1990 and 1998

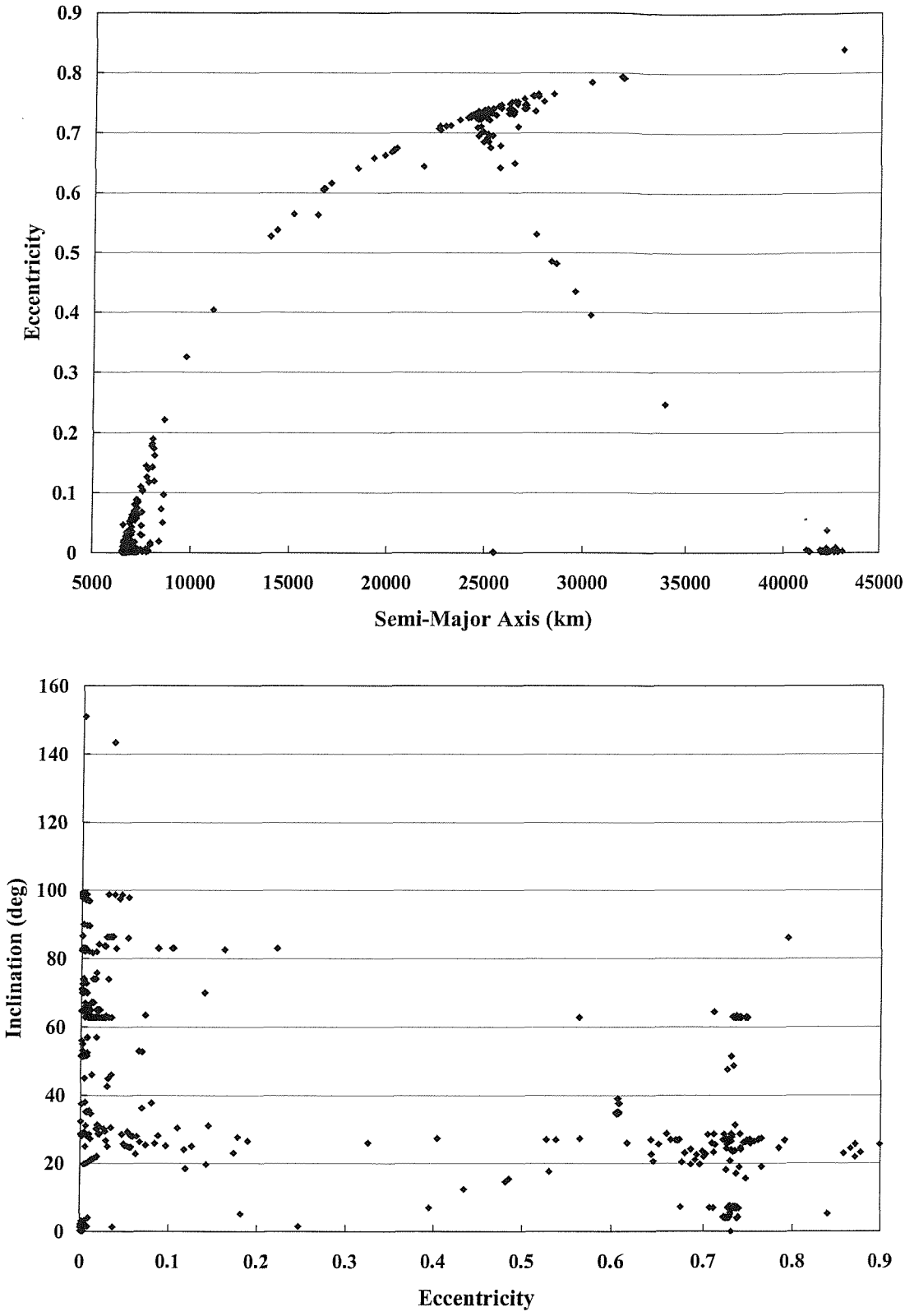

Figure 3-5: Orbital distributions of rocket bodies launched between 1990 and 1998

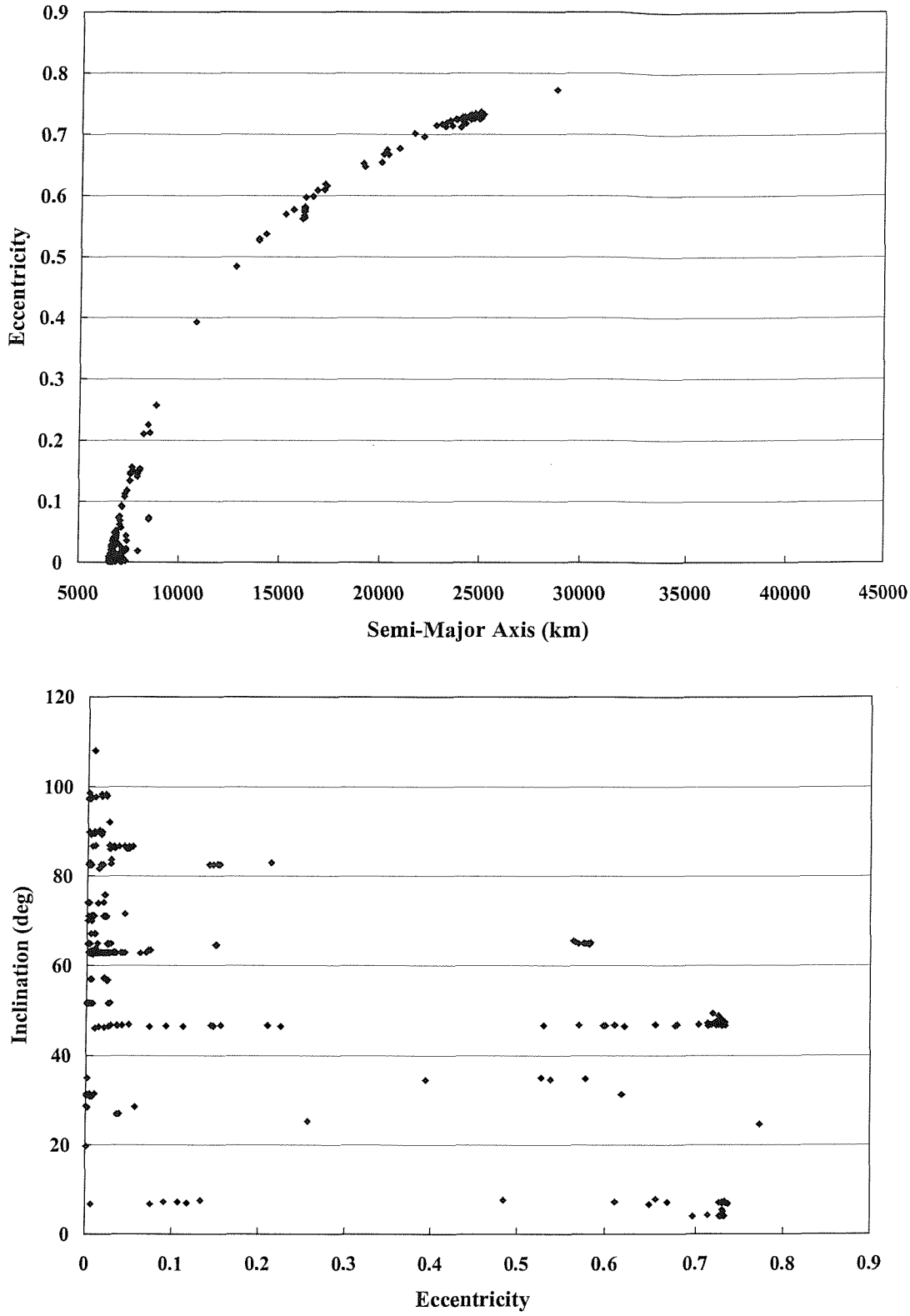

Figure 3-6: Orbital distributions of rocket body operational debris launched between 1990 and 1998

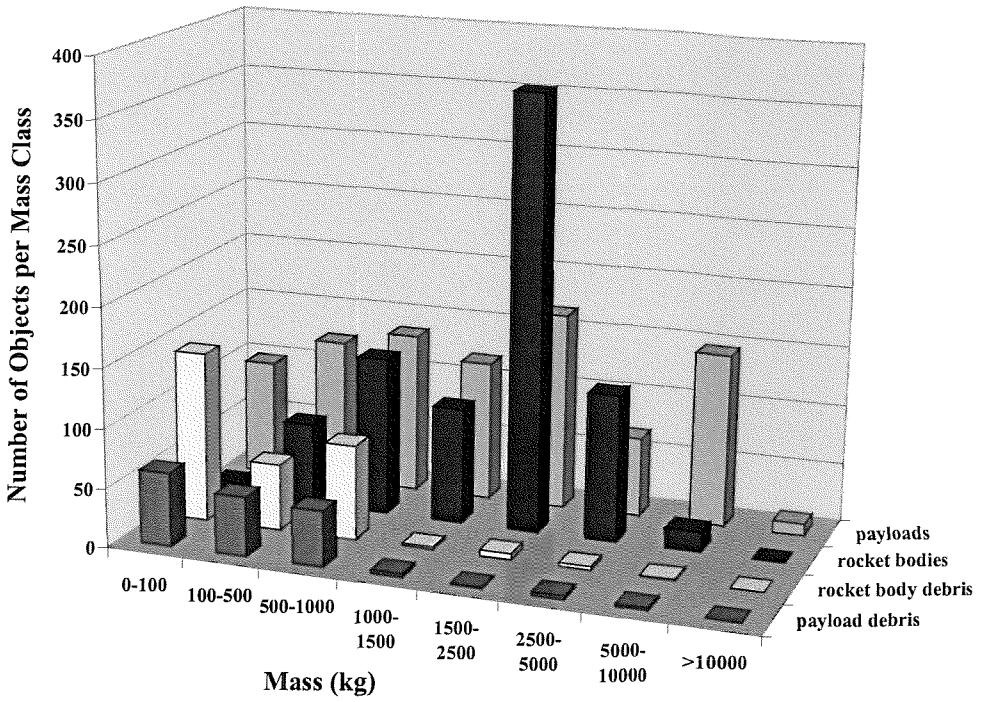

Figure 3-7: Mass distribution of various categories of launch-related objects deposited from 1990 to 1998

Future Launch Traffic Database

The assignment of the 9-digit classification code to each launch-related object in the historical launch event database has enabled a high level of detail to be attained in the IDES future launch traffic database. The object classification code, initial orbital element, mass and area data assigned to the last 8 years of launch-related objects in the historical launch event database have been analysed in order to derive a high fidelity future launch traffic model. This comprises representative data on each of the object classes. The representative data derived for each object class includes orbit, mass, and cross-sectional area. Also as part of this analysis, a relational database has been constructed that establishes links between object classes. This 'object-oriented' approach enables the launch vehicle upper stage and operational debris objects that are historically associated with the launch of a given payload to be added to the evolving IDES population at the same time as the payload. In fact, the future launch traffic database consists of three data files, described in Table 3-1. These data files define the payload class launch rates, associations between the payload classes and other object classes, and the summary orbit/mass data on each of the 410 object classes.

File name	Description
PAYLOAD.DAT	for each payload class code launching between 1990 and 1998: -mean launch rate (per year) -mean number of payloads per launch -mean operational lifetime (years)
ASSOC.DAT	for each payload class code launching between 1990 and 1998: -associated object class code -mean number of objects per launch for the associated object class -fraction/share of associated payload class launch rate (if associated object class is a launch vehicle upper stage class)
CLASS.DAT	for each object class code launching between 1990 and 1998: -representative (mean) semi-major axis (km) -representative (mean) eccentricity -representative (mean) inclination (deg) -representative mass (kg) -representative mean geometric cross-sectional area (m^2) -lethality ratio (J/g) of the object class (default of 40 J/g)

Table 3-1: Description of the future launch traffic data files

Examples of each of these files can be found in Appendix A. The relational database aspects of this approach enable a realistic replication of launch-related object patterns into the long-term future. The other main strength of the approach is the replication of the historical orbit and mass distribution of launch-related objects. Figure 3-8 shows the semi-major axis versus eccentricity and eccentricity versus inclination distribution of all object classes in the future launch traffic model. With the high-resolution classification scheme used, a total of 410 different object classes have been identified from the historical launch data of the last 8 years and used to generate future launch-related objects. It is clear that if one represents the individual historical object orbit distribution from Figure 3-3 to Figure 3-6 in one plot, then the orbit distributions of the future launch traffic database in Figure 3-8 show a very strong correlation. The future traffic database distributions display the clusters manifested in the historical data, and exhibit a realistic scattering around those clusters. All key orbit regimes are well represented, such as near-circular LEO, MEO, and GEO, and also high eccentricity GTO and Molniya orbits. It is evident from the eccentricity-inclination plot, that the future launch traffic database accounts for all the key features of the historical launch data, including the clusters within specific inclinations bands and the scatter in the eccentricity range.

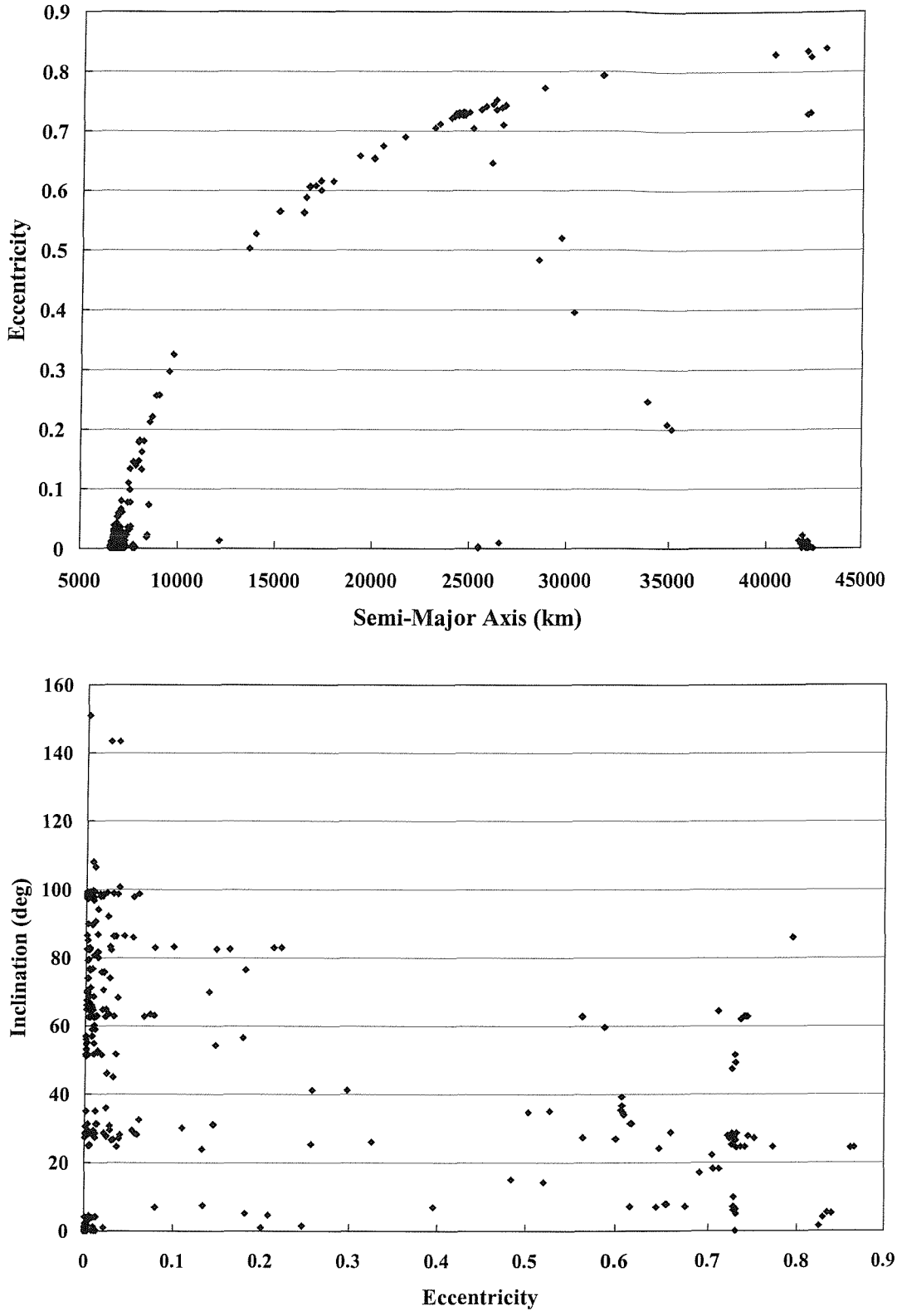

Figure 3-8: Orbital distributions of all object classes in the future launch traffic model

Due to the fact that the future launch traffic database has been derived from historical launch activity of the past 8 years (including the launch rates), it represents a 'Business As Usual' future launch traffic scenario. Overall, the model will predict an average of approximately 330 launch-related objects per year to be added to the long-term projections in IDES. This corresponds to a mean overall launch rate of 89 per year from 226 different payload classes, covering the entire Earth orbit regime. The relational database file (ASSOC.DAT) contains 475 different associations between payload classes and other debris object classes such as launch vehicle upper/final stages, launch vehicle operational debris, and payload operational debris. Note that the launches of the Mir space station supply spacecraft, the Space Shuttle, and constellations such as Iridium, Globalstar and Orbcomm have been filtered out of the analysis and are not included in the future launch traffic database.

Statistical Prediction of Future Launch Events

The three files of the future launch traffic database are utilised in order to predict specific launch events and their associated objects for the long-term evolution simulation. IDES uses a separate software pre-processing program for future launch event modelling. The output of this program is a launch manifest containing the launch data of each launch-related object to add to the evolving debris population within IDES at the predicted time. This launch data includes deployment epoch, classification code, initial orbital elements, mass, area etc.

The PAYLOAD.DAT file is the driving influence in the predictive process. Just as the main environment evolution program in IDES steps forward in user-defined time intervals, the future launch event program assumes the same progressive approach. For each timestep in the simulation, the pre-processor takes the launch rate of each payload class in the file and interrogates the ASSOC.DAT file to find any associations of that payload class with a launch vehicle upper stage class.

For each association of the payload class with an upper stage class, the model calculates the launch rate by multiplying the overall payload class launch rate by the launch rate fraction of the association. In other words, launch event prediction is based on the launch rate of the payload-upper stage combination over a single timestep duration. The predicted number of

events for that payload-upper stage combination is statistically derived using a Poisson distribution from n = 0 to N events, to obtain N event probabilities, P_n, given by

$$P_n = \frac{\lambda^n}{n!} e^{-\lambda} \tag{3-1}$$

where λ = mean launch rate (per year) × timestep interval (years).

Values of P_n are accumulated to give an overall probability, P_N, and then each event probability is normalised by this value. All normalised event probabilities lie in the range of 0 to 1. A high precision uniform random number is generated and the predicted number of events corresponds to the maximum normalised event probability that has been exceeded by this random number.

If a launch (or a number of launches) is predicted for the payload-upper stage combination for the given timestep, then the average number of objects for the payload class, upper stage class, and associated payload/upper stage operational debris classes are added to the launch manifest. All these objects will be assigned semi-major axis, eccentricity, inclination, mass and area values based on their respective classification code summary data contained in the CLASS.DAT file. In fact, the semi-major axis for each predicted object is slightly randomised in a ± 20 km range centred around the mean value given in CLASS.DAT. Right ascension of ascending node and argument of perigee values are randomly derived in the 0 to 360° range for each predicted object. All objects associated with the predicted launch event assume the same beginning-of-life epoch, which is randomly obtained in the range between epoch t and epoch $t+\Delta t$ of the timestep. All payload objects associated with the predicted launch event are given an end-of-life epoch, based on the beginning-of-life epoch and mean operational lifetime value given for the payload classification code in the PAYLOAD.DAT file. For flexibility, the IDES user is able to specify a future launch profile whereby the 'Business As Usual' launch rates for any year can be scaled up or down by a user-defined launch rate scaling factor.

Satellite Constellation Launch Traffic

A review of LEO satellite constellation proposals has been conducted, and a database of realistic constellation designs has been defined. Only five out of the fifteen proposals appear

to have received anywhere near the necessary financial investment in order to design, manufacture, launch, test and operate a complete system. Design data, such as semi-major axis, eccentricity, inclination, mass and area of the constellation satellites can be seen in the constellation launch database, given in Table 3-2. Estimated system start dates are also specified.

Start Date	Name	Sats	Planes	Sats/ plane	SMA (km)	ECC	INC (°)	Mass (kg)	Area (m^2)
1/11/1998	Iridium	72	6	12	7158	0	86.4	689	4.3
1/1/2002	Teledesic	324	12	27	7753	0	84.7	1400	12
1/12/1999	Globalstar	48	8	6	7792	0	52	450	10
1/6/2002	Skybridge	80	8	5	7847	0	55	800	12
31/11/1998	Orbcomm	28	4	7	7203	0	45	42	9.6

Table 3-2: Default satellite constellation traffic database

In order to add constellation satellites to the future launch manifest generated by the future launch traffic model, a constellation pre-processor takes each constellation design in the database and produces individual constellation satellite data from the design values given. The orbit of each satellite in the constellation assumes the same semi-major axis, eccentricity and inclination as given for the whole constellation, but the right ascension of ascending node and argument of perigee values are determined by consideration of the Walker-type constellation phasing method[71]. This is still the most popular constellation design methodology used in today's planned constellation systems. The orbital planes of the constellation are distributed evenly in right ascension of ascending node between 0 and 360°. The argument of perigee values of the orbit planes are staggered by an angle equal to 360° divided by the total number of satellites in the constellation.

Once all constellation-related object launch data have been produced by the constellation pre-processor, they are merged in the chronological order into the launch event manifest containing the background launch-related objects. The launch event manifest is then ready to be used by the IDES main environment evolution program at the designated time in the simulation.

3.3.2 Fragmentations

Up to 31st March 1998 there have been a total of 149 recorded breakup events that have contributed a large proportion to the debris population. The ability to model a varied number of different fragmentation scenarios with good accuracy must therefore be a vital part of any debris environment model. The main goal of a breakup model is to reproduce the mass distribution of an event and its resulting debris cloud. Orbital dynamics can then be applied to all debris clouds to predict the current state of the population. There are a wide range of causes for breakups, but the events can be classified into three main categories: low intensity explosions (mostly from propulsion-related accidents or electrical faults); high intensity explosions (mostly from deliberate or accidental detonations of spacecraft); and catastrophic collisions. For each of these breakup categories, debris models tend to use different distributions for the cumulative number of fragments versus fragment mass and for the velocity imparted to fragments according to their size. Low intensity explosions are assumed to generate many large-size, trackable fragments and very few smaller debris objects. In contrast, high intensity explosions and collisions are usually assumed to generate less large-size fragments, but many thousands of sub-decimetre sized debris objects. In addition to this, satellites and other large objects such as rocket bodies may be damaged by hypervelocity impacts with debris. These damaging impacts do not have enough energy to totally fragment the object, but instead have a cratering effect that ejects secondary fragments from the crater area. All these event types are modelled in IDES.

The modelling process determines the physical properties of each fragment (e.g. mass, size, area), the velocity imparted to each fragment as the structure breaks apart, and the resulting orbit. Some breakup models have many degrees of freedom to enable the mass spectra to fit the tracked fragments from each of the historical fragmentation events. However, for the purposes of simulating future breakup events, IDES uses a more generalised set of relationships that only require information on the orbit and mass of the breakup object. If the event is a collision, then the mass and velocity of the impactor are also required. The following relationships have been selected on the basis that they are supported by deterministic data and comply with normal physical laws (i.e. mass and energy conservation).

Debris Fragment Mass to Size/Area Relationship

Fragment mass, M (kg), can be related to size, d (m), and area, A_{eff} (m^2), by

$$M = \begin{cases} 46.81 d^{2.26} & \text{if } d > 0.0062 \text{ m}, \\ 2094 d^{3} & \text{if } d \le 0.0062 \text{ m}, \end{cases} \tag{3-2}$$

$$M = \begin{cases} 61.5 A_{eff}^{1.13} & \text{if } A_{eff} > 3.0 \times 10^{-5} \text{ m}^2, \\ 3009 A_{eff}^{1.5} & \text{if } A_{eff} \le 3.0 \times 10^{-5} \text{ m}^2. \end{cases} \tag{3-3}$$

These relationships were derived from the size-dependent debris material density defined in ref. 72.

Fragments of common mass have a spreading about the effective area, which is modelled by sampling the actual object area from a statistical log-normal distribution with a standard deviation of 0.8 with respect to the mean or effective area, A_{eff}, as recommended by Jehn[73].

Debris Fragment Mass Distribution

The cumulative number of fragments, CN, greater than mass, m (kg), are given for the different breakup scenarios listed below. For low intensity explosions, we have[47]

$$CN = \begin{cases} 171 \exp\left(-0.6514\sqrt{m\, f_m}\right) & \text{for } m \ge 1.936 kg / f_m, \\ 869 \exp\left(-1.8215\sqrt{m\, f_m}\right) & \text{for } m < 1.936 kg / f_m, \end{cases} \tag{3-4}$$

where f_m is the ratio of 1000 kg over the breakup mass, M_t (kg).

The coefficients were chosen to ensure mass conservation. Figure 3-9 shows the mass spectrum of the breakup of a 1000 kg object caused by a low intensity explosion, using the above relationship. The majority of the fragments have masses that centre around approximately 0.1 kg. The split exponential law applied to events of this type is clearly visible at 1.9 kg. There are very few small size fragments predicted for low intensity explosions.

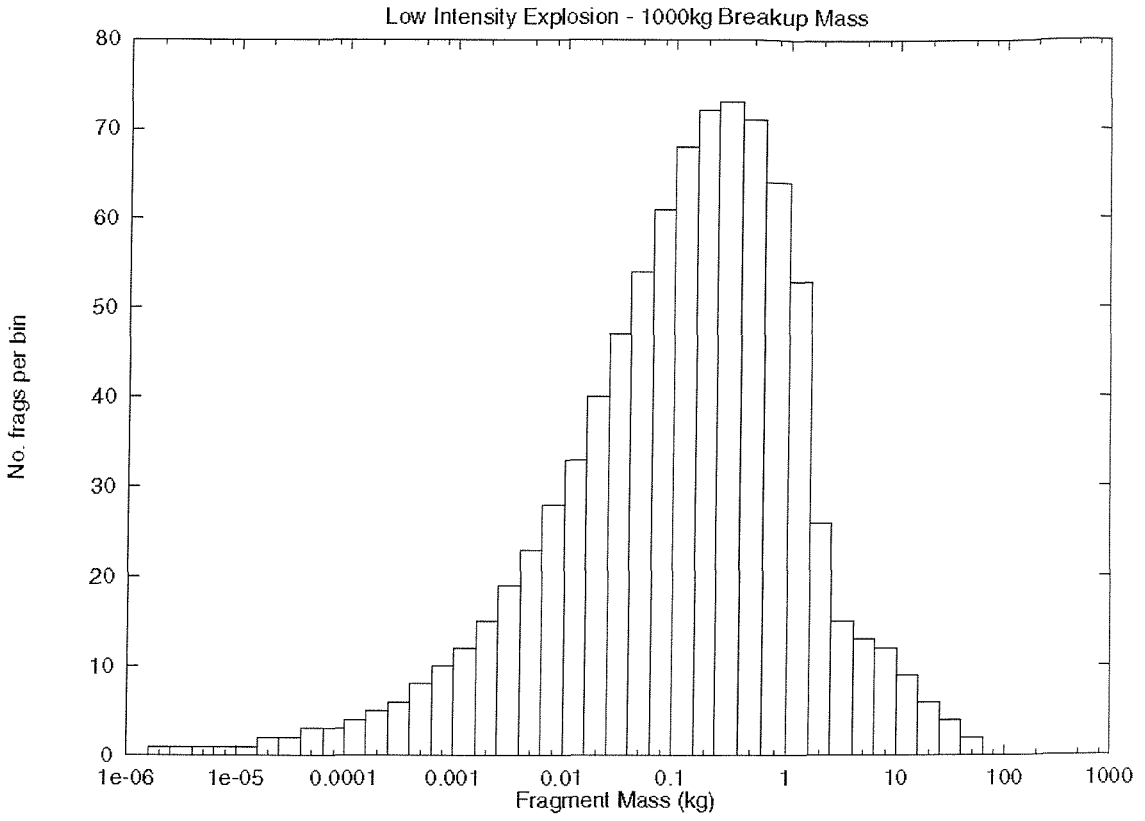

Figure 3-9: Mass spectrum for a low intensity explosion

For high intensity explosions, we have two distributions in the mass range, defined by

$$CN = \begin{cases} 171 \exp\left(-0.6514\sqrt{m\, f_m}\right) & for\ m \geq 1.936 kg / f_m\ , \\ 869 \exp\left(-1.8215\sqrt{m\, f_m}\right) & for\ m < 1.936 kg / f_m\ , \\ \quad + & \\ 0.331\left(\dfrac{m}{0.5\, M_t}\right)^{-0.78} & . \end{cases} \tag{3-5}$$

For this type of explosion, we assume that 50% of the breakup mass follows the low intensity exponential law (upper equation), and 50% of the breakup mass follows the power law (lower equation). In the case of the low intensity portion, f_m is the ratio of 1000 kg over 50% of the breakup mass, M_t. The power law coefficients are derived from the maximum power measured in the SOCIT series of ground tests summarised by McKnight *et al*[74]. In reality, it is not known exactly what the split is between power law and exponential law, since the ground test data for this type of event is very sparse. A 50/50 split has been assumed here, in order to limit the number of large-size debris coming from the exponential

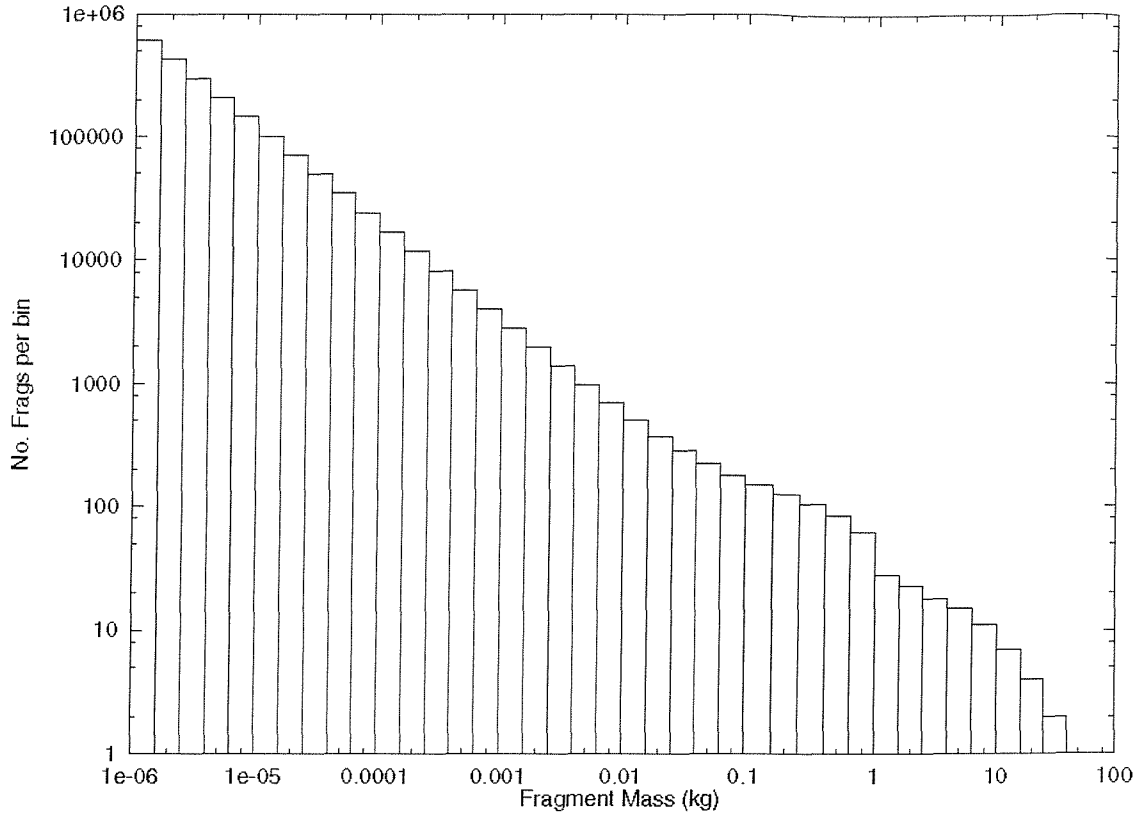

Figure 3-10: Mass Spectrum of a high intensity explosion (1000 kg breakup mass)

law and, more importantly, to maximise the number of small/medium-size fragments. Debris models tend to under-predict debris environment measurement data by up to an order of magnitude or more at sub-100 micron particle sizes, and this is a justifiable way of reducing the under-prediction, until non-fragmentation source models are mature enough to implement and can fill the 'under-prediction gap'. Figure 3-10 shows the mass distribution of the same breakup mass of 1000 kg resulting from a high intensity explosion event. Again, we can see the low intensity split exponential law at 1.9kg, but below 1kg the power law dominates the spectrum with over 600,000 fragments in the lowest mass bin of 1 mg.

For catastrophic collisions (EMR > 40 J/gram), we have[74]

$$CN = A\left(\frac{m}{M}\right)^{-B} \tag{3-6}$$

where

$$B = 0.60 + 0.18\,P\left[\frac{EMR - 40}{EMR}\right],\quad A = 1.6290 - 1.6636\,B\text{, and } M = M_t + M_p\ .$$

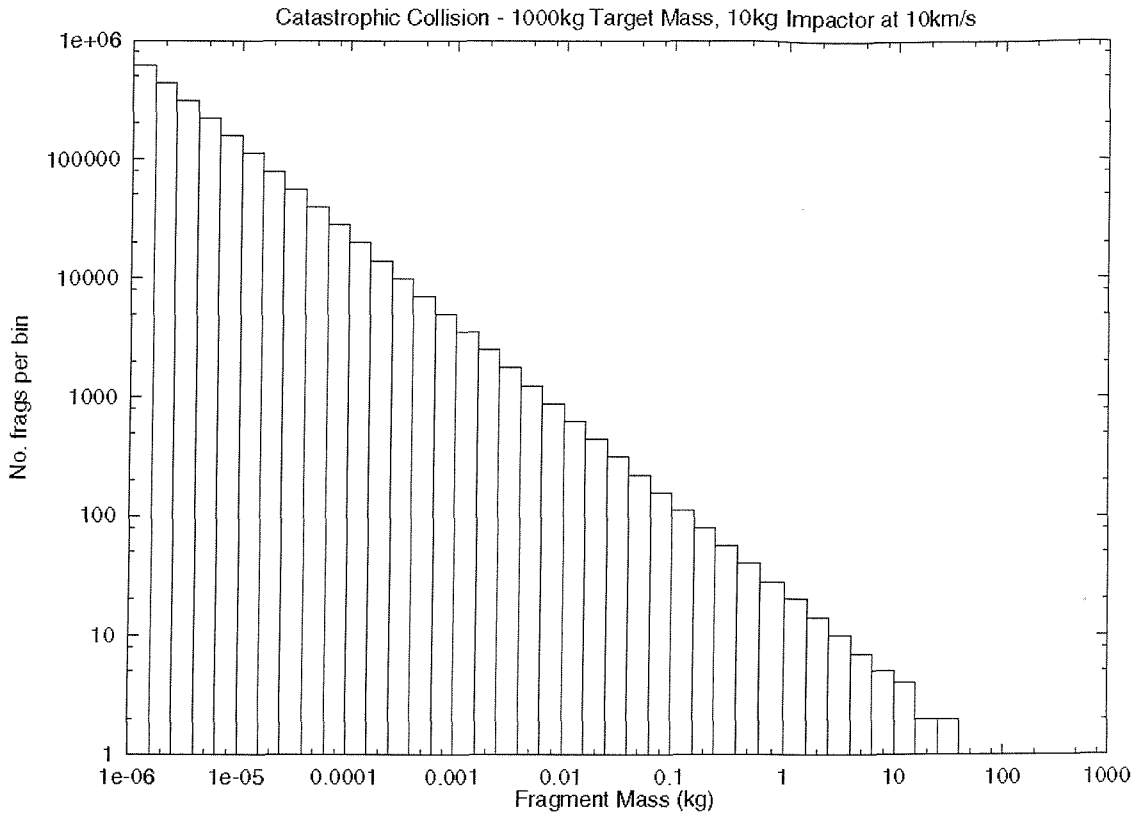

Figure 3-11: Mass spectrum for a catastrophic collision breakup

Here, *EMR* is the impactor kinetic energy-to-target mass ratio in joules per gram and P is the energy coupling coefficient. McKnight[74] recommends a value of 0.9 for this coefficient. M_p (kg) is the projectile mass, and M_t (kg) is the target mass prior to the collision. The coefficients have been chosen to ensure mass conservation. As we can see from Figure 3-11, the modelled mass spectrum of a catastrophic collision follows a pure power law approach with its gradient and scaling dependent upon the specific conditions relating to the impactor and target (and therefore the EMR value). For a 10 kg impactor colliding at 10 km/s with a 1000 kg target mass, the model produces very few large fragments and more than 500,000 fragments in the lowest mass bin of 1 mg.

For damaging collisions (EMR < 40 J/gram), we use[75]

$$CN = 0.4478\left(\frac{m}{M}\right)^{-0.7496}, \tag{3-7}$$

where

$$M = M_e + M_p, \text{ and } M_e = kM_p v^2 .$$

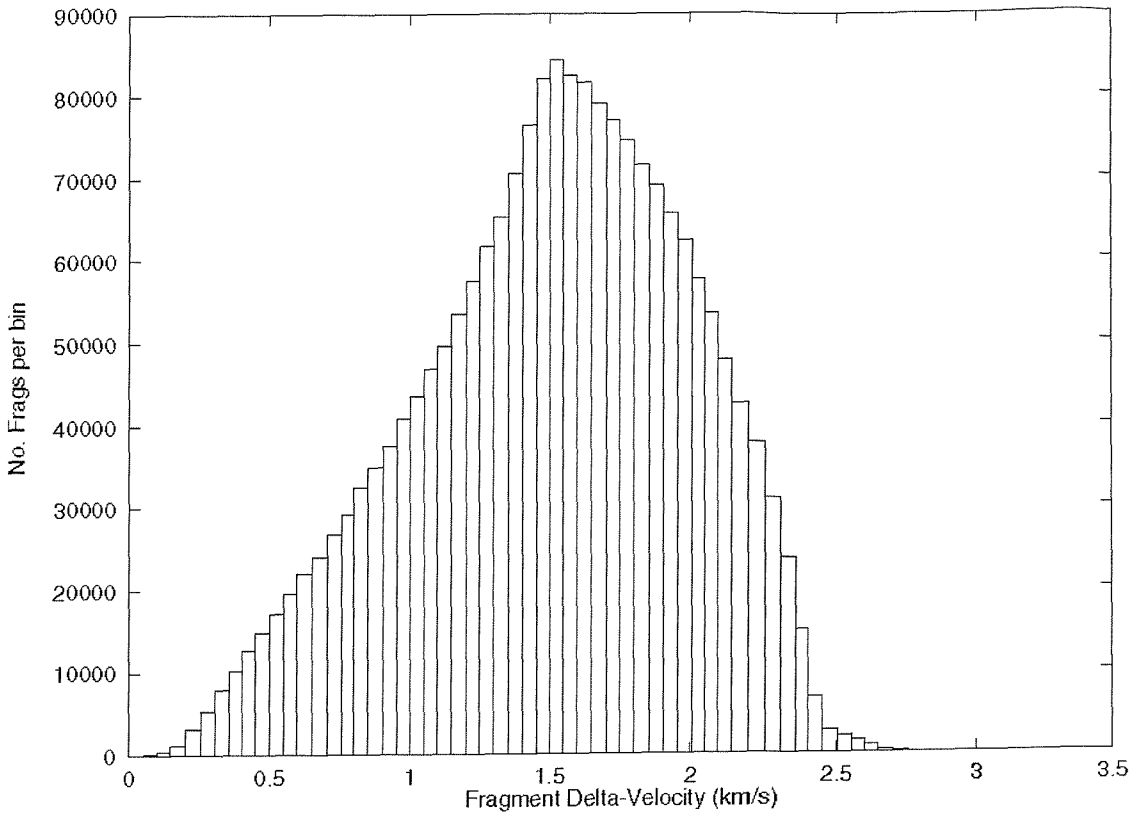

Figure 3-12: Fragment delta-velocity distribution for a high intensity explosion

Here, v is the relative impact velocity in km/s. k is a coefficient equal to 1 s^2/km^2. In order to account for a loss of mass from the target object, the residual target mass is found by debiting the total ejected mass, M_e (kg), from the original target mass, M_t (kg).

Debris Fragment Delta-Velocity Distribution

The delta-velocity, ΔV, imparted to a fragment of size, d, depends upon the type of breakup. For both low and high intensity explosions, we have[76]

$$\log_{10}\Delta V_{peak} = -0.0676(\log_{10} d)^2 - 0.804(\log_{10} d) - 1.514 \ , \tag{3-8}$$

where ΔV_{peak} is the characteristic delta-velocity in km/s and d is the debris size in m. The corresponding equation for collisions is given by[52]

$$\log_{10}(\Delta V_{peak}) = \begin{cases} 0.875 - 0.0676\left(\log\dfrac{d}{d_m}\right)^2 & for\ d > d_m \ , \\ 0.875 & for\ d \le d_m \ , \end{cases} \tag{3-9}$$

where

$$d_m = \frac{\sqrt[3]{E_p}}{c} \quad \text{and} \quad E_p = \frac{1}{2} M_p \, v^2 \ .$$

Here, ΔV_{peak} is the characteristic delta-velocity in km/s, d_m is the cut-off diameter in metres, c is a coefficient of value 8×10^8 $kg^{1/3}s^{-2/3}m^{-2/3}$, and v is the impact velocity (in m s^{-1}).

The above relationships determine characteristic or peak delta-velocities according to a particular fragment size/mass. The spreading of delta-velocity for fragments of a constant mass is modelled by a triangular spreading function[52]. This spreading effect is shown in Figure 3-12, which is derived from a high intensity explosion of a 1000 kg breakup mass. The minimum mass considered was 1 mg and the peak of 1.5 km/s corresponds to the characteristic imparted velocity at this minimum mass. The relationship used for collisions yields a similar peak in the fragment velocity distribution of 1.4 km/s for the same breakup mass of 1000 kg and an impactor of 10 kg colliding at 10 km/s. The actual delta-velocity for a particular fragment is derived by taking a random variant from this triangular distribution. All breakups simulated by IDES are assumed to be isotropic in terms of the direction of fragment ejection from the parent object centre of mass reference frame. Random ejection angles are selected for each fragment, and with the actual delta-velocity, these are used to compute the fragment's initial orbit.

An historical fragmentation database is used by IDES to model the known fragmentation events during the historical environment evolution process in order to predict the current debris environment. This database, shown fully in Appendix B, is mainly derived from the official Inter-Agency Debris Co-ordination Committee (IADC) breakup list and breakup notification details from the NASA Johnson Space Center.

Future Explosion Database

Taking the same approach to the future launch traffic model, the future explosion model employs constant or steady-state average event rates for the different object classes. Similarly, these event rates are derived from historical explosion activity occurring between 31st March 1990 and 31st March 1998 specified in the historical fragmentation database.

There are a total of 149 fragmentation events in the historical fragmentation database, but only events from the breakup of object 1990-081D onward have occurred within this time period.

In order to derive the future explosion database, the breakup object of each of the historical fragmentation events considered was assigned with its 9-digit classification code from the historical launch database. Firstly, all events were grouped into their classes by sorting by their classification code. However, the classes still required further sorting into sub-classes because, of course, objects of the same class may have several different groupings of common breakup semi-major axis, eccentricity, inclination and mass values. Therefore, sub-classes were derived by sorting the objects in a given object class by the common (or similar) values of these parameters.

Once collected into sub-classes, the semi-major axis, eccentricity, inclination and breakup mass fraction parameter values were averaged to derive the representative values for the sub-class. The explosion type and object mass parameter values are the same in each sub-class and so it is simple to take them as the representative values of each sub-class. Finally, the explosion rate of the sub-class was derived by counting the number of events in the sub-class and dividing by the 8-year time period. These representative parameters of each sub-class were then listed in a data file, along with the classification code and corresponding class description (from the object class database file CLASS.DAT), to produce the IDES future explosion database (see Appendix B).

Statistical Prediction of Future Explosion Events

The method used by IDES to predict future explosion events is the same as that used for predicting future launch events. Here, the future explosion software program considers each sub-class in the future explosion database file and predicts the number of explosion events of the sub-class occurring over each progressive timestep (e.g. every month) by utilising the Poisson distribution algorithm. The predicted number of events for that sub-class in the timestep is statistically derived using the Poisson distribution in equation (3-1) from n = 0 to N events, to obtain N event probabilities, P_n.

Values of P_n are accumulated to give an overall probability, P_N, and then each event probability is normalised by this value. All normalised event probabilities lie in the range from 0 to 1. A high precision uniform random number is generated and the predicted number of events corresponds to the maximum normalised event probability that has been exceeded by this random number. If one or more, explosion events are predicted for the sub-class for the given timestep, then its event parameters are taken from the sub-class entry in the future explosion database. The breakup epoch for an event is randomly derived between epoch t and epoch $t+\Delta t$ of the timestep. Also, right ascension of ascending node, argument of perigee and true anomaly of the breakup event are randomly derived in the 0 to 360° range. The semi-major axis and inclination for the breakup event are randomised in a ± 20 km range and 2° range respectively, centred around the mean values given in the database.

3.3.3 Nuclear Reactor Coolant Leakage

In 1997, Kessler *et al*[77] completed a comprehensive study of a previously unknown source of orbital debris. This analysis centred around a new debris object population first detected by the Haystack radar. The large population of objects were measured to be spherical in shape, of centimetric proportions, and with near-circular, 65° inclination orbits within the 800 to 1000 km altitude band. The narrow altitude band containing the new population was not consistent with the source being a fragmentation event or solid rocket motor burn. High ejection velocities associated with both of these event types tend to lead to a very wide dispersal of resulting debris in the altitude range. This new debris population had to be produced by a source process with low particle ejection velocities. A specific swarm of objects belonging to this population passed through the beam of the Goldstone radar during an observation campaign and could be correlated with the orbit of the Cosmos 1900 spacecraft, a Russian Radar Ocean Reconnaissance Satellite (RORSAT). RORSATs are powered by nuclear reactors with primary and secondary liquid metal coolant circuits, and were suspected to be leaking their sodium-potassium (NaK) coolant mixture. The source of this debris was confirmed, when a co-ordinated observation campaign between the Haystack, Millstone Hill, and Tradex radars, and the Firepond telescope, acquired and tracked 11 of the suspected NaK droplets[78]. The decay profiles of these tracked objects were analysed and were consistent with spherical objects with material densities near 1 g/cm^3, very close to that of the NaK liquid metal mixture.

The most likely source mechanism of liquid NaK droplets was postulated to occur during the routine ejection of the nuclear fuel rods of the RORSAT nuclear reactor, when the RORSAT reaches its nominal graveyard orbit at 950 km altitude. After the rods are ejected, it has been speculated that there is no valve to close the primary coolant circuit, thus allowing the liquid NaK coolant mixture to leak out of the thin-diameter primary coolant supply pipe. This leakage process may produce thousands of millimetre and centimetre-sized droplets, and possibly millions of very small vapour droplets at sub-millimetre sizes[59]. However, the only measurement data that allows us to infer the existence and magnitude of these very small droplets are two NaK craters found on the retrieved surfaces of the LDEF spacecraft[77]. Therefore, because of the lack of a more statistically reliable measurement dataset, and the fact that these very small vapour droplets will have decayed from orbit by now, we have only formed a model for the millimetre and centimetre-sized droplets. Most of these larger droplets will still be in orbit today and for many years to come because their evaporation times have been estimated to be much longer than their orbital lifetimes[79]. In order to model this phenomenon, a new source model has been developed here and will be improved upon when more measurement data on sub-millimetre sized droplets are obtained.

Droplet Mass-to-Size Relationship

Sodium-potassium liquid mixture has a material density of 900 kg/m^3. NaK droplets are assumed to be homogeneous in composition and spherical in shape, giving

$$m = 150\pi\, d^3 \quad \text{or} \quad d = \sqrt[3]{\frac{m}{150\pi}} \quad , \tag{3-10}$$

where m is the droplet mass (kg) and d is the droplet diameter (m).

Droplet Mass-to-Cross-Sectional Area Relationship

For a homogeneous sphere of material density 900 kg/m^3, the relationship between droplet mass and cross-sectional area is simply

$$A = 1.297 \times 10^{-2}\, m^{2/3} \quad \text{or} \quad m = 677\, A^{3/2} \quad , \tag{3-11}$$

where A is the droplet cross-sectional area (m^2).

Droplet Mass Distribution

In order to model the mass distribution of the NaK droplet population, the exponential law proposed by Bess[80] is used to achieve an empirical fit to the limited measurement data available. The exponential law can have a peak number of droplets (given the correct fit of coefficients) in the millimetre size range, near the detection size threshold of the most reliable measurement data (i.e. the Haystack radar), and it will generate very few sub-millimetre droplets. The Bess exponential law is defined by

$$CN = N_o \exp\left(-C\sqrt{m}\right) \tag{3-12}$$

where CN is the cumulative number of objects, m is the object mass in kg, N_o is the total number of objects in the distribution (an 'intensity' parameter) and C is the slope parameter. N_o and C are the distribution coefficients that must be derived so that the distribution fits as many measurement data points as possible (but at least one). The fitted distribution must also possess mass conservation, i.e. the sum of the droplet masses must equal the total mass of NaK coolant material released.

The measurement data available to estimate the NaK droplet population originates from Kessler *et al*[77], who estimated 78,400 droplets larger than 6 mm from Haystack radar data. Sridharan *et al*[78] identified at least 10 droplets larger than 3.4 cm in diameter from Haystack, Millstone, TRADEX radar and Firepond telescope tracking data.

To ensure mass conservation in the Bess exponential law, Jehn[81] has derived C from the constraint that the total mass of the objects should equal the total ejected mass, M_e (kg), by

$$C = \sqrt{\frac{2\left(N_o - \ln N_o - 1\right)}{M_e}} \tag{3-13}$$

This implies that C is dependent upon N_o and so the number-mass distribution has now only one degree of freedom, i.e. the variation in N_o to fit the measurement data.

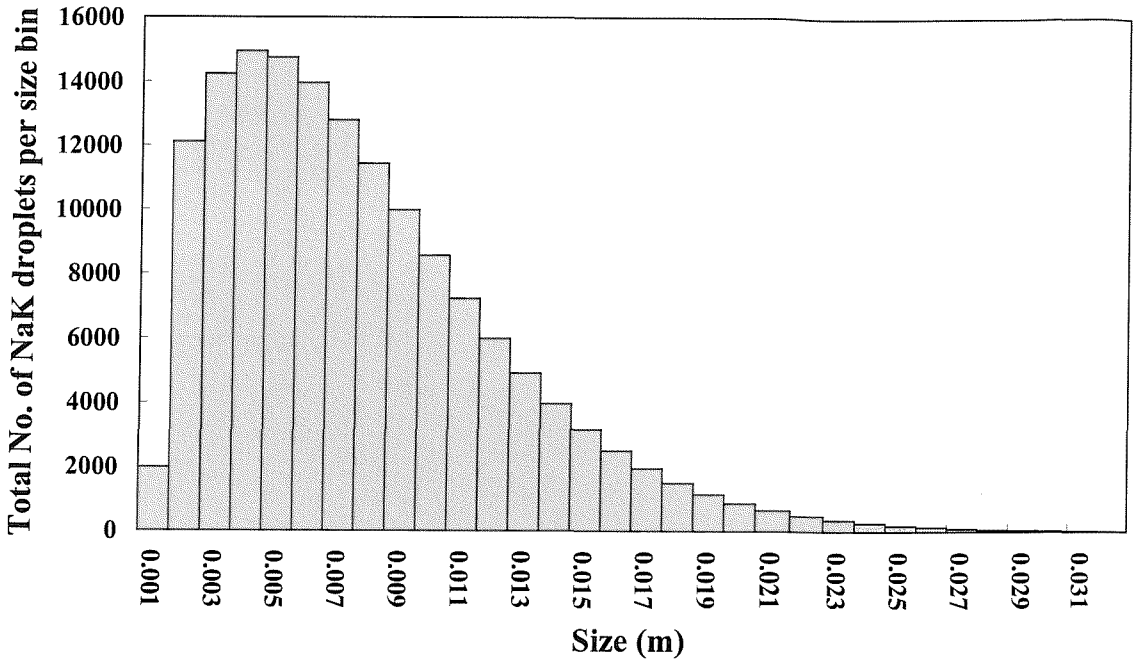

Figure 3-13: Exponential size spectrum of the total generated population of NaK coolant droplets as predicted by the new source model in IDES

Kessler *et al*[77] estimated the volume of NaK coolant released from the primary circuit during core ejection to be about 5 litres. Given that NaK has a mass density of 900 kg/m^3, 5 litres would have a mass of 4.5 kg. Although there have been over 30 RORSATs placed in a graveyard orbit between 850 and 1000 km altitude (except Cosmos 1900, which only reached a 695 km perigee by 763 km apogee orbit), the RORSATs up to Cosmos 954 did not eject their cores and therefore would not have released any NaK coolant by this mechanism. There have been 15 RORSAT core ejections between 850 and 1000 km altitude since Cosmos 954, which may have released a total NaK coolant mass of 67.5 kg. Hence, to derive a fit to the measurement data, a value of M_e = 67.5 kg has been chosen.

A fit of the Bess exponential law distribution to the most reliable measurement data point of Kessler (78,400 droplets > 6 mm between 750 and 1000 km altitude) gives N_o = 155,500 and C = 67.87. However, IDES needs to model the NaK droplets released by each event in order to obtain a realistic orbit and spatial density distribution of the NaK droplet population. Given that 155,500 droplets is the total number of droplets (N_o) between 750 and 1000 km predicted by this approach, then each of the 15 RORSAT core ejections in that altitude range is predicted to have released a total of 10,367 droplets (on average). This

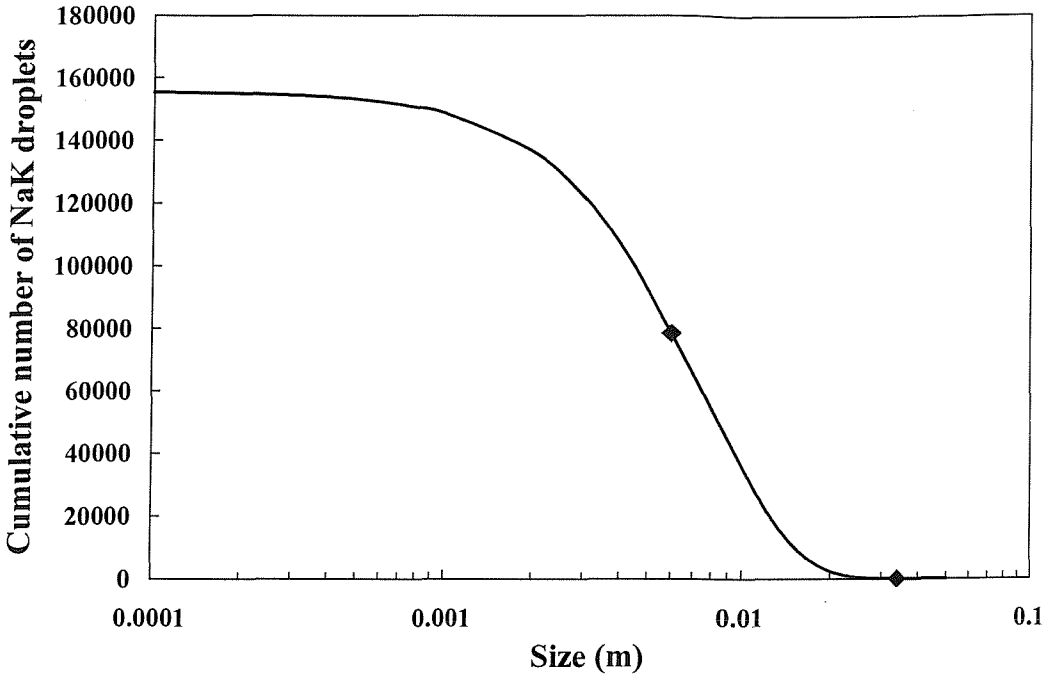

Figure 3-14: Cumulative size distribution of the total generated NaK droplet population as predicted by the new source model in IDES

gives the single core ejection event coefficients of N_o = 10,367 and C = 67.845. Therefore, the cumulative number-mass distribution for each core ejection event is derived as

$$CN = 10367\, e^{-67.845\sqrt{m}} \tag{3-14}$$

where CN is the number of NaK droplets per event greater than mass, m (kg).

Using equations (3-10) and (3-14), the modelled size distribution of the total NaK droplet population released into the orbital debris environment can be seen in Figure 3-13. As the exponential distribution shows, the peak number of droplets occurs at a droplet size of 4 mm, which is slightly below the detection size threshold of the Haystack radar of 6 mm at 850 to 1000 km range. As Figure 3-14 shows, the derived cumulative number-size distribution fits the Kessler data point of 78,400 droplets larger than 6 mm and produces 15 droplets larger than 3.4 cm, slightly higher than the 10 tracked droplets of the Sridharan data point. Below a droplet diameter of 4 mm, the distribution levels off to maximum of 155,000 droplets. The distribution gives approximately 34,000 NaK droplets released at sizes larger

than 1 cm. Since development and implementation of this NaK droplet mass distribution in IDES, additional measurement data from the Goldstone radar has been published by Matney *et al*[30]. This data has placed the number of NaK droplets with sizes between 2.5 and 6 mm at 500,000 which is somewhat higher than the maximum 155,000 droplets generated by the derived exponential law at these sizes. Therefore, it is planned to revise the NaK droplet mass distribution for IDES in order to fit this additional data and also extend the distribution down to 0.1 mm droplet sizes to account for the two NaK impact craters found on the LDEF spacecraft.

Delta-Velocity Distribution

According to Wiedemann[59], the velocity imparted to the larger droplets as they leak from the primary coolant supply pipe is independent of droplet size and very low (about 10 m/s). This is negligible compared to the RORSAT orbital velocity and therefore each droplet will essentially assume the graveyard orbit parameters of the RORSAT itself.

3.4 Orbital Debris Evolution

3.4.1 Orbit Propagation Techniques

IDES propagates the orbits of individual large objects with respect to atmospheric drag, geopotential gravity, luni-solar gravity and solar radiation pressure perturbations. The small object population is binned by its distribution over perigee radius, eccentricity, inclination, and mass. This matrix is evolved by a Monte Carlo technique, which randomly selects the orbits of 10 representative particles (each with a weighting factor representing a tenth of the number of real objects) from each orbit-mass bin (see Figure 3-2). Each representative particle's orbit is propagated with respect to geopotential gravity, atmospheric drag, luni-solar gravity, and solar radiation pressure perturbations over the timestep Δt. The particle (with its weighting factor) is then added to the orbit-mass bin to which it has migrated, corresponding to the propagated orbital elements of the particle at epoch $t+\Delta t$.

3.4.2 Long-Term Orbit Perturbations

During a long simulation run over many years, there are a large number of orbit calculations that need to be performed for the population. Clearly, it would be very computationally

intensive to consider the short-term variations of the orbital paths of all debris greater than 10 microns. Therefore, IDES uses a fast analytical, one-step orbit propagation method to determine the variations in an object's orbital elements due to the major perturbations over a time interval, Δt. The model determines rate of change in the object's orbital elements at the start of the integration step due to each perturbation component. In a linear technique, the orbital element rates of change are multiplied by the time interval Δt, to obtain the absolute changes in the orbital elements over the integration step. The absolute changes from each perturbation component are added together to give overall changes in the orbital elements. These include changes in the semi-major axis, Δa, eccentricity, Δe, inclination, Δi, argument of perigee, $\Delta\omega$, and right ascension of the ascending node, $\Delta\Omega$. New elements are finally derived by adding each change to the original value, e.g. $a_1 = a_0 + \Delta a$ for semi-major axis. The orbital element changes from each perturbation component are summarised in the following sections.

Geopotential Gravity

The geopotential gravity perturbation equations used in IDES are summarised by Roy[82]. The most important component of the geopotential perturbation is that due to the first order J_2 (second harmonic) secular variations over time, Δt. The orbital elements that are constantly varying periodically due to this component are the right ascension of the ascending node, Ω, and the argument of perigee, ω. These change according to

$$\overline{\Delta\Omega_{\text{sec}}} = -\frac{3}{2}\frac{J_2 R^2}{\left[a\left(1-e^2\right)\right]^2} n\left(\cos i\right)\Delta t, \tag{3-15}$$

$$\overline{\Delta\omega_{\text{sec}}} = \frac{3}{2}\frac{J_2 R^2}{\left[a\left(1-e^2\right)\right]^2} n\left(2-\frac{5}{2}\sin^2 i\right)\Delta t, \tag{3-16}$$

where a is the semi-major axis (km), e is the eccentricity, i is the inclination angle (deg), R is the Earth's mean equatorial radius (km), and n is the satellite mean motion (1/s).

Long-period oscillations in the elements due to the third harmonic, J_3, are also accounted for in the long-term orbit propagation. Eccentricity and inclination for example, vary according

to secular variations in argument of perigee, ω as follows

$$\Delta e_{lp} = -\frac{3}{2}\frac{n J_3 R^3}{a^3\left(1-e^2\right)^2}\sin i\left(1-\frac{5}{4}\sin^2 i\right)\cos\omega\ \Delta t, \tag{3-17}$$

$$\Delta i_{lp} = \frac{3}{2}\frac{n J_3 R^3}{a^3}\frac{e}{\left(1-e^2\right)^3}\cos i\left(1-\frac{5}{4}\sin^2 i\right)\cos\omega\ \Delta t. \tag{3-18}$$

Atmospheric Drag

The extensive research of King-Hele[83] is used to compute changes in semi-major axis and eccentricity by analytical methods. IDES employs the CIRA (Cospar International Reference Atmosphere) of 1972 to give values of atmospheric density and density scale height according to the perigee height of the object orbit and the exospheric temperature, T_{ex} (K). This atmospheric data model has been chosen for computational efficiency and the goodness of CIRA for these applications. CIRA has been derived from the long-term atmospheric decay profiles of satellites with known cross-sectional area, mass and drag coefficient. It is therefore more suited for use with the King-Hele equations than other atmosphere models, which are derived from Mass Spectrometer and Incoherent Scatter (MSIS) data on nitrogen density and temperature. Such data is limited to specific altitudes at specific points in time and would lead to inaccurate long-term atmospheric drag decay predictions for debris objects in IDES. The exospheric temperature is proportional to the 30-day mean solar flux, $F_{10.7}$, at a wavelength of 10.7 cm (in units of 10^{-22} W m^{-2} Hz^{-1}) according to

$$T_{ex} = 1.15\,(\,379 + 3.24\,F_{10.7}\,). \tag{3-19}$$

Solar flux (and therefore the orbital decay rate) is modulated by the 11-year solar cycle, with maximum decay rate occurring during solar maximum conditions. The $F_{10.7}$ dataset shown in Figure 3-15 and used by IDES, has been taken from the NASA Goddard historical records, and their predictions of the next two solar cycles[84]. The NASA solar activity predictions have then been repeated over the next 50 years in order to account for solar cycle effects in the future debris environment projections. The predictions were derived using statistical estimation techniques applied to activity observed in many previous solar cycles. King-Hele has shown that for a spherically symmetric atmosphere (which is assumed in the

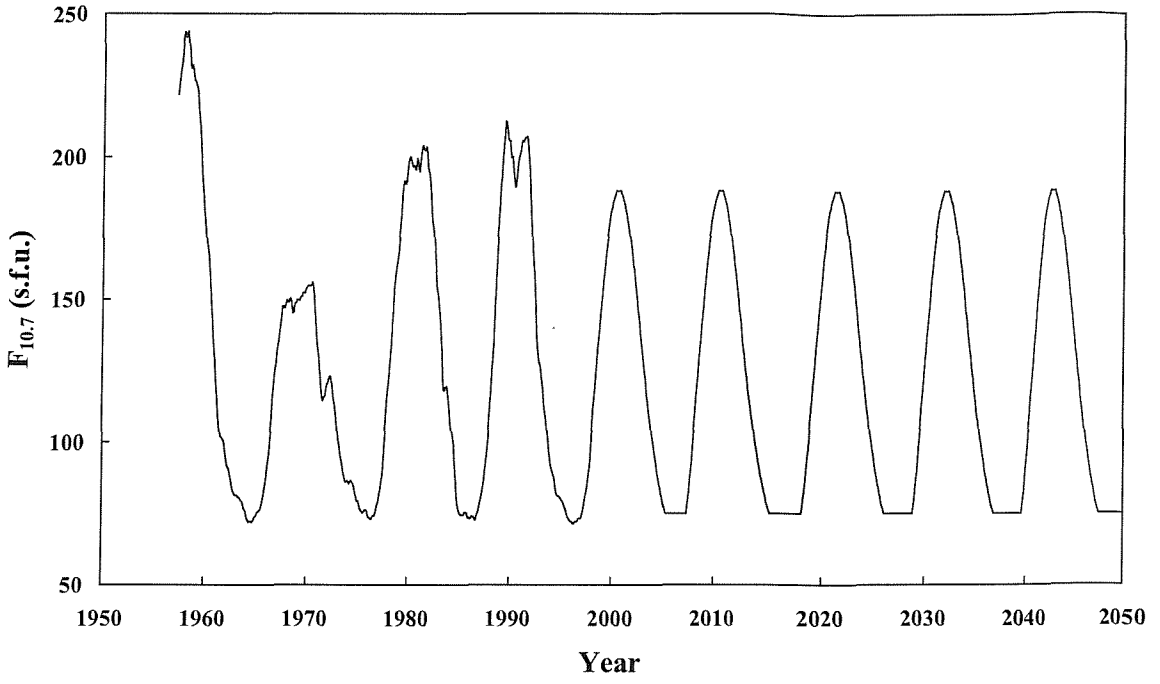

Figure 3-15: IDES historical and future solar activity dataset (13-month smoothed solar flux at 10.7 cm wavelength, $F_{10.7}$, in solar flux units, s.f.u.)

CIRA model), the changes in semi-major axis, Δa (m), and eccentricity, Δe, are essentially a function of the object area, A (m^2), object mass, M (kg), atmospheric density at perigee, ρ_p (kg/m^3), and drag coefficient, C_D, and given by

$$\Delta a = -2\pi \frac{A C_D}{M} a^2 \rho_p \exp[a_0 - a - a_0 e_0] f_1(I_0, I_1, I_2, I_3) , \qquad (3\text{-}20)$$

$$\Delta e = -2\pi \frac{A C_D}{M} a \rho_p \exp[a_0 - a - a_0 e_0] f_2(I_0, I_1, I_2, I_3, I_4) , \qquad (3\text{-}21)$$

where f_1 and f_2 are functions of I_n (n=1,…,4), which are Bessel functions of the first kind with argument of $z = ae/H$. H is the density scale height (km).

Luni-Solar Gravity Perturbations

IDES considers the luni-solar gravity perturbation effects on all orbits intersecting LEO by using the theory developed by Cook[85]. Cook derived analytical expressions for the rate of change of the orbital elements from luni-solar effects based upon the integration of Lagrange's planetary equations and the astronomical parameters of the Sun and Moon.

These may be expressed in first derivative form as

$$\frac{de}{dt} = -\frac{15K}{2n} e\sqrt{1-e^2}\left[AB\cos 2\omega - \tfrac{1}{2}\left(A^2 - B^2\right)\sin 2\omega\right], \tag{3-22}$$

$$\frac{di}{dt} = \frac{3KC}{4n\sqrt{1-e^2}}\left[A\left(2+3e^2+5e^2\cos 2\omega\right)+5Be^2\sin 2\omega\right], \tag{3-23}$$

$$\frac{d\Omega}{dt} = \frac{3KC}{4n\sqrt{1-e^2}\sin i}\left[5Ae^2\sin 2\omega + B\left(2+3e^2-5e^2\cos 2\omega\right)\right], \tag{3-24}$$

$$\frac{d\omega}{dt} = \frac{3K}{2n}\sqrt{1-e^2}\left[5\left\{AB\sin 2\omega + \tfrac{1}{2}\left(A^2-B^2\right)\cos 2\omega\right\}\right. \tag{3-25}$$

$$-1+\tfrac{3}{2}\left(A^2+B^2\right)+\frac{5a}{2e\,r_d}\left\{1-\tfrac{5}{4}\left(A^2-B^2\right)\right\}$$

$$\left.\times\ \left(A\cos\omega + B\cos\omega\right)\right] - \frac{d\Omega}{dt}\cos i\ ,$$

where

$$K = \frac{GM_d}{r_d^3}\ .$$

The coefficients A, B, and C are functions of trigonometric expressions that relate the orbit of the disturbing body to the satellite orbit. G is the gravitational constant ($km^3\ kg^{-1}\ s^{-2}$), n is again the mean orbital motion (s^{-1}), M_d is the mass of the disturbing body (kg), and r_d is the distance to the disturbing body (km).

Solar Radiation Pressure Perturbations

Many small-size debris objects have high area-to-mass ratios and consequently their orbits are influenced by solar radiation pressure (SRP), as well as atmospheric drag. By a similar treatment to the luni-solar perturbation theory, Cook[85] gives the rate of change of the orbital elements due to SRP effects, taking account of the satellite's entry to the Earth shadow and

exit from this shadow. The expressions are defined by

$$\frac{da}{dt} = \frac{1}{na\pi}\left[(r_c \sin\theta_c - r_o \sin\theta_o)T_p + a(\cos E_c - \cos E_o)S_p\right], \tag{3-26}$$

$$\frac{de}{dt} = \frac{T_p}{2\pi n a^3}\left[3a^2\sqrt{1-e^2}\left\{\tan^{-1}\left(\frac{\sqrt{1-e^2}\tan\left(\tfrac{1}{2}\theta_c\right)}{1+e}\right)\right.\right. \tag{3-27}$$

$$\left.\left. - \tan^{-1}\left(\frac{\sqrt{1-e^2}\tan\left(\tfrac{1}{2}\theta_o\right)}{1+e}\right)\right\} - \frac{1}{2e}\left(r_c^2 \sin\theta_c - r_o^2 \sin\theta_o\right)\right.$$

$$\left. + \frac{a}{2e}\left(1-4e^2\right)\left(r_c \sin\theta_c - r_o \sin\theta_o\right)\right] - \frac{S_p}{4\pi n a^3}\left[\left(r_c^2 - r_o^2\right)\right.$$

$$\left. + \frac{a\left(1-e^2\right)}{e^2}\left(r_c - r_o\right) + \frac{1}{e}\left(r_c^2 \cos\theta_c - r_o^2 \cos\theta_o\right)\right],$$

$$\frac{di}{dt} = \frac{W}{2\pi n a^3}\left\{\left[\frac{r_c^2 \sin\theta_c - r_o^2 \sin\theta_o}{2\left(1-e^2\right)} + \frac{a\left(1+2e^2\right)}{2\left(1-e^2\right)}\left(r_c \sin\theta_c - r_o \sin\theta_o\right)\right.\right. \tag{3-28}$$

$$\left.\left. - \frac{3a^2 e}{\sqrt{1-e^2}}\left(\tan^{-1}\left(\frac{\sqrt{1-e^2}\tan\left(\tfrac{1}{2}\theta_c\right)}{1+e}\right) - \tan^{-1}\left(\frac{\sqrt{1-e^2}\tan\left(\tfrac{1}{2}\theta_o\right)}{1+e}\right)\right)\right]\cos\omega\right.$$

$$\left. - \frac{\left(r_c^2 - r_o^2\right)}{2e}\sin\omega\right\},$$

$$\frac{d\Omega}{dt} = \frac{W}{2\pi n a^3 \sin i}\left\{\frac{\left(r_c^2 - r_o^2\right)}{2e}\cos\omega + \left[\frac{r_c^2 \sin\theta_c - r_o^2 \sin\theta_o}{2\left(1-e^2\right)}\right.\right. \tag{3-29}$$

$$\left.\left. + \frac{a\left(1+2e^2\right)}{2\left(1-e^2\right)}\left(r_c \sin\theta_c - r_o \sin\theta_o\right)\right.\right.$$

$$\left.\left. - \frac{3a^2 e}{\sqrt{1-e^2}}\left(\tan^{-1}\left(\frac{\sqrt{1-e^2}\tan\left(\tfrac{1}{2}\theta_c\right)}{1+e}\right) - \tan^{-1}\left(\frac{\sqrt{1-e^2}\tan\left(\tfrac{1}{2}\theta_o\right)}{1+e}\right)\right)\right]\sin\omega\right\}$$

$$\frac{d\omega}{dt} = -\frac{S_p}{2\pi n a^3 e}\left[3a^2\sqrt{1-e^2}\left\{\tan^{-1}\left(\frac{\sqrt{1-e^2}\,\tan\left(\frac{1}{2}\theta_c\right)}{1+e}\right)\right.\right. \tag{3-30}$$

$$\left.\left. - \tan^{-1}\left(\frac{\sqrt{1-e^2}\,\tan\left(\frac{1}{2}\theta_o\right)}{1+e}\right)\right\} + \frac{1}{2e}\left(r_c^2 \sin\theta_c - r_o^2 \sin\theta_o\right)\right.$$

$$\left. - \frac{a}{2e}\left(1-2e^2\right)\left(r_c \sin\theta_c - r_o \sin\theta_o\right)\right]$$

$$+ \frac{T_p}{4\pi n a^3 e^3}\left[e\left(r_c^2 \cos\theta_c - r_o^2 \cos\theta_o\right) + a\left(1-e^2\right)\left(r_c - r_o\right)\right] - \frac{d\Omega}{dt}\cos i \ .$$

where

$$S_p = F\, l_1(i,\omega,\Omega,L,\varepsilon), \quad T_p = -F\, l_2(i,\omega,\Omega,L,\varepsilon),$$

$$W = \frac{F}{2\cos\omega}\, l_3(i,\omega,\Omega,L,\varepsilon), \text{ and } F = -\frac{4.5\times10^{-6}(1+\beta)A}{M} \ .$$

The equation for the solar radiation force per unit mass, F (N kg^{-1}), was taken from Roy[82]. β is the surface reflectivity coefficient, which can vary between 0 (no reflection of solar radiation) and 1 (complete reflection of solar radiation). An average value of 0.5 for solar reflectivity is assumed here. The parameters S_p, T_p and W are perturbing forces per unit mass, or accelerations, acting on the satellite. W is the perturbing acceleration perpendicular to the osculating orbit plane. They are directly proportional to F. The trigonometric expressions l_1, l_2 and l_3 are influenced by the angular elements of the object orbit, the geometric mean longitude of the Sun, L, and the mean obliquity of the ecliptic, ε. Here, θ_c, r_c, and E_c are the true anomaly, geocentric radius, and eccentric anomaly of the orbit at Earth shadow entrance. The corresponding parameters at Earth shadow exit are θ_o, r_o, and E_o. In this set of equations, the semi-major axis, a, is expressed in metres.

The entrance true anomaly is found by searching through the true anomaly range in 1° steps between 0° and 360° for the step that turns the Earth shadow function[86], S, from a negative value to a positive value. The Earth shadow function is given by

$$S = R_e^2(1+e\cos\theta)^2 + p^2(\beta\cos\theta + \xi\sin\theta)^2 - p^2 \tag{3-31}$$

where

$$\beta = \frac{X_S P_x + Y_S P_y + Z_S P_z}{\sqrt{X_S^2 + Y_S^2 + Z_S^2}} \quad \text{and} \quad \xi = \frac{X_S Q_x + Y_S Q_y + Z_S Q_z}{\sqrt{X_S^2 + Y_S^2 + Z_S^2}} \ .$$

X_S, Y_S and Z_S, are the geocentric rectangular co-ordinates of the Sun at a given epoch, as defined in the American Ephemeris and Nautical Almanac. P_x, P_y, and P_z, are components of a unit vector, $\vec{P}$, that points from Earth's centre of mass to the perigee of the orbit. Q_x, Q_y, and Q_z are also components of a unit vector, $\vec{Q}$, that is defined as being perpendicular to unit vector $\vec{P}$, and pointing out of the orbit plane. R_e is the mean Earth radius, and p is the semi-latus rectum of the orbit.

The exit true anomaly step is located when the shadow function undergoes a sign change from positive to negative. Once both entrance and exit true anomaly steps have been found at 1° resolution, the search technique then divides the given 1° range into 10 further steps in order to locate the entrance or exit true anomaly with 0.1° resolution. This numerical search technique has been found to be very efficient, whilst retaining a reasonable accuracy.

3.5 Orbital Debris Environment

3.5.1 Debris Flux Determination

The determination of debris flux for discrete sectors of the Low Earth Orbit (LEO) regime is an essential component of the IDES model. The techniques used, provide snapshots of the LEO flux environment in order to predict future collision events and facilitate directional collision risk analysis of a single target mission (in both current and long-term environments). In an approach developed by Klinkrad[58], the debris flux environment is

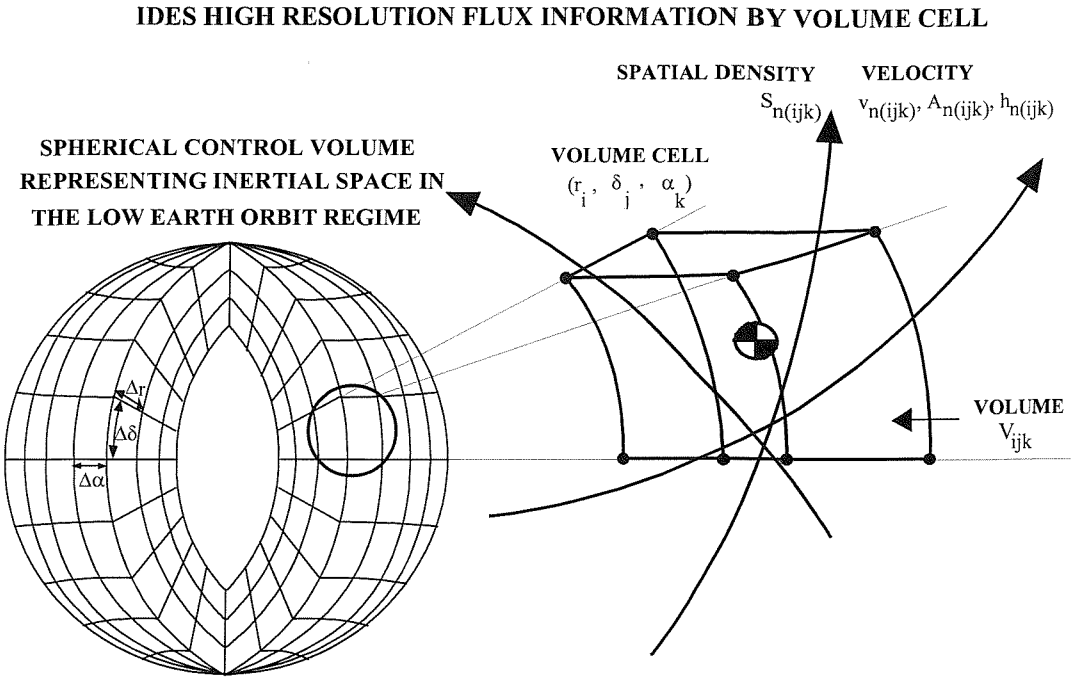

Figure 3-16: Representation of the debris flux environment in LEO

represented by a three-dimensional inertial control volume divided into volume cells by the spherical co-ordinate parameters of geocentric radius, declination and right ascension. The transformation of the orbital state of the debris population into spatial densities and intersection velocity vectors for each of the volume cells in the control volume, makes it possible to construct spatial density profiles over altitude/declination for environment analysis. Alternatively, the fluxes encountered by a single target orbit corresponding to different particle size ranges can be determined for collision risk assessment.

The method of determining debris flux in IDES uses a technique similar to Klinkrad[58]. This technique is applicable because each large object is represented individually by its full orbital element set. For the small-size debris population that is divided into many perigee radius-eccentricity-inclination-mass bins, the model assumes that the argument of perigee and right ascension of the ascending node values of each debris object orbit are randomly distributed. These characteristics are certainly true of the small-size debris population where fragment clouds that have been ejected from breakup locations are randomly dispersed after a period of months. Therefore, the theory and assumptions are suitable for the model and provide a high precision method of calculating directional fluxes.

Large Object Flux

For each large object with individual orbital elements of semi-major axis, a, eccentricity, e, inclination, i, right ascension of ascending node, Ω, and argument of perigee, ω, the method determines the true anomalies, θ, of the orbit which intersect the respective cell borders of the inertial control volume (see Figure 3-16). These borders are defined by the discrete, regularly spaced values of geocentric radius, r_i, declination, δ_j, and right ascension, α_k. The method uses the equations derived by Sven Hauptmann[87]. The intersection true anomalies, as a function of these borders are given by

$$\theta(r_i) = \cos^{-1}\left(\frac{a\left(1-e^2\right)/r_i - 1}{e}\right) \tag{3-32}$$

$$\theta(\delta_j) = \sin^{-1}\left(\frac{\sin\delta_j}{\sin i}\right) - \omega \tag{3-33}$$

$$\theta(\alpha_k) = \sin^{-1}\left(\frac{\sin(\alpha_k - \Omega)}{\sqrt{1-\sin^2 i\cos^2(\alpha_k - \Omega)}}\right) - \omega \tag{3-34}$$

Each of the true anomalies are converted to an intersection time and then the intersections are sorted in ascending chronological order. The time between these intersections (t_2 - t_1) is used, along with the orbital period, T, to determine the residential probability, $P_{n(ijk)}$, of the object during passage through the respective cell volume, V_{ijk}. Hence the spatial density, $S_{n(ijk)}$, is found by dividing the residential probability by the cell volume. The velocity vector is defined at the mid-point of cell passage ($\theta_{mid(ijk)}$) by the velocity magnitude, $v_{n(ijk)}$, azimuth, $A_{n(ijk)}$ and elevation, $h_{n(ijk)}$. These quantities are expressed as

$$P_{n(ijk)} = \frac{t_2 - t_1}{T}, \quad S_{n(ijk)} = \frac{P_{n(ijk)}}{V_{ijk}}, \quad v_{n(ijk)} = \sqrt{\mu\left(\frac{2}{r_i} - \frac{1}{a}\right)} \tag{3-35}$$

$$A_{n(ijk)} = -\cos^{-1}\left(\frac{\sin i\,\cos\left(\omega + \theta_{mid(ijk)}\right)}{1-\sin^2 i\,\cos^2\left(\omega + \theta_{mid(ijk)}\right)}\right) \tag{3-36}$$

$$h_{n(ijk)} = \cos^{-1}\left(\frac{-e\sin\theta_{mid(ijk)}}{\sqrt{1+e^2+2e\cos\theta_{mid(ijk)}}}\right) - \frac{\pi}{2} \tag{3-37}$$

Klinkrad defines azimuth as the angle between the object velocity vector in the local horizontal plane with respect to the meridian. Azimuth is measured from the north direction and is counted positive eastwards. Elevation is the angle between the object velocity vector and the local horizontal plane, and is counted positive spacewards. The flux magnitude of each debris intersection in the cell is simply the spatial density multiplied by the velocity magnitude (and a conversion factor to change the flux units to $1/m^2/yr$). The flux vector of each cell intersection is defined by the spatial density, velocity magnitude, azimuth and elevation values.

Instead of storing every flux vector of every cell intersection of every debris orbit, the author has developed a technique to significantly reduce data storage and processing requirements by computing mean flux vectors in each cell. For each cell intersection, the velocity, azimuth and elevation values are weighted by the residential probability and added to their respective running totals. The residential probability is also accumulated. The mean velocity vector for each cell after all debris intersections is then derived by dividing each of the velocity, azimuth and elevation running totals by the total residential probability of the cell. The spatial density for each cell is determined by the total residential probability divided by the volume of the cell. Thus, the mean flux vector is defined. However, having just one mean flux vector per cell is not sufficient to represent the wide variation in directionality. In fact, a minimum of 8 mean flux vectors are required per cell in order to cover this variation. The 8 vectors come from the combinations of 4 sectors in azimuth angle (-180 to -90, -90 to 0, 0 to 90, and 90 to 180 degrees) and 2 sectors in elevation angle (-90 to 0, and 0 to 90 degrees). In order to minimise data storage, the IDES model uses this configuration when producing snapshots of the debris flux environment.

Small Object Flux

The mass-binned contributions to the debris flux matrix from the small-size debris population are derived by assuming that a number of debris on similar orbits can be represented by a single common orbit, taken from the parameter space in the population

orbit matrix. For each bin of the population orbit matrix, the state variable $N_t(r_p,e,i,m)$, and the bin's centroid orbit co-ordinate in perigee radius-eccentricity-inclination space, are used to determine the *group* spatial density and velocity vector in the respective mass bin of each intersected cell volume. Again, the theory is used in the same way as described above for large debris objects. However, this time the assumption is that all debris objects within a particular bin of the population orbit matrix traverse the centroid orbital path and so the unit spatial density (due to one object) in each intersected cell volume can be scaled by the number of objects in the bin, $N_t(r_p,e,i,m)$ to determine the group spatial density.

3.5.2 Target-Centred Collision Event Prediction

Collision event prediction is treated in the simulation by a novel 'target-centred' approach, developed by the author. It combines rapid collision risk assessment of large target objects in the population relative to the mass-dependent debris/meteoroid flux environment with statistical Monte Carlo prediction of events. The lethality of each predicted collision event is also assessed. This method allows the triggering of catastrophic collision breakups, as well as non-lethal damaging impacts that produce secondary fragments, and surface impacts that deposit paint flakes into the environment.

Each member of the debris population with a mass greater than 50 kg is considered as a target which encounters an orbit-integrated flux from debris of the various mass ranges defined for the debris flux environment snapshot. The Klinkrad method[58] of determining relative flux to a target orbit is used. Firstly, the cell intersections of the target orbit are found in the same way as for the debris flux calculations. For each cell intersection, the target velocity components in geocentric cartesian co-ordinates, $\dot{x}_m, \dot{y}_m, \dot{z}_m$, the target declination, δ_m, and right ascension, α_m, and target residential probability are computed. Then, for each mass bin of the intersected cell, the velocity components of each of the 8 debris mean flux vectors relative to the target, $\Delta\dot{x}_{n.m}$, $\Delta\dot{y}_{n.m}$, $\Delta\dot{z}_{n.m}$, are derived from

$$\begin{pmatrix} \Delta\dot{x}_{n.m} \\ \Delta\dot{y}_{n.m} \\ \Delta\dot{z}_{n.m} \end{pmatrix} = v_n \begin{pmatrix} c\alpha_m(-s\delta_m ch_n cA_n + c\delta_m sh_n) - s\alpha_m sA_n \\ s\alpha_m(-s\delta_m ch_n cA_n + c\delta_m sh_n) + c\alpha_m sA_n \\ c\delta_m ch_n cA_n + s\delta_m sh_n \end{pmatrix} - \begin{pmatrix} \dot{x}_m \\ \dot{y}_m \\ \dot{z}_m \end{pmatrix} \qquad (3\text{-}38)$$

where c=*cos*, s=*sin*, n denotes the debris flux vector (from a particular mass bin) and m denotes the target. A_n, h_n, and v_n, are the transient debris azimuth, elevation and velocity magnitude values of the mean flux vector. In order to express the relative velocity vector in the target-centred moving reference frame, the target right ascension of ascending node, Ω, inclination, i, and argument of true latitude, u_m, (the addition of argument of perigee and true anomaly at mid-cell intersection) are used in a matrix transformation given by

$$\vec{v}_{n.m} = \begin{pmatrix} v^u_{n.m} \\ v^v_{n.m} \\ v^w_{n.m} \end{pmatrix} = \begin{pmatrix} cu_m c\Omega - su_m s\Omega ci & cu_m s\Omega + su_m c\Omega ci & su_m si \\ -su_m c\Omega - cu_m s\Omega ci & -su_m s\Omega + cu_m c\Omega ci & cu_m si \\ s\Omega si & -c\Omega si & ci \end{pmatrix} \begin{pmatrix} \Delta\dot{x}_{n.m} \\ \Delta\dot{y}_{n.m} \\ \Delta\dot{z}_{n.m} \end{pmatrix} \tag{3-39}$$

The relative velocity vector, $\vec{v}_{n.m}$, has three orthogonal components representing relative velocity for the directions u, v, and w in the target-centred reference frame. The u direction denotes the radial direction, the v direction denotes the along-track direction, and the w direction denotes the out-of-plane direction. The relative velocity *magnitude* between the mean debris flux vector and the target is then simply

$$v_{rel} = |\vec{v}_{n.m}| = \sqrt{\left(v^u_{n.m}\right)^2 + \left(v^v_{n.m}\right)^2 + \left(v^w_{n.m}\right)^2} \tag{3-40}$$

The relative flux magnitude between the mean debris flux vector and target is given by the debris vector's spatial density multiplied by this relative velocity (with a conversion factor to express the correct flux units of $1/m^2/yr$). The orbit-integrated mean relative flux to the target, F_t, is then a summation of each of the relative flux magnitudes encountered in each of the target cell intersections, weighted by the target residential probability in the respective volume cells. The expected mean number of impacts to the target (in a given mass bin), λ, is then computed from the orbit-integrated mean flux to the target, F_t, the target cross section, σ_t, the average debris cross section for the mass bin, σ_p, and the time interval, Δt, as follows

$$\lambda = F_t \sqrt{\sigma_t^2 + \sigma_p^2}\ \Delta t \tag{3-41}$$

Using this expected mean number of impacts to the target, λ, the *predicted* number of collision events from a particular debris mass range can be statistically derived using a Poisson distribution from n = 0 to N events, to obtain N event probabilities, P_n, (as performed in refs. 10 and 52) where

$$P_n = \frac{\lambda^n}{n!} e^{-\lambda} \quad . \tag{3-42}$$

Values of P_n are accumulated to give an overall probability, P_N, and then each event probability is normalised by this value. All normalised event probabilities lie in the range from 0 to 1. A high precision uniform random number is generated and the predicted number of collision events corresponds to the maximum normalised event probability that has been exceeded by this random number.

If one or more collisions are predicted for the target, then the lethality of the encounter is assessed by the calculating the impactor energy-to-target mass ratio (*EMR*) from parameters of target mass, M_t, average projectile mass for the mass bin, M_p, and the impact velocity, v_{imp}. The impact velocity is obtained from the relative velocity at the peak encountered flux to the target. This is given by

$$EMR = \frac{\frac{1}{2} M_p v_{imp}^2}{M_t} \quad . \tag{3-43}$$

If the *EMR* is greater than the lethality ratio of the target (default of 40 J/g), a catastrophic collision is executed by the breakup model, using the target's orbital elements and with the true anomaly of the breakup set to the value where the peak relative flux was encountered. However, if the *EMR* is less than the target's lethality ratio then the crater depth of the impact is determined by the equation[88]

$$P_\infty = 5.24\, d_p^{19/18} H_t^{-1/4} \left(\frac{\rho_{proj}}{\rho_t} \right)^{1/2} \left(\frac{v_{imp}}{c} \right)^{2/3} \quad . \tag{3-44}$$

In this equation, the projectile size, d_p, is in centimetres. The projectile material and the target material are assumed to be aluminium with densities ρ_{proj} and ρ_t of 2.785 g/cm^3, giving a Brinell Hardness of the target, H_t of 90, and a speed of sound, c of 5.4 km/s. If the depth of the crater is more than 1 mm, then a craterization (damaging impact producing aluminium secondary ejecta) is performed by the breakup model. If the crater depth is less than 1 mm, a surface impact (pit) is assumed and an equation can be employed to calculate the number of paint flakes ejected according to flake mass/size from around the surface pit. However, a reliable equation (based on ground test data) to define the paint flake ejecta mass distribution does not exist due to a lack of experimental data. If and when an empirical equation is derived in the future, this can be plugged into the IDES model and the paint flake ejecta source can be simulated.

The collision event prediction process can also be repeated for meteoroid impacts using the Grün *et al*[89] relationship to express the interplanetary meteoroid flux, F_{ip}, as a function of particle mass, m. In order to derive the sporadic meteoroid flux, F_{spo}, to a stationary target at LEO altitudes, the interplanetary flux must be multiplied by the earth focussing factor, G_E, and the earth shielding factor[90], ζ. All equations involved in this computation are described as follows

$$F_{ip} = c_0\left[\left(c_1 m^{0.306} + c_2\right)^{-4.38} + c_3\left(m + c_4 m^2 + c_5 m^4\right)^{-0.36} + c_6\left(m + c_7 m^2\right)^{-0.85}\right] \tag{3-45}$$

where $c_0 = 3.15576\times10^7$ $\quad c_1 = 2.2\times10^3$

$c_2 = 15$ $\quad c_3 = 1.3\times10^{-9}$

$c_4 = 10^{11}$ $\quad c_5 = 10^{27}$

$c_6 = 1.3\times10^{-16}$ $\quad c_7 = 10^6$

$$G_E = 1 + \frac{R}{R + H_{alt}} \tag{3-46}$$

$$\zeta = \frac{1 + \cos\Theta}{2} \quad \text{where} \quad \sin\Theta = \frac{R + 100}{R + 100 + H_{alt}} \tag{3-47}$$

$$F_{spo} = F_{ip}\ G_E\ \zeta \tag{3-48}$$

Here, F_{ip}, is the interplanetary meteoroid flux at 1 Astronomical Unit (AU) in units of $1/m^2/s$, R is the mean Earth radius (km), and H_{alt} is the target orbit altitude (km).

Techniques included in another piece of software developed at DERA[91], are used to compute the sporadic meteoroid flux relative to the moving target satellite at steps of true anomaly around its orbit. This is done by obtaining the stationary flux (as defined in the above equations) for the specific altitude at each true anomaly step and then scaling the flux by the k correction factor[92] that is determined using the target velocity, v_t, and an average sporadic meteoroid velocity, v_m. This accounts for the bias in directionality introduced in the ram direction by the target's motion and gives the mean relative impact velocity at each true anomaly step after numerical integration of the impact angle, α_{imp}, over 2π (due to isotropic sporadic meteoroid velocity vectors). The k correction factor is calculated by

$$v^* = \sqrt{v_m^2 - v_t^2 \sin^2 \alpha_{imp}} \tag{3-49}$$

$$v_{imp} = v_t \cos \alpha_{imp} + v^* \tag{3-50}$$

$$k = \frac{v_{imp}^3}{v_m^2 v^*} \tag{3-51}$$

The orbit-integrated sporadic mean meteoroid flux and velocity relative to the target are then obtained by numerical integration over all true anomaly steps. These flux and velocity values are then used to assess the impact effects as done with the man-made debris impactors above.

Consideration of Satellite Constellations in Collision Event Prediction

Multiple satellite constellation systems, such as the many commercial communications architectures being proposed for deployment in LEO, must be modelled as a special case in the collision event prediction process presented above. This is because within the system, spacecraft are being controlled collectively by a single operator so that they are maintained within specific volumes (absolute station-keeping) or with the same minimum distance from one another (relative station-keeping). Either way, satellites within a constellation system should not collide with one another during nominal operations. The target-centred approach

to collision event prediction uses the flux environment snapshot to compute flux relative to large object targets. Without any special handling, the flux environment snapshot would include flux contributions from the constellation satellites and the flux relative to each constellation satellite target would include contributions from all the other members in the constellation system. In effect, the model would predict collisions between satellites in the same system.

This possibility is eliminated by using the algorithm presented in Figure 3-17. Two snapshots of the debris flux environment are taken at the same epoch. The first flux environment snapshot includes flux contributions from both the background debris population (with size bins larger than 1 mm) and all the constellation satellites. The second flux environment snapshot includes flux contributions from the background debris population only (no constellation flux contributions). There is a negligible computer runtime overhead from taking two snapshots simultaneously, and only a modest increase in computer memory. Having the target-centred approach to collision event prediction and details on the type of each large target object, means that IDES is able to recognise whether the target is a constellation satellite or a large background object (satellite, upper stage etc.).

In this algorithm, if the target object is a constellation satellite then its collision risk (and possible collision event) is computed from the second flux environment snapshot, which only includes contributions from the background debris population. However, if the target object is a large background object, then its collision risk is computed from the first flux environment snapshot, which includes flux from both background debris and constellation satellites. This means that constellation satellites will not 'see' other constellation satellites, but constellation satellites will 'see' debris induced by constellation satellite collisions with the background debris population (since fragments from constellation satellite collision-induced breakups become part of the background population). As before, large background objects will 'see' both the constellation satellites and other objects in the background debris population. Thus, the collision fragmentation source is being handled correctly within IDES by this method of avoiding the false prediction of collisions between operational constellation satellites.

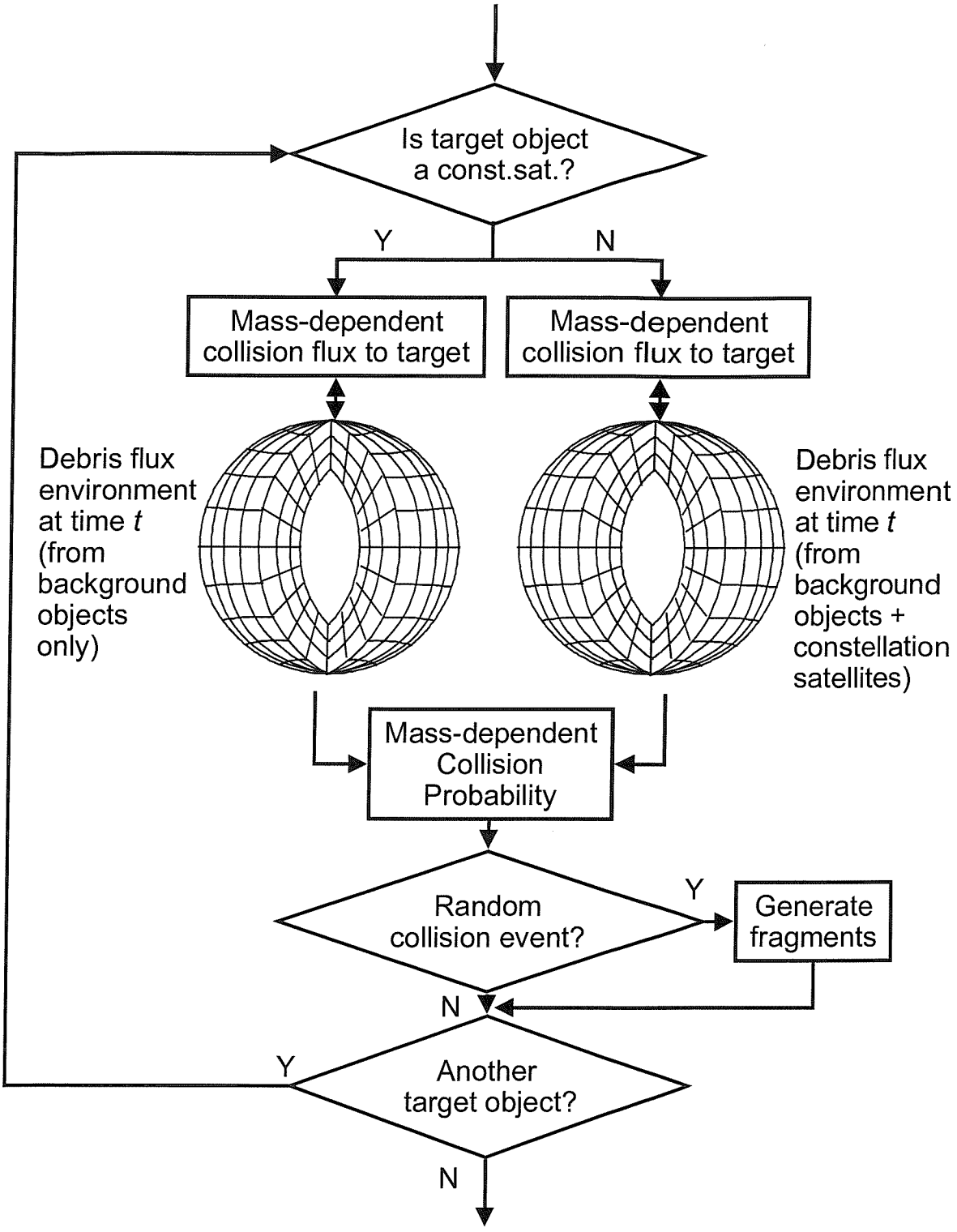

Figure 3-17: Algorithm for the handling of satellite constellations in the IDES long-term debris environment evolution program

3.5.3 Long-Term Collision Risk Prediction

Collision risk analysis of a single target mission is available based upon any of the debris flux environment snapshots produced by the simulation. Analysis in the present-day environment or in a future environment may be performed. Such data can be incorporated into future space platform vulnerability and shielding studies. Mission analysis in IDES can be coupled with tools that model satellite geometries and impact analysis for assessing the most effective debris protection strategies. The IDES collision risk assessment program operates upon the flux evolution model which has been output by DEEM, the main program of IDES. The flux evolution model is a data file composed of a series of debris flux environment snapshots appended to the file at every time step. The risk assessment program has direct access to all these snapshots and so a fast analysis of relative flux around the target orbit at any epoch is possible. In the case of the future environment snapshots, 10 Monte Carlo simulations of the IDES model are conducted in order to account for the randomness of debris source events and to obtain an average of environment evolution trends from these different statistical permutations. Each of these 10 Monte Carlo runs outputs a Flux Evolution model file. Predictions of impact flux on the target must therefore be produced for each of the 10 Monte Carlo environments and then averaged.

Directional Collision Flux Variation

The technique employed is identical to that used in the collision event prediction process, except only one user-defined target orbit is considered. However, the risk assessment is more detailed than just determining the orbit-integrated mean relative flux per size bin. In addition to the relative flux magnitude and relative velocity magnitude for each debris flux vector encountered by the target around its orbit, the target-centred encounter angles of azimuth and elevation are also determined by

$$A_{rel} = \tan^{-1}\left(\frac{v_{n.m}^{w}}{v_{n.m}^{v}}\right) \tag{3-52}$$

$$h_{rel} = \sin^{-1}\left(\frac{v_{n.m}^{u}}{v_{rel}}\right) \tag{3-53}$$

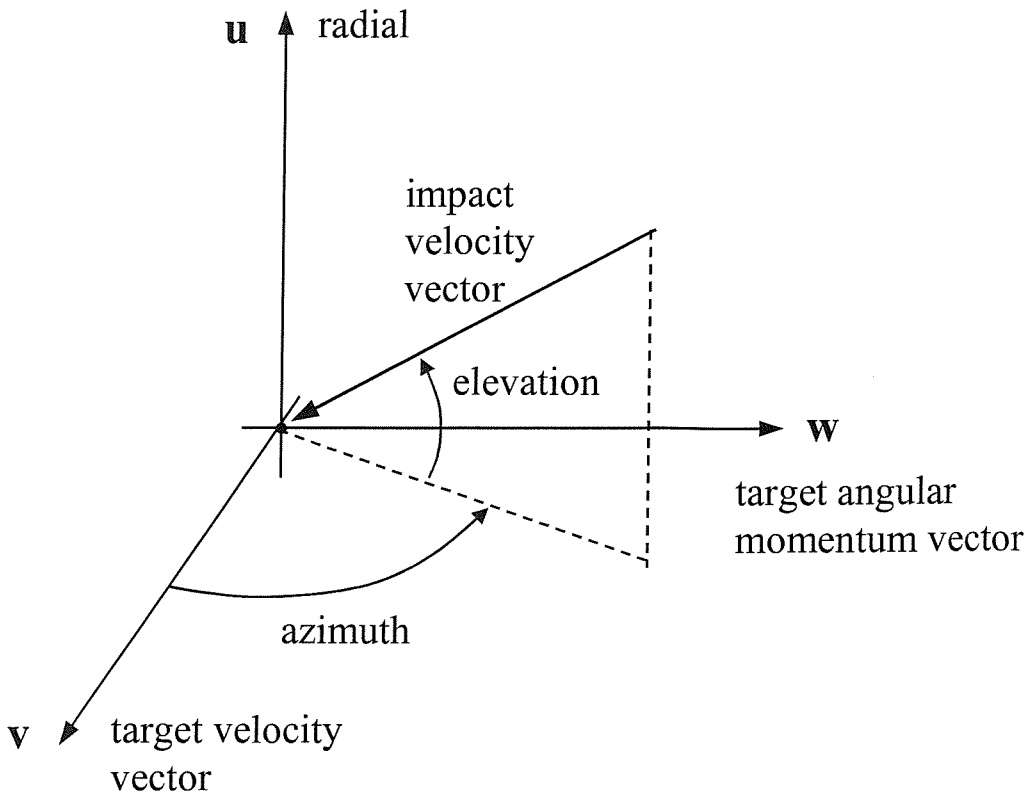

Figure 3-18: The target-centred moving reference frame for the determination of directional debris impact flux relative to an arbitrary target orbit

Figure 3-18 shows these angles in relation to the reference frame. Encounter azimuth, A_{rel}, is the direction of the impact in the target's local horizontal plane and is evaluated in the range -180 to +180 degrees (with 0 degrees azimuth representing the target's direction of motion). Encounter elevation, h_{rel}, is the direction of impact outside the target's horizontal plane and is evaluated in the range -90 to +90 degrees (with 0 degrees elevation representing the target's local horizontal plane). The contributions of relative flux magnitude from each mean debris flux vector encountered are used to derive distributions of relative flux over encounter velocity, azimuth, elevation and target true anomaly for debris larger than a user-defined size threshold. These distributions are output and visualised for mission analysis purposes and can be sampled by space platform shielding analysis software.

Long-Term Collision Flux Variations

The velocity and directional distributions of flux on an arbitrary target orbit are found by accessing the flux environment snapshot in the flux evolution model file that is closest to

the determination epoch specified by the IDES user. The long-term temporal variation in orbit-integrated mean debris flux to a user-defined target orbit (for a specified size threshold) can be found using the same theory described in section 3.5.2 and also by accessing every flux environment snapshot appended to the flux evolution model file. It would be very wasteful to read in all flux vector data in all volume cells of every flux environment snapshot, since the user-defined target orbit will only intersect a small fraction of the volume cells in the control volume. An efficient 'direct access' algorithm has been developed so that the IDES risk assessment program only 'grabs' the relevant data from the correct location in the flux evolution model file at the appropriate point in the processing. This minimises file input effort and therefore computer runtime.

Once averaged over 10 or more Monte Carlo iterations, the mean flux to target versus time curve can be multiplied by the user-defined cross-sectional area of the target object and the time interval between snapshots, and then accumulated to obtain the cumulative mean collision probability versus time (for the selected size threshold).

3.6 Operation of the Model

A powerful way of managing the data and processing associated with the Integrated Debris Evolution Suite has been built for the user in the form of a Graphical User Interface (GUI). The purpose of the IDES GUI is to prepare formatted input data files, direct the inputs/outputs, run each of the programs, and manage data analysis and visualisation of the results. The GUI has been designed to make the software easy to use, when the simulation running behind it is very complex. IDES operates on a UNIX operating system in the X-Windows environment, and the main data set-up window for the environment evolution program, DEEM, can be seen in Figure 3-19. This window is used to describe the specific scenario to be run, define the boundaries and resolutions of the main matrices within DEEM, set options for particular debris source processes, enter the frequency of model output, and fix the initial random number seed for the random number generators. There are also buttons to clear the window of all data, select default settings, cancel the set-up altogether, or accept the settings to produce the input file. Overall, the GUI has enabled IDES to be much more user-friendly and quicker to operate than the basic approach of manual input file editing and command line execution.

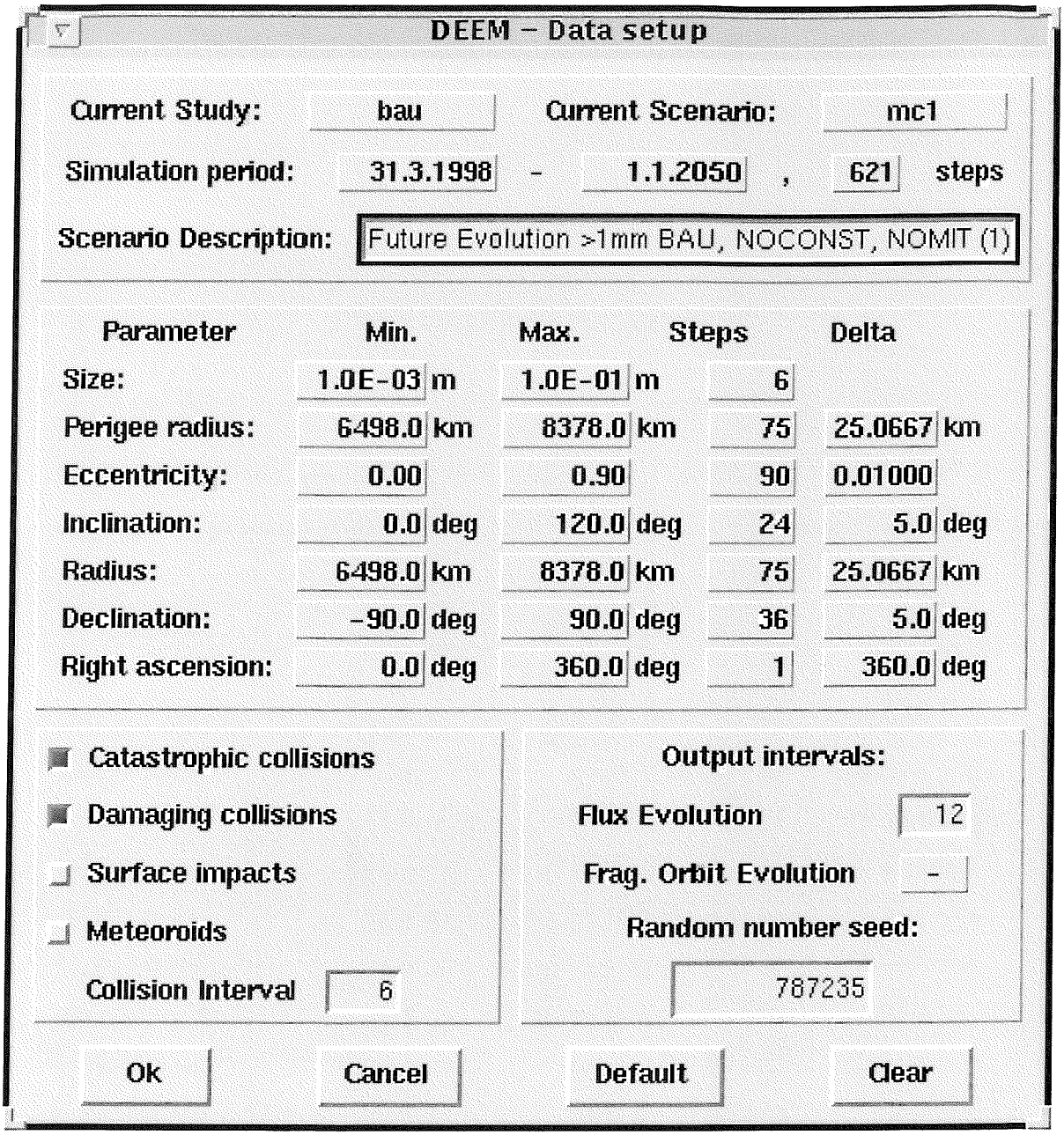

Figure 3-19: A user's view of IDES in the X-Windows environment

4 Model Validation

4.1 Introduction

Orbital debris models are essential for characterising the entire debris environment, especially for orbit and size regimes where measurements have poor coverage. These models are required to provide an accurate assessment of collision risk to current and future spacecraft missions. Therefore, the ultimate test of any environment simulation model is a comparison with the real world that the model is designed to represent. For a model such as IDES, this validation process should compare model predictions with reliable measurements of the debris population. The validation process is essential in determining the accuracy of the model, and can serve to improve accuracy in later model upgrades, once the potential reasons for any discrepancies are well understood. Confidence in the model predictions is strongly dependent upon a rigorous validation programme, particularly for simulations of future debris population evolution where no comparison with measurement data is possible.

The most deterministic debris measurement data currently available is the USSPACECOM Catalogue which contains the orbital elements of over 8500 Earth orbiting objects tracked by ground sensors of the US Space Surveillance Network (SSN). The catalogue data is suitable for validating the debris source and sink sub-models that are employed in deterministic environment models such as IDES, including the breakup and orbit perturbation models. The USSPACECOM catalogue contains data on decimetre-sized objects and larger in low Earth orbit (LEO) and so it can also be used to validate the modelled environment above this size threshold. Two of the most reliable sources of measurement data for the smaller-sized untrackable debris population are the detections of the US Haystack ground radar[93] and the impact analysis of the retrieved Long Duration Exposure Facility (LDEF) spacecraft[94]. These measurements are used to validate the IDES predictions of the sub-decimetre sized debris population.

Haystack has been statistically sampling the LEO environment of debris larger than about 6 mm since 1990 by counting the number of objects passing through its radar beam, which is operated in various fixed orientation 'beam-park' modes. Haystack can detect, but does not

routinely track and hence derive the orbital elements of debris objects at these sizes. The LDEF spacecraft was exposed to the debris environment for 5.76 years between 1984 and 1990. It was placed at an initial near-circular orbit with an altitude of 509 km and an inclination of 28.4°. The orbit later decayed over the course of the mission lifetime to an altitude of 324 km, before being retrieved by the Space Shuttle. LDEF received over 30,000 debris and meteoroid impacts from micron to near-millimetre sized particles. Many of the impact sites were counted and analysed upon return to Earth, enabling the directionality and magnitude of meteoroid/debris fluxes encountered for various impactor sizes to be inferred.

4.2 Validation of Debris Source and Sink Models

4.2.1 Long-Term Orbit Perturbation Model

The orbit perturbation model is validated by comparing long-term orbital evolution predictions of stable catalogued objects with the variation in the measured orbital elements selected from their two-line element histories contained in the weekly USSPACECOM catalogues.

For the validation of the IDES orbit perturbation model, two examples of stable tracked orbit histories from the USSPACECOM catalogue data were chosen between 1993 and 1998. In both cases, the initial orbital elements from a 1993 epoch were used as initial conditions for the orbit perturbation model. Firstly, the Ariane 4 third stage (COSPAR ID 1991-050F), which was used to launch the ERS-1 spacecraft, was selected as a representative debris object in a high inclination, near-circular low Earth orbit. In this orbit, luni-solar, solar radiation pressure and atmospheric drag perturbations are expected to be small and geopotential perturbations will have the largest influence. An area-to-mass ratio of 0.0196 m^2/kg was taken from the IDES historical launch database described in section 3.3.1. Although the Ariane 4 stage 3 mass is well known, there is uncertainty in the cross-sectional area presented to the direction of motion (and therefore the atmospheric drag force). Any error in the drag predictions would be due to an inaccurate value of the area-to-mass ratio, the drag perturbation theory, the atmospheric model, or the historical solar flux.

Figure 4-1 shows the evolution of the semi-major axis for the IDES predictions and two line element (TLE) measurements. The IDES orbit propagator appears to predict a decay rate

that is three times faster than the TLE data for semi-major axis, as it decreases due to atmospheric drag decay. However, the maximum absolute error in the predictions is about 2 km after 6 years of propagation, which is not unreasonable at the altitude of 770 km where the atmospheric density is low. It is likely that this error has been caused by incorrect estimation of the area-to-mass ratio.

The TLE data in Figure 4-2 displays periodic fluctuations in eccentricity which are modelled accurately by IDES in terms of period. However, the magnitude of the fluctuations are much larger for the IDES orbit propagator predictions. This is because the long-period fluctuations are due to the effects of odd zonal harmonics in Earth's gravitational field (predominantly the coefficient J_3), which are known to be poorly represented by the TLE data. In processing two-line element sets, USSPACECOM attempt to remove the eccentricity oscillations. However, these oscillations are not successfully removed in some TLE data (mainly at very low eccentricities). Therefore, given the deficiencies in the TLE data, the IDES orbit propagator produces an accurate prediction for the eccentricity of this object.

Figure 4-3 shows the long-term variations in inclination for the ERS-1 upper stage. The object is in a sun-synchronous orbit with an initial retrograde inclination of 98.4°. The decrease in inclination over nearly 6 years is quite insignificant at around 0.2° and appears to be a very long-period oscillation because the decrease levels off during 1998. The long-period oscillation is most likely due to a resonance with the solar radiation pressure effects in this sun-synchronous orbit (SSO). The predictions of the IDES orbit propagator agree very well with the TLE data here, both in trend and magnitude.

The secular precession of argument of perigee with time due to the effect of the second harmonic in Earth's gravitational field is presented in Figure 4-4. This secular drift is roughly at a frequency of 3 revolutions per year, and is typical of a near-circular low Earth orbit. The IDES orbit propagator produces very good predictions for this orbital element. Not shown here is the evolution of the right ascension of the ascending node, which increases in a secular manner through its 360° range with a period of about 1 year. The 98° inclination is designed to rotate the SSO plane at the same rate as the Sun around the Earth.

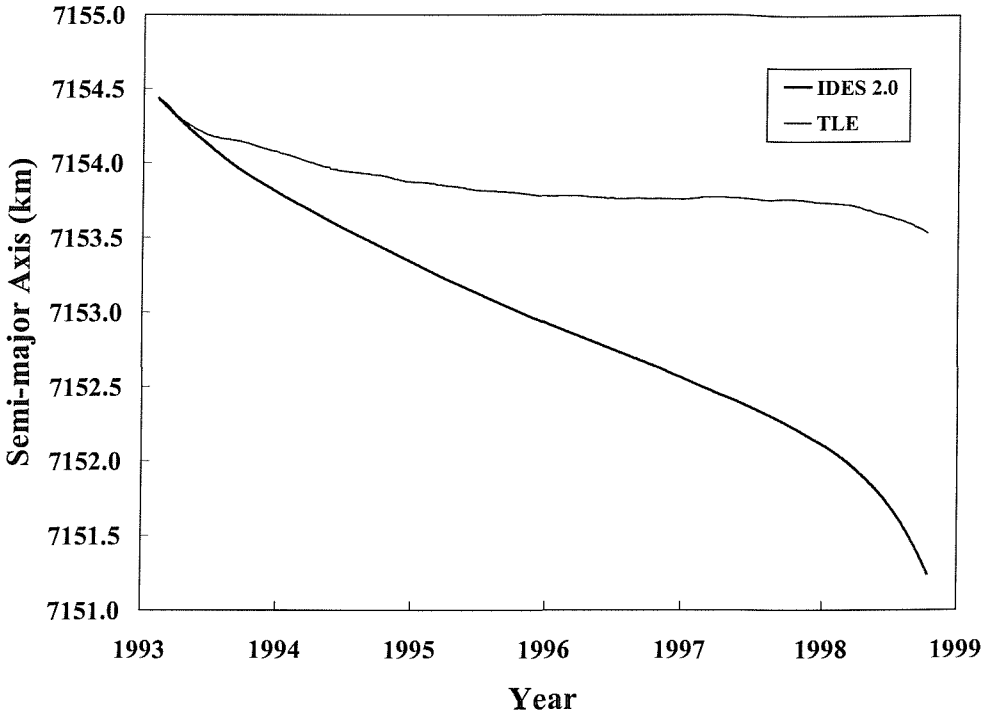

Figure 4-1: IDES long-term predictions of semi-major axis for an Ariane 4 stage 3 (1991-050F) in LEO compared to two line element (TLE) data

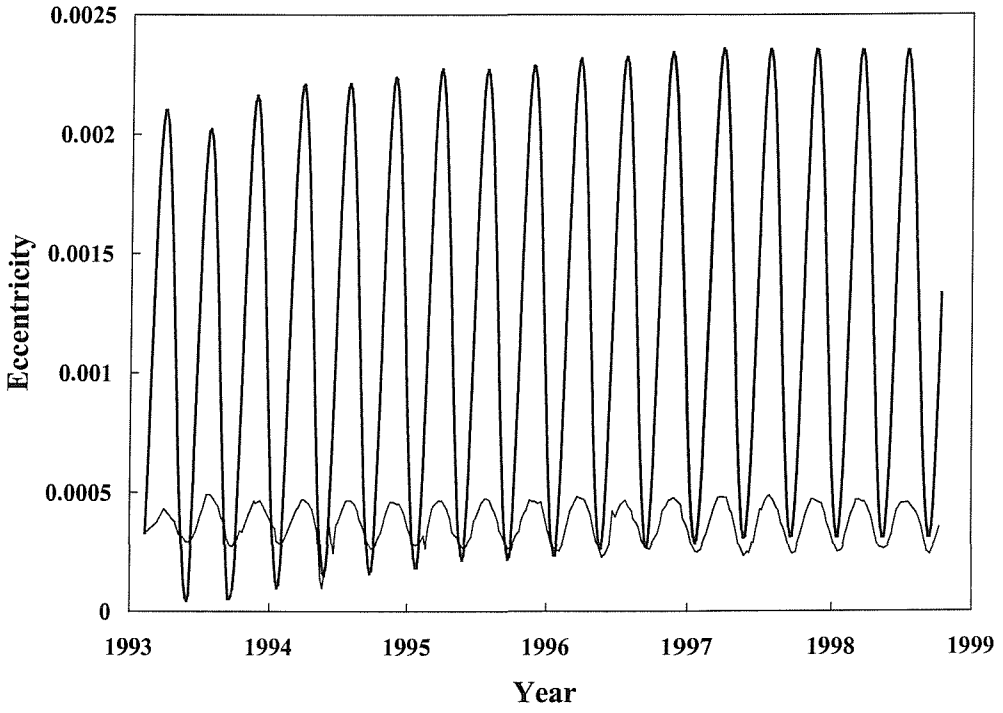

Figure 4-2: IDES long-term predictions of eccentricity for an Ariane 4 stage 3 (1991-050F) in LEO compared to two line element (TLE) data

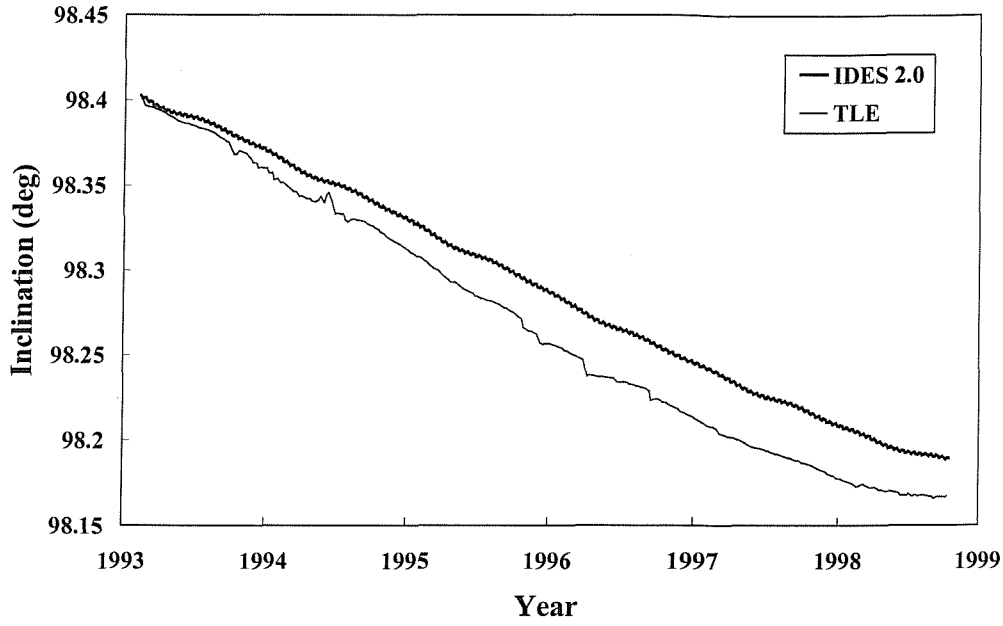

Figure 4-3: IDES long-term predictions of inclination for an Ariane 4 stage 3 (1991-050F) in LEO compared to two line element (TLE) data

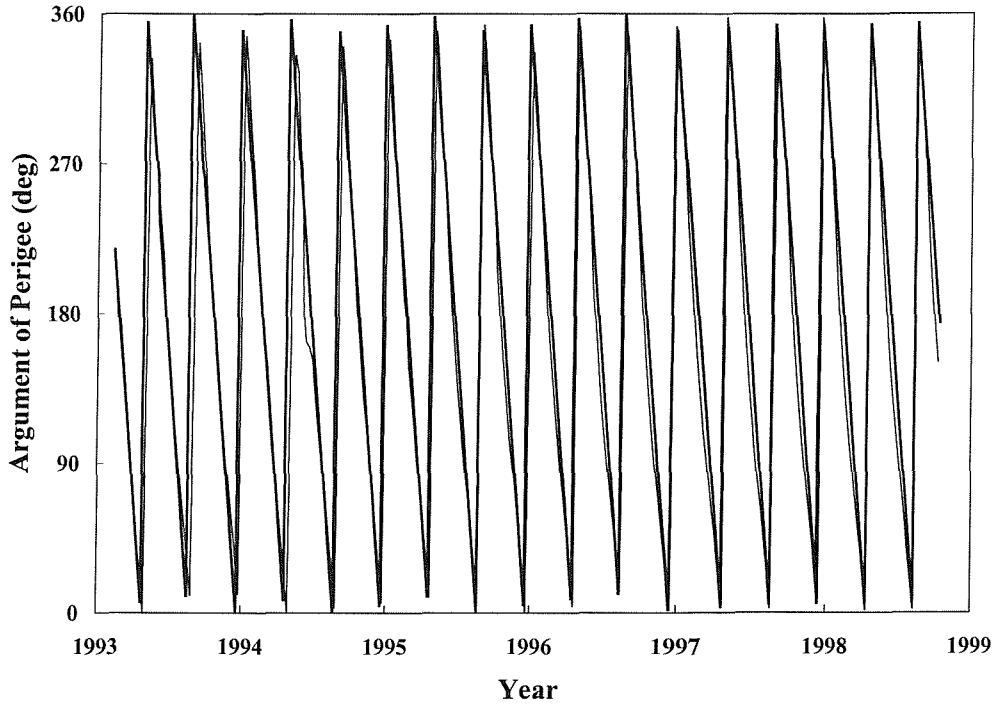

Figure 4-4: IDES long-term predictions of argument of perigee for an Ariane 4 stage 3 (1991-050F) in LEO compared to two line element (TLE) data

As the second example of orbit evolution, a Russian Molniya launch vehicle 4th stage (COSPAR ID 1993-002D) was chosen. This upper stage is in a Molniya-type orbit with high eccentricity (~0.7) and inclination near the critical inclination of 63.4°. In this orbit, luni-solar and geopotential perturbations are expected to dominate the orbit evolution. The object has a low area-to-mass ratio and Molniya orbits tend to have perigee height oscillations that give a minimum height of about 500 km, so the atmospheric drag effects are expected to be small. Solar radiation pressure perturbations should also be insignificant due to the low area-to-mass ratio.

Figure 4-5 presents the evolution of semi-major axis for this object. The scatter in the TLE data between 1993 and 1998 is a measure of tracking errors because it is known that the Space Surveillance Network (SSN) has difficulty cataloguing objects in Molniya-type orbits. In both the predictions and the TLE data, semi-major axis decreases slightly between 1993 and 1995, before levelling off after 1995. This is due to atmospheric drag decaying the orbit as the luni-solar perturbations lower the perigee height to a minimum of 500 km at the beginning of 1994. The perigee then rises well above the atmosphere to a maximum height of 1900 km in 1998. There are small oscillations in semi-major axis that were found to be due to solar radiation pressure effects. The small changes occurred at times when portions of the orbit were in the Earth's shadow. Overall, the orbit propagator shows a reasonable agreement with the TLE data for semi-major axis (only 3 km maximum difference) over the six year period of evolution.

The evolution of the Molniya object's eccentricity between 1993 and 1998 is given in Figure 4-6. There is a very low frequency, long-period oscillation that causes eccentricity to vary between 0.69 and 0.75. This was found to be due to the effects of luni-solar perturbations. Much shorter period oscillations can be observed that have much lower amplitudes, and these are again due to the third body gravitational attractions of the Sun and Moon. The IDES orbit propagator displays a very close correlation with the TLE data and shows a very good accuracy for eccentricity.

The long-term variations in inclination for this object are dominated by luni-solar perturbations (see Figure 4-7) which cause a very long-period oscillation that passes through the critical inclination of 63.4° to a maximum at 65°. Overall, luni-solar effects cause a 2°

change in inclination of this Molniya-type orbit over the 6 years of evolution. Again, the IDES orbit propagator is very effective at closely matching the TLE data.

For an object in a Molniya-type orbit such as the example chosen, the argument of perigee behaviour over time is very different from the normal secular drift observed for near-circular, low Earth orbits. This can be seen in Figure 4-8 where argument of perigee remains almost constant at a maximum of 288° between 1993 and 1994. As one would expect, this is where the inclination is very close to or at the critical inclination of 63.4°, where the rate of change in argument of perigee is zero. After 1994, the inclination increases towards its maximum of 65° between 1996 and 1998 and the rate of argument of perigee precession increases again. This produces what appears to be a linear decrease in argument of perigee between 1996 and 1998. The behaviour in the evolution of this orbital element is being driven by the first order, second zonal (J_2) spherical harmonic coefficient in the Earth gravitational field, relating to the Earth's oblateness. The IDES orbit propagator predicts this behaviour with very good accuracy. The J_2 perturbation is also responsible for a slow, constant secular regression in the right ascension of ascending node of this Molniya orbit.

Generally, it can be concluded that the IDES orbit propagator is able to predict the long-term evolution of Molniya-type orbits with very little error. This is due to the fact that the orbit evolution is dominated by luni-solar and geopotential perturbations, and the analytic theory used to model these effects is found to be extremely effective.

Many other upper stages have been chosen as test cases, including low inclination, near-circular LEOs, and highly eccentric, low inclination geostationary transfer orbits. The figures presented above are purely illustrative of the validation process, but do indicate that the analytic IDES orbit propagator considers all perturbation effects and is sufficiently accurate for the purpose of debris population evolution. Further tests of the IDES orbit propagator were conducted over much longer projection periods of 100 years. The propagator remained stable with integration timesteps of up to 8 days (4 day timesteps were used in the above results), and took as little as 1.5 seconds of computer processing time on a 170 MHz Sun Ultra workstation to propagate an orbit over the 100 year period.

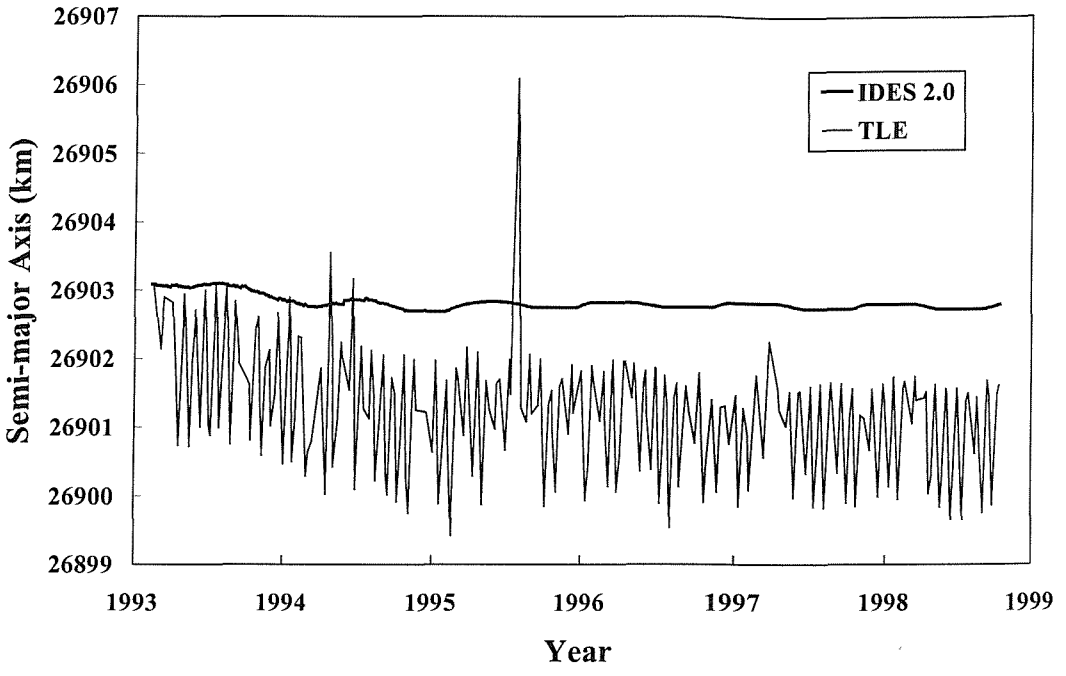

Figure 4-5: IDES long-term predictions of semi-major axis for a Molniya stage 4 (1993-002D) in highly-eccentric Molniya-type orbit compared to TLE data

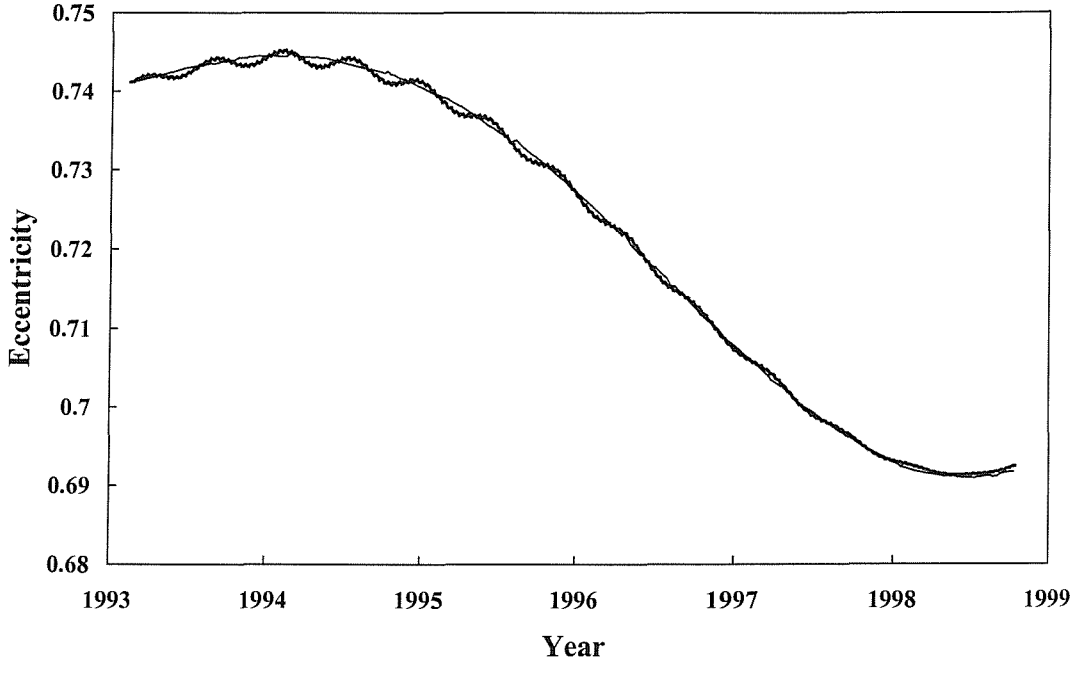

Figure 4-6: IDES long-term predictions of eccentricity for a Molniya stage 4 (1993-002D) in highly-eccentric Molniya-type orbit compared to TLE data

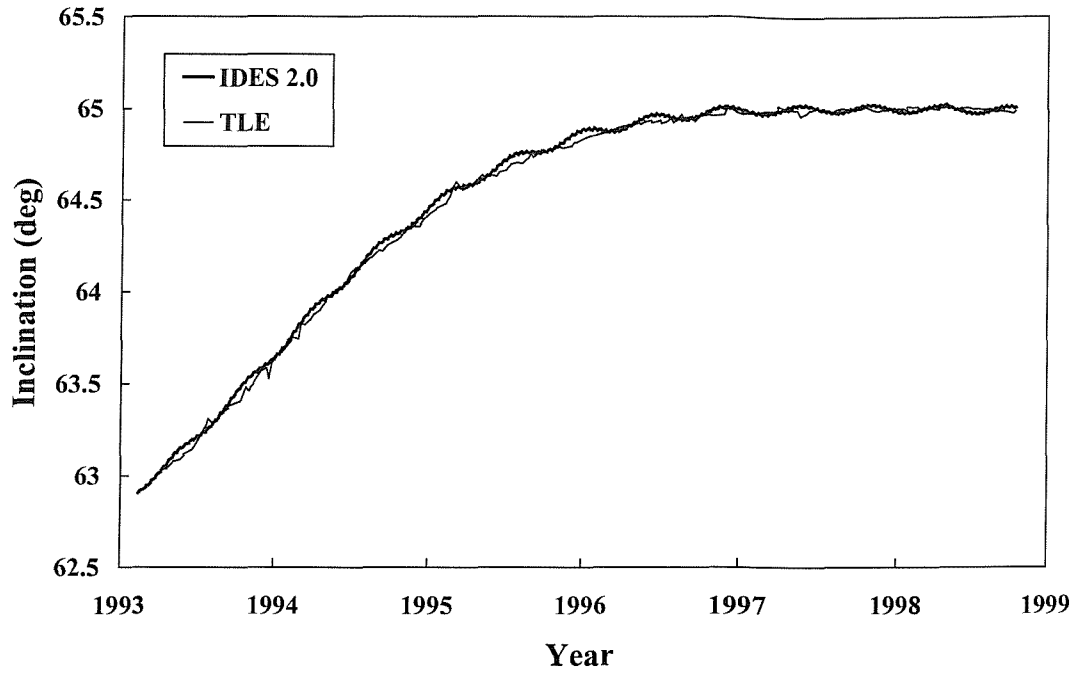

Figure 4-7: IDES long-term predictions of inclination for a Molniya stage 4 (1993-002D) in highly-eccentric Molniya-type orbit compared to TLE data

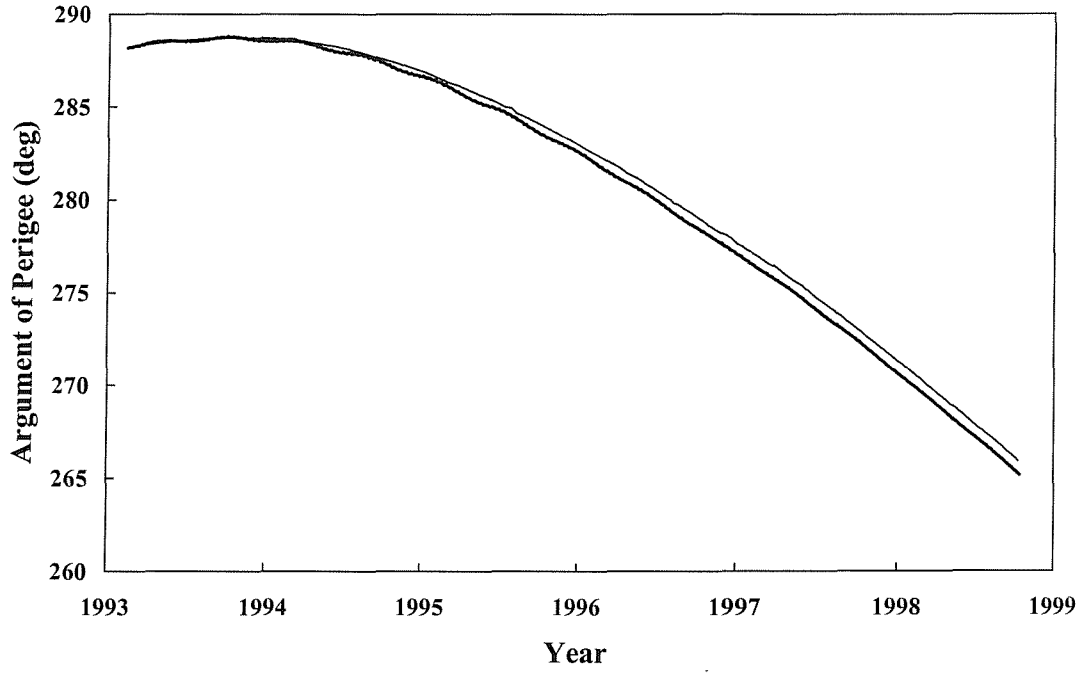

Figure 4-8: IDES long-term predictions of argument of perigee for a Molniya stage 4 (1993-002D) in highly-eccentric Molniya-type orbit compared to TLE data

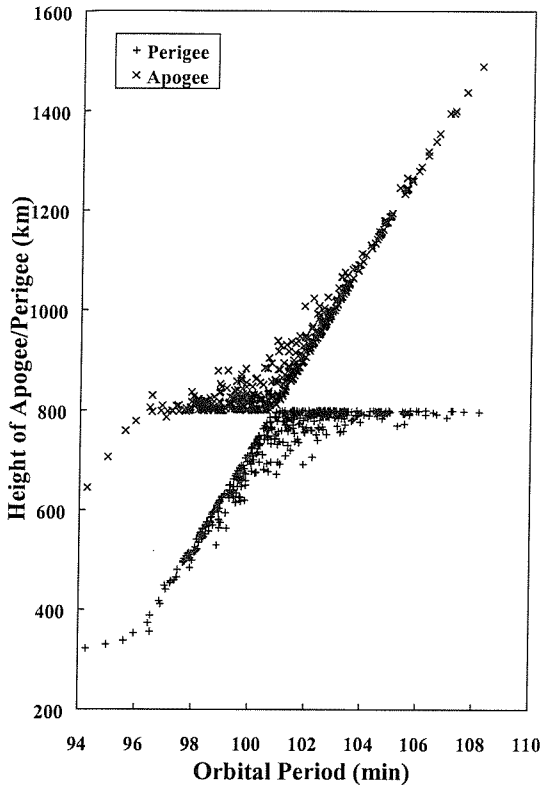

Figure 4-9: Gabbard diagram for the IDES simulation of the SPOT-1 rocket body fragmentation

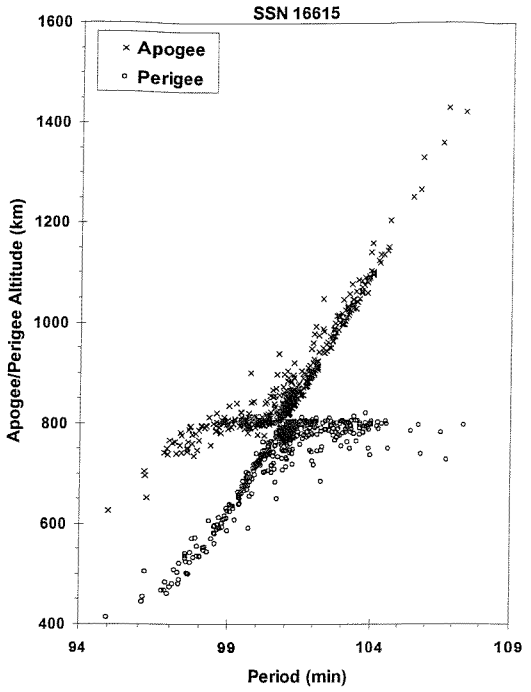

Figure 4-10: Gabbard diagram of the tracked fragments from the SPOT-1 rocket body fragmentation[95]

4.2.2 Fragmentation Model

Validation of the IDES breakup model can be performed by simulating selected historical on-orbit fragmentations and then comparing the orbital distribution of modelled debris clouds with distributions of the actual debris clouds, as recorded in the USSPACECOM catalogue.

The accuracy of the IDES breakup model was tested by simulating the fragmentation of the SPOT-1 rocket body in November 1986 at 800 km altitude. The orbital distribution of the simulated debris cloud of >10 cm fragments can be compared to the distribution of tracked fragments from the breakup[95]. However, the tracked fragment data was presented for an epoch 3 months after the event had occurred. Therefore, the validated IDES orbit perturbation model was used to propagate the simulated fragments by this time interval.

With a breakup mass of 1634 kg, the breakup model generated 421 fragments, which compares well with the catalogued number of 489.

The Gabbard diagrams of Figure 4-9 and Figure 4-10 show the distribution of apogee and perigee heights against orbital period 3 months after the breakup event for the simulated and tracked clouds respectively. The simulated cloud has a very similar distribution to that of the tracked cloud, particularly for orbital periods of lower than 97 minutes, where fragments have perigee heights deep in the atmosphere below 600 km. Atmospheric drag causes these fragments to decay, thus lowering their perigee and apogee heights before disintegration in the lower atmosphere. Most fragments still remain spread within 200 km above and below the 800 km breakup altitude. Even at decimetre sizes (where delta-velocities are lower than for centimetre and millimetre sizes), fragments are dispersed with perigees at the breakup altitude and apogees as high as 1500 km (see the right hand limbs of the Gabbard diagrams). These fragments correspond to impulses imparted in the direction of motion of the parent object. Some fragments receive delta-velocities that oppose the direction of motion, leading to apogees remaining at the breakup altitude and perigees as low as 400 km (see the left hand limbs of the Gabbard diagrams).

4.3 Validation of the Low Earth Orbit Debris Environment Model

4.3.1 Historical Evolution of the Orbital Debris Environment

During an historical evolution simulation, IDES calculates the size-dependent debris density environment in high-resolution, three-dimensional space (discretised by geocentric radius, declination, and right ascension) at regular time intervals of 6 months. Figure 4-11 and Figure 4-12 show the spatial density versus altitude versus year for >10 cm and >1 cm debris sizes respectively. They are a good visualisation of historical evolution and allow a 'first-look' validation by correlating the occurrence of certain spatial density peaks with historical debris source events. The debris environment larger than 10 cm is partly dominated by fragments from breakup events and partly by launch-related objects. Breakup events can be seen in the figures as sharp steps in spatial density around a specific altitude at a particular point in time. An example is in Figure 4-11 at 950 km altitude in the year 1961. This was the first ever recorded breakup event and was identified as a low intensity, propulsion-related explosion of the Ablestar rocket upper stage which was used to launch

the US Transit 4A spacecraft. It can be seen that the breakup cloud was distributed with a peak spatial density at the breakup altitude and a spread 400 km above and below this altitude. Since the event was modelled as a low intensity explosion, very few fragments were generated at sub-decimetre sizes. This explains the fact that the breakup cloud is not visible in the >1 cm debris environment evolution in Figure 4-12. The influence of launch-related objects on the >10 cm environment evolution is evident by the smooth, gradual build-up in spatial density over time at some of the most popular operational altitudes. For example, Figure 4-11 shows distinct ridges developing over time at 800 km, 1000 km, 1400 km and 1500 km altitudes.

The historical debris environment at sizes larger than 1 cm is dominated by fragments from high intensity explosions and by the sodium-potassium (NaK) coolant droplets. The centimetre-sized environment did not really exist until the deliberate detonations of the Russian Cosmos 50 and Cosmos 57 spacecraft between 200 and 400 km altitude at the turn of the year 1965. While the Cosmos 50 debris cloud decayed very quickly due to fragment perigee heights near the 200 km breakup altitude, the Cosmos 57 cloud has a peak at 400 km with longer fragment orbital lifetimes. In Figure 4-12, a sharp step in spatial density can be seen throughout LEO in 1965. The Cosmos 57 cloud is widely dispersed throughout the LEO regime. After 1965, the figure clearly shows that the centimetre-sized debris environment continued to be defined by these events. Although some events occurred at very low altitudes, many self-destruct events were executed at higher altitudes leading to fragments with long orbital lifetimes and growth in the >1 cm population. These events were most prevalent in the 1980's (between 2 and 3 per year) and this can be observed by the large increases in spatial density at altitudes up to 800 km during that decade. After 1988, most detonation events ceased and the fragment population decayed moderately during the following solar maximum around 1990. The dominating effect of NaK coolant droplets on the >1 cm environment at altitudes between 800 and 1000 km can be clearly seen in Figure 4-12. Droplet leakage has been associated with Russian RORSATs in their nominal graveyard orbit. Some 16 such leakage events were identified and these occurred between 1980 and 1988. During this period the spatial density around 900 km increased to a factor of 7 above the fragment background environment, according to IDES. After 1988, the droplet peak decayed to a factor of 5 higher than the fragment background in 1998.

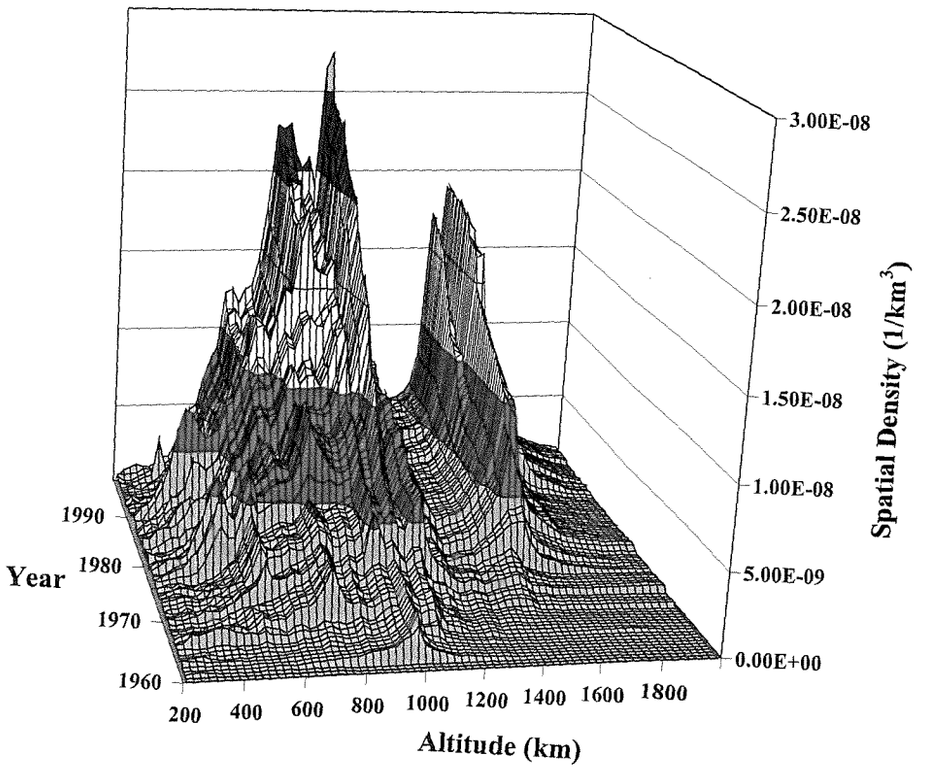

Figure 4-11: Historical evolution of the >10 cm debris environment in low Earth orbit from 1/10/1957 to 31/3/1998

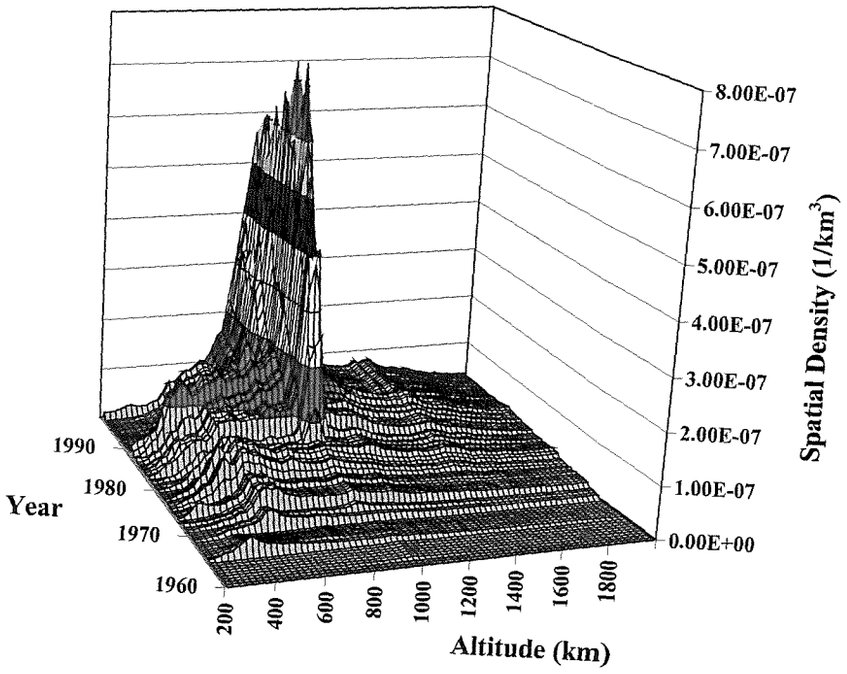

Figure 4-12: Historical evolution of the >1 cm debris environment in low Earth orbit from 1/10/1957 to 31/3/1998

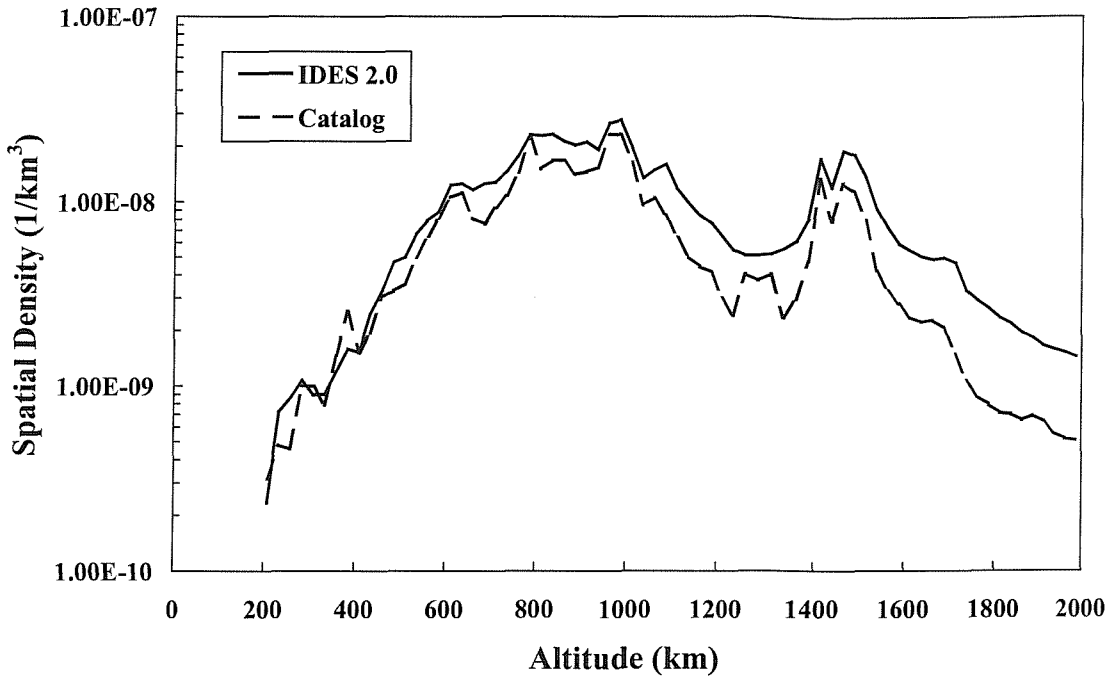

Figure 4-13: Comparison of IDES >10cm and USSPACECOM catalogue spatial density distributions on 31st March 1998

4.3.2 Comparison to Measurements at Decimetre Sizes

The historical flux environment snapshots output by IDES are accessed in order to produce the model predictions for comparison with measurement data. Firstly, the IDES 1998 spatial density distribution of >10 cm debris over LEO altitudes is determined and compared with the spatial density distribution of objects in the 31st March 1998 USSPACECOM catalogue. For validation of the large-size debris environment predictions, the comparison of the IDES spatial density distribution of >10 cm objects in LEO with the corresponding USSPACECOM catalogue distribution is shown in Figure 4-13. Both curves display the characteristic peaks in spatial density at 800, 1000, 1400 and 1500 km. The IDES predictions are generally in good agreement with the catalogue.

At some altitudes, particularly above 1000 km, the model predictions are up to a factor of 2 higher than the measured environment. However, the IDES model accuracy is considered to be reasonable since there is evidence to suggest that the catalogue is incomplete[24] due to the reduced sensitivity of the ground radar sensors, for the 10 cm size limit at these higher LEO altitudes. In fact, the detection threshold of 10 cm is estimated to increase as altitude

increases up to 2000 km. Therefore, some decimetre-sized breakup fragments will not be tracked or catalogued in this region, whereas the model does simulate and include these breakup fragments in its population. In some regions, the spatial density is strongly influenced by launch-related debris. Thus, the figure shows that the use of the historical launch database (and subsequent propagation of launch-related objects) is valid and retains the accuracy of the model.

4.3.3 Comparison to Measurements at Centimetre Sizes

In order to compare the IDES predictions of the centimetre-sized debris environment with Haystack radar measurements, it is necessary to use a radar simulation model that can convert an IDES flux environment snapshot into the number of debris objects per hour crossing the field-of-view of the Haystack radar beam. The field-of-view model developed by NASA to compare the EVOLVE model with the Haystack data is used here[29]. The radar beam, in a fixed staring (near-vertical) mode, is divided into 5 km range intervals from 350 km to 1250 km. The centre of each range interval is a 'detection site', which lies within a particular radius-declination cell of the IDES control volume containing a number of debris flux vectors. Each debris flux vector consists of a spatial density value and a velocity vector represented by velocity magnitude, azimuth and elevation in the cell reference frame.

The velocity magnitude perpendicular to the beam is determined and multiplied by the spatial density to obtain the debris flux of that vector crossing the beam. After a summation of the contributions from all debris flux vectors in the cell, the total flux perpendicular to the detection site is multiplied by the perpendicular cross-sectional area of the beam range interval and the unit time is adjusted to 1 hour. The resulting value is the detection rate (the number of debris objects detected per hour) for a given range interval, assuming the Haystack radar has a 100% probability of detection for debris of 1 cm and larger. The distribution of detection rate over all 5 km range intervals is then averaged every 50 km and directly compared to the Haystack data from fiscal year (FY) 1995, which is the closest to the IDES flux environment snapshot of 1st January 1996.

This IDES snapshot of the >1cm debris environment was post-processed by the radar simulation model for the Haystack radar beam orientation during the observation period. The predicted detection rate distribution over altitude is compared to the measured

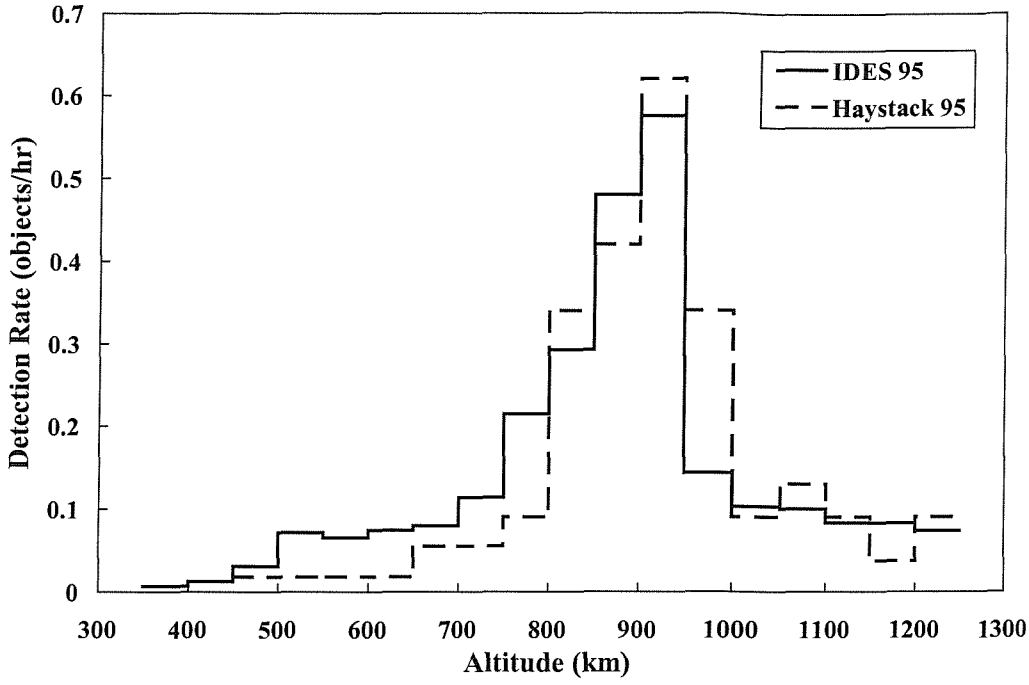

Figure 4-14: Comparison of IDES predictions and measured detection rates of debris larger than 1 cm in LEO for the US Haystack radar

distribution in Figure 4-14. In order to make a direct comparison, the Haystack data is presented for the detection of objects larger than 1 cm, rather than for the total data set which also contains the detection of debris of a few millimetres.

The plot shows that IDES is in very good agreement with Haystack measurement data at altitudes above 1000 km and is a factor of 2 or less over-predicting the detection rate between 450 and 800 km altitude. This is reasonable, considering the possible differences between the fragment size-to-mass relationship used in IDES and the estimated size distribution inferred from Haystack calibration experiments. Between the altitudes of 850 km and 1000 km, the Haystack measured detection rates increase sharply by a factor of 5, due to the NaK droplet population[77]. IDES is now able to predict this debris source population, and is therefore able to match the Haystack measurements very well in this region. Another potentially significant source of centimetre-sized orbital debris is the operation of Solid Rocket Motors which can, according to many authors[96,97,98], release 'slag' particles near or after the completion of the burning process. Slag particles are a hot liquid mixture of aluminium oxide and unburnt aluminium solidifying upon ejection. While it is not currently necessary to include this source in the IDES model (due to the reasonable

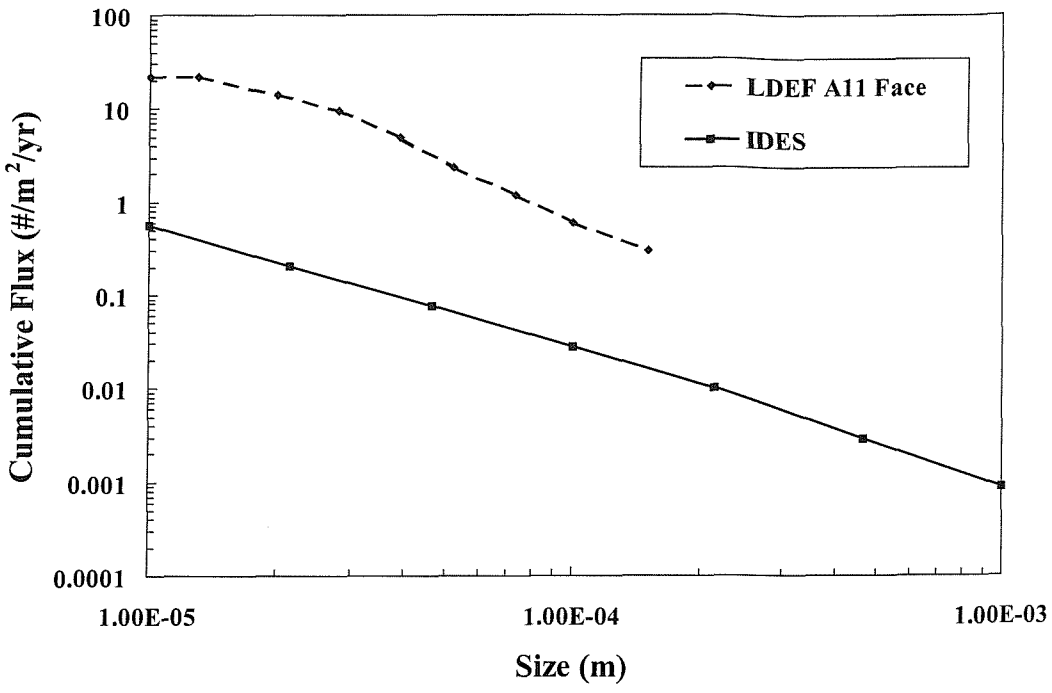

Figure 4-15: Comparison of size-dependent debris impact flux as predicted by IDES and the inferred measurement data from the A11 (52 deg) forward face of the retrieved LDEF spacecraft

comparison of the model with the Haystack measurements) it should be considered in a future version of IDES in order to further refine the model's accuracy at centimetre sizes.

4.3.4 Comparison to Measurements at Sub-millimetre Sizes

The historical flux environment snapshot output by IDES for the epoch 1st July 1987 (near the mid-point of the LDEF mission) is utilised by the IDES risk assessment program to predict the average cumulative debris flux relative to the LDEF orbit for 7 different size thresholds, ranging from 10 microns to 1 mm. The LDEF orbit of 416 km altitude, 28.4° inclination at this epoch is used to transform the debris flux vectors, encountered in the volume cells intersected by the orbit, into relative flux vectors in the spacecraft-centred moving reference frame. The relative flux vectors are multiplied by the residential probability of the orbit in the respective intersected cells, and summed to obtain the orbit-integrated mean debris flux to LDEF for each size threshold. The predictions can then be compared with the LDEF debris flux data given in the same format by Hörz *et al*[94].

The comparison of predicted debris impact flux for the LDEF orbit on 1st July 1987 with the measured flux for the A11 (52°) forward face (which encountered most of the impacts) is

shown in Figure 4-15. At a size threshold of 0.1 mm, the IDES predictions are an order of magnitude lower than the measurement data. At the lower size threshold of 10 microns, the under-prediction increases to a factor of 40. Possible reasons for this are discussed in the chapter summary (section 4.5)

4.4 Comparison with Other Debris Models

In March 1997, some IDES model predictions were compared to those of other major space debris environment models in use world-wide. Jehn *et al*[99] compared IDES, MASTER (ESA), CHAINEE (TU Braunschweig, Germany), ORDEM96 and EVOLVE (NASA, USA), SDM/STAT (CNUCE, Italy), and the Nazarenko SDPA model (Russia) in the centimetre size range for low Earth orbit. All these models have good agreement with each other for sizes larger than 10 cm because the environment is well known, due to the data on tracked objects from the US and Russian space surveillance catalogues. The models include these comprehensive measurements in one way or another. However, this was the first time that so many international models had been compared at these smaller sizes where measurement data is more sparse and hence where the environment is less well understood. As a result of the poor amount of measurement data at these sizes, both on the debris environment and debris source processes, there are many uncertainties in debris environment modelling. Each of the models employs a different set of source/sink sub-models and so unsurprisingly, the comparison found large differences between the models. Each model predicted a spatial density distribution of debris >1 cm between 150 km and 2000 km altitude in 50 km altitude bins for a reference epoch of 1st January 1997. The spatial density distributions of all the models were plotted together on a linear scale and compared in detail (see Figure 4-16).

In some cases, particularly at 900 km and 1500 km, the uncertainties between models were as high as an order of magnitude. The IDES model results were generally in the middle of the bounds of uncertainty, except between 800 and 1000 km where the NaK liquid coolant droplet population of centimetre-sized objects has been found by radar measurements. The American and Russian models feature this peak, whilst others such as IDES, SDM and MASTER did not include this source at the time the comparison was made. However, these models have since been upgraded to include the NaK droplet population[59,100], and therefore, a new comparison between the models would be much closer in this region. At all other

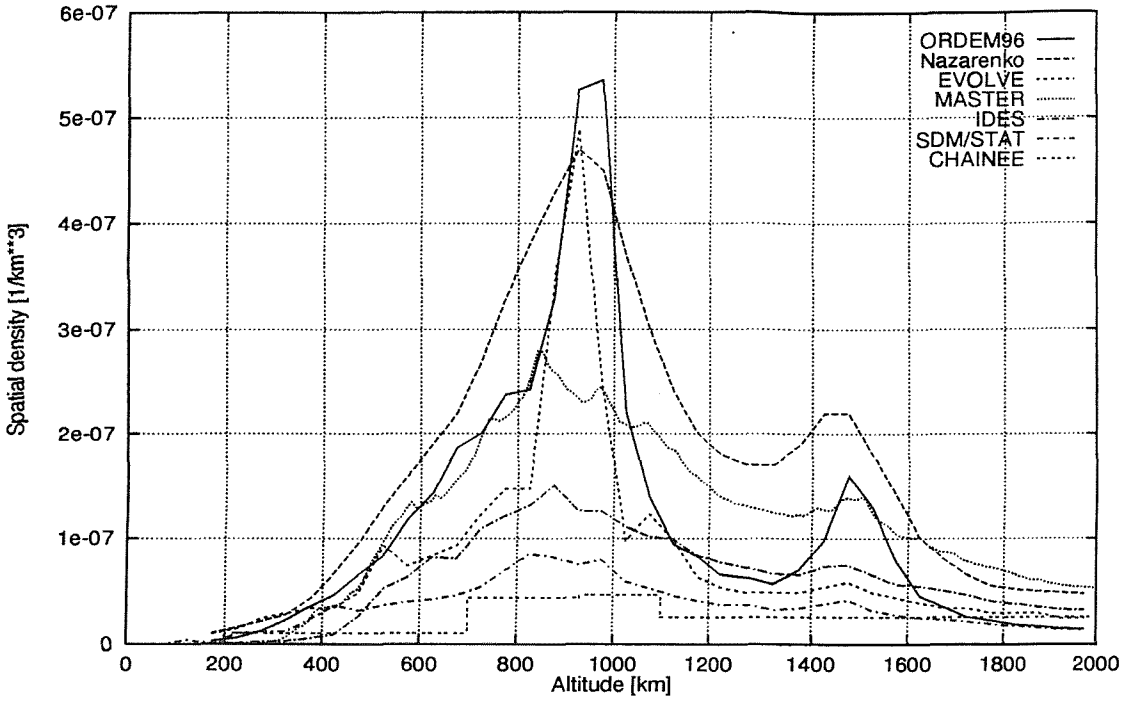

Figure 4-16: Spatial density distributions for objects >1 cm on 1/1/97 predicted by different space debris models[99]

altitudes, IDES compared very well with the NASA EVOLVE model. NASA's ORDEM96 model and ESA's MASTER model were generally a factor of 2 higher than IDES at most altitudes except between 800 to 1000 km. It should be noted that the spatial densities of the ESA MASTER model were scaled by a factor of 4.4, for objects larger than 1 cm. Without this scaling, the actual simulated MASTER results would have been about a factor of 2 below the IDES predictions and quite similar to the SDM/STAT model values.

In the same paper, Jehn also derived a method for taking the measured detection rate of the Haystack radar (the main source of measurement data at this size range) in a given altitude bin and calculating the spatial density confidence intervals based on the number of observation hours of Haystack. This enabled the model spatial densities to be directly compared with the statistical uncertainties in the measurement spatial densities. Jehn found that between 700 and 750 km, only IDES and EVOLVE were within the confidence interval of the Haystack radar measurements. MASTER (with its 4.4 scaling factor) and ORDEM96 were 20% higher than the confidence interval in this altitude range. This is a very good technique for comparing models with measurements and Jehn and Klinkrad have applied it over the entire LEO altitude regime when comparing the MASTER model with detection

data from the COBEAM 1/96 radar measurement campaign[101]. It should be applied more widely to validate all debris models against the altitude-dependent detection data from all ground-based radar measurements worldwide.

IDES has also participated in a comparison of long-term evolution models as part of a United Nations paper on space debris modelling. Future environment projections from IDES, EVOLVE, SDM, CHAINEE, CHAIN, and the SDPA model were compared for a 'business as usual' scenario (constant launch and explosion rates as in the recent past) over the next 100 years. It was found that the IDES predictions (with no constellations modelled) and the EVOLVE predictions were very similar to each other for the cumulative number of catastrophic collisions and the growth in the centimetre-sized LEO debris population over the next 50 years. Further comparisons between long-term evolution models are being conducted for the ongoing activities of the Environment and Database Working Group of the Inter-Agency Debris Co-ordination Committee (IADC). In the comparison for the United Nations paper, there was a very wide divergence between the long-term projections of different models because initial/boundary conditions and input data were not standardised or co-ordinated. The IADC working group has been instrumental in agreeing on a standardised framework and common datasets for model comparisons in the future, and this should eventually resolve most of the large differences seen in previous long-term projection comparisons.

4.5 Summary

Simulations of the historical evolution of the low Earth orbit debris environment have been made using the IDES model. These simulations have provided a valuable insight into the dynamics of the debris environment and its emerging characteristics at particular altitudes, points in time, and particle sizes. For object sizes larger than 10 cm, step increases in the spatial density were observed due to discrete breakup events. Gradual build-up in spatial density at the most popular operational altitudes could be seen due to objects associated with launch activity. For object sizes larger than 1 cm, the spatial density in the 800 to 1000 km altitude band was found to have increased by up to a factor of 7 during the 1980s, due to the assumed leakage of liquid metal coolant from Russian RORSATs. This modelled peak did not decay significantly during the 1990s. The mechanism of these leakages seems to have arisen from the procedure to dispose of RORSAT nuclear power systems in a safe,

high altitude graveyard orbit. The procedure was implemented following the hazardous atmospheric re-entry of the Cosmos 954 nuclear powered spacecraft in 1978. Such a substantial increase in object density demonstrates that the methods of post-mission disposal and the use of graveyard/storage orbits must be considered very carefully in the future.

The current debris environment predicted by IDES has also been validated by comparison with measurement data. The IDES >10 cm debris environment for 31st March 1998 shows a good agreement with the USSPACECOM catalogue environment, except at altitudes above 1000 km where IDES is a factor of 2 higher than the catalogue. However, these discrepancies may be explained by the incompleteness of the catalogue at these altitudes. The IDES >1 cm debris environment produces detection rates in the Haystack radar beam that are reasonably similar to the measured rates at all altitudes. There are no longer significant under-predictions by the IDES model around 900 to 1000 km, since the latest version (2.0) introduced a model of the NaK coolant droplet debris source. It has been deduced that this source is responsible for the sharp peak in the centimetre-sized population in this region. At a size threshold of 0.1 mm, the IDES predictions for the debris flux to the LDEF spacecraft are an order of magnitude lower than the measurement data. At the lower size threshold of 10 microns, the under-prediction increases to a factor of 40.

This significant discrepancy at small sizes can be partially explained by the possible under-prediction of breakup models. However, non-fragmentation sources not currently modelled by IDES may be a more significant cause of this under-prediction. Such sources include paint flakes generated by surface degradation due to atomic oxygen erosion, thermal cycling, and UV radiation, and also alumina (Al_2O_3) particles expelled as by-products during Solid Rocket Motor (SRM) burns. All of these particle types are known to be present at very small sizes in the LEO environment, because they have been found as residues in the impact craters of space-returned surfaces on LDEF[94] and the Space Shuttle[102]. By including these source processes in a future version of IDES, it may be possible to narrow the model under-prediction of the small-size debris population. As an example, a research programme in this area is currently being conducted at the Queen Mary and Westfield College, University of London with a requirement to develop a paint flake source model from thermal cycling/atomic oxygen/ultra violet radiation effects[103]. Once completed, this source model will be integrated into the IDES model.

5 The Effects of a Large Satellite Constellation on Long-Term Debris Evolution

5.1 Introduction

An increasing number of multiple satellite constellations providing global mobile telecommunications will be launched into the low Earth orbit region within the next decade. These systems could be utilised for many years in a growing debris environment that presents a significant long-term collision hazard. Most LEO constellations will be deployed in the regions of peak debris density at high inclinations where the debris collision risk is greatest.

The modern day concept of satellite constellations that provide optimal, continuous multiple whole Earth or 'global' coverage for communications purposes was proposed by Walker[71] in 1971. Walker suggested a design for satellites operating in a number of equally spaced, highly inclined circular orbit planes, such that their relative phasing formed either a 'delta' or 'star' pattern. Other phasing strategies were developed later by Adams and Rider[104]. The constellations to be deployed in the next few years are mostly based on these designs, but they vary widely in size, operational orbits and function. For example, the Globalstar design comprises 48 satellites just above 1400 km altitude and will provide mobile narrowband voice communications[105]. In contrast, the original Teledesic constellation design had an 840 satellite configuration to be operated at 700 km altitude and offering high rate broadband data transmission for services such as video-conferencing or high performance Internet access[106]. Indeed, it was the sheer size of proposals such as this, which prompted the study of the possible long-term effects of a large constellation on the debris environment in low Earth orbit. A large constellation is defined here as a system of more than 100 satellites. Although the Teledesic design has now been scaled back to 324 satellites (including spares), it was necessary to consider the long-term effects of deploying and operating a constellation of over 800 satellites in order to find the upper boundary of constellation-debris collision interactions in such an extreme case.

Until recently, orbital debris research associated with constellations has mainly been concerned with short-term and long-term collision cascading within the system itself[7]. Only a limited study had previously been performed with IDES to model the potential long-term collision interactions between constellations and the background debris environment[107]. This suggested that a large generic constellation placed in a region of high debris density would suffer a number of fatalities, resulting in a larger debris population in the next 20 years. At the same time, research into long-term environmental effects of constellations has also been conducted by Anselmo/Rossi *et al*[55,67,108,109] in Italy, Reynolds *et al*[53,110] in the United States and Bendisch *et al*[111] in Germany. There has been concern by researchers that the large increase in mass and area at critical altitudes due to constellations may accelerate long-term debris growth in LEO and trigger collision cascading in the background debris environment much earlier than previously estimated.

The extent of accelerated population growth due to constellations depends upon the level of collision interactions between the constellations and the background debris environment. A large constellation system may suffer a number of satellite fatalities from collisions with debris fragments in the long-term. A fatality is defined as a collision event that has enough energy to cause a catastrophic fragmentation of the target object. Each of these breakup events will spread more fragments into the environment local to the large constellation, thus increasing the collision risk to both the constellation and large background objects, such as spacecraft, rocket upper stages and operational debris. This increase in risk may produce more collisions for large background objects near the constellation altitude, which would further enhance the risk to produce more constellation collisions and so on. This localised effect can be considered as a *long-term collision coupling* between a large constellation and the background debris population. The IDES model is used to study this phenomenon. No detailed study of these problems has previously been performed.

In the same time-frame as the planned satellite constellation deployments, a number of different measures have been proposed in order to mitigate the long-term growth of the debris population and the possibility of collision cascading. These debris mitigation measures are the steps taken during launch and mission operations in order to avoid or reduce debris generation now and in the future. Research conducted into the long-term evolution of orbital debris has found that the debris population may grow exponentially[64],

eventually leading to a self-sustaining chain reaction of collisions[5]. As a consequence, this could pose a significant collision risk to future space systems in LEO. Various mitigation measures have been proposed in order to reduce the production of different types of debris. These include: tethering launch and operations-related objects to the vehicle; venting residual fuel and discharging batteries on spacecraft and launcher upper stages to prevent on-orbit explosions (eg. on ESA Ariane launchers[112]); and performing end-of-life manoeuvres using chemical or electric propulsion[113] to de-orbit or reduce the post-mission orbital lifetime of spacecraft and upper stages. The latter option is recognised to be the most effective mitigation measure because it minimises the growth rate of the large objects that contain most of the mass and area which could be involved in further collisions. It has been found that a combination of explosion prevention and routine de-orbiting (or lifetime reduction) could stabilise or even control long-term population growth[46,54, 66,111].

A significant increase in collision activity associated with large LEO constellations has implications for reducing the effectiveness of routine mitigation measures. Enhanced collision activity would spread additional debris fragments and tend to cause increases in the population growth, thus acting against decreases in the population growth due to the mitigation measures. The IDES model is also used here to reveal the balance between these two factors and hence their net effect on the long-term evolution of the orbital debris environment. The study presented in this chapter was published elsewhere[114,115] and was conducted with version 1.0 of the IDES model, before major enhancements were made for the version 2.0. The most notable differences are that in the earlier version, there is a lack of RORSAT NaK droplet modelling, a lower resolution launch traffic database and an earlier reference epoch of 1st January 1996. However, the lack of these enhancements does not invalidate the study, and valuable insights into the long-term impact of a large constellation on the debris environment can still be gained.

5.2 Modelled Future Traffic Scenarios

Due to the statistical nature of modelling future debris sources such as collisions, explosions and launches, IDES is used in a Monte Carlo mode to represent different statistical permutations. In order to obtain a reasonable statistical average of the impact of large-scale constellation operations on long-term debris evolution, 10 Monte Carlo simulations are run

for each of four distinct cases. This yields results with a standard deviation of about 10-20% from the mean. All cases use the IDES 1996 debris population (pre-generated from an historical evolution simulation run) and a 'business as usual' (BAU) future traffic model to predict long-term evolution from 1996 to 2050 in 4 month time intervals. Only *catastrophic* collisions were assessed at every timestep. The four cases are defined as follows:

- *BAU*

  IDES 1996 population as initial conditions, future 'business as usual' launch & explosion rates;

- *BAUCONST*

  IDES 1996 population as initial conditions, future 'business as usual' launch & explosion rates, plus all 4 constellations in Table 5-1;

- *BAUMIT*

  IDES 1996 population as initial conditions, future 'business as usual' launch & explosion rates, explosion prevention from 2000, immediate de-orbiting of upper stages from 2000, end-of-life de-orbiting of spacecraft from 2030;

- *BAUCONMIT*

  IDES 1996 population as initial conditions, future 'business as usual' launch & explosion rates, explosion prevention from 2000, immediate de-orbiting of upper stages from 2000, end-of-life de-orbiting of spacecraft from 2030, plus all 4 constellations in Table 5-1.

The above package of mitigation measures have been chosen to represent the most severe scenario for controlling future debris growth that is feasible with today's technology and achievable within reasonably modest additional costs. Active retrieval and de-orbit of large debris objects by dedicated 'space tugs' is not currently considered to be a viable option and so has been neglected in these studies. The most severe proposed mitigation measures have

System Name	Year of Launch	Altitude (km)	Inclination (°)	Total No. Sats	Satellite Area (m^2)	Satellite Mass (kg)
CONSTEL1	2000	700	98	924	40	700
CONSTEL2	1998	780	86	72	40	700
CONSTEL3	1999	1400	52	56	36	450
CONSTEL4	1998	775	45	28	14	45

Table 5-1: Generic constellation designs modelled in IDES

been chosen in the context of this study in order to explore the boundaries of long-term evolution. These mitigation measures would tend to produce the largest achievable reduction in debris population growth. On the other hand, the high level of collision-induced breakup activity associated with a very large constellation of over 800 satellites could produce the most significant acceleration in debris population growth. From another perspective, the most severe mitigation measures might be required to counteract the significant long-term impact of a very large constellation on future population growth.

Besides the consideration of collisions, factors such as the future launch rate and future explosion rate can influence the long-term evolution of the LEO debris environment over the next 50 years. In both cases, the future launch rate was assumed to remain constant at around 80 per year, and the future explosion rate was set to a constant 4 per year. These rates are called the 'Business As Usual' rates and were derived from the average of the 8 years of LEO activity between 1988 and 1996. This assumes that future activity will continue at the same level as the recent past, hence the term 'Business As Usual'. Since all four cases have the same average launch and explosion rates, then the differences in the future collision rate and hence population growth will be exclusively due to the operation of the constellations and the implementation of routine debris mitigation measures. Geopotential and atmospheric drag perturbation models are used to propagate the debris population in these scenarios.

In addition to the 924-satellite CONSTEL1 system (similar to the original Teledesic design), three other smaller constellations (similar to the Iridium, Globalstar and Orbcomm designs) are also included in the simulation in order to make the scenario more realistic. The launch

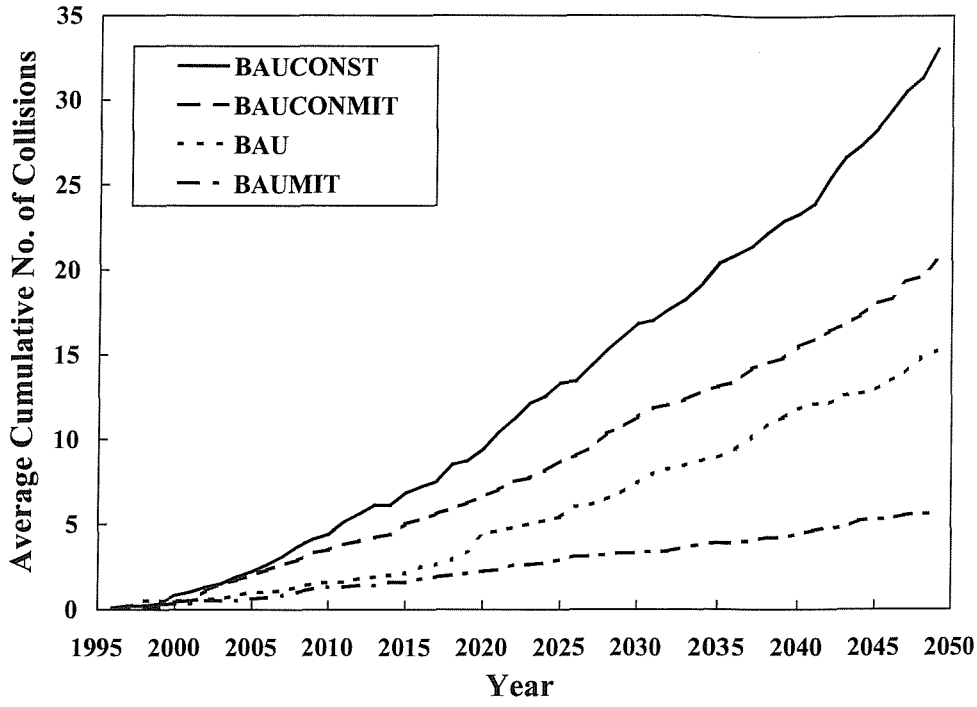

Figure 5-1: Predicted catastrophic collision rates in LEO with and without constellations and mitigation measures

vehicle upper stages associated with the deployment of all four constellations were assumed not to explode and to be de-orbited immediately after delivering their payloads into an initial parking orbit. The constellations were assumed to be operational throughout the 54 year time span with expended satellites de-orbited and replaced by spare satellites on demand. Any constellation satellites fragmented by a collision were assumed to be replaced in a similar way, so that the operational configuration is maintained throughout the simulation. Constellation satellites were assumed not to explode, and assumed to be de-orbited if they fail during operation. This set of strict constellation mitigation measures were assumed in order to solely evaluate the influence of the operational presence of constellations on the level of collision interactions and debris population growth.

5.3 Constellation Impact

5.3.1 Future Collision Activity

Figure 5-1 shows how the deployment of the 4 satellite constellations and the implementation of routine de-orbiting and explosion prevention can influence the collision rate in LEO. The *BAUMIT* case shows that the mitigation measures are very effective in

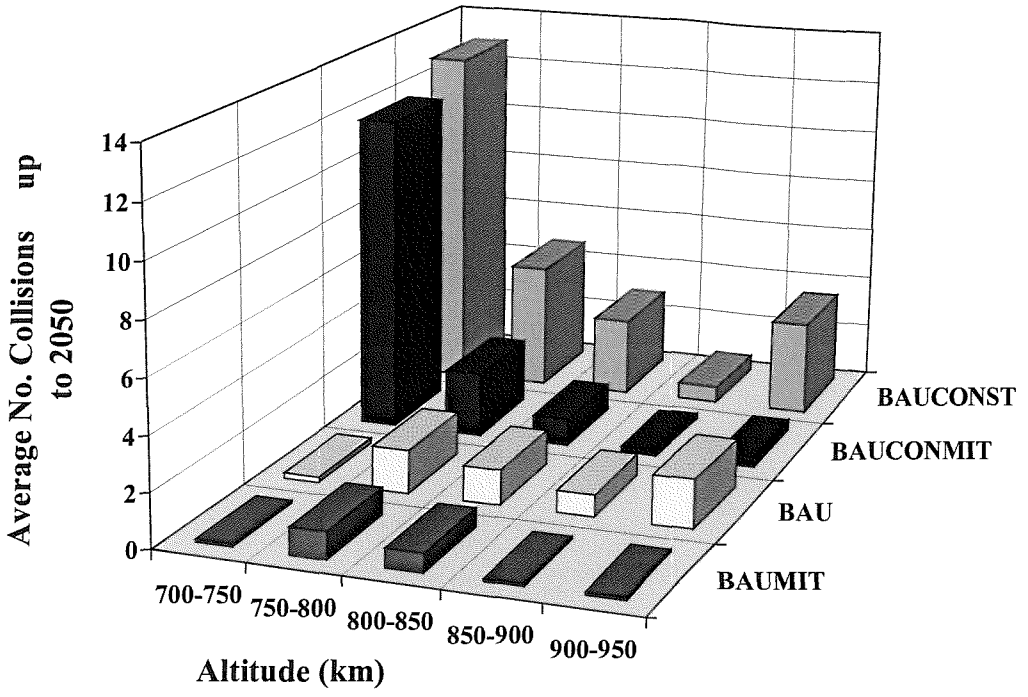

Figure 5-2. The average number of catastrophic collisions up to the year 2050 in various altitude bands for different future space flight scenarios

controlling the future collision rate, when no constellations are present. An average of only 5 collisions were predicted by the IDES model up to the year 2050 in this case. This is because the lethal collision risk is still mostly due to fragments from explosion events, and stopping these events after the year 2000 reduces the explosion fragment population as they are removed from orbit by atmospheric drag decay. This reduces the growth of collision risk (and hence the collision rate) experienced by large background objects like spacecraft and upper stages. In addition, the de-orbiting of spacecraft and upper stages prevents an increase in the number of large background objects available to undergo collisions. This results in a constant minimal collision rate and consequent linear increase in the cumulative number of collisions with time.

Comparison between the *BAU* and *BAUCONST* cases shows that the constellations (especially the large 924 satellite design) can double the overall collision rate in LEO. There are over 30 catastrophic collisions predicted up to 2050 in the *BAUCONST* case, compared to only 15 in the *BAU* case. The *BAUCONMIT* case gives an average of 20 collisions up to 2050, which is higher than the number predicted for the *BAU* case. From this, one can deduce that the increase in collision activity due to constellation systems would be more

dominant than the decrease due to the effectiveness of mitigation measures. Again, the reduction in collision risk by explosion prevention and removal of large background objects by routine de-orbiting is very effective in controlling the background object collision rate. However, the overall collision rate is still dominated by the collision-induced breakups of constellation satellites in the *BAUCONMIT* case, since they represent a significant proportion of the total number of large target objects. The collision rate for the *BAUCONMIT* case is predicted to be 40% lower than the *BAUCONST* case. This is mainly as a result of the decrease in the background object collision rate due to the mitigation measures, as mentioned above.

The dominance of constellation-related collisions over background object collisions is confirmed by Figure 5-2. The altitude breakdown shows that in the 700 to 750 km altitude band, there are at least 60 times more collisions in the cases involving constellations than in the cases with no constellations. This is mainly due to the collisions suffered by the 924-satellite CONSTEL1 design. The mitigation measures have hardly any effect on the number of collisions in this altitude band when CONSTEL1 is present.

The average number of collision-induced breakups (up to 2050) sustained by constellations in the *BAUCONST* case was predicted to be 12.1 for CONSTEL1 and 1.9 for CONSTEL2. This is compared to 10.8 for CONSTEL1 and 1.4 for CONSTEL2 in the *BAUCONMIT* case. Therefore, there are only small reductions in the fatality rates of CONSTEL1 and CONSTEL2 as a result of explosion prevention and routine de-orbiting. Again, this is likely to be because the decrease in the catastrophic collision risk by explosion prevention is almost balanced by the collision risk created from the collision-induced breakups of the large CONSTEL1 design. Since there are no constellations modelled in the 800 to 850 km altitude band, this gives a useful picture of how the fragments dispersed from constellation collision-induced breakups can influence the local background object collision rate. For the *BAU* and *BAUCONST* cases where no mitigation measures are implemented, the number of background object collisions is doubled due to the constellation collision activity at lower altitudes. However, when the mitigation measures are applied, there is hardly any increase in the number of background object collisions due to the constellations. This is because routine de-orbiting keeps the number of background target objects in the altitude band at a constant level, as the removal rate approximately matches the launch rate. In general, the action of

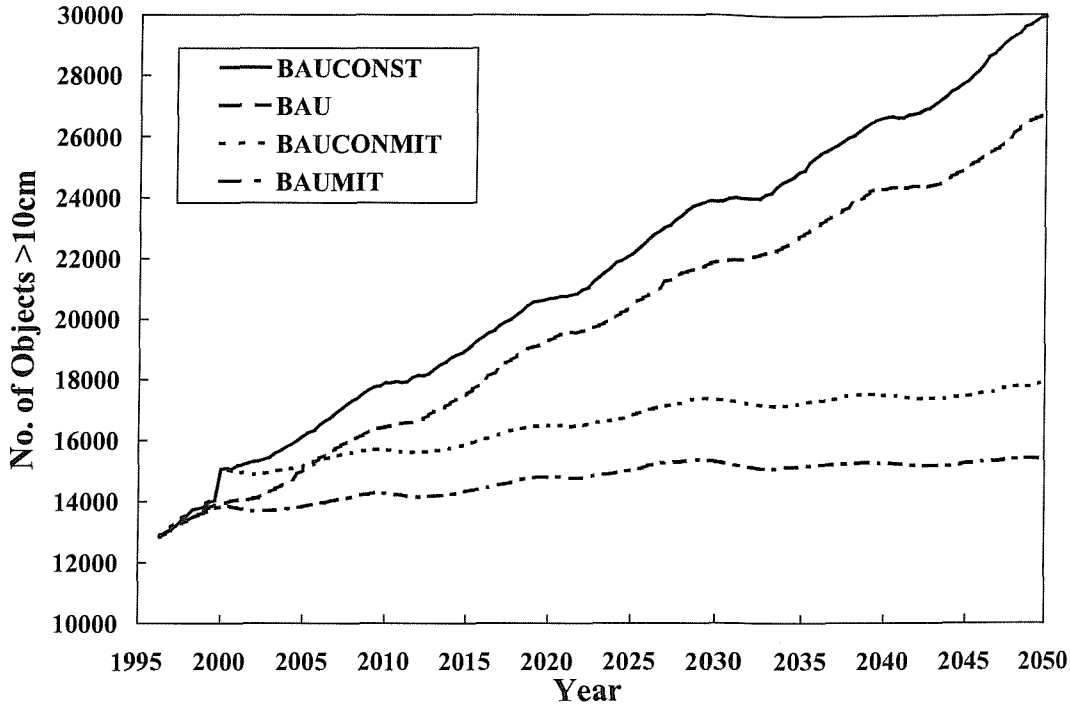

Figure 5-3. The average impact of constellations and mitigation measures on the long-term evolution of debris >10 cm in or intersecting LEO

mitigation measures can reduce the collision rate by half in this altitude band, irrespective of the presence of the constellations at the lower altitudes.

5.3.2 Future Population Trends

Now that the long-term constellation collision interactions have been examined for the four different future traffic scenarios, the next step is to determine their effect on the projections of future population growth for various sizes of debris.

Figure 5-3 shows that the population growth for debris larger than 10 cm is linear for the cases without the implementation of mitigation measures (*BAU* and *BAUCONST*). In the *BAU* case, the population doubles from ~13,000 in 1996 to ~26,000 in 2050. This is expected because in the past, the main source of objects larger than 10 cm has been low intensity explosions, which the study assumes will continue to occur at the same constant rate into the future. When the constellations are deployed in the *BAUCONST* case, they add a total of 1080 objects to the population. This is indicated by the sharp increase in the year 2000 when the 924-satellite CONSTEL1 design is launched. By the end of the simulation in the year 2050, the population for the *BAUCONST* case is approximately 4000 objects larger

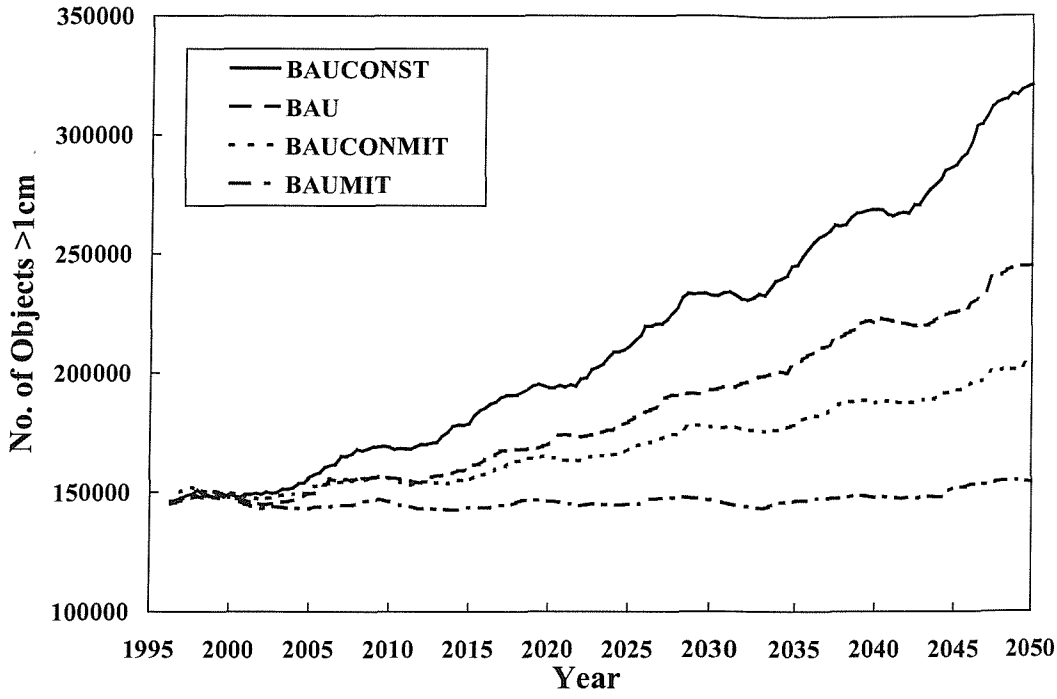

Figure 5-4. The average impact of constellations and mitigation measures on the long-term evolution of debris >1 cm in or intersecting LEO

than the *BAU* case. Therefore, an extra 3000 objects larger than 10 cm are orbiting in addition to the 1080 constellation satellites. These are likely to be due to fragments generated from the constellation fatalities relating to the large CONSTEL1 design and the enhanced background object collision rates local to this constellation system.

When mitigation measures are applied in the *BAUMIT* case, the same linear population growth can be observed from 1996 to 2000. After the year 2000, the low intensity explosions are prevented and upper stages are de-orbited. The growth rate then decreases dramatically and the population slowly rises linearly with time until the year 2030, when de-orbiting of spacecraft commences. Subsequently, the population completely stabilises and remains at a constant level. With only a 10% to 20% increase over 54 years, the mitigation measures modelled here seem to be very effective for controlling the decimetre-sized debris population in the long-term. This is important because, in general, only debris larger than 10 cm are capable of causing collision-induced breakups in LEO. Again, there is a sharp increase in the population for the *BAUCONMIT* case when CONSTEL1 is introduced in the year 2000. However, there are not quite as many additional fragments produced due to the collision interactions between constellations and the background debris environment over

54 years. This is because the implementation of mitigation measures slightly reduces the level of constellation-related collision activity.

Figure 5-4 presents the population evolution for debris larger than 1 cm in size. Generally, the temporal trends display more exponential growth, instead of the linear increases seen in the decimetre-sized population evolution. Here, the effect of the solar cycle is more prevalent. Smaller particles have higher ballistic coefficients than larger ones, and therefore will be more susceptible to atmospheric drag decay. During periods of high solar activity the atmosphere will be heated, resulting in a higher atmospheric density and drag decay in LEO, thus removing some of the 1 cm debris population from orbit. This has the effect of lowering the population. Correspondingly during solar minimum, atmospheric density and drag are at a minimum. This allows debris objects to accumulate as fragmentation events occur, hence producing an increase in the population.

In Figure 5-4, the *BAUCONST* case more than doubles the centimetre-sized population over 50 years. By contrast, the *BAU* case produces a rise of only 60% above the initial value. Therefore, in the absence of routine mitigation measures, the constellations (mainly the 924 satellite design) would cause an increase the centimetre-sized population growth by 35% in the long-term.

When mitigation measures are implemented, and constellations are *not* deployed (the *BAUMIT* case), then the population does not increase at all over 50 years. Clearly, mitigation measures are very effective at stabilising the centimetre-sized population in this scenario. When the constellations are operating in LEO, the mitigation measures of routine de-orbiting and explosion prevention are not so effective at *stabilising* centimetre-sized debris population growth. This is because the *BAUCONMIT* case shows a shallow exponential population growth of 30% over the initial 1996 value, as opposed to a near-constant population with no net increase over time. However, the mitigation measures are still quite effective at *partially reducing* the centimetre-sized population growth. The population level in the *BAUCONMIT* case remains below that observed in the *BAU* case. This implies that the mitigation measures are effective at moderately reducing the centimetre-sized population growth, even after the deployment of the constellation systems.

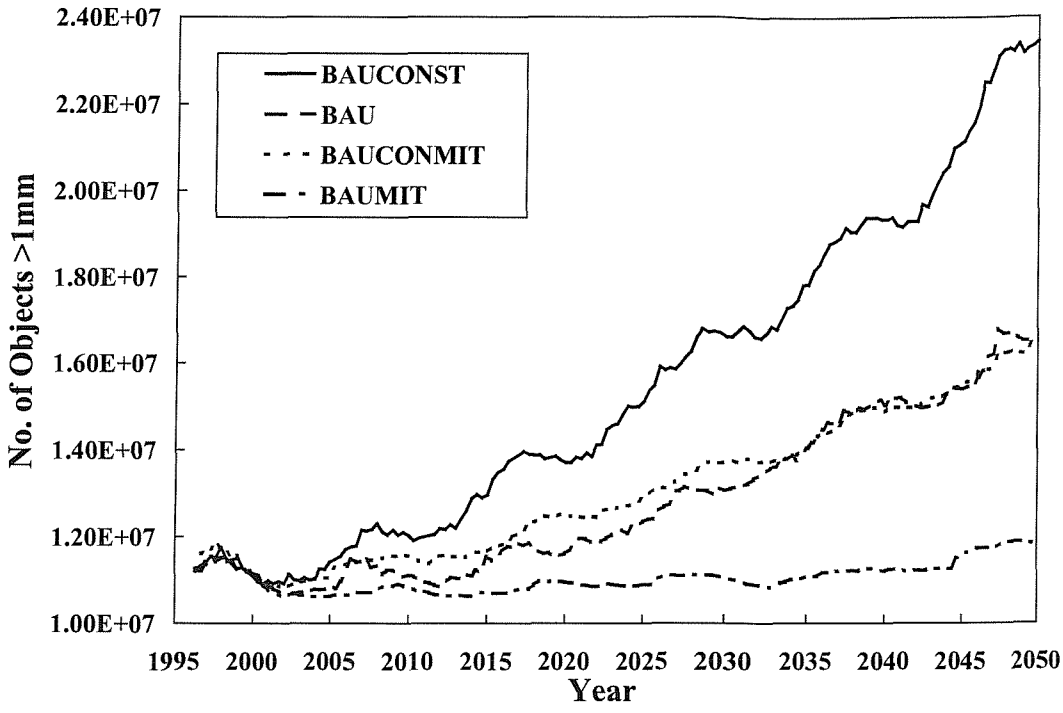

Figure 5-5. The average impact of constellations and mitigation measures on the long-term evolution of debris >1 mm in or intersecting LEO

Figure 5-5 shows general exponential growth trends in the >1 mm population over the 54 years due to the influence of an increasing number of catastrophic collisions over time. The exception to exponential growth is again the *BAUMIT* case, which maintains an approximately constant population level over time. This shows that the millimetre-sized population is well controlled by routine de-orbiting and explosion prevention, in the absence of the constellations. However, the modelled constellations reduce the effectiveness of the mitigation measures because the population increases by 50% over the initial 1996 value in the *BAUCONMIT* case, instead of remaining constant as in the *BAUMIT* case.

In fact, the number of objects larger than 1 mm for the *BAUCONMIT* case is very similar to the number in the *BAU* case throughout the long-term evolution. This implies that the effectiveness of mitigation measures in *reducing* the millimetre-sized population growth would be cancelled out by the collision activity associated with the constellations, and in particular the 924-satellite CONSTEL1 design.

5.4 Summary

The investigation has shown that the deployment of a large constellation of over 900 satellites would have a significant, dominating effect on long-term debris evolution trends in low Earth orbit. Such a large system would seriously inhibit the effectiveness of routine debris mitigation measures at some object sizes. The introduction of the debris mitigation measures considered would be sufficient to overcome the long-term impact of constellations in order to completely stabilise decimetre-sized debris population growth. The measures would partially reduce the growth of centimetre-sized debris after the deployment of a large satellite constellation. However, the enhanced collision activity associated with a large LEO multi-satellite system of over 900 spacecraft deployed in a region of high collision risk, would be sufficient to cancel out the effectiveness of mitigation measures in reducing the millimetre-sized debris growth. Most significantly, such a system would suffer enough collision-induced breakups to completely cancel out the reduction in the overall collision rate enabled by the mitigation measures. Spacecraft de-orbiting measures would need to be implemented much earlier than 2030 in addition to the other modelled mitigation measures, if the long-term effects of operating such a large constellation system are to be avoided.

6 The Effects of New Satellite Constellation Traffic on Long-Term Debris Evolution

6.1 Introduction

Since the long-term impact of a large constellation of over 900 satellites was studied extensively in 1997 and documented in Chapter 5, the IDES model was significantly enhanced and upgraded to version 2.0 (see Chapter 3 for the full description of IDES 2.0). During this upgrade, the reference epoch was advanced from 1st January 1996 to 31st March 1998, involving the update of the historical launch and fragmentation databases. A new future launch traffic model was derived from the historical launch database, reaching even higher levels of resolution and detail. A new debris source model describing the release of sodium-potassium coolant droplets from Russian RORSATs was developed and integrated into the IDES model. These improvements, namely the inclusion of NaK droplets and the high quality of historical launch data, also lead to the successful validation of the IDES model predictions against measurement data at >1 cm and >10 cm size thresholds respectively. With the greater accuracy achieved in the initial population and a higher resolution future traffic model, there was an opportunity to perform an improved assessment of the long-term impact of constellations on the LEO debris environment.

Since the previous study in 1997, there have also been a number of changes in the LEO satellite constellation launch traffic projections. Firstly, many of the narrowband voice and data/messaging systems are no longer projections, but they have become reality. The Iridium global mobile phone constellation has been fully deployed (with in-orbit spares) and has been offering a full service since November 1998. Iridium's competitor, Globalstar, has over 30 satellites in orbit at the time of writing, and the remaining number are expected to be launched during 1999, allowing service to commence in late 1999 or early 2000. The Orbcomm data/messaging constellation has almost reached full deployment status, but is already providing a global service to a growing customer base. In the broadband communications arena, the design of the planned Teledesic constellation has been revised, with a reduction in the number of satellites from 924 down to 324 (including in-orbit spares)

and an increase in the operational altitude from 700 km up to nearly 1400 km. These two changes will significantly reduce the system's through-life collision risk, in terms of both catastrophic and failure-inducing collisions. In addition to Teledesic, a new player has emerged in the broadband multimedia/internet marketplace. The French-led Skybridge constellation is being planned for deployment by 2002, with 80 satellites operating in the 1400 to 1500 km altitude band. In this band, there are secondary peaks in the lethal >10 cm debris environment and no atmospheric drag to remove fragments generated by collision-induced or explosion-induced satellite breakups. Such changes in the projected constellation traffic have substantial implications for a realistic prediction of the constellation collision interactions with the background debris population and hence their long-term effects on the debris environment in the future.

Given the dominant effect of a constellation of over 900 satellites on the overall collision rate and debris population growth described in Chapter 5, one might expect that a reduced level of constellation traffic might lead to a reduced impact on collision/population trends and mitigation measure effectiveness. Thus, a new study is needed in order to evaluate this factor. Following current trends and indications, most (if not all) commercial LEO constellation systems should have a debris mitigation strategy in place, such as explosion prevention or de-orbiting (as in the case of Iridium satellites), if only to avoid polluting their own operational orbit. Certainly, the issue of orbital debris and the need to employ mitigation techniques is being taken seriously by most existing or potential constellation operators. The objectives of the study described in this chapter is a realistic assessment of long-term constellation effects, based on currently foreseen constellation launch traffic and on the assumption that the constellations employ strict debris mitigation measures.

6.2 Modelled Future Traffic Scenarios

As in the previous study described in the Chapter 5, the stochastic nature of modelling future debris sources such as collisions, explosions and launches requires IDES to be used in a Monte Carlo mode to represent different statistical permutations of long-term evolution. In order to obtain a reasonable statistical average of the impact of the foreseen LEO satellite constellation operations on long-term debris evolution, 10 Monte Carlo simulations are run for each of four distinct scenarios. All cases use the IDES 2.0 1998 debris population

(including the newly modelled NaK droplet source), which has been pre-generated from an historical evolution simulation run and validated against debris measurement data (see Chapter 4). All cases use the updated 'business as usual' future traffic model (see Chapter 3) to predict long-term evolution from 1998 to 2050 in 6 month time intervals. Only *catastrophic* collisions were assessed at every timestep. The four scenarios are similar to those assumed in the previous study, except that different constellation designs and mitigation measure implementations are being simulated. These scenarios are defined as follows:

- *BAU*

  Validated IDES 1998 population as initial conditions, future 'business as usual' launch & explosion rates;

- *BAUCONST*

  Validated IDES 1998 population as initial conditions, future 'business as usual' launch & explosion rates, plus all 5 constellations in Table 6-1;

- *BAUMIT*

  Validated IDES 1998 population as initial conditions, future 'business as usual' launch & explosion rates, mission-related object limitation from 2005, explosion prevention from 2010, immediate de-orbiting of upper stages from 2005, and end-of-life de-orbiting of spacecraft from 2015;

- *BAUCONMIT*

  Validated IDES 1998 population as initial conditions, future 'business as usual' launch & explosion rates, mission-related object limitation from 2005, explosion prevention from 2010, immediate de-orbiting of upper stages from 2005, and end-of-life de-orbiting of spacecraft from 2015, plus all 5 constellations in Table 6-1.

System Name	Year of Launch	Altitude (km)	Inclination (°)	Total No. Sats	Satellite Area (m^2)	Satellite Mass (kg)
CONSTEL1	2002	1375	85	324	12	1400
CONSTEL2	1998	780	86	72	9	700
CONSTEL3	1999	1414	52	56	10	450
CONSTEL4	1998	775	45	28	9.6	42
CONSTEL5	2002	1457	55	80	12	800

Table 6-1: Description of the new constellation designs modelled in IDES

In order to perform a realistic assessment of long-term constellation effects, the constellation designs given in Table 6-1 have been chosen to reflect actual systems launched or being planned for deployment in LEO in the next few years. Based on available information, the configurations of CONSTEL1 to CONSTEL5 are similar to Teledesic, Iridium, Globalstar, Orbcomm and Skybridge respectively. In the absence of design data, some values have been estimated, and therefore the modelled designs may not accurately represent the actual systems that they are meant to emulate.

The mitigation measures to be simulated here are based upon an updated, more realistic assessment of their likely global implementations. Previously, explosion prevention was assumed to apply from the year 2000. However, it was felt that this estimate was too optimistic because not all launchers have implemented procedures to preclude the occurrence of an explosion (called passivation), or could not be expected to do so by that epoch. Even if all new launchers were to apply preventative measures from now on, there would still be enough upper stages in orbit to continue explosions over the next few years. The year 2010 is seen as a reasonable epoch for all launcher and satellite manufacturers to implement passivation and for in-orbit unpassivated upper stages and satellites to be safe from the threat of explosion. The policy of immediate de-orbiting of upper stages has been delayed by five years (to 2005) with respect to the previous study and the immediate post-mission de-orbiting of satellites has been brought forward by 15 years (to 2015), compared to the implementation date modelled in Chapter 5. It was felt that satellite de-orbiting could be implemented much sooner than 2030 because of the raised awareness of satellite manufacturers to the debris problem and to national agency guidelines/standards. In

addition, technology that could make immediate post-mission de-orbiting a cost-effective operation could become common place within the next 15 years, e.g. ion thrusters.

In this updated study of the long-term effects of constellations and mitigation measures, the overall future launch rate was assumed to remain constant at 89 events per year and the future explosion rate was set to a constant 5.5 events per year. These rates are called the 'Business As Usual' (BAU) rates and were derived from the average of the 8 years of LEO to GEO activity between 1990 and 1998. The detailed future launch and explosion traffic models were updated and improved since the previous study was conducted. These state-of-the-art traffic models are described in sections 3.3.1 and 3.3.2. As stated before, since all four scenarios described above have the same average launch and explosion rates, then the differences in the future collision rate and hence population growth will be exclusively due to the operation of the new constellation designs and the implementation of the modelled debris mitigation measures.

As in the previous study, geopotential and atmospheric drag perturbation models are used to propagate the debris population in these scenarios.

The assumptions concerning constellation deployment and operations have remained the same as in the previous study. Namely, the launch vehicle upper stages associated with the deployment of all five constellations were assumed not to explode and to be de-orbited immediately after delivering their payloads into an initial parking orbit. The constellations were assumed to be operational throughout the 52-year time span with expended satellites de-orbited and replaced by spare satellites on demand. Any constellation satellites fragmented by a collision were assumed to be replaced in a similar way, so that the operational configuration is maintained throughout the simulation. Constellation satellites were assumed not to explode and to be de-orbited if they fail during operation. Again, these set of strict constellation mitigation measures were assumed in order to evaluate solely the influence of the operational presence of the foreseen constellation designs on collision interactions and hence on debris population/environment evolution trends.

By comparing results from the BAU and BAUCONST scenarios, it becomes possible to determine the long-term impact of the new satellite constellation traffic on the debris

environment, when no routine mitigation measures are implemented in the background population. A comparison between predictions from the BAUMIT and BAUCONMIT scenarios would show the long-term impact of the constellation designs *with* routine mitigation measures applied. Additionally, further comparison between the BAU and BAUMIT scenarios would reveal the effectiveness of the mitigation measures, without the new constellation traffic deployed. Lastly, a comparison between BAUCONST and BAUCONMIT scenarios enables an assessment of the mitigation measure effectiveness, when these constellations are present.

6.3 Constellation Impact

6.3.1 Future Collision Activity

The average catastrophic collision activity predicted by IDES for the 4 different modelled future traffic scenarios is presented in Figure 6-1, starting from the initial epoch of 31st March 1998 to the final epoch of 1st January 2050. In both the BAU and BAUCONST curves, there is an exponential trend in the overall cumulative number of collisions, ending with approximately 11 and 13 collisions predicted after 50 years respectively. This exponential trend implies that the collision rate increases with time under the 'business as usual' scenarios with no mitigation. Observing the BAU and BAUCONST curves relative to one another, the presence of the new constellation traffic appears to have only a minor impact on the overall LEO collision activity without mitigation measures. Only 2 additional collision events are predicted on average over the next 50 years. This small increment is largely due to the average total 1.2 collision-induced breakups predicted for the 324 satellite constellation. Only 0.2 collision-induced breakups were predicted for the other constellations, on average.

Comparison between the collision activity predicted for the BAUMIT and BAUCONMIT shows that the two curves are almost the same. Thus, the new constellation traffic would have no effect on the LEO collision rate, if the modelled routine mitigation measures are applied in the background population. The average number of collision-induced breakups predicted for any of the constellations is negligible here. In fact, in both these scenarios, the predictions suggest that the modelled mitigation measures are very good at stabilising and actually reducing the LEO collision rate, with or without the new constellation designs

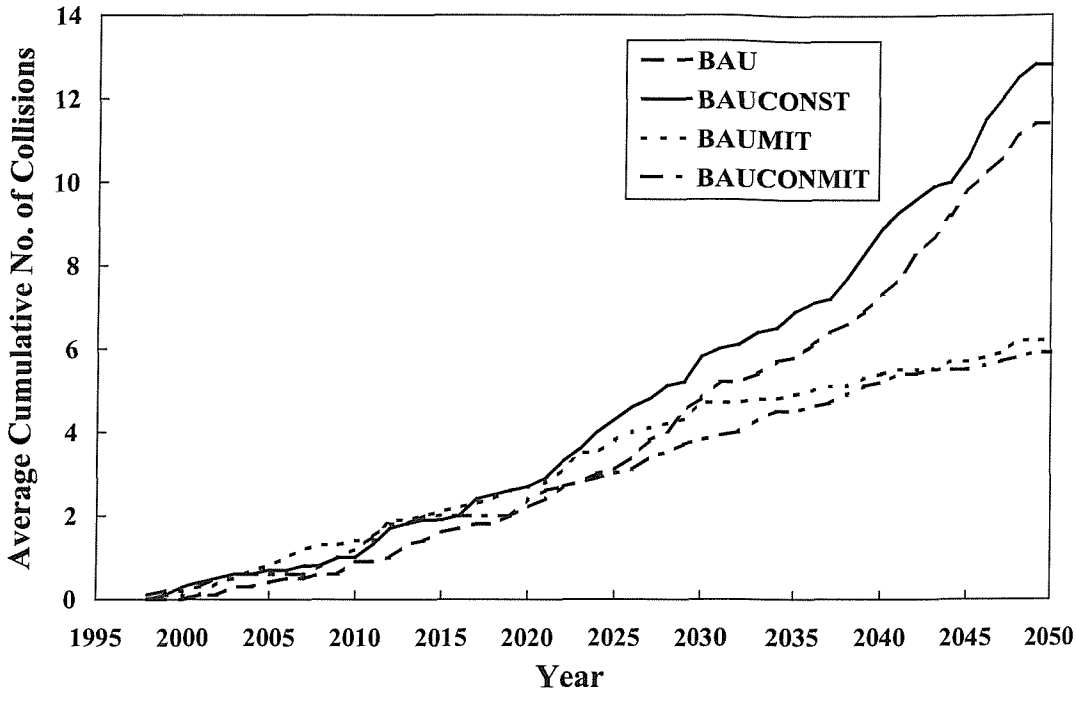

Figure 6-1: Predicted LEO catastrophic collisions for the 'Business As Usual' future traffic scenario with and without the new constellation traffic and the mitigation measures

deployed. This is evident as the two cumulative curves start to decrease in gradient and tend to flatten out after approximately 2035, ending at 6 catastrophic collisions predicted up to 2050. The mitigation measures of explosion prevention and immediate post-mission de-orbiting would be efficient enough to cut the predicted number of catastrophic collisions by 50% after 50 years. This is likely to be due to the fact that the de-orbiting would reduce the growth in the number of large target objects which could be involved in catastrophic collision events. Also, the explosion prevention policy would immediately halt the increase in the number of decimetre-sized debris population, and therefore the catastrophic fragmentation risk experienced by the large target objects.

In this and other figures in this Chapter, the predictions for the BAUCONMIT scenario appear to be lower than those for the BAUMIT scenario. This is due to the statistical uncertainties introduced by the Monte Carlo simulation method. There were a slightly lower number of explosions predicted for the BAUCONMIT scenario than for the BAUMIT scenario in the mid-section of the projections, thus accounting for the difference. However, both sets of mean predictions are within each others' 10-20% standard deviation region.

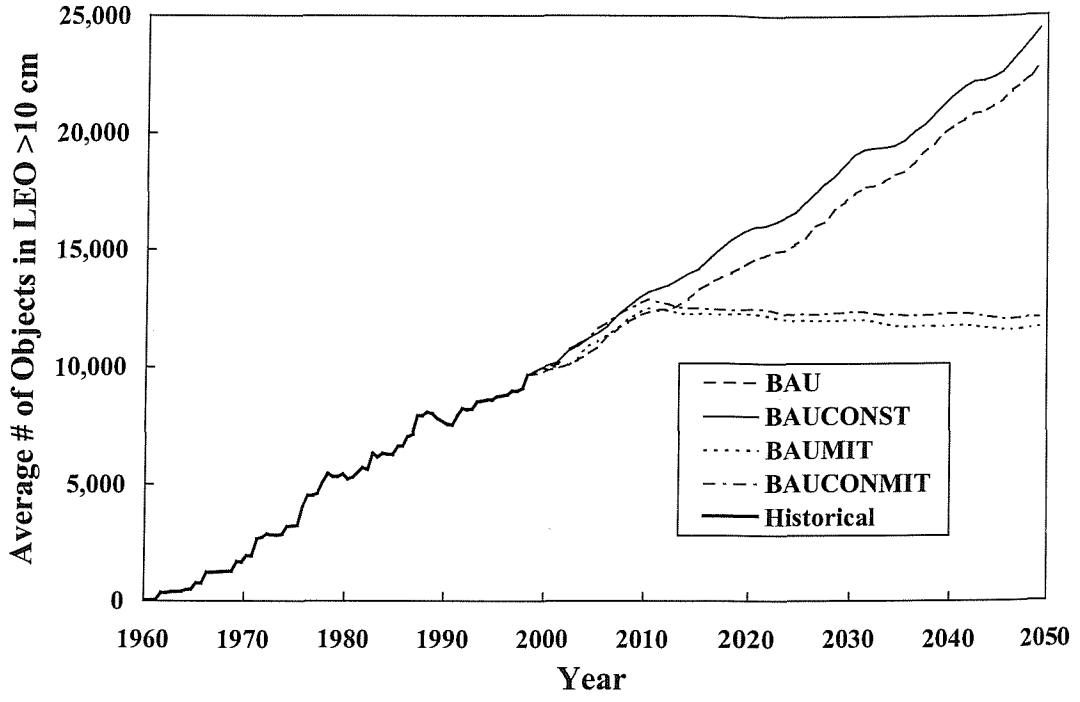

Figure 6-2: Predicted >10 cm LEO population evolution for the 'Business As Usual' future traffic scenario with and without the new constellation traffic and the mitigation measures

6.3.2 Future Population Trends

The IDES model predictions presented and discussed in this section represent the projected 50-year evolution of the average LEO population of >10 cm, >1 cm, and >1 mm debris for the 4 different future traffic scenarios. In order to put these projections into perspective, the corresponding historical population evolution predictions (running from 1957 to 1998) are also included in the results. Therefore, one is able to gain knowledge of how population levels varied in the past, through to the present-day and how these levels might comparatively extend as trends into the long-term future. Of course, the long-term model predictions are subject to certain assumptions on launch/explosion traffic input, mitigation measures, solar activity, and collision event prediction.

The predicted LEO population evolution of objects larger than 10 cm is shown in Figure 6-2. Historically, the >10 cm population evolution has exhibited a net linear growth trend to reach just under 10,000 objects in 1998. There is a periodic modulation in the historical curve due the influence of the 11-year solar cycle and of differing rates of launch/explosion

activity. At solar maximum, for example in 1990, the orbital decay rates are augmented and orbital lifetimes are shortened, leading to a decrease in the population level as the object removal rate is higher than the object generation rate. Correspondingly at solar minimum, atmospheric drag decay tends to be much reduced, allowing the population to rapidly increase again.

The long-term projections for the BAU and BAUCONST scenarios tend to continue this linear growth trend throughout the next 50 years, reaching 23,000 and 24,500 objects respectively. This is because the >10 cm population is dominated by fragments from explosions and objects related to launch events. In the 'business as usual' future traffic scenarios, explosion and launch events are assumed to continue to occur in the future at the same constant rates as observed during the 1990s. Again, the projections for both scenarios display the small modulation of the 11-year solar cycle as explained above. A comparison between the BAU and BAUCONST scenarios reveals that the new constellation traffic may have a minor impact on the decimetre-sized population, when mitigation measures are not applied. There are about 1,500 objects more in the BAUCONST scenario due to the 560 constellation satellites and the fragments generated from the average 1.4 extra collision-induced breakups sustained by the constellation designs over the next 50 years.

Comparison between the BAUMIT and BAUCONMIT scenarios shows that there would be a negligible impact on the decimetre-sized population due to the presence of the new constellation traffic, when the modelled package of mitigation measures are implemented. There is an increase of about 500 objects in the BAUCONMIT scenario due to the constellation satellites launched. There is a negligible average number of collision-induced breakups predicted for the constellations designs in this scenario and hence very few extra collision fragments are generated by the constellations during the application of the mitigation measures. In both BAUMIT and BAUCONMIT scenarios, the long-term projections show that the historical >10 cm population growth trend continues until 2010, when the explosion prevention mitigation measure is implemented. Thereafter, the population displays no growth at all and even decreases slightly from its 2010 level over the following 40 years. This because there is no input from explosion fragments after 2010 and the in-orbit explosion fragment population starts to decay due to atmospheric drag. Furthermore, rocket bodies and satellites are being removed from orbit after 2005 and 2015

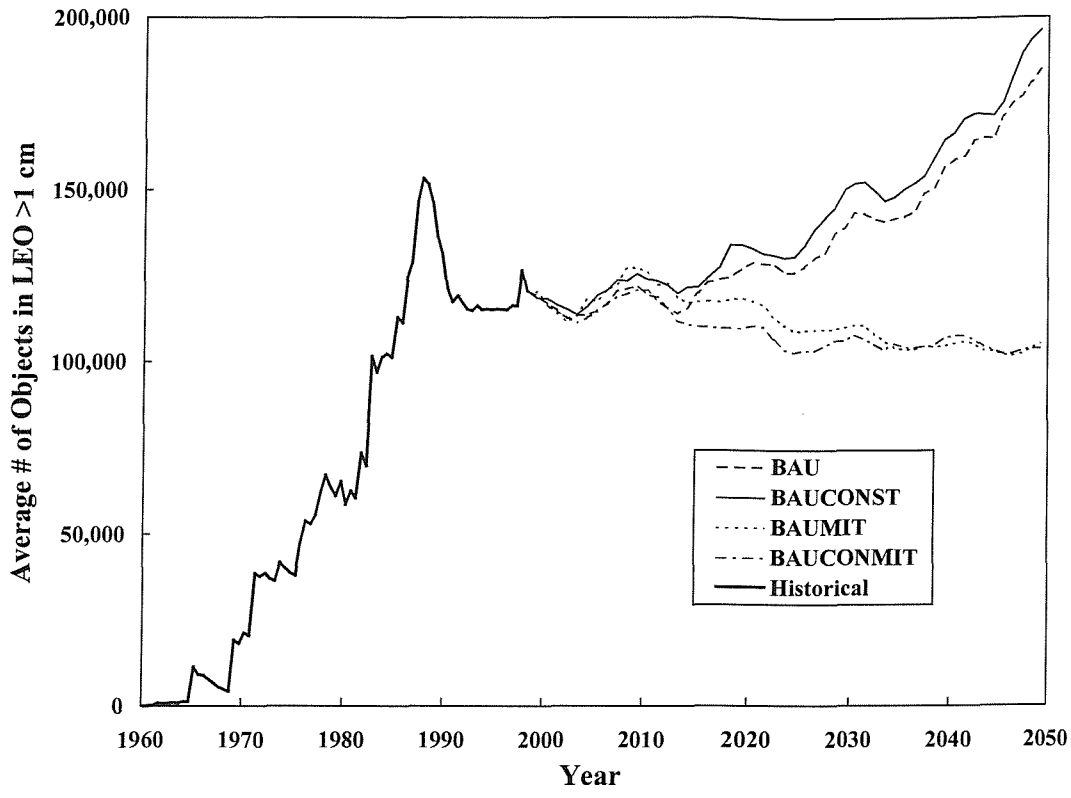

Figure 6-3: Predicted >1 cm LEO population evolution for the 'Business As Usual' future traffic scenario with and without the new constellation traffic and the mitigation measures

respectively due to the implementation of immediate post-mission de-orbiting. The >10cm population is only prevented from decreasing significantly due to these factors by the continued 'business as usual' launch-related object input and fragments from the average 6 collision-induced breakups, predicted over the course of the 52-year simulation period.

The historical and future projections of the population of objects larger than 1 cm can be seen in Figure 6-3. Historically, the >1 cm population has been dominated by fragments generated from high intensity explosions (mainly the deliberate detonation of spacecraft) and, of course, the NaK liquid coolant droplets leaking from Russian RORSATs. As stated in Chapter 4, the centimetre-sized population did not start to grow until 1965. Thereafter, there were sporadic step increases in the population level at given points in time, corresponding to the occurrence of specific high intensity explosions. According to the historical simulation, this activity caused the >1 cm population to grow to nearly 70,000 objects in LEO in 1980. During the 1980s, the rate of high intensity explosions rose to

between 2 and 3 events per year. Also during that decade, all 16 of the RORSAT sodium-potassium coolant leakage events were deemed to have occurred. These two factors combined to produce a dramatic increase in the predicted centimetre-sized population, which reached 150,000 objects in 1988, according to IDES.

After 1988, there were no assumed RORSAT coolant leakage events, and the rate of high intensity explosions declined to an average of approximately 1 event per year. Coincidentally, the sharp decrease in centimetre-sized object generation occurred just before the solar maximum in 1990. The high level of solar activity in 1989/1990 heightened the removal rate of fragments from high intensity explosions, and the population level dropped as rapidly as it had increased. The estimated 34,000 NaK droplets >1 cm in orbit were largely unaffected by the solar maximum because most droplets have orbital altitudes higher than 750 km where atmospheric density is very low, leading to orbital lifetimes of several decades. After 1990 and up to 1998, the high intensity explosion rate remained low at an average of just over 1 event per year and also these events occurred at low altitude leading to relatively short orbital lifetimes of the generated fragments. Consequently, in times of low solar activity and low particle input rate, the centimetre-sized population remained at an approximately constant level of 120,000 objects, according to the IDES model.

The low rate of high intensity explosions observed during the 1990s is extrapolated into the future in the 'business as usual' future explosion traffic model. Catastrophic collision events also greatly influence the >1 cm population levels. The high kinetic energies involved in the impact can produce thousands of small fragments as the mass distribution of these events (like high intensity explosions) is assumed to take the form of a power law. The predicted rising rate of catastrophic collisions given in Figure 6-1, leads to exponential growth trends in the BAU and BAUCONST long-term projections. The underlying gradient of the population growth over the next 50 years is, however, mainly due to the larger rate of high intensity explosions. In both BAU and BAUCONST scenarios, the >1 cm population is projected to increase from 120,000 objects in 1998 to nearly 200,000 objects on average in 2050. The effects of the solar cycle are evident in these projections, and the magnitude of these periodic effects is larger than for objects >10 cm in size. This is because centimetre-sized objects have a higher area-to-mass ratio, and therefore a faster orbital decay due to atmospheric drag. A comparison between the BAU and BAUCONST long-term projections

reveals that the new constellation traffic would only have a minor impact on the centimetre-sized population growth, when no mitigation measures are implemented. This is because of the very low average number of collision-induced breakups predicted for the constellation satellites in the BAUCONST scenario over the 52-year simulation period.

Even when the routine mitigation measures are applied in the BAUMIT and BAUCONMIT scenarios, the comparison between these cases shows that there would be essentially no increase in the centimetre-sized population due to the new constellation traffic. This is because an average of less than 1 extra collision-induced breakup was predicted for the constellation satellites in the BAUCONMIT scenario. The long-term population projections for both BAUMIT and BAUCONMIT scenarios show that explosion prevention, implemented in 2010 here, would produce a short-term reduction in the input of centimetre-sized debris. Following 2010, the in-orbit high intensity explosion fragments and NaK droplets would start to decay from orbit, actually causing the LEO population to decrease from 125,000 objects in 2010 down to approximately 100,000 objects in the year 2050. Due to the immediate post-mission de-orbiting of satellites and rocket bodies, the centimetre-sized fragments generated from the reduced number of predicted catastrophic collisions (an average of 6 events over 50 years) are unable to prevent this decline in the population.

The historical and future population projections for debris larger than 1 mm in size are presented in Figure 6-4. The historical population evolution trends are similar to those seen with the >1 cm population in Figure 6-3. However, the current particle size distribution of the NaK droplet source model does not produce many millimetre-sized objects in comparison to those generated by high intensity explosion events. Therefore, the predicted millimetre-sized population can be assumed to be entirely dominated by the latter source. There are three distinct phases to the historical evolution of the >1 mm population, corresponding to different rates of the high intensity explosions. In the first phase, the population started to grow sporadically due to the occurrence of these events with a net linear trend from 1965 to 1982, with the predicted population level reaching 3 million objects in 1982. In the second phase from 1982 to 1988, the rate of high intensity explosions doubled, and this led to a sharp rise in the predicted population level to reach 6 million objects in 1988. After 1988, the number of high intensity explosions fell dramatically and this, coupled with the occurrence of high atmospheric drag decay of orbits at solar

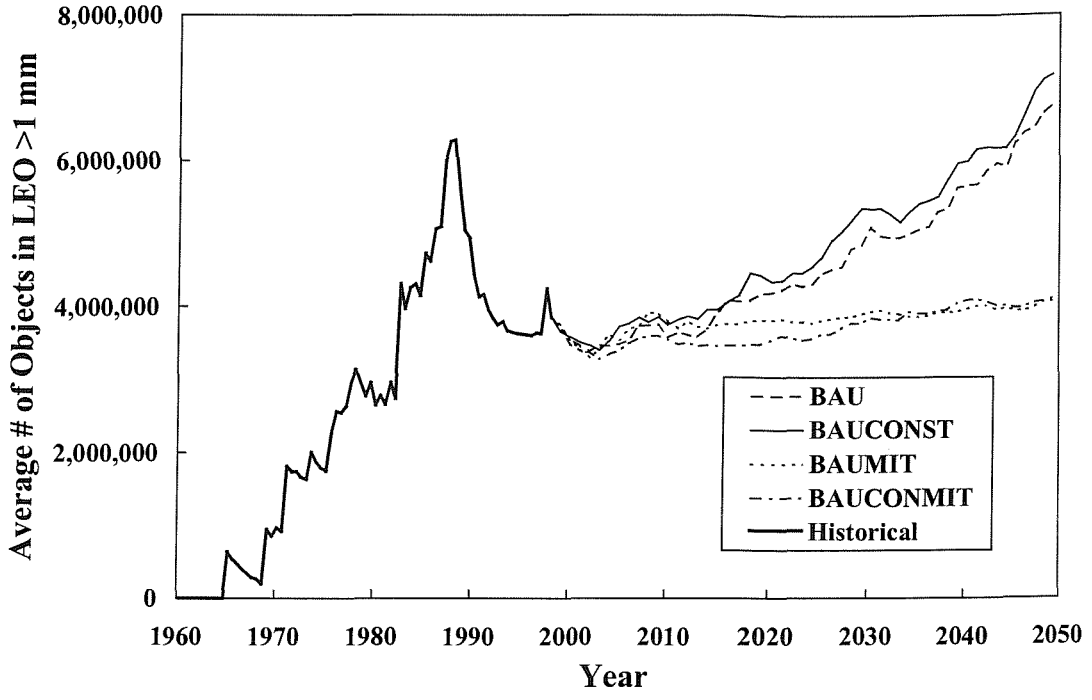

Figure 6-4: Predicted >1 mm LEO population evolution for the 'Business As Usual' future traffic scenario with and without the new constellation traffic and the mitigation measures

maximum in 1990, produced an equally sharp decline in the millimetre-sized population. The predicted population level then stabilised during the following solar minimum and reached almost 4 million objects in 1998.

As in the >1 cm long-term population projections, the presence of the new constellation traffic appears to have little impact on the millimetre-sized debris population, with or without the implementation of the mitigation measures. Without the mitigation measures applied, the 'business as usual' predictions of the BAU and BAUCONST scenarios exhibit exponential growth with periodic modulation by the solar cycle, and reach a level of approximately 7 million objects by the year 2050. However, when the mitigation measures are promptly applied in the BAUMIT and BAUCONMIT scenarios, explosion prevention and immediate post-mission de-orbiting would avoid significant population growth. Consequently, the millimetre-sized population would be stabilised to near present-day levels in the long-term.

6.3.3 Future Environment Trends

The long-term population projections have indicated that the new constellation traffic would only have a minor impact on population evolution trends, with or without the modelled mitigation measures implemented (assuming that the constellation operators themselves also apply these measures). Therefore, the results presented in this section only relate to the constellation-related 'business as usual' future traffic scenarios (BAUCONST and BAUCONMIT). The equivalent BAU and BAUMIT scenario projections are very similar in characteristic and hence are not shown here in order to avoid duplication.

The results described in the previous section gave solely the temporal behaviour of the total number of objects in LEO larger than a given size threshold for the 4 different scenarios. They are useful for comparative purposes, and for drawing overall conclusions concerning long-term constellation impact and mitigation measure effectiveness. However, those results do not give any information on the evolution of the debris environment at different LEO altitudes. The debris environment projections given in this section represent high resolution forecasts of the debris spatial density distributed over altitude and time, for a given particle size threshold and future traffic scenario. The altitude range is partitioned into 25 km intervals from 200 km up to 2000 km, and the spatial density-altitude profile is given for each year from 2000 to 2050. The resulting three-dimensional surface plots represent an average debris environment projection which is derived from the individual projections output from each of the 10 Monte Carlo simulation runs of the IDES model for a particular traffic scenario. This has ensured that the spatial density distributions are smooth in appearance, devoid of stochastic aberrations and statistically significant.

Figure 6-5 shows the LEO debris environment evolution of objects >10 cm under a 'business as usual' future traffic scenario, with the new constellation traffic and without the application of any mitigation measures. Initially in the year 2000, the main peaks in spatial density are located at 775 km, 825 km and 1000 km altitude with density values lying between 2×10^{-8} and 3×10^{-8} objects/km^3. The peak at 775 km is due to the addition of 100 satellites from the CONSTEL2 (780 km) and CONSTEL4 (775 km) constellation designs launched during 1998 and 1999. Also, there are smaller, secondary spatial density peaks of just under 2×10^{-8} objects/km^3 at 1400 km and 1475 km altitude. It can be observed that the

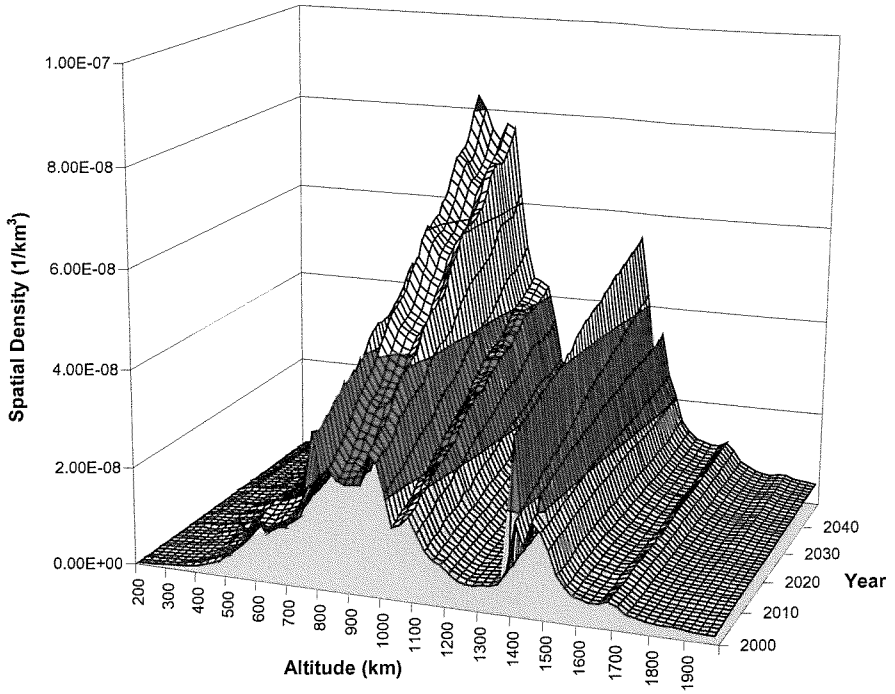

Figure 6-5: Future projection of the >10 cm LEO debris environment for a 'business as usual' future traffic scenario including the new constellation traffic

peak at 1475 km increases slightly in 2002 due to the introduction of the 80-satellite CONSTEL5 constellation. A completely new spatial density peak emerges in 2002 at 1375 km altitude due to the launch of the 324-satellite CONSTEL1 system. The background spatial density is initially low at 1375 km, and the addition of so many satellites within a 25 km altitude band causes the spatial density to increase by a factor of about 7. This CONSTEL1 peak is actually higher in spatial density than the primary peaks described above between 775 and 1000 km.

Figure 6-5 reveals that the predicted spatial density of objects >10 cm increases linearly with time at all LEO altitudes in this scenario. The gradient of this linear trend, however, appears to be highly altitude dependent. This is because of the significant differences in the recent historical launch and explosion rates for the different altitude regions, and these rates are assumed by the model to continue into the long-term future. One can see that the peak spanning the 800 to 1000 km altitude region has the highest predicted increase over the next 50 years, almost a factor of 4 larger than the year 2000 environment. At higher altitude regions (e.g. between 1400 and 1500 km), the increase in >10 cm spatial density is only a factor of 2 over the initial value for the same time period. Small periodic modulations in the

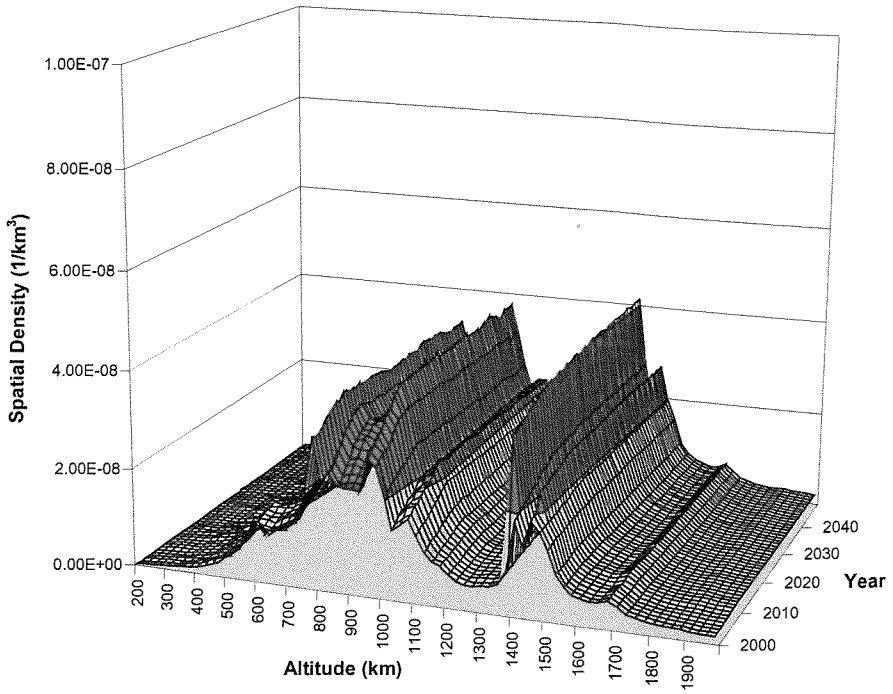

Figure 6-6: Future projection of the >10 cm LEO debris environment for a 'business as usual' future traffic scenario including the new constellation traffic and mitigation measure implementation

projected spatial density evolution at 800 to 1000 km altitudes are evident in Figure 6-5. These are due to the effects of the 11-year solar cycle on atmospheric drag. The drag force becomes exponentially higher at lower and lower altitudes, and thus the orbital lifetimes of objects are severely reduced. This factor accounts for the exponentially decreasing spatial density as altitude decreases from 600 km. Atmospheric drag becomes negligible at altitudes above 1000 km. This explains why there are no periodic solar cycle effects in the long-term projections of the 1375 km, 1400 km and 1475 km peaks in spatial density.

Figure 6-6 shows the prediction of the >10 cm LEO debris environment with both the new constellation traffic and the modelled mitigation measures implemented. The spatial density-altitude profile and its evolution from the year 2000 to 2010 has exactly the same characteristics and linear growth behaviour as the BAUCONST scenario projection in Figure 6-5. However, explosion prevention is implemented in 2010 and there is no significant linear growth in spatial density at all LEO altitudes after this year. In fact, there is no predicted growth at all in the spatial density profile, and the spatial density values below 1000 km remain constant over time. This is especially true for the spatial density peaks at

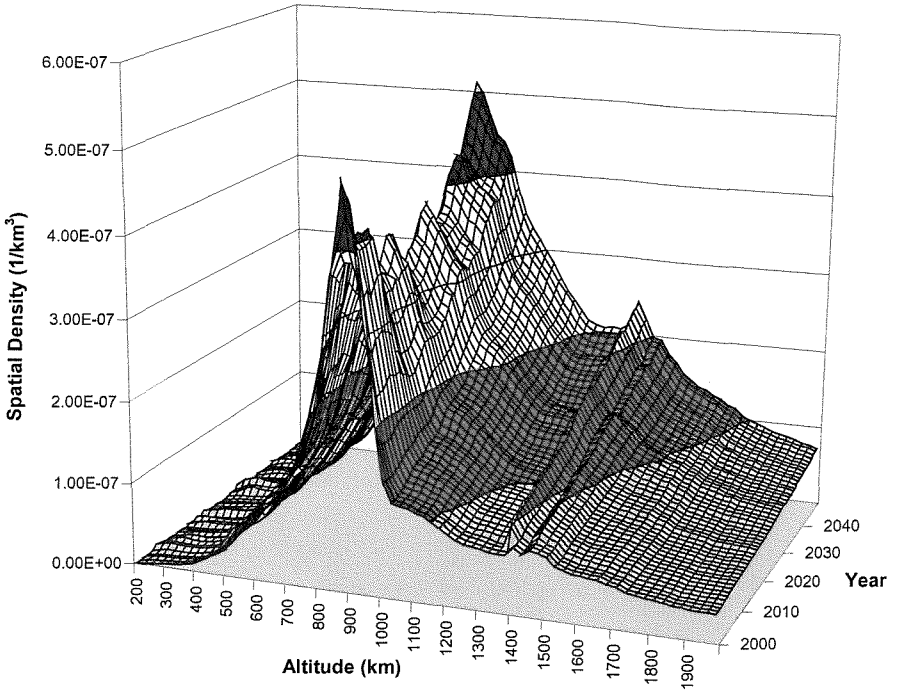

Figure 6-7: Future projection of the >1 cm LEO debris environment for a 'business as usual' future traffic scenario including the new constellation traffic

775 km, 825 km and 1000 km, which stay just below 4×10^{-8} objects/km^3, throughout the period 2010 to 2050. This is because no more explosion fragments are assumed to be generated after 2010. The removal of objects larger than 10 cm due to atmospheric drag and immediate post-mission de-orbiting appears to balance the addition of objects from 'business as usual' launch activity, and fragments from the low number of predicted catastrophic collisions in this scenario. The collision rate is stabilised and brought under control in the long-term due to the removal of target objects by immediate post-mission de-orbiting of satellites and rocket bodies. At altitudes higher than 1000 km, there is no atmospheric drag sink and the removal of objects by immediate post-mission de-orbiting is not sufficient to completely counteract the addition of objects from launch activity and the catastrophic collisions. Hence, the peaks in spatial density between 1375 km and 1475 km altitude still increase slightly, but at a slowing rate due to the reduction in the collision rate.

Figure 6-7 shows the projected evolution of the >1 cm debris environment over LEO altitudes for the 'business as usual' traffic scenario, with the new constellation traffic and without the modelled mitigation measures. Initially in the year 2000, the predicted LEO spatial density-altitude profile is dominated by the NaK droplet population between 750 and

1000 km altitude, which produces a peak spatial density of 4.5×10^{-7} objects/km^3 at about 900 km. This peak is approximately a factor of 4 higher than the underlying spatial density due to fragments from high intensity explosions. At other altitudes, the >1 cm debris density is quite widely spread over the full LEO altitude range due to the dispersal of many fragments into highly eccentric orbits. Emerging just above this spread, at altitudes between 1375 and 1475 km are the smaller contributions from the >10 cm debris environment, especially the 1375 km spatial density peak relating to the 324-satellite CONSTEL1 constellation design. The projected long-term temporal behaviour of spatial density between 750 and 1000 km altitude is very interesting in Figure 6-7, and appears as a dipping ridge-like structure. The spatial density peak centred around 900 km shows a net decrease over the next 25 years. This is because the dormant NaK droplet population is undergoing slow orbital decay due to the influence of atmospheric drag. After about the year 2025, the peak spatial density of this population reduces further and the eruption of fragments from high intensity explosions and catastrophic collisions displace the droplets as the dominant source in the 750 to 1000 km region. An ever-increasing collision rate and the continuation of the constant high intensity explosion rate up to 2050 ensures the accelerated development of a spatial density peak in this region. This peak grows to eventually replace the initial NaK droplet peak at a similar value of 5×10^{-7} objects/km^3. Hence, this scenario provides the unique conditions of a decaying NaK droplet population and the subsequent emergence of explosion/collision fragments in the same region that produces this spatial density 'ridge' for the evolving >1 cm environment at 900 km altitude.

At altitudes higher than 1000 km, the NaK droplets do not have an influence on the spatial density of objects larger than 1 cm. Therefore, the general exponential growth trends, due to explosions and the increasing number of collisions, can be seen in Figure 6-7 throughout the 52-year projection period. The periodic modulation effects of the solar cycle are clearly visible on the spatial density 'ridge' at 900 km altitude. The magnitude of the oscillations is greater than that seen in the >10 cm debris environment projections because of the higher area-to-mass ratios of centimetre-sized fragments and droplets. In fact, the solar cycle effects are large enough to actually cause periodic decreases in the spatial density at altitudes lower than 900 km. At altitudes higher than about 1200 km, atmospheric drag becomes negligible for centimetre-sized debris and therefore the solar cycle does not have an influence, resulting in the smooth exponential growth trends of the spatial density.

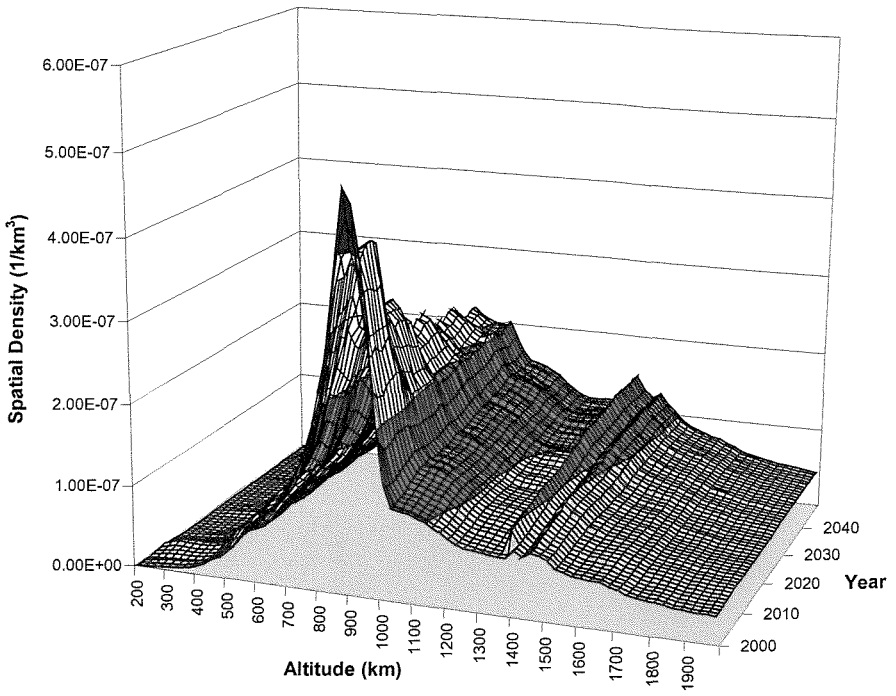

Figure 6-8: Future projection of the >1 cm LEO debris environment for a 'business as usual' future traffic scenario including the new constellation traffic and mitigation measure implementation

Figure 6-8 shows the long-term projection of the >1 cm debris environment with both the new constellation traffic and the mitigation measures applied. The initial characteristics of the >1 cm spatial density-altitude profile in the year 2000, described for the BAUCONST scenario in Figure 6-7, are also the same here. The other similarity between the two figures is the orbital decay of the dormant NaK droplet population residing between 750 and 1000 km altitude, producing a reduction in the spatial density peak at 900 km over the next 25 years. However, the difference with this BAUCONMIT scenario is that explosion prevention and immediate post-mission de-orbiting severely limits the future generation of centimetre-sized fragmentation debris. Hence, there is no emerging fragment-related peak in spatial density around 900 km to replace the decaying NaK in the latter 25 years of the simulation. In fact, without an exponentially growing peak in this region, the decay of the NaK droplet peak in spatial density can be seen to extend beyond the next 25 years, through two further solar cycle oscillations up to the year 2050. At this point, most of the droplets have decayed from orbit and the spatial density profile would be entirely dominated by the limited fragment population. After 2010, the spatial density values at altitudes above 1000 km still increase very slightly over the following 40 years of the simulation. This is because

the low number of catastrophic collisions predicted for this scenario still disperse new centimetre-sized fragments into eccentric orbits with apogees reaching up to these higher LEO altitudes. Most collision events tend to occur in the 800 to 1000 km altitude region, leading to collision fragments with perigees/apogees in this region. Atmospheric drag is very low at these altitudes and would not be able to remove these collision fragments for decades. Hence, spatial density slowly accumulates above 1000 km in this scenario.

6.4 Summary

The new constellation traffic modelled in this chapter is an approximate reflection of the current design status of systems being planned for deployment into LEO in the next decade. It was found that this new constellation traffic (including a 324-satellite system) would have only a minor impact on the long-term evolution of the LEO debris environment, with or without the implementation of routine mitigation measures, provided that the constellation operators themselves implement strict debris mitigation measures. In this context, the modelled constellation designs were predicted to sustain very few collision-induced breakups over the next 50 years. Hence, the number of generated collision fragments from these breakups were low in comparison to the background population at all LEO altitudes.

Significantly, it was found that the timely implementation of routine explosion prevention and immediate post-mission de-orbiting within the next 10-15 years was very effective at stabilising and even reducing the future LEO collision rate. These measures were found to stabilise population growth and prevent further increase in population levels at millimetre, centimetre and decimetre particle sizes. The centimetre-sized and decimetre-sized population levels even reduced in the long-term, due to these efficient mitigation measures.

The consequences of not implementing these kinds of measures within the next 10 to 15 years would be: continued linear growth in spatial density at all LEO altitudes for debris larger than 10 cm; and accelerating long-term exponential growth in the spatial density for centimetre-sized objects. This is particularly the case in the 750 km to 1000 km altitude band, where most of the collision activity is predicted to occur in the future. Without the implementation of the modelled debris mitigation measures, the decaying NaK droplet spatial density peak at 900 km would be replaced by the emergence of a fragment-related peak within 50 years.

7 Long-Term Constellation Collision Risk Analysis

7.1 Introduction

As awareness of the orbital debris issue continues to spread throughout the space industry, those designing space missions and spacecraft are learning that mission lifetime collision risks are significant in some regions of LEO and are on the increase. These risks must be properly assessed in order to make the trade-off against other risk factors to achieve acceptable reliability/system availability figures. If mission lifetime collision risks are unacceptably high, they must be effectively mitigated through changes to mission or spacecraft design. To facilitate this collision risk assessment, mission designers must have access to long-term collision risk forecasts for various target orbits over the planned mission lifetime. These forecasts are best provided by the most sophisticated models, which are able to simulate the long-term evolution dynamics of the debris flux environment over the next few decades and translate this into the evolving debris flux levels that could be encountered.

Models of the current debris flux environment, although valuable for near-term collision risk assessments, tend to estimate long-term future collision risks by applying analytical expressions to extrapolate their current debris environment into the future. These expressions take into account simple growth factors in the debris source terms and modulations due to potential solar cycle effects at the altitude of interest. However, we have seen that the application of these extrapolation methods can lead to large discrepancies, when compared to long-term evolution model predictions of mission collision risk[116]. It is therefore necessary to have models which can simulate long-term debris environment evolution in detail, and determine the directional/temporal collision risks that might be encountered by a spacecraft orbiting in that evolving debris environment. The IDES model has been designed specifically for this purpose and will be utilised in this chapter to perform long-term collision risk analysis for LEO satellite constellations operating in the future environments predicted by IDES and presented in Chapter 6.

In fact, constellations are a special case in long-term collision risk analysis because they may not only be exposed to the background debris environment, but also to additional 'self-

induced' risks due to fragments generated by any collision-induced breakups of satellite members within the system. These collision-induced breakups would be caused by long-term exposure of the large number of LEO constellation satellites to the catastrophic background environment (debris sizes larger than approx. 10 cm). A number of these collision-induced breakups were predicted to occur over the next 50 years by IDES in Chapter 6. Apart from the distribution of collision flux to a sample constellation satellite over impact angles and velocity, this chapter also presents the forecast of collision flux to the chosen satellite over the next 50 years. This is done for different impactor size thresholds and for the four future traffic scenarios considered. These temporal flux predictions are then used to estimate the number of debris-induced failures of the selected constellation system during the course of the mission. The same method is employed to provide debris-induced failure forecasts for two other constellation systems. Finally, the debris-induced failure rates are compared to the equivalent rates expected from component/sub-system reliability problems. It is these forecasts that are of most interest to constellation system designers, since they will give an estimate of the number of extra replacement satellites that need to be built and launched in order to maintain continuous global service coverage.

7.2 Directional Collision Flux Analysis for a Constellation Satellite

The method of computing the debris flux relative to the moving satellite target reference frame, through the range of different impact angles and velocities, has been described in section 3.5.3. The dependency of debris flux in the target reference frame over impact direction and velocity is of direct interest to spacecraft designers in particular. The spacecraft may have varying or fixed attitude within this reference frame and this information can serve as a direct input to tools such as ESABASE/DEBRIS[117] or NASA's BUMPER[118] code for impact damage risk assessment of the spacecraft surfaces and external shielding designs. In this context, the ESA MASTER model[48] is able to provide a very high resolution prediction of direction and velocity dependent flux to a target orbit, and is valid in the very near-term future debris environment. Other models in use with a published near-term directional collision flux capability are the NASA 1989 and 1996 engineering models[40,41], and the Russian SDPA model[45]. The IDES model is able to provide long-term direction and velocity dependent debris flux to a target orbit in any of the yearly flux

environment snapshots taken between 1998 and 2050, for any of the future traffic scenarios simulated in Chapter 6. In this section, the reference 'business as usual' (BAU) future traffic scenario has been chosen as a basis for the directional debris impact flux predictions. All results are an average of the individual results obtained from the 10 Monte Carlo simulations performed for this BAU scenario. As a case study, a satellite in the CONSTEL2 constellation (similar to Iridium) has been selected. The parameters used in this risk analysis case study are shown in Table 7-1.

Parameter	**Value**
Satellite semi-major axis	7158 km
Satellite eccentricity	0.0001
Satellite inclination	86.4°
Satellite cross-sectional area	9 m^2
Debris impactor size threshold	>1 cm
Analysis date	1st January 2020

Table 7-1: Data for the directional collision risk analysis of a constellation satellite

The variation of >1 cm debris flux to the constellation satellite with true anomaly angle can be seen in Figure 7-1 for the year 2020. True anomaly is the angle swept out in the orbit plane as the satellite traverses its orbital path, starting from the perigee point. Therefore, at 0° and 360° true anomaly, the satellite is at perigee, and apogee is reached at 180° true anomaly. The argument of perigee for the near-circular satellite orbit was randomly selected as 327°. Therefore, given the near-polar inclination of the satellite orbit, true anomalies of 33° and 213° are when the satellite passes through approximately 0° declination (i.e. the equatorial region). It can be seen that there are primary peaks in encountered flux at 96°, 150°, 276°, and 330° true anomaly. These peaks correlate to the intersection of the satellite orbit with approximately +63° and -63° declination respectively. At these declinations, there are modelled peaks in the >1 cm debris spatial density at most LEO altitudes, due to the fragments generated by high intensity explosion events occurring at orbital inclinations between 63° and 65°. There are secondary peaks in the encountered flux at 117°, 129°,

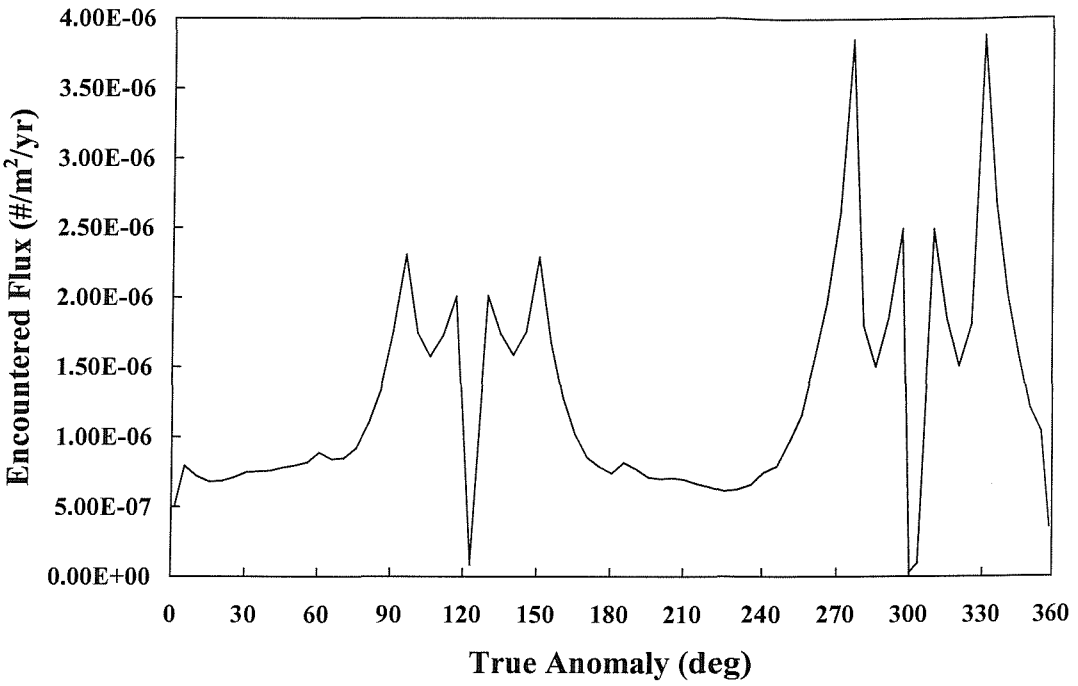

Figure 7-1: Average debris flux (>1 cm) encountered by the chosen constellation satellite around its orbit for the BAU scenario (1/1/2020)

297°, and 309° true anomaly and these correspond to the intersection of the satellite orbit with +84° and -84° declination respectively. Again, the IDES model predicted a growing peak in >1 cm debris spatial density at these declinations, due to the fragments generated by the collision-induced breakups simulated by IDES for the population of large objects on near-polar orbital inclinations (in the 700 to 1000 km altitude region).

It can also be observed that the encountered flux drops very sharply to almost zero at the true anomaly values of 123° and 303°. This is when the satellite orbit reaches maximum declination (+86.4°) and minimum declination (-86.4°) respectively, where the debris spatial density is very low. This is due to the fact that most of the near-polar inclination debris objects are actually concentrated around 82° and 98° inclination, and so would not reach the higher declinations traversed by the target orbit. There are also much wider troughs in the encountered flux centred around 33° and 213° true anomaly. This is because the satellite orbit is in a region of low declination of between -50° and +50°, where the lowest debris spatial densities are predicted. The stated true anomaly values correspond to satellite intersection of 0° declination where the high inclination debris cuts through the equatorial regions very quickly, leading to low residence durations and hence low spatial densities.

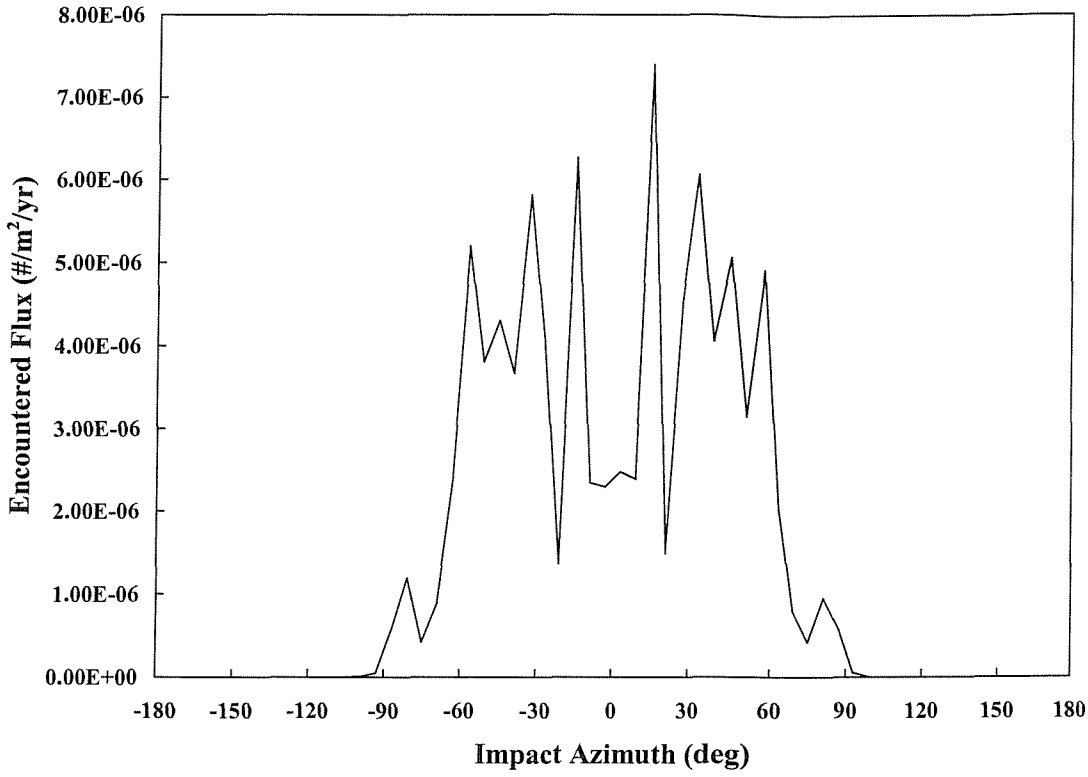

Figure 7-2: Predicted average impact azimuth angle distribution of the debris flux (>1 cm) encountered by the chosen constellation satellite in the BAU scenario (1/1/2020)

Overall, the plot shows how encountered flux can be precisely correlated to the passage of the satellite orbit through volumes of space with either high or low debris spatial density.

The variation of predicted >1 cm debris flux encountered by the target orbit over impact azimuth angle can be seen in Figure 7-2. This is the angle of impact in the target satellite's local horizontal plane. One can see that almost all of the debris impacts would be constrained within azimuth angles of between -90° and +90°, i.e. coming from within 90° to the left and to the right of the satellite velocity vector at 0° azimuth (the 'ram' direction or direction of motion). The debris flux is distributed about 0° azimuth angle in a reasonably symmetric manner with the largest flux peaks predicted to be encountered at ±15° azimuth angle. With an almost 'head-on' collision geometry, these peaks are due to debris on similar near-polar orbital inclinations to the target orbit and with a wide separation of their ascending nodes with respect to the target orbit. There are also peaks of slightly lower encountered flux at a range of angles between -60° and -30° azimuth, and between +30° and

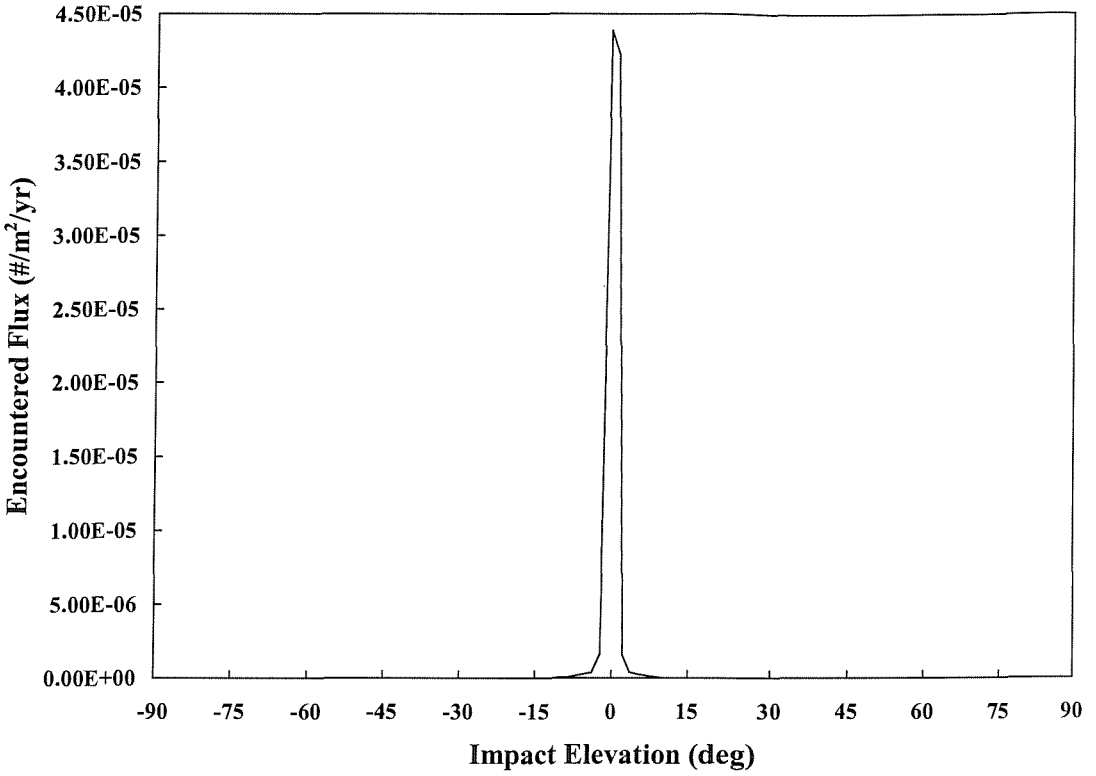

Figure 7-3: Predicted average impact elevation angle distribution of the debris flux (>1 cm) encountered by the chosen constellation satellite in the BAU scenario (1/1/2020)

+60° azimuth respectively. These secondary peaks are likely to result from debris impactors with lower orbital inclinations of between 60° and 70°. Much smaller 'side-lobes' in the encountered flux distribution may be observed at ±80° azimuth angle, due to debris on similar near-polar inclinations and similar ascending nodes as the target orbit.

The variation of predicted >1 cm debris flux encountered by the target orbit over impact elevation angle is presented in Figure 7-3. Elevation angle is defined as the angle of debris impact outside the target orbit's local horizontal plane. A positive elevation angle describes an impact from above the local horizontal plane and a negative elevation angle from below this plane. Only elliptical debris orbits are able to produce significant impact elevation angles. It can be observed that there is a single, discrete peak in encountered flux at 0° impact elevation angle and the peak is almost entirely constrained within +/- 5° elevation. This implies that the impacts will be mostly encountered by the target satellite in the local horizontal plane. This is due to the near-circular orbit of the satellite and the near-circular

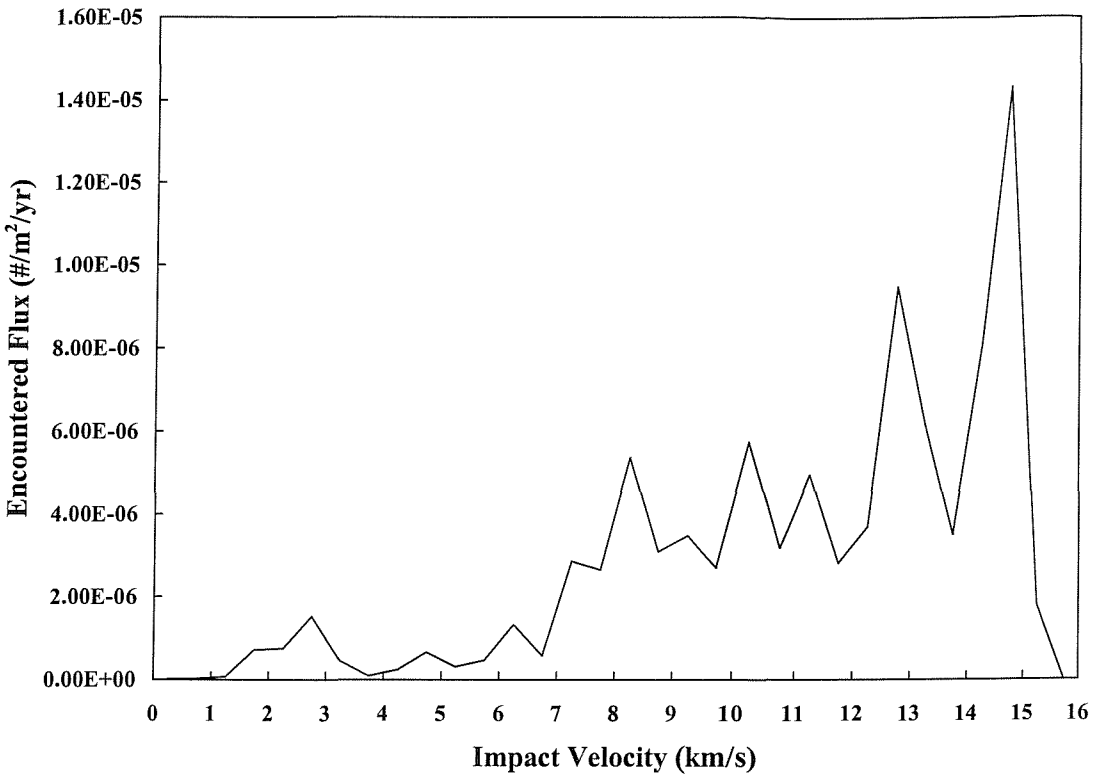

Figure 7-4: Predicted average impact velocity distribution of the debris flux (>1 cm) encountered by the chosen constellation satellite in the BAU scenario (1/1/2020)

nature of the debris orbits at the target orbit altitude of 780 km. The debris encountered are either on near-circular orbits, or alternatively the debris have elliptical orbits and are being encountered by the circular target orbit near their perigee altitudes.

Figure 7-4 shows the variation of the predicted >1cm debris flux encountered by the target orbit over impact velocity magnitude. Given that the encountered debris flux is predicted to be in the satellite's local horizontal plane, it is the impact azimuth distribution presented in Figure 7-2 that has the greatest influence on the impact velocity distribution. Head-on impacts close to 0° azimuth angle would tend to lead to the largest impact velocities between target and impactor. At the target orbit altitude of 780 km, orbital velocities are about 7.5 km/s and so the dominant head-on impacts produce impact velocities of close to 15 km/s. This is confirmed by the largest encountered flux peak at 14.8 km/s in Figure 7-4. There are secondary encountered flux peaks in the impact velocity distribution between 7 and 13 km/s. These are due to the secondary flux peaks in Figure 7-2 at wider azimuth angles from -60° to -30°, and from +30° to +60°. There is a very minor peak in encountered

flux at impact velocities between 2 and 3 km/s in Figure 7-4. This peak correlates to the small 'side-lobe' peaks in the impact azimuth distribution at +/- 80°.

7.3 Long-Term Collision Flux Trends for a Constellation Satellite

The detailed analysis of the debris flux encountered by a target satellite in terms of direction and velocity of impact at any point in time during the mission is directly applicable to the spacecraft design process. Additionally, the IDES model has an advanced capability to forecast the long-term temporal variation of debris flux to any target orbit intersecting LEO for a given debris particle size threshold and future traffic scenario. This forecasting capability can be of direct interest initially to the orbit selection process in the mission design phase. Then, these long-term forecasts can be updated reasonably frequently before launch and throughout mission operations as the model predictions of the current debris environment and future launch traffic are improved with time. This capability, whilst subject to the uncertainties that are inherent in the long-term environment projections, can at least give the mission designer and mission analyst a useful picture of the through-life collision risk trends in various orbits, compared to just simply extrapolating the current collision risks.

The long-term encountered debris flux forecasts are produced by using the theory presented in section 3.5.3 to obtain the orbit-integrated mean flux to the target orbit. This is done for each of the yearly flux environment snapshots output by a single IDES Monte Carlo simulation of debris environment evolution. The orbit-integrated mean flux to target versus year is obtained for each of the 10 Monte Carlo simulations in the given future traffic scenario. These 10 results are then averaged to produce the average long-term variation of encountered flux to the chosen target orbit in the given future traffic scenario. This processing has been performed for the constellation satellite given in Table 7-1, exposed to the long-term flux environment projections of the four different future traffic scenarios studied in Chapter 6.

Before presenting the long-term encountered flux forecasts for the chosen constellation satellite, it is worthwhile to note the meaning of the forecasts in each of the four different future traffic scenarios of BAU, BAUCONST, BAUMIT, and BAUCONMIT. The

encountered flux trends predicted for the BAU scenario represent the flux to target posed by the 'business as usual' background debris environment (with no mitigation measures implemented). The encountered flux trends predicted for the BAUCONST scenario represent the collision risk from the background debris environment, plus the average 'self-induced' collision risk posed by the fragments generated from the collision-induced breakups of other constellation satellites. Hence, comparison between the encountered flux trends of the BAUCONST and BAU scenarios infers this 'self-induced' collision risk. The encountered flux trends predicted for the BAUMIT and BAUCONMIT scenarios are equivalent to BAU and BAUCONST respectively, and contain the 'business as usual' background debris environment when the modelled mitigation measures are applied. Comparison between the encountered flux trends of BAUCONST and BAUCONMIT reveal the effect of the modelled mitigation measures in reducing the collision risk to the target constellation satellite.

Figure 7-5 shows the encountered flux trends predicted for the constellation satellite target orbit with debris of >10 cm in size. As seen in the population and environment evolution trends presented in Chapter 6 for this size threshold, the encountered flux trends in the scenarios of 'business as usual' without mitigation measures (BAU and BAUCONST) display an overall linear growth trend. There are small periodic modulations in this trend due to the solar cycle effects on atmospheric drag decay rates of object orbits, at the constellation satellite orbital altitude of 780 km. The periodic modulations are only small in magnitude due to the low atmospheric density and therefore long object dwell times in this region. Starting at an encountered flux level of 7.5×10^{-6} impacts/m^2/year in 1998, this linear growth is due to the linear extrapolation of historical launch and explosion activity into the future. This activity is sufficient to more than double the average encountered flux level to 1.8×10^{-5} impacts/m^2/year over the next 50 years. A comparison between the predictions in the BAU and BAUCONST scenarios, and between BAUMIT and BAUCONMIT scenarios, suggests that the chosen constellation satellite would encounter negligible 'self-induced' flux from debris >10 cm, with or without the implementation of the modelled mitigation measures. This is because, on average, the constellations modelled in this study were predicted to sustain less than two collision-induced breakups over the 50 year forecast. Hence, very few collision fragments are generated from constellation collision activity, and they could not produce a significant flux to the target orbit compared to the encountered flux

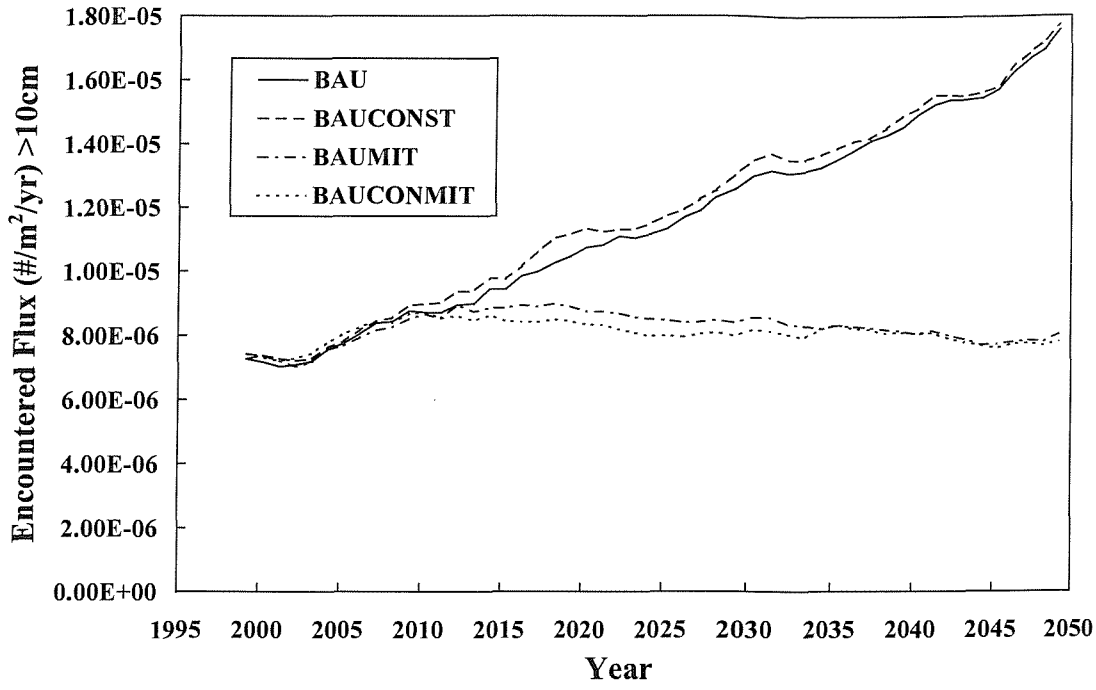

Figure 7-5: Forecast of the average flux of debris larger than 10 cm encountered in the chosen constellation satellite orbit over the next 50 years under four different future traffic scenarios

from the background environment. In this, and other figures in this Chapter, the mean collision risk to the target in the BAUCONMIT scenario appears to be less than the mean collision risk in the BAUMIT scenario. This is not because the satellite constellations are reducing the background collision risk, but is merely due to the statistical uncertainties introduced by the Monte Carlo simulation technique. There were a slightly lower number of random explosions predicted for the BAUCONMIT scenario than for the BAUMIT scenario in the mid-section of the projections, thus accounting for the difference. If more than 10 Monte Carlo runs were performed for each future traffic scenario, then the statistical uncertainties in the mean collision risk predictions would be reduced in magnitude. However, factors such as computer runtime currently prevent more Monte Carlo runs being executed.

The effect of the modelled mitigation measures on the >10 cm debris flux to the constellation satellite can be clearly seen by the comparison between the predictions for the BAUCONST and BAUCONMIT scenarios. Up to 2010, both scenarios produce similar linear encountered flux trends. Afterwards in the mitigation scenarios, explosion prevention

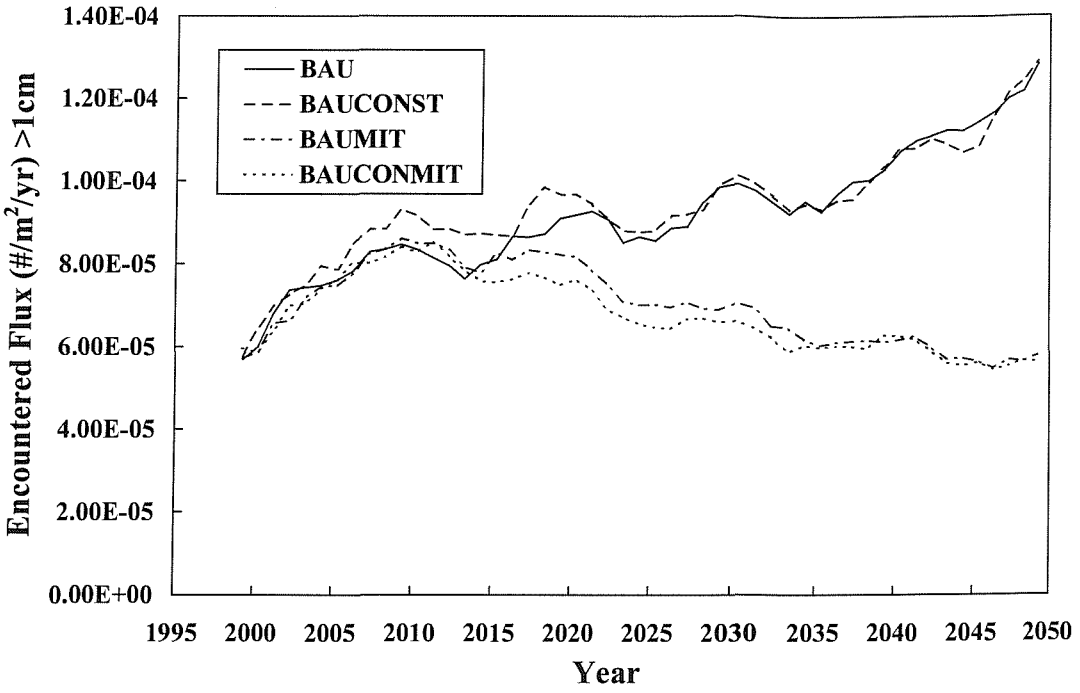

Figure 7-6: Forecast of the average flux of debris larger than 1 cm encountered in the chosen constellation satellite orbit over the next 50 years under four different future traffic scenarios

comes into operation and predicted encountered flux levels start to fall. This is because there is no fresh input of explosion fragments, and the in-orbit explosion fragment population at, and above the constellation satellite orbital altitude reduces due to atmospheric drag decay. The encountered flux levels are only prevented from falling more rapidly by the fragments generated from the few collision-induced breakups in this region. These breakups are limited by the immediate post-mission de-orbiting of rocket bodies and satellites in 2005 and 2015 respectively. In fact for debris >10 cm in size, the modelled mitigation measures are sufficient to return the encountered flux back to its initial 1998 level after 50 years.

Figure 7-6 presents the average flux of debris >1 cm that would be encountered in the constellation satellite target orbit. The flux predicted for all future traffic scenarios actually increases from 6×10^{-5} impacts/m^2/year in 1998 to a peak of about 9×10^{-5} impacts/m^2/year in 2008, even though there is a solar maximum in 2000/2001. Usually, the solar maximum causes a decrease in encountered flux, as seen in Figure 7-5 for debris >10 cm. However, the target orbit altitude of 780 km is only 100 km below the peak in the centimetre-sized debris environment due to the NaK coolant droplet population. This population is assumed

to remain dormant from 1988 and is set to decay from orbit under the action of atmospheric drag over the next couple of decades. Therefore, the increase in >1 cm encountered flux between 1998 and 2008 is likely to be caused by many of the NaK droplets decaying through the 780 km target orbit altitude during and after the solar maximum. After 2010, the encountered flux trends in the 'business as usual' scenarios without mitigation measures (BAU and BAUCONST) show a gradual overall exponential growth to reach 1.3×10^{-4} impacts/m^2/year in 2050. This is due to the ever increasing explosion and collision fragment population dominating over the ever decreasing influence of the decaying NaK droplet population in the centimetre size range at the target orbit altitude. The periodic modulation of the overall exponential growth trend due to solar cycle effects can be clearly seen in Figure 7-6. The solar cycle oscillations are larger in magnitude for centimetre-sized debris than for decimetre-sized objects, due to the generally higher ballistic coefficients of objects at smaller sizes.

In contrast, the implementation of the modelled mitigation measures tends to produce an overall gradual decrease in >1 cm flux to the target orbit after 2010. Between 2010 and 2050, the encountered flux is predicted to eventually drop back down to the initial 1998 level. Almost all of the NaK droplet population will have decayed below the 780 km target orbit altitude by about 2025, but the application of explosion prevention in 2010 ensures the decay of the in-orbit explosion fragment population. Also, the immediate post-mission de-orbiting after 2005/2015 severely constrains the generation of centimetre-sized collision fragments in the main collision region between 700 and 1000 km altitude. These factors result in the net overall decrease in >1 cm encountered flux seen in the mitigation scenarios after 2010. Once again, it can be observed in Figure 7-6 that there is a negligible 'self-induced' flux posed by constellation collision-induced breakup activity.

Figure 7-7 displays the IDES prediction of the long-term flux to the constellation satellite target orbit from debris larger than 1 mm. At this size threshold, the IDES model produces a very small NaK droplet population relative to the fragmentation debris population. This is because the modelled NaK droplet size distribution has a cut-off of 150,000 droplets larger than 4 mm. Therefore, the initial rapid increase in encountered flux trends observed for centimetre-sized debris in Figure 7-6 is not predicted at millimetre sizes. This is due to the relatively few NaK droplets decaying through the target orbit altitude, compared to the flux

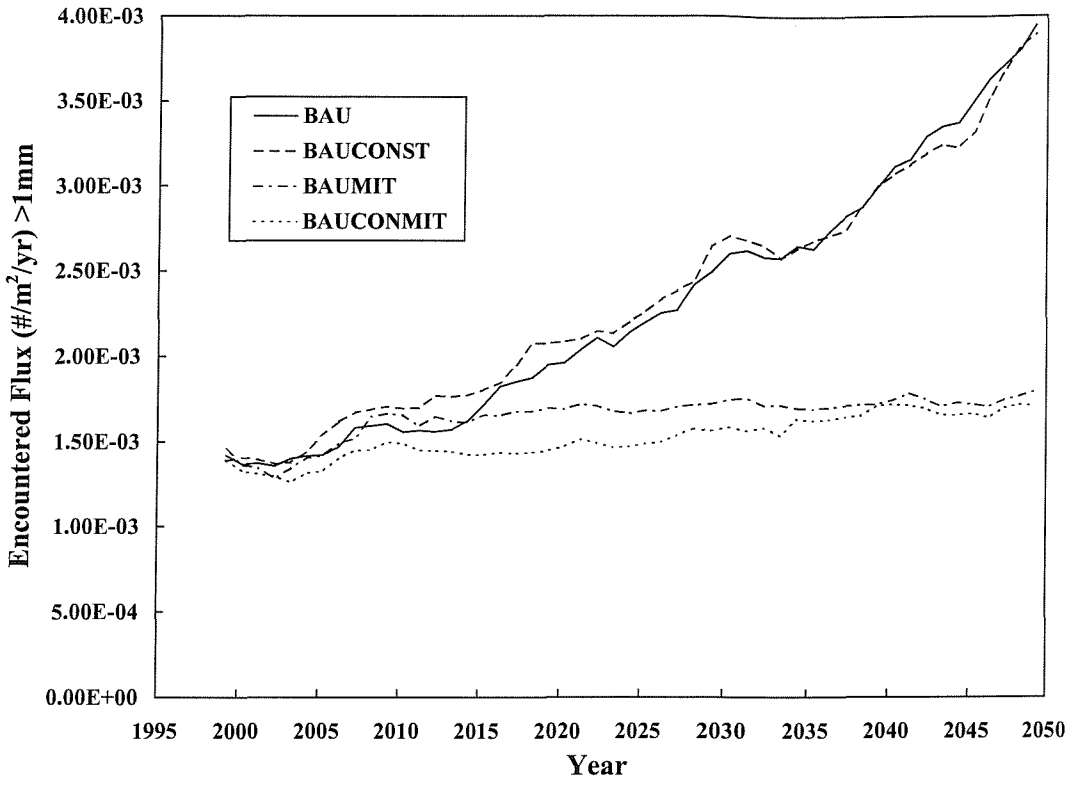

Figure 7-7: Forecast of the average flux of debris larger than 1 mm encountered in the chosen constellation satellite orbit over the next 50 years under four different future traffic scenarios

levels induced by explosion and collision fragments. Hence in Figure 7-7, the exponential growth in >1 mm encountered flux is evident throughout the entire 52-year simulation period for the 'business as usual' scenarios with no mitigation. In the BAU and BAUCONST scenarios, the average >1 mm encountered flux exponentially increases from 1.4×10^{-3} impacts/m^2/year in 1998 to 4×10^{-3} impacts/m^2/year in 2050, which is a rise of almost a factor of 3. Small solar cycle effects causing the periodic modulations in the overall exponential growth are visible in these trends.

For the BAUMIT and BAUCONMIT mitigation scenarios, the implementation of explosion prevention in 2010 and of immediate post-mission de-orbiting in 2005/2015 is predicted to stabilise the millimetre-sized flux to the target orbit at an almost constant level between 2010 and 2050. There is no predicted decrease in encountered flux, as seen for centimetre-sized debris in Figure 7-6. At this target orbit altitude, the generation rate of millimetre-sized collision fragments counter-balances the decay rate of the fragment population, after

the halting of explosions in 2010. Additionally, the decay rate is low because the millimetre-size fragment population is generally biased towards orbits with high eccentricity, leading to extended orbital lifetimes and a slower time to decay below the target altitude. Thus, a predicted constant encountered flux level is reached after the implementation of the mitigation measures. For debris >1 mm, there is a negligible 'self-induced' flux produced by constellation collision activity.

7.4 Debris-Induced Constellation Satellite Failure Rates

The encountered debris flux trends predicted for a single satellite in a constellation system can give a useful insight into the long-term variability of collision risk in the operational orbit. However, the information that is of most interest to constellation designers is the estimated number of satellite failures induced by debris impacts over the planned system operational lifetime. This directly indicates the potential number of extra replacements (and the extra manufacture and launch costs) that would be required to ensure continuous service availability. When forecasting the cumulative number of debris-induced failures for different constellation systems in previous IDES studies[119], it has been assumed that only debris larger than 1 cm could cause a satellite failure upon impact. By using this assumption, the only step necessary to obtain the cumulative number of debris-induced failures over time is to derive the cumulative number of impacts from debris >1 cm to the constellation over time. This was done by effectively applying the long-term encountered flux trends predicted for one constellation satellite to all satellites within the system. This is a reasonable assumption since the constellations studied here all have satellites with near-circular orbits at a common altitude and inclination. Hence, the only differences between the satellite orbits within a system are their right ascension of ascending nodes and argument of perigees (which are orbital plane dependent). The debris population is assumed to be randomly distributed in these orbit plane orientation parameters.

In these previous studies, the single-satellite encountered flux for debris >1 cm (in impacts/m^2/year) was simply multiplied by the total cross-sectional area of the whole constellation to get the constellation impact rate. The impact rate at each flux environment snapshot epoch was then multiplied by the time interval between snapshots (1 year) in order to obtain the expected number of impacts >1 cm to the constellation during each time

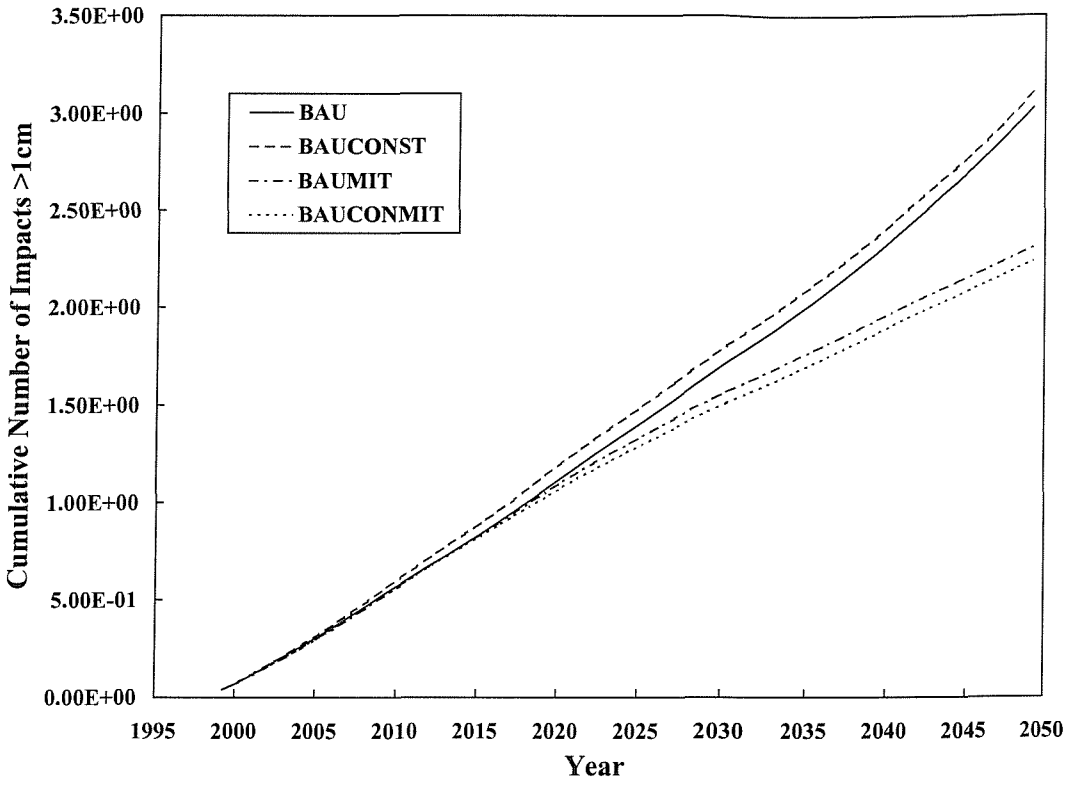

Figure 7-8: Forecast of the average expected number of impacts from debris >1 cm to the 72-sat. constellation system operating at 780 km altitude and 86.4° inclination for different future traffic scenarios

interval. The expected number of impacts was accumulated over successive time intervals from the constellation deployment epoch to produce the cumulative number of impacts >1 cm to the constellation over time.

This method was applied to calculate the cumulative number of impacts >1 cm over time for the CONSTEL2 system, based on the long-term encountered debris flux trends predicted by the IDES model for the chosen CONSTEL2 constellation satellite in Figure 7-6. The forecasts provided for the four different modelled future traffic scenarios can be seen in Figure 7-8. In the scenarios which relate to 'business as usual' future traffic without mitigation measures (BAU and BAUCONST), the CONSTEL2 system is predicted by IDES to encounter an average of 3 impacts with debris >1 cm over 50 years of exposure to the environment. An average of 1 impact is expected over the first 20 years of exposure. From the forecasts presented for the BAUMIT and BAUCONMIT scenarios, it is evident that the modelled mitigation measures do not have a discernable effect on the cumulative

constellation collision risk until after 2025. This is when most of the centimetre-sized NaK droplets have decayed through the 780 km operational altitude and the fluxes due to explosion and collision fragments are on the decline. In fact, in cumulative terms, the modelled mitigation measures are predicted to reduce the mean expected number of impacts >1 cm by only one third after 50 years of exposure to the projected debris environment.

Debris particles larger than 1 cm impacting a LEO constellation satellite at velocities of between 10 and 15 km/s can be assumed to cause failure. However, it is possible that smaller debris in the millimetre size range would cause more localised damage, which might still lead to failure if the strike occurs near the location of a critical component. Therefore, the previous assumption that *only* debris larger than 1 cm causes failure upon impact would tend to result in *very* conservative predictions of the cumulative number of debris-induced failures. In order to make the debris-induced failure predictions more realistic, a crude estimate of impact failure probability has been assumed in four different size ranges and is presented in Table 7-2. These probabilities are not based on detailed simulations of satellite damage assessment, but have been selected on the basis that small debris impactors produce more localised damage and therefore the resulting ejecta (if any) have less likelihood of striking the critical components.

Debris size range	Impact failure probability
1 mm - 2.2 mm	10%
2.2 mm - 4.7 mm	30%
4.7 mm - 1 cm	60%
>1 cm	100%

Table 7-2: Estimated satellite failure probabilities for debris impactors in various logarithmic size ranges of the IDES model

Given this size-dependent impact failure distribution, the cumulative number of failures for a particular constellation can be found by following these steps:

1. Calculate the cumulative number of impacts over time for debris >1 mm, >2.2 mm, >4.7 mm, and >1 cm (using the method described above);

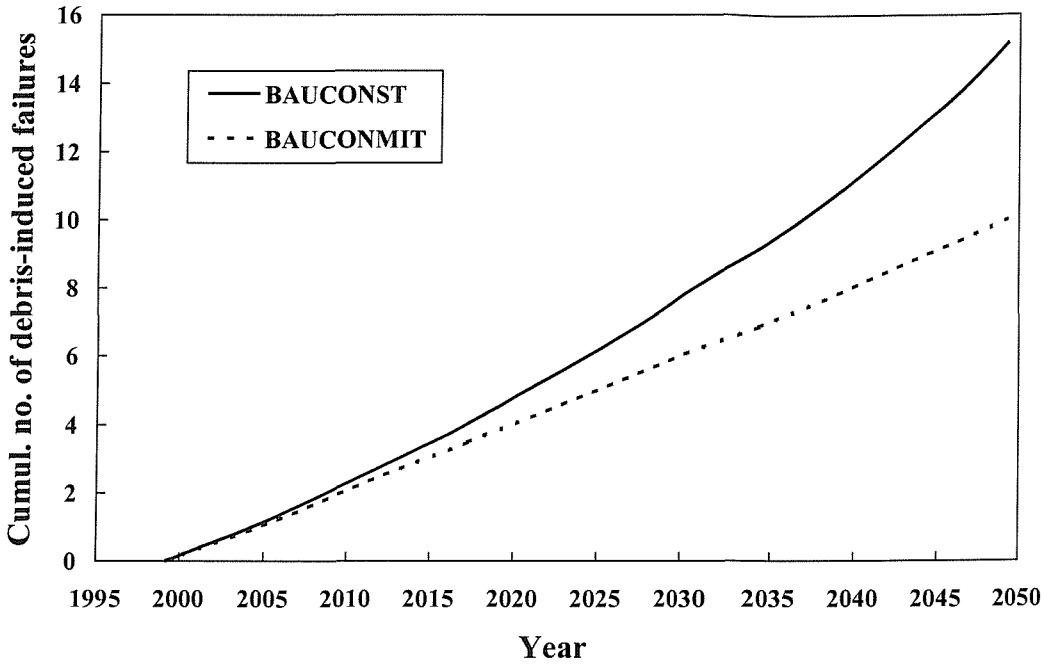

Figure 7-9: Forecast of the average expected number of satellite failures due to debris impacts for the 72-sat. constellation system operating at 780 km altitude and 86.4° inclination in two different future traffic scenarios

2. Find the differentials between these distributions to obtain the cumulative number of impacts for debris of 1 mm to 2.2 mm, 2.2 mm to 4.7 mm, 4.7 mm to 1 cm;
3. Multiply the differential distributions by their respective impact failure probabilities, e.g. 0.1 × (cumulative number of impacts for debris between 1 mm and 2.2 mm);
4. Sum the probability-weighted differential distributions together with the distribution for debris >1 cm to get the cumulative number of failures for the constellation.

By employing this procedure, the estimated cumulative number of debris-induced failures predicted for the 72-satellite CONSTEL2 system with and without the influence of the modelled mitigation measures can be seen in Figure 7-9. Without the application of the mitigation measures (BAUCONST), exposure to the projected 'business as usual' debris environment produces an exponentially increasing number of failures with exposure time. On average, 15 satellites are predicted to fail due to debris impacts after 52 years of debris environment exposure, and just over 4 failures after the first 20 years. This represents about 20% and 6% of the constellation respectively. The implementation of the modelled mitigation measures (BAUCONMIT) appear to produce a constant debris-induced failure

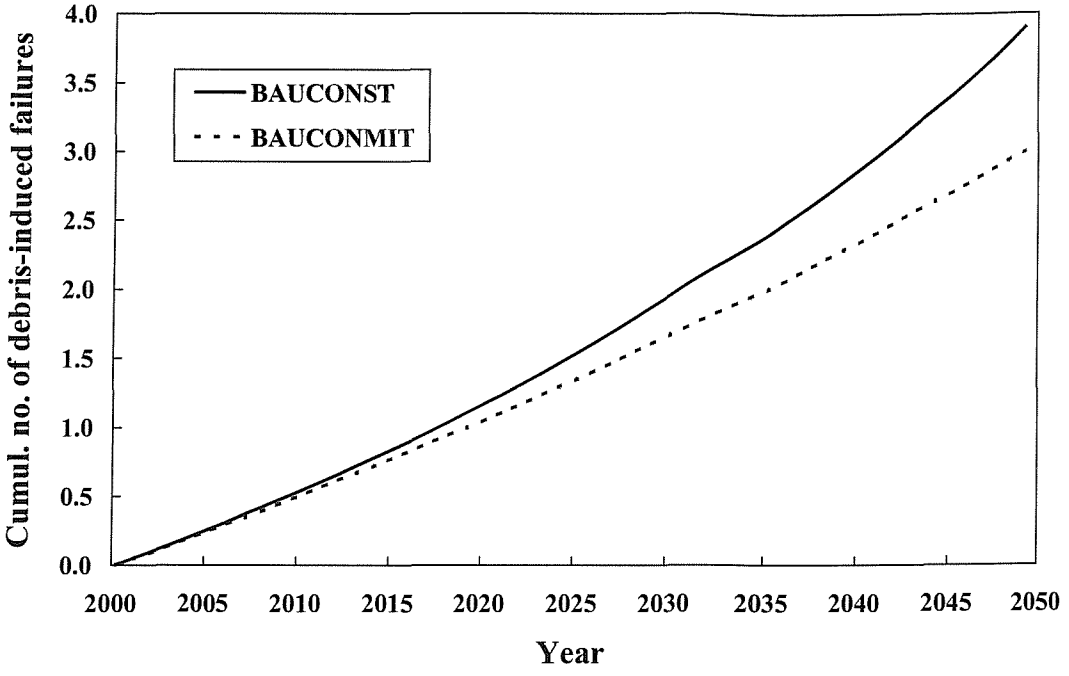

Figure 7-10: Forecast of the average expected number of satellite failures due to debris impacts for the 56-sat. constellation system operating at 1414 km altitude and 52° inclination in two different future traffic scenarios

rate over time, leading to a linearly increasing cumulative trend which reaches 10 failures after 52 years of exposure and an average of 3.5 failures after the first 20 years. A comparison between Figure 7-8 and Figure 7-9 reveals that the introduction of additional satellite failures from debris impactors in the millimetre-size range (with the estimated impact failure probability distribution), increases the predicted debris-induced failure rate substantially. However, this new method is considered to be more realistic and consistent with the predictions of other models, e.g. the NASA CONSTELL model[53]. Therefore, the new results given in Figure 7-9 should be used as a guideline by constellation operators.

The equivalent predictions for the 56-satellite CONSTEL3 system operating at 1414 km altitude and 52° inclination are displayed in Figure 7-10. Compared to CONSTEL2, the number of satellites in the system is slightly smaller, but the numbers of debris-induced failures predicted for CONSTEL3 are nearly a factor of 4 lower. This is because, unlike CONSTEL2, this higher altitude, lower inclination operational orbit is not in the peak density regions of the debris environment (at all sizes) and hence the encountered debris flux is much lower. Approximately 4 debris-induced failures are forecast for the

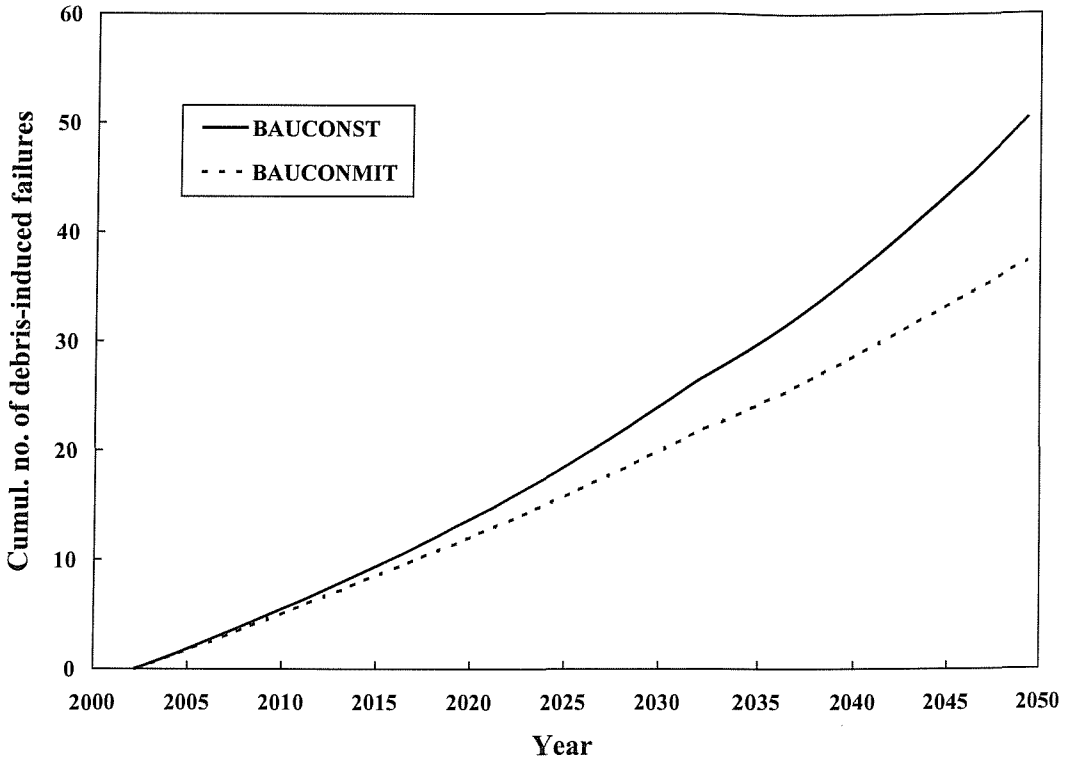

Figure 7-11: Forecast of the average expected number of satellite failures due to debris impacts for the 324-sat. constellation system operating at 1375 km altitude and 85° inclination in two different future traffic scenarios

CONSTEL3 system after more than 50 years of exposure to the 'business as usual' debris environment, and only an average of 1 failure is predicted during the first 20 years of operations. These values represent 7% and 1.8% of the constellation respectively. It can be observed that the effect of the mitigation measures on the failure rate for this higher altitude constellation is a 25% reduction, which is a less significant factor than at the lower 780 km altitude of the CONSTEL2 system. This is because above 1000 km there is negligible atmospheric density and therefore drag to remove debris objects from this region and hence mitigation measures appear less effective here.

Figure 7-11 shows the predicted debris-induced failure rate forecast for the 324-satellite CONSTEL1 system. The operating altitude of 1375 km is very similar to that of the CONSTEL3 design at 1414 km. However, proportionately more debris-induced satellite failures are predicted for the much larger CONSTEL1 constellation, principally due to the higher 85° inclination used. As many as 50 satellites are predicted to fail after 48 years of

exposure to the 'business as usual' debris environment, and an average of 15 failures after the first 20 years. These values represent 15% and 4.6% of the constellation system respectively.

In order to put these debris-induced constellation satellite failure predictions into perspective, they must be compared to the failure rates expected from normal reliability problems. If, for example, satellites in a constellation system are considered to be 80% reliable over an operational lifetime of 8 years, then the system would expect to lose an average of 20% of those satellites over the 8 year lifetime. If the constellation system is designed to operate for 20 years, then two generations of constellation satellites would need to be replaced (after 8 and 16 years respectively), and the third generation would operate for half of their designed operational lifetimes. Therefore, the percentage of the constellation system failing after 20 years would be 2.5 times the percentage after 8 years of operations, or 50% in this example. Table 7-3 shows the failure percentages for different figures of satellite reliability and duration of constellation system operations.

Satellite Lifetime (yrs)	Satellite Reliability	Proportion of system failed after 8 years	Proportion of system failed after 20 years
8	80%	20%	50%
8	90%	10%	25%
8	95%	5%	12.5%

Table 7-3 : Constellation failure percentages for different reliability values

The highest value predicted for the debris-induced failure percentage of a constellation system after 20 years of operation was 6.3% for the CONSTEL2 system. Hence for high reliability constellation satellites, mean debris-induced failure rates are found to be at least a factor of 2 lower than failure rates expected from reliability problems. For lower reliability constellation satellites, the debris-induced failure rates are at least a factor of 8 lower than the normal failure rates.

7.5 Summary

The direction/velocity dependent future collision risk analysis of a constellation satellite with a near-circular orbit at 780 km altitude and 86° inclination in the year 2020 has enabled the detailed understanding of a constellation's operating environment in LEO. The constellation chosen in this case study would encounter the highest collision risks from debris larger than 1 cm at high latitude regions. The debris would most likely to strike from a near 'head-on' direction in the local horizontal plane at high velocities of around 15 km/s.

The time dependent predictions of the debris flux encountered by the same constellation satellite for different size thresholds and future traffic scenarios has provided a good insight into the potential collision risk levels in a constellation orbit over the next 50 years. It was found that with current estimates of constellation traffic, the systems would pose a negligible 'self-induced' risk to themselves at all debris sizes, provided that they conduct strict mitigation measures such as satellite post-mission and failure de-orbiting. Without the implementation of the routine mitigation measures in the background population, including explosion prevention and immediate de-orbiting of satellites/rocket bodies, the 'business as usual' encountered flux increased linearly with time for debris >10 cm, and exponentially for debris >1 cm and >1 mm. This growth in collision risk was at least a factor of two above present levels after 50 years. An unusually large rise of the encountered flux in the centimetre debris size range was predicted for the next 10 years. This is believed to result from the centimetre-sized NaK droplet population decaying through the constellation satellite orbit altitude due to strong atmospheric drag during the next two solar maxima. It was found that when the routine mitigation measures were implemented, they were efficient enough to decrease or halt the growth in encountered flux levels at all debris sizes.

The long-term encountered flux trends were also used to estimate debris-induced satellite failure rates for different constellation systems. These rates were very dependent upon orbit selection, number of satellites in the system, and satellite cross-sectional area. The highest debris-induced failure rate was predicted for a constellation operating at 780 km altitude and 86° inclination. This rate lead to 6% and 20% of the constellation failing after 20 years and 50 years of exposure respectively. This was found to be about a factor of 2 to 8 lower than the expected 'reliability' failure rates, depending upon the satellite reliability value chosen.

8 Conclusions

8.1 Overview

The high-resolution simulation of the historical and long-term future evolution of the LEO debris environment, and the detailed long-term prediction of collision risk to any target orbit intersecting LEO is not trivial to achieve within a single model. By taking a tightly integrated, system-level approach to the design and development of a debris model, the Integrated Debris Evolution Suite (IDES) has been produced as an extremely flexible tool with a wide scope of state-of-the-art capabilities required to provide advanced solutions in all these areas.

A highly novel aspect of the IDES model is the new target-centred approach to the prediction of future collision events. Developed as part of this PhD research, the target-centred approach has made an advance over other traditional methods in the area of future collision event prediction, and has improved the accuracy of modelling the all-important future collision fragment source within long-term evolution models. The focus on large objects in the population as targets for rapid collision risk assessment, and stochastic prediction of collision events, has preserved knowledge of the exact orbit and mass of target objects during collision-induced fragmentation. This is problematic for other methods because the required information defining the breakup object is not known, and hence the breakup object's orbit and mass must be generated on a random basis. This can lead, in other models, to a systematic loss of accuracy in the number and orbit distribution of the collision fragment population.

The IDES simulation software has been developed to the highest standards and has undergone a rigorous validation programme to assess its accuracy. The results of this model validation are presented in Chapter 4. The IDES model was then applied extensively to study the long-term effects of constellations on the LEO debris environment in Chapters 5 and 6, and the long-term collision risks to constellation systems in Chapter 7. Detailed findings of these studies have been summarised at the end of each of these chapters. It is the intention of this chapter to provide a synopsis of these findings and their implications for

satellite constellation design. Clearly, there is more research to be done in the area of long-term debris environment and collision risk modelling, and therefore the thesis is closed with an outlook on future work.

8.2 Model Accuracy

Simulations of the historical evolution of the low Earth orbit debris environment have been performed using the IDES model. These simulations have provided a first-look validation of the model and a new insight into the emerging characteristics of the debris environment at particular altitudes, points in time, and particle sizes. Step increases in parts of the spatial density profile over altitude at specific epochs could be correlated to the occurrence of discrete breakup events. Gradual build-up in the spatial densities within specific altitude bands due to launch activity could be identified. The assumed leakage of liquid metal coolant from Russian RORSATs was observed to produce a pronounced peak in the centimetre-sized debris environment, which was (and still is) many times more dense than the underlying fragment population within a narrow altitude band.

The historical debris environment simulated by IDES has also been validated by comparison with reliable measurement data. The predicted debris environment for objects larger than 10 cm shows a good agreement with the equivalent USSPACECOM catalogue environment, given the known incompleteness of the catalogue at higher LEO altitudes at sizes close to 10 cm. The predicted debris environment for objects larger than 1 cm produces ground-based radar detection rates that are similar to the measured rates at all altitudes, including the large peak due to the sodium-potassium coolant droplet population. At a size threshold of 0.1 mm, the IDES debris environment produces a debris flux to a retrieved spacecraft surface that is an order of magnitude lower than the flux inferred from the measurement data. At the lower size threshold of 10 microns, the under-prediction increases to over an order of magnitude. It is believed that the inclusion of non-fragmentation sources in the IDES model, such as paint flakes and alumina solid rocket motor particles, will considerably improve the accuracy of IDES at these small sizes (see section on 'Future Work').

The main purpose of the IDES model is to predict the long-term evolution of the orbital debris environment (including constellation effects) and the long-term variation of collision

risk to low Earth orbit systems, particularly from centimetre and decimetre-sized debris which can cause satellite failure or fragmentation upon impact. Since IDES has good accuracy compared with reliable measurements at LEO altitudes for these sizes, confidence in the model for these applications has greatly improved.

8.3 Implications for Constellation Operations

The long-term collision interactions of a wide range of different constellation designs with the low Earth orbit debris environment have been extensively simulated for a 'business as usual' future traffic scenario, both with and without the application of mitigation measures. From these comprehensive state-of-the-art studies, it is concluded that the debris environment cannot sustain the long-term operation of a constellation with over 900 satellites deployed in orbits associated with the highest collision risk. In such a case, the constellation would have a long-term collision coupling with the local debris environment, leading to greatly enhanced collision risks and collision-induced breakup activity at the operational altitude due to the generated fragments. This additional collision activity associated with the large constellation would be sufficient to dominate the overall LEO collision rate, population growth, and collision risks to other orbiting systems. As a result, strict mitigation measures such as explosion prevention and immediate post-mission de-orbiting would be rendered extremely inefficient and unable to achieve long-term environment stability.

However, the IDES simulations have shown that the debris environment could sustain the long-term operation of medium-sized constellations of up to 100 satellites deployed in orbits associated with the highest debris collision risk, or alternatively larger constellations of up to 350 satellites deployed in low collision risk orbits. These types of system are representative of the current design status of constellations being planned for deployment into LEO in the next decade. In these cases, the number of collision-induced breakups sustained by the constellation systems would be extremely low, provided that these systems employ strict debris mitigation strategies such as explosion prevention and immediate post-mission/failure de-orbiting of their satellites. Consequently, the number of generated collision fragments from these limited breakups would be small in comparison to the background population. Thus, the long-term impact of the currently foreseen constellation

traffic on the LEO debris environment would be negligible, again provided that the constellations implement the strict mitigation measures stated above.

8.4 Mitigation Measure Effectiveness

According to the sophisticated IDES model simulations, the combined implementation of explosion prevention and immediate post-mission de-orbiting of satellites and rocket bodies was found to be very effective in stabilising and even reducing the future LEO collision rate. These measures would also stabilise population growth, and prevent further increase in population levels at millimetre, centimetre and decimetre particle sizes. In addition to this stabilisation, the centimetre-sized and decimetre-sized debris population levels even showed a reduction in the long-term, due to these efficient, combined mitigation measures. It should be noted that these measures would only retain their high efficiency if they are implemented within the next 10 to 15 years. After this time, it may be too late to prevent the collision cascading process from occurring without more drastic, costly action. The consequences of not implementing these kinds of measures would be continued linear growth in the decimetre-sized debris environment, and long-term exponential growth in the centimetre and millimetre debris size ranges. Without the implementation of the measures, the decaying peak in sodium-potassium droplet spatial density would be replaced by the emergence of a wider fragment-related peak within the next few decades.

8.5 Constellation Risk Assessment

The highest collision risks that would be encountered by constellations were found to be in near-circular orbits at altitudes between 700 and 1000 km and with near-polar inclinations. Constellation satellites in these orbits are most likely to be struck almost head-on from the ram direction, and in the local horizontal plane at high velocities of around 15 km/s. At these velocities, debris impacts have the potential to cause significant damage to a satellite and could lead to system failure or complete breakup in the case of the larger impactors. The long-term forecasts of collision risk for LEO constellations provided by the IDES model are state-of-the-art and should be of direct interest to mission designers. It was found that with current estimates of constellation traffic, the systems would pose a negligible 'self-induced' risk to themselves at all debris sizes, provided that they conduct strict mitigation measures such as immediate satellite post-mission/failure de-orbiting. Estimated debris-induced

satellite failure rates were produced for different constellation architectures. These rates were found to be very sensitive to orbit selection, number of satellites in the system, and satellite cross-sectional area. The highest proportion of debris-induced failures within a system was predicted for a constellation operating in the peak collision risk orbit described above. Approximately 6% and 20% of the constellation was predicted to fail due to debris impacts after 20 years and 50 years of exposure respectively. Debris-induced failure rates were found to be at least a factor of 2 to 8 lower than the failure rates expected from 'reliability' problems, depending upon the satellite reliability value chosen. However, in absolute terms, even an additional two or three launches carrying a number of extra replacement satellites represents a significant cost. For a large constellation, this cost can be minimised by optimal orbit selection in the design phase.

8.6 Further Work

Improvements to Model Accuracy

The development and improvement of non-fragmentation source models as new measurement data becomes available, will be an important area for all debris environment models in the future. Currently, most non-fragmentation debris source models are in their infancy and need to reach a mature state in order to be used with some confidence. At small particle sizes between 10 microns and 1 mm, the paint flake source generated via surface degradation or ejected by meteoroid/debris impacts may be a significant debris source. However, this is the source that is least well characterised. Research into the physical and chemical processes inducing paint flake release should be studied in depth, in order to improve understanding and eventually reduce the inaccuracy of debris environment models such as IDES at these sizes. A research programme to this effect is currently being conducted at the Queen Mary and Westfield College, University of London with a requirement to develop a paint flake source model from thermal cycling/atomic oxygen/ultra violet radiation effects. This model should be validated against measurement data from ground-based 'space environment simulation' facility tests. Once completed, the paint flake degradation source model will be integrated into the IDES model. A paint flake ejecta source model should also be developed, based upon the empirical size distributions of paint flakes ejected during ground-based hypervelocity impact tests. Additionally, alumina dust and slag particles ejected during/after SRM burns are known to contribute to the orbital

debris population at sub-100 micron and centimetre sizes respectively. An alumina dust and slag source model will be implemented in the IDES software in the future to further improve IDES capabilities and accuracy.

Since development and implementation of the NaK droplet mass distribution in IDES, additional measurement data from the Goldstone radar has been published. This data has placed the number of NaK droplets with sizes between 2.5 and 6 mm at 500,000. This is somewhat higher than the maximum 155,000 droplets generated by the exponential law in IDES at these sizes. Therefore, it is planned to revise the NaK droplet mass distribution for IDES in order to fit this additional data and also extend the distribution down to 0.1 mm droplet sizes to account for the two NaK impact craters found on the LDEF spacecraft.

The impact failure probability distribution used to estimate debris-induced failure rates for the constellation systems is currently derived from a simple assumption on the magnitude of impactor damage potential at different particle sizes. This distribution is not based upon any ground-based hypervelocity impact test data or upon any results from impact damage assessment simulations. This is because there is little published research on the failure mode analysis of satellite systems in response to damage caused by the penetration of particles of different sizes/velocities and at different locations. The accuracy of debris-induced failure rate forecasts for constellations would certainly benefit from an impact failure probability distribution derived by satellite impact damage codes. However, these codes must first be extended to model the criticality and failure modes of major components/sub-systems, and the damage effects of secondary ejecta particle clouds internal to a spacecraft design for different primary impact scenarios. This will be a major challenge, but not beyond the realms of possibility.

Further Constellation Studies

The extensive studies conducted into the long-term impact of constellation systems on the low Earth orbit debris environment have so far assumed that the constellation systems would implement strict debris mitigation measures. These assumed measures included immediate de-orbiting of constellation satellites at end-of-life and upon failure. However, some constellation operators may be tempted to neglect debris mitigation measures because of the cost implications, or operators may simply lose control of satellites. In this scenario,

uncontrolled defunct constellation satellites would be left in or near the constellation operational orbit, thus increasing the number of constellation satellites (since the defunct satellites will be replaced). It has been shown in Chapter 7 that up to 50% of satellites within a constellation system may fail due to reliability problems during a 20-year period of constellation operations. Furthermore, systems may have 1 or 2 complete satellite replacement cycles within the constellation system operational lifetime. Hence, if no mitigation is employed, the total number of satellites associated with a given constellation after 20 years of operations may be a factor of 2.5 higher than the number of operational satellites in the nominal configuration. Such an increase would cause the number of collision-induced breakups sustained by constellation satellites to rise. In turn, these extra breakups would disperse fragments and increase the long-term impact of constellations on the environment and collision risk trends. The IDES model would require enhancement to study this phenomenon.

Currently, constellation operators may volunteer to comply with national agency mitigation standards. These standards mainly recommend two different options for post-mission disposal of satellites in LEO. The first option involves performing a de-orbit manoeuvre, ensuring that the residual post-mission orbital lifetime due to natural perturbations is less than a certain number of years. In practice, it is least costly to simply perform a single burn to lower perigee into a region of high atmospheric density, for example 300 km altitude. This will result in a population of constellation satellites with decaying elliptical orbits, and is likely to apply to systems with operational altitudes below 900 km due to fuel requirements. The second option involves boosting satellites to a storage orbit region above LEO in order to remove mass from the more crowded LEO altitudes. In this case, multiple burns would be executed in order to achieve near-circular orbits above 2000 km, and is likely to be attractive for constellations with operational altitudes above 1300 km due to fuel requirements. However, given that the total number of satellites associated with a constellation may be significantly more than the operational number (due to replacement cycles and failures rates), the storage orbit may soon be over-used and collisions may start to occur in that region. The IDES model would require enhancement to simulate the long-term effects of post-mission lifetime limitation and storage orbit mitigation policies, applicable to both constellations and the general satellite population.

Future IDES Applications

Presently, the IDES model is constrained to simulating the long-term evolution of the LEO debris environment. Constellations systems are also being planned for deployment in Medium Earth Orbit (MEO) and Inclined Geo-Synchronous Orbit (IGSO). Prominent members of the international debris community are calling for the use of a graveyard orbit above the geostationary ring[3,120,121] in order to preserve GEO as a valuable operational resource. National agency debris standards[18] also propose post-mission disposal above/below semi-synchronous orbit in MEO. There is concern that these graveyard orbits may be over-used in the future, particularly if MEO and GEO become increasingly popular for commercial reasons. A large population of satellites and rocket bodies in those graveyard orbits would increase the probabilities of explosion and collision fragmentations, thus potentially increasing the collision risk to operational systems from the dispersed fragments[34]. Much attention must be given to debris management in MEO and GEO regions in the future, including the avoidance of long-term debris problems in the graveyard orbits. The extension of the IDES model to study long-term LEO, MEO and GEO debris environment evolution and the implications of associated mitigation practices will be an important application for the future, and one that will have a wide scope for new research.

Looking ahead to possible spaceflight activity in the next few decades, new technologies that are emerging from the concept stages must be considered for their potential effects on the debris environment. One such example is the application of Micro and Nano Technology (MNT) to satellites. In the future, it is envisaged that hundreds or even thousands of tiny micro-satellites with masses less than 1 kg could be designed to work co-operatively in a constellation or a swarm formation, to perform the missions that would conventionally be performed by just a few expensive large satellites. These micro-satellite swarms might be too small and too numerous to be tracked by space surveillance networks. In this scenario, the large operational satellites might not be able to 'see' the micro-satellite swarms in terms of tracking data for close approach predictions. However, the micro-satellites would be sufficient in mass to cause, on impact, either the failure or the fragmentation of a large satellite. The deployment of manoeuvrable micro-satellite swarms might lead to large variations in lethal collision risks in very specific orbits, and indeed presents a very complex modelling problem for the future.

8.7 Summary

The IDES model has been developed as an extremely flexible tool with a wide scope of state-of-the-art capabilities, providing a high-resolution simulation of the historical and long-term future evolution of the LEO debris environment, and associated mission collision risks. Novel techniques have been developed to greatly improve the level of detail and accuracy of collision event prediction, incorporating the simulation of collision interactions between satellite constellations and background debris environment. Comprehensive studies using IDES have added to our knowledge of the constellation designs that can and cannot be sustained by the LEO debris environment in the long-term. The research presented in this thesis has proven that low Earth orbit is not a limitless resource. It must be managed carefully in the future. This means that the space debris community must keep a watching brief on the scale of satellite constellation proposals. The long-term forecasts of collision risk for LEO constellations provided by the IDES model are state-of-the-art and should be of direct interest to mission designers. The forecasts have enhanced our knowledge of the potential magnitude of debris-induced failure rates, for a wide range of constellation design parameters and future traffic scenarios. These debris-induced failure rates were found to be lower than the rates expected from normal satellite component or sub-system failure. However, failures from debris impacts are significant enough that constellation operators must now fully consider orbital debris hazards during the design of their systems.

Bibliography

[1] Kessler, D.J., "Collisional Cascading: The Limits of Population Growth in Low Earth Orbit", Adv. Space Res. Vol. 11, No. 12, pp. 63-66, 1991.

[2] Hechler, M., van der Ha, J.C., "Probability of Collisions in the Geostationary Ring", J. of Spacecraft and Rockets, Vol.18, No.4, 1980.

[3] Flury, W., "Collision Probability and Spacecraft Disposition in the Geostationary Orbit", Adv. Space Res., Vol.11, No.12, pp. 67-79, 1991.

[4] Johnson, N.L., "History of On Orbit Fragmentations", Teledyne Brown Engineering, Colorado Springs, CS92-TR-JSC-007, Sixth Edition, 1992.

[5] Eichler, P., Rex, D., "Debris Chain Reactions", AIAA 90-1365, AIAA/NASA/DOD Orbital Debris Conference: Technical Issues & Future Directions, Baltimore MD, April 1990.

[6] Office of Science and Technology Policy, "Interagency Report on Orbital Debris", 1995.

[7] Crowther, R., Stokes, H., Walker, R., Barrows, S., Swinerd, G.G., "Characterisation of the Potential Impact of Space Systems on the Orbital Debris Environment: Satellite Constellations", Proceedings on Space Environmental, Legal, and Safety Issues, SPIE, Vol. 2483, pp. 88-99, 1995.

[8] Mazza, C., Fairclough, J., Melton, B., de Pablo, D., Scheffer, A., Stevens, R., "Software Engineering Standards", Prentice Hall, Hemel Hempstead, England, 1994.

[9] Law, A.M., Kelton, W.D., "Simulation Modeling and Analysis", McGraw-Hill, 1991.

[10] Rossi, A., Cordelli, A., Pardini, C., Anselmo, L., Farinella, P., "Modelling the Space Debris Evolution: Two New Computer Codes", AAS 95-186, Advances in the Astronautical Sciences, Space Flight Mechanics 1995, pp. 1217-1231, 1995.

[11] Royal Aircraft Establishment, "The R.A.E. Table of Earth Satellites 1957-1989", 1990.

[12] Siebold, K., Matney, M.J., Ojakangas, G.W., Anderson, B.J., "Risk Analysis of 1-2 cm Debris Populations from Solid Rocket Motors and Mitigation Possibilities for GEO-Transfer

Orbits", Proceedings of the 1st European Conference on Space Debris, Darmstadt, Germany, ESA publication SD-01, 1993.

[13] Mueller, A.C., Kessler, D., "The Effects of Particulates from Solid Rocket Motors Fired in Space", Adv. Space Res., Vol. 5, No. 2, 1985.

[14] Akiba, R., Ishii, N., Inatani, Y., "Behaviour of Alumina Particles Exhausted by Solid Rocket Motors", ISAS, Sagamihara, Kanagawa, AIAA 90-1367, Baltimore, 1990.

[15] National Research Council, "Orbital Debris: A Technical Assessment", National Academy Press, 1995.

[16] Stansbery, E.G., Settecerri, T.J., Matney, M.J., Zhang, J., Reynolds, R.C., "Haystack Radar Measurements of the Orbital Debris Environment; 1990-1994", NASA Johnson Space Center, JSC-27436, 1996.

[17] Maclay, T.D., McKnight, D.S., "The Contribution of Debris Wakes from Resident Space Objects to the Orbital Debris Environment", IAA-94-IAA.6.4.692, 45th Congress of IAF, Jerusalem, Israel, Oct. 9-14, 1994.

[18] NASA Safety Standard, "Guidelines and Assessment Procedures for Limiting Orbital Debris", NSS 1740.14, August 1995.

[19] Spencer Campbell, W., Sorge, M., Spencer, D., Maethner, S., "Proposed Development of Department of Defense (DOD) Debris Mitigation Guidelines", Paper AAS 96-112, AAS/AIAA Space Flight Mechanics Meeting, Austin TX, February 1996.

[20] Kato, A., "Current Status of NASDA Orbital Debris Mitigation Standards", Paper IAA.-95-IAA.6.5.02, 46th International Astronautical Congress, Oslo, Norway, October 1995.

[21] Orbital Debris Program Office, NASA Johnson Space Center, "Orbital Debris Quarterly News", Vol. 4, Issue 1, January 1999.

[22] Crowther, R., "The Trackable Debris Population in Low Earth Orbit", JBIS, Vol. 47, pp. 128-133, 1994.

[23] Klinkrad, H., Jehn, R., "The Space Debris Environment of the Earth", ESA Journal, Vol. 16, No. 1, 1992.

[24] Henize, H., Stanley, J., "Optical Observations of Orbital Debris", Paper AIAA-90-1340, AIAA/NASA/DOD Orbital Debris Conference, 1990.

[25] Stansbery, E.G., Bohannon, G., Pitts, C., Tracy, T., Stanley, J., "Radar Observations of Small Space Debris", Adv. Space Res., Vol. 13, No. 8, pp. 43-48, 1993.

[26] Mehrholz, D., "Space Object Observation with Radar", Adv. Space Res., Vol. 13, No. 8, pp. 33-42, 1993.

[27] Taft, L.G., Beatty, D.E., Yakutis, A.J., Randall, P.M.S., "Low Altitude, One Centimeter, Space Debris Search at Lincoln Laboratory's (MIT) Experimental Test System", Adv. Space Res., Vol. 5, No. 2. pp. 35-45, 1985.

[28] Settecerri, T.J., Stansbery, E.G., Matney, M.J., "Haystack Measurements of the Orbital Debris Environment", Advances in Space Research, Volume 23, Issue 1, pp. 13-22, 1999.

[29] Reynolds, R., Matney, M., "A Comparison of Haystack Radar Measurements with EVOLVE Debris Environment Predictions", Paper IAA-95-IAA.6.3.08, 46th International Astronautical Congress, Oslo, Norway, October 1995.

[30] Matney, M., Goldstein , R., Kessler, D., Stansbery, E., "Recent Results from the Goldstone Orbital Debris Radar", Advances in Space Research, Volume 23, Issue 1, pp. 5-12, 1999.

[31] Mulholland, J.D., Singer, S.F., Oliver, J.P., Weinberg, J.L., Cooke, W.J., Montague, N.L., Wortman, J.J., Cassel, P.C., Kinard, W.H., "IDE Spatio-Temporal Impact Fluxes and High Time-Resolution Studies of Multi-Impact Events and Long-Lived Debris Clouds", LDEF-69 Months in Space: Proceedings of the First Post-Retrieval Symposium, Kissimmee FL, NASA CR-3134, 1991.

[32] Drohlshagen, G., McDonnell, J.A.M., Stevenson, T., Aceti, R., Gerlach, L., "Post Flight Measurements of Meteoroid/Debris Impact Features on EURECA and the Hubble Solar Array", Adv. Space Res., Vol. 16, No. 11, pp. 85-89, 1995.

[33] Zhang, J., Kessler, D.J., Rex, D., "Interpretation of the Distribution of Large Craters on the Long Duration Exposure Facility (LDEF) ", Proceedings of the First European Conference on Space Debris, Darmstadt, Germany, ESA SD-01, 1993.

[34] Kessler, D.J., "The Current and Future Environment: An Overall Assessment", Preservation of Near Earth Space for Future Generations, pp.19-36, Cambridge University Press, 1994.

[35] Zolensky, M.E., See, T.H., Bernhard, R.P., Barrett, R., Hörz, F., Warren, J.L., Dardano, C., Leago, K.S., Kessler, D., Foster, T.R., "Final Activities and Results of the Long Duration Exposure Facility Meteoroid and Debris Special Investigation Group", Adv. Space Res., Vol. 16, No. 11, pp. 53-65, 1995.

[36] Kessler, D.J., "Space Debris: More Than Meets the Eye", Sky & Telescope, June 1987.

[37] United Nations Committee On the Peaceful Uses of Outer Space, "Report of the Scientific and Technical Subcommittee on the Work of its Thirty-Fourth Session", February 1997.

[38] Space News, "Orbital Debris Strikes French Defense Satellite", 6th August 1996.

[39] Kessler, D.J., Reynolds, R.C., Anz-Meador, P.D., "Current Status of Orbital Debris Environment Models", AIAA 95-0662, 33rd Aerospace Sciences Meeting and Exhibit, Reno, NV, 9-12 January 1995.

[40] Kessler, D.J., Reynolds, R.C., Anz-Meador, P.D., "Orbital Debris Environment for Spacecraft Designed to Operate in Low Earth Orbit", NASA-TM-100471, 1988.

[41] Zhang, J., Kessler, D.J., Matney, M.J., Eichler, P., Reynolds, R.C., Anz-Meador, P.D., Stansbery, E.G., "The NASA Engineering Model: A New Approach", Adv. Space Res., Volume 19, Issue 2, pp. 281-290, 1997.

[42] Kessler, D.J., "Derivation of the Collision Probability Between Orbiting Objects: The Lifetimes of Jupiter's Outer Moons", ICARUS 48, pp. 39-48, 1981.

[43] Eichler, P., Reynolds, R.C., "The Four Phases of the Collisional Evolution of an Unstable Earth Environment", Orbital Debris Monitor, Vol. 9(1), January 1996.

[44] Bendisch, J., "Analysis of Debris Mitigation Measures", Final report of ESOC Contract 11263/95/D/IM(SC), April 1996.

[45] Nazarenko, A.I., "The Development of the Statistical Theory of a Satellite Ensemble Motion and its Application to Space Debris Modeling", Proceedings of the Second European Conference on Space Debris, ESA SP-393, pp. 233-238, May 1997.

[46] Eichler, P., Reynolds, R.C., "Mid- and Long-Term Debris Environment Projections Using the EVOLVE and CHAIN models", Paper IAA-95-IAA.6.4.07, 46th International Astronautical Congress, Oslo, Norway, October 1995.

[47] Reynolds, R., "Documentation of Program EVOLVE: A Numerical Model to Compute Projections of the Man-Made Debris Environment", System Planning Corporation report OD91-002-U-CSP, 1991.

[48] Sdunnus, H., Klinkrad, H., "An Introduction to the ESA Reference Model for Space Debris and Meteoroids", Proceedings of the First European Conference on Space Debris, Darmstadt, Germany, ESA SD-01, 1993.

[49] Eichler, P., Anz-Meador, P., "A New and Detailed Evaluation of the Number and Masses of Objects in Earth Orbit", Paper AAS 96-115, AAS/AIAA Space Flight Mechanics meeting, Austin TX, February 1996.

[50] NASA Orbital Debris Program Office, "Orbital Debris Quarterly News", Volume 3, Issue 2, April 1998.

[51] NASA Orbital Debris Program Office, "Orbital Debris Quarterly News", Volume 3, Issue 4, October 1998.

[52] Ojakangas, G.W., Anz-Meador, P., Reynolds, R., "Orbital Debris Environment", AIAA 90-3863, AIAA Space Programs and Technologies Conference, Huntsville AL, Sept. 1990.

[53] Reynolds, R., Bade, A., Siebold, K., Johnson, N., "Debris Environment Interactions with Low Earth Orbit Constellations", Proceedings of the Second European Conference on Space Debris, ESA SP-393, pp. 351-357, May 1997.

[54] Anselmo, L., Cordelli, A., Farinella, P., Pardini, C., Rossi, A., "Study on Long-Term Evolution of Earth Orbiting Debris", Final report of ESOC contract 10034/92/D/IM(SC), February 1996.

[55] Rossi, A., Anselmo, L, Pardini, C., Farinella, P., Cordelli, A., "Interaction of the Satellite Constellations with the Low Earth Orbit Debris Environment", presented at the International Workshop on the Mission Design & Implementation of Satellite Constellations, Toulouse, France, November 17-19, 1997.

[56] Sdunnus, H., "ESA MASTER Final Report", ESOC contract 10453/93/D/CS, July 1995.

[57] Fucke, W., Sdunnus, H., "Population Model of Small-Size Space Debris", Final report of ESOC contract 9266/90/D/MD, June 1993.

[58] Klinkrad, H., "Collision Risk Analysis for Low Earth Orbits", Adv. Space Res., Volume 13, Issue 8, pp. 177-186, 1993.

[59] Wiedemann, C., Bendisch, J., Klinkrad, H., Krag, H., Wegener, P., Rex, D., "Debris Modeling of Liquid Metal Droplets Released by RORSATs", paper IAA-98-IAA.6.3.03, 49th International Astronautical Congress, Melbourne, Australia, Sept. 28-Oct. 2, 1998.

[60] Wegener, P., Krag, H., Rex, D., Bendisch, J., Klinkrad, H., "The Orbital Distribution and Dynamics of Solid Rocker Motor Particle Clouds for an Implementation into the MASTER Debris Model", Adv. Space Res., Volume 23, Issue 1, pp. 161-164, 1999.

[61] Anz-Meador, P., "Future Planned Space Traffic: 1990-2010 and Beyond", Paper AIAA-90-1360, AIAA/NASA/DOD Orbital Debris Conference: Technical Issues & Future Directions, Baltimore MD, 1990.

[62] Kleinau, W., Bombled, J.P., "Potential Mission Scenarios (Post 2000) for Future European Launchers", Paper IAF-90-194, 41st IAF Congress, Dresden, Germany, 1990.

[63] Reynolds. R., P. Anz-Meador, G.W. Ojakangas, "The Impact of Alternative Mission Models on the Future Orbital Debris Environment", Advances in Space Research, Vol. 11, No. 12, pp. 29-32, 1991.

[64] Kessler, D.J., Cour-Palais, B.G., "Collision Frequency of Artificial Satellites: The Creation of a Debris Belt", Journal of Geophysical Research, Vol. 83, No. A6, 1978.

[65] Alby, F., Lansard, E., Michal, T., "Collision of CERISE with Space Debris", Proceedings of the Second European Conference on Space Debris, ESA SP-393, pp. 589-596, May 1997.

[66] Klinkrad, H.(editor), "ESA Space Debris Mitigation Handbook", version 1.0 issued by the European Space Agency in June 1998.

[67] Anselmo, L., Rossi, A., Pardini, C., "Updated Results on the Long-Term Evolution of the Space Debris Environment", Adv. Space Res., Volume 23, Issue 1, pp. 201-211, 1999.

[68] Madler, R.A., Culp, R.D., "The Impact of Satellite Breakup Parameters on Long-Term Orbital Debris Environment Evolution", SPIE Vol. 2483, pp. 64-76, 1995.

[69] Walker, R., "Architectural Design Document: IDES Software", report ref. DRA/CIS(CIS2)/ADD/95/01, July 1995.

[70] Madler, R.A., "Sensitivity of the Near-Earth Orbital Debris Environment to Satellite Fragmentation Parameters", PhD dissertation, University of Colorado, USA, 1994.

[71] Walker, J.G., "Some Circular Orbit Patterns Providing Continuous Whole Earth Coverage", Journal of the British Interplanetary Society, Vol. 24, pp.369-384, 1971.

[72] Space Station Freedom Program Office, "Space Station Natural Environment Definition for Design", Revision A, SSP 30425, Reston VA, June 1991.

[73] Jehn, R., "Fragmentation Models", ESOC/MAS Working Paper 312, ESOC, Darmstadt, 12/90.

[74] McKnight, D., Maher, R., Nagl, L., "Refined Algorithms for Structural Breakup Due to Hypervelocity Impact", Hypervelocity Impact Society Symposium, Sante Fe, NM, Oct.16-20 1994.

[75] Su, S.-Y., Kessler, D.J., "Contribution of Explosions and Future Collision Fragments to the Orbital Debris Environment", Advances in Space Research, Vol. 10, No.2, p. 25-34, 1985.

[76] Reynolds, R.C., "A Review of Orbital Debris Environment Modelling at NASA/JSC", Orbital Debris Conference, AIAA-90-1355, Baltimore, MD, Apr. 16-19 1990.

[77] Kessler, D.J., Matney, M.J., Reynolds, R.C., Bernhard, R.P., Stansbery, E.G., Johnson, N.L., Potter, A.E., Anz-Meador, P.D., "The Search for a Previously Unknown Source of Orbital Debris: The Possibility of a Coolant Leak in Radar ocean Reconnaissance Satellites", NASA Report no. JSC-27737, NASA Johnson Space Center, Houston, TX, USA, 1997.

[78] Sridharan, R., Beavers, W., Lambour, R., Gaposchkin, E.M., Kansky, J., Stansbery, E., "Remote Sensing and Characterization of Anomalous Debris", Proceedings of the Second European Conference on Space Debris, ESA SP-393, pp. 239-246, May 1997.

[79] Meshcheryakov, S.A., "Analysis of One Line of Evidence of Orbital Debris Population Bred by RORSAT Satellites", Space Forum, Vol.1, pp. 119-123, 1996.

[80] Bess, T.D., "Mass Distribution of Orbiting Man-made Space Debris", NASA Report no. TN D-8108, NASA Langley Research Center, USA, 1975.

[81] Jehn, R., "Modelling Debris Clouds", PhD thesis, Shaker Verlag, Germany, 1996.

[82] Roy, A.E., "Orbital Motion" 3rd ed. Hilger, 1988.

[83] King-Hele, D.G., "Satellite Orbits in an Atmosphere: Theory and Applications", Blackie, 1987.

[84] Schatten, K., NASA/GSFC, Solar flux predictions, Solar Geophysical Data Bulletin, published by the National Geophysical Data Center, June 1998.

[85] Cook, G.E., "Luni-Solar Perturbations of the Orbit of an Earth Satellite", RAE Technical Report No. G.W. 582, 1961.

[86] Escobal, P.R., "Methods of Orbit Determination", Robert E. Krieger Publishing Company, Huntington, New York, 1976.

[87] Walker, R., Hauptmann, S., Crowther, R., Stokes, H., Cant, A., "Introducing IDES: Characterising the Orbital Debris Environment in the Past, Present and Future", AAS 96-113, Advances in the Astronautical Sciences, Space Flight Mechanics 1996, Vol. 93, Part I, pp. 201-220, 1996.

[88] Christiansen, E.L., et al., "Highly Oblique Impacts Into Thick and Thin Targets", International Journal of Impact Engineering, Nov. 1992.

[89] Grün, E., Zook, H.A., Fechtig, H., Giese, R.H., "Collisional Balance of the Meteoroid Complex", Icarus 62, pp 244-272, 1985.

[90] Kessler, D.J., "A Guide to Using Meteoroid-Environment Models for Experiment and Spacecraft Design Applications", NASA TN D-6596, 1972.

[91] Cant, A., "The Prediction of Meteoroid Impacts on Satellites", Technical Report DRA/CIS(CSC3)/TR/95/01/1.0, January 1995.

[92] ESABASE/DEBRIS; Environment Models; Section 2.2, Meteoroids Environment, p2.1-2.26.

[93] Settecerri, T.J., Stansbery, E.G., Opiela, J.N., Henderson, R., "Haystack Radar Measurements of the Orbital Debris Environment; 1994-1996", NASA Report no. JSC-27842, NASA Johnson Space Center, Houston TX, USA.

[94] Hörz, F., Bernhard, R.P., See, T.H., Brownlee, D.E., "Natural and Orbital Debris Particles on LDEF's Trailing and Forward-Facing Surfaces", LDEF - 69 Months in Space, Third Post - Retrieval Symposium, NASA CP 3275 Part 1, pp. 415-429, 1993.

[95] Johnson, N., Bade, A., Eichler, P., Cizek, E., Robertson, S., Settecerri, T., "History of On-Orbit Satellite Fragmentations", 11th Edition, NASA Report no. JSC 28383, July 1998.

[96] Jackson, A., Eichler, P., Reynolds, R., Potter, A., Johnson, N., "The Historical Contribution of Solid Rocket Motors to the One Centimeter Debris Population", Proceedings of the Second European Conference on Space Debris, ESA SP-393, pp. 279-284, May 1997.

[97] Stansbery, E.G., Kessler, D.J., Matney, M.J., "Recent Results of Orbital Debris from the Haystack Radar Measurements", paper AIAA 95-0664, 33rd Aerospace Science Meeting and Exhibit, 9-12 January 1995.

[98] Kessler, D., Johnson, N., Stansbery, E., Reynolds, R., Siebold, K., Matney, M., Jackson, A., "The Importance of Nonfragmentation Sources of Debris to the Environment", Adv. Space Res., Volume 23, Issue 1, pp. 149-160, 1999.

[99] Jehn, R., Nazarenko, A., Ihringer, C., Walker, R., "Comparison of Space Debris Models in the Centimetre Size Range", Proceedings of the Second European Conference on Space Debris, ESA SP-393, pp. 309-316, May 1997.

[100] Rossi, A., Pardini, C., Anselmo, L., Cordelli, A., Farinella, P., "Effects of the RORSAT NaK Drops on the Long-Term Evolution of the Space Debris Population", paper IAA-97-IAA.6.4.07, 48th International Astronautical Congress, Turin, Italy, Oct 6-10, 1997.

[101] Jehn, R., Klinkrad, H., "From Measurement Results to Space Debris Environment Models", paper IAA-97-IAA.6.3.10, 48th International Astronautical Congress, Turin, Italy, Oct 6-10, 1997.

[102] Christiansen, E., "Orbiter Meteoroid/Orbital Debris Impacts: STS-50 (6/92) through STS-86 (10/97)", NASA report no. JSC-28033, 1998.

[103] Stark, J., Nombro, A., Walker, R., Crowther, R., "A Model for the Generation of Micro-debris Resulting from Atomic Oxygen Impact", Proceedings of the Second European Conference on Space Debris, ESA SP-393, pp. 285-288, May 1997.

[104] Adams, W.S., Rider, L., "Circular Polar Constellations Providing Continuous Single or Multiple Coverage Above a Specified Latitude", The Journal of the Astronautical Sciences, Vol. 35, No. 2, pp. 155-192, 1987.

[105] Wilson, A. (editor), Jane's Space Directory, Twelfth Edition, 1996-1997.

[106] Teledesic Corporation World Wide Web Home Page, http://www.teledesic.com/.

[107] Walker, R., Crowther, R., Swinerd, G.G., "The Long-Term Implications of Operating Satellite Constellations in the Low Earth Orbit Debris Environment", Adv. Space Res., Volume 19, Issue 2, pp. 355-358, 1997.

[108] Battaglia, P.E., Rossi, A., "A Survey of the Italian Space Debris Related Activities", paper IAA-96-IAA.6.4.08, 47th International Astronautical Congress, Beijing, China, October 7-11, 1996.

[109] Anselmo, L., Cordelli, A., Farinella, P., Pardini, C., Rossi, A., "Modelling the Evolution of the Space Debris Population: Recent Research Work at Pisa", Proceedings of the Second European Conference on Space Debris, ESA SP-393, pp. 339-344, May 1997.

[110] Mendell, W., Reynolds, R., Kessler, D., "Telecommunications Satellite Constellations and the LEO Debris Population", paper IAA-97-IAA.6.5.05, 48th International Astronautical Congress, Turin, Italy, Oct 6-10, 1997.

[111] Bendisch, J., Rex, D., "The Long-Term Evolution of Orbital Debris - New Findings Concerning Collisional Cascading", IAA-95-IAA.6.4.08, 46th International Astronautical Congress, Oslo, Norway, October 1995.

[112] Bonnal, Ch. Sanchez, M., Naumann, W., "Ariane Debris Mitigation Measures", Proceedings of the Second European Conference on Space Debris, ESA SP-393, pp. 681-688, May 1997.

[113] Ryden, K., Fearn, D. G., "End-of-life disposal of satellites using electric propulsion: an aid to mitigation of the space debris problem", paper IAF-95-IAA.6.5.04, 46th International Astronautical Congress, Oslo, Norway, October 1995.

[114] Walker, R., Crowther, R., Marsh, V., Stokes, P.H., Swinerd, G.G., "Satellite Constellations and their Long Term Impact on the Debris Environment in Low Earth Orbit",

Proceedings of the Second European Conference on Space Debris, ESA SP-393, pp. 359-366, May 1997.

[115] Walker, R., Crowther, R., Cosby, M., Stokes, P.H., Swinerd, G.G., "The Long-Term Impact of Constellations on the Debris Environment after the Implementation of Debris Mitigation Measures", paper IAF-97-IAA.6.4.3, 48th International Astronautical Congress, Turin Italy, October 1997.

[116] Sdunnus, H., Stokes, H., Walker, R., Bendisch, J., Klinkrad, H., "Consideration of Solar Activity in Models of the Current and Future Particulate Environment of the Earth", paper presented at the ESA Workshop on Space Weather, ESTEC, Noordwijk, The Netherlands, 11-13 November 1998.

[117] Drolshagen, G., Borde, J., "ESABASE/DEBRIS Meteoroid/Debris Impact Analysis", Technical Description, ESABASE-GD-01/1, 1992.

[118] Christiansen, E.L., Hyde, J.L., Lear, D., "Meteoroid/Orbital Debris Impact Damage Predictions for the Russian Space Station MIR", Proceedings of the Second European Conference on Space Debris, ESA SP-393, pp. 503-508, May 1997.

[119] Walker, R., Crowther, R., Wilkinson, J., Stokes, P.H, "Orbital Debris Collision Risks to Satellite Constellations", Mission Design and Implementation of Satellite Constellations, p. 317-326, J.C. van der Ha (ed.), Kluwer Academic Publishers, 1998.

[120] Flury, W., McKnight, D., "Policy Aspects of Orbital Debris Mitigation", paper IAF 92-0223, 43rd International Astronautical Congress, Washington, Aug. 28-Sept. 5, 1992.

[121] Johnson, N.L., "Protecting the GEO Environment: Policies and Practices", Space Policy, Vol. 15, Issue 3, pp. 127-135, 1999.

Appendix A

Examples of the IDES Future Launch Traffic Database Files

EXAMPLE PAYLOAD.DAT FORMAT:

Class no.	Class description	Launch rate (/yr)	obj./launch	op. life (yrs)
130552504	"FR VLP VLA VHI HM OBSSATS P"	0.125	1	4.98
240253104	"JP VLP VLA LI ESM SCISATS P"	0.250	1	2.50
440358304	"FSU VLP VLA MI SM MILSATS P"	0.375	1	0.00
440358504	"FSU VLP VLA MI HM MILSATS P"	3.000	1	2.90
451658004	"GB VLP HA VLI ISM MILSATS P"	0.125	2	1.00
466150304	"US HP HA VLI SM COMSATS P"	0.625	1	12.53
546150404	"EUTEL HP HA VLI MM COMSATS P"	0.250	1	12.96

EXAMPLE ASSOC.DAT FORMAT:

Primary Class no.	Primary Class description	Assoc. Class no.	Assoc. Class description	obj./ launch	assoc. r/body launch rate frac.
246152104	"JP HP HA VLI ESM OBSSATS P"	240252107	"JP VLP VLA LI ESM OBSSATS PMORO"	4	0.000
440358404	"FSU VLP VLA MI MM MILSATS P"	440303702	"FSU VLP VLA MI Molniya LVFS"	1	0.125
440358404	"FSU VLP VLA MI MM MILSATS P"	440306202	"FSU VLP VLA MI Tsyklon LVFS"	1	0.875
440353404	"FSU VLP VLA MI MM SCISATS P"	440306202	"FSU VLP VLA MI Tsyklon LVFS"	1	1.000
440353404	"FSU VLP VLA MI MM SCISATS P"	440306203	"FSU VLP VLA MI Tsyklon LMORO"	5	0.000
466150304	"US HP HA VLI SM COMSATS P"	461702002	"US VLP HA LI Delta II LVFS"	1	0.200
466150304	"US HP HA VLI SM COMSATS P"	462200702	"US VLP VHA LI Atlas II LVFS"	1	0.200
466150304	"US HP HA VLI SM COMSATS P"	440304503	"FSU VLP VLA MI Proton K LMORO"	1	0.000
466150304	"US HP HA VLI SM COMSATS P"	445204502	"FSU MP HA LI Proton K LVFS"	1	0.200
466150304	"US HP HA VLI SM COMSATS P"	511600203	"ESA VLP HA VLI Ariane 4 LMORO"	1	0.000
466150304	"US HP HA VLI SM COMSATS P"	511600202	"ESA VLP HA VLI Ariane 4 LVFS"	1	0.400
466150304	"US HP HA VLI SM COMSATS P"	510100203	"ESA VLP VLA VLI Ariane 4 LMORO"	1	0.000

EXAMPLE CLASS.DAT FORMAT:

Class no.	Class description	a (km)	e	i (deg)	mass (kg)	area (m2)	leth. (J/g)
070354404	"CN VLP VLA MI MM TECSATS P"	6632.660	0.00690000	56.95	2099.000	4.1937	40.0
440306602	"FSU VLP VLA MI Zenit LVFS"	7164.160	0.00123000	70.39	8300.000	38.5691	40.0
440306603	"FSU VLP VLA MI Zenit LMORO"	7310.863	0.01957791	70.59	233.083	2.8290	40.0
461358304	"US VLP MA MI SM MILSATS P"	16659.660	0.60570002	39.19	1075.000	2.4936	40.0
461600702	"US VLP HA VLI Atlas II LVFS"	24312.160	0.73049998	0.00	1802.000	29.1778	40.0
511600203	"ESA VLP HA VLI Ariane 4 LMORO"	24354.357	0.72793883	6.02	384.736	7.9567	40.0
511600202	"ESA VLP HA VLI Ariane 4 LVFS"	24631.053	0.73044270	6.31	1780.000	27.7412	40.0

Appendix B

IDES Historical Fragmentation & Future Explosion Databases

IDES Historical Fragmentation Database													
Breakup Epoch (MJD)	COSPAR ID	Class Number	Breakup Type	Semi-major Axis (km)	Eccentricity	Inclination (deg)	Right Ascension of Node (deg)	Argument of Perigee (deg)	True Anomaly (deg)	Object Mass (kg)	Breakup Mass Fraction	Impactor Mass (kg)	Impactor Velocity (km/s)
37482	1961 015C	460305702	3	7316.1	0.007	66.88	96.15	296.38	206	625	1	0	0
37971	1962 057A	440356204	3	6608.1	0.0055	55.15	320.83	89.97	158	1500	0.0189	0	0
38360	1963 047A	460200602	3	7512.3	0.0873	30.34	163.86	106.25	155	4600	0.0063	0	0
38705	1964 070A	440358504	1	6589.2	0.0033	51.23	163.4	354.64	318	4750	0	0	0
38814	1965 012A	440354604	1	6672.1	0.0192	64.74	299.73	70.91	134	5500	0	0	0
38837	1965 020D	440301202	3	7420.6	0.1065	56.12	357.78	105.6	144	1600	0.1642	0	0
39051	1965 082B	460206002	3	7091.3	0.0071	32.2	84.67	194.12	117	1500	1	0	0
39141	1965 088A	440358104	3	6743	0.023	48.4	27.7	226.4	56	400	0.1803	0	0
39174	1966 012C	460558004	3	6594.4	0.0117	96.5	147.42	127.02	70	4	1	0	0
39296	1966 046B	460200502	3	6641.6	0.0028	28.81	215.72	138.79	75	3400	0.0219	0	0
39316	1966 059A	460255704	3	6581.6	0.0024	31.98	4.4	22.27	126	26600	0.0016	0	0
39390	1966 088A	440358504	3	6983.4	0.0638	49.63	342.6	78.99	0	3000	0.0265	0	0
39436	1966 101A	440358504	3	6893.8	0.0542	49.58	54.91	83.61	74	3000	0.0178	0	0
39880	1968 003A	440358604	1	6658	0.012	65.63	208.4	151.9	0	5500	0	0	0
39960	1968 025B	460205102	3	6663.8	0.0115	32.59	290.63	284.3	306	30000	0.0006	0	0
40150	1968 091A	440858504	1	7703.4	0.1098	62.35	118.76	76.78	213	1400	0	0	0
40162	1968 090A	440358404	1	6884.8	0.0042	62.25	77.29	305.17	166	1400	0	0	0
40162	1968 097A	440858504	1	7715.1	0.1051	62.32	77.62	73.67	358	1400	0	0	0
40311	1969 029B	440303902	3	7031.9	0.0217	81.21	32.55	180.68	304	1440	0.0258	0	0
40431	1969 064B	460701802	3	9231.8	0.2794	30.37	132.62	183.37	359	1100	0.226	0	0
40501	1969 082AB	460303102	1	7380.6	0.0127	69.64	279.98	107.91	12	600	0.5	0	0
40881	1970 025C	460503102	3	7450.4	0.0013	99.89	204.07	180.33	128	600	1	0	0
40887	1970 089A	440858504	1	7701.8	0.104	62.95	129.1	60.5	274	1400	0	0	0
40894	1970 091A	440858504	1	7689.9	0.1031	62.82	104.7	56.03	10	1400	0	0	0
41012	1971 015A	440858504	1	7765.3	0.1055	65.73	355.11	50.94	12	1400	0	0	0
41288	1971 106A	440358404	1	7392.7	0.1072	65.75	297.12	54.13	6	1400	0	0	0
41778	1973 017B	440304502	3	6597.9	0.0039	51.48	332.55	16.5	96	4000	0.0074	0	0
41811	1973 021A	440358604	1	6634.6	0.0142	72.85	303.56	25.41	238	6300	0	0	0
42047	1973 086B	460501802	3	7881.9	0.0013	102.06	44.2	112.95	208	800	1	0	0
42519	1974 103A	440358504	1	6804.5	0.0012	69.33	273.26	308.47	233	3000	0	0	0
42554	1972 058B	460501802	3	7146.2	0.02	98.51	196.22	40.09	285	800	0.5625	0	0

Breakup Epoch (MJD)	COSPAR ID	Class Number	Breakup Type	Semi-major Axis (km)	Eccentricity	Inclination (deg)	Right Ascension of Node (deg)	Argument of Perigee (deg)	True Anomaly (deg)	Object Mass (kg)	Breakup Mass Fraction	Impactor Mass (kg)	Impactor Velocity (km/s)
42605	1966 056A	462953004	3	10555.6	0.1187	87.14	209.49	66.58	328	55	1	0	0
42644	1974 089D	460501902	3	7828.3	0.0018	101.55	277.87	69.15	166	900	0.9859	0	0
42661	1975 080A	440358604	1	6624.8	0.0124	67.14	188.66	69.01	326	6200	0	0	0
42802	1975 102A	440358504	1	6812.6	0.0001	69.33	302.64	80.64	343	3000	0	0	0
42817	1975 004B	460501903	3	7202.1	0.0121	97.83	95.58	142.68	354	900	0.4639	0	0
42985	1976 072A	440358604	1	6638.6	0.0146	67.15	151.39	71.68	54	6700	0	0	0
43140	1976 126A	440358504	1	7823	0.1084	65.85	336.91	198.79	124	1400	0	0	0
43142	1976 123A	440358604	1	6608	0.011	65.05	52.1	350.8	0	6300	0	0	0
43281	1976 105A	441858304	1	26586.8	0.7305	62.81	97.29	318.67	85	1250	0	0	0
43283	1976 063A	440358504	1	6805.6	0.0012	69.33	129.36	299.44	251	3000	0	0	0
43341	1977 065B	460201901	3	7663.3	0.0977	28.68	270.58	52.56	98	900	0.3534	0	0
43418	1976 067A	440858204	3	7917	0.0705	65.86	82.06	351.04	226	650	0.3033	0	0
43443	1977 068A	441858304	1	26537.4	0.733	62.96	304.27	318.79	59	1250	0	0	0
43501	1977 121A	440358404	1	7419.3	0.0138	65.16	281.68	114.6	203	1400	0	0	0
43504	1976 077B	460501902	3	7889.1	0.0016	102.08	42.09	54.32	264	900	1	0	0
43672	1977 027A	441858304	1	26556.8	0.7103	62.84	114.88	319.86	161	1250	0	0	0
43690	1977 092A	446150404	3	42183.7	0.0001	0.4	315.03	34.69	212	1750	0.5736	0	0
43796	1978 083A	441858304	1	26590.9	0.7338	62.8	335.62	318.39	191	1250	0	0	0
43844	1976 120A	440358204	3	6962.6	0.0042	65.85	10.38	311.18	314	650	0.1074	0	0
43962	1977 047A	441858304	1	26596	0.6973	62.91	155.63	322.53	306	1250	0	0	0
44125	1979 077A	441858304	1	26565.5	0.7315	62.98	287.48	318.37	97	1250	0	0	0
44133	1979 033A	440358504	1	6769.8	0.0009	69.33	271.12	327.85	275	3000	0	0	0
44284	1979 058A	441858304	1	26569.5	0.723	62.89	104.38	318.53	178	1250	0	0	0
44345	1979 104B	511700102	1	22990.5	0.7151	18.1	93.17	279.47	174	1400	0	0	0
44348	1980 030A	440358504	1	7395.7	0.0858	65.15	251.07	248.42	164	1400	0	0	0
44632	1978 026C	460501903	3	7282.6	0.0009	98.95	68.58	127.76	146	900	0.5991	0	0
44727	1981 031A	441858304	1	26571.3	0.736	62.95	278.51	316.59	165	1250	0	0	0
44741	1980 057A	441858304	1	26562.9	0.717	62.67	197.92	319.7	226	1250	0	0	0
44803	1980 021A	440358504	1	6779.8	0.0059	69.33	173.78	245.21	127	3000	0	0	0
44812	1981 053A	440358204	2	7362.5	0.0044	82.96	118.98	127.62	302	800	1	1	10000
44861	1981 088F	441303702	3	13577.7	0.4852	62.82	70.77	286.57	232	1100	0.0058	0	0
44900	1981 016A	441858304	1	26559.1	0.723	62.93	213.69	318.47	195	1250	0	0	0

Breakup Epoch (MJD)	COSPAR ID	Class Number	Breakup Type	Semi-major Axis (km)	Eccentricity	Inclination (deg)	Right Ascension of Node (deg)	Argument of Perigee (deg)	True Anomaly (deg)	Object Mass (kg)	Breakup Mass Fraction	Impactor Mass (kg)	Impactor Velocity (km/s)
44932	1981 071A	441858304	1	26787.2	0.735	62.96	248.93	317.15	194	1250	0	0	0
44967	1978 098B	460501903	3	7320.3	0.002	99.13	277.15	68.7	16	900	0.0082	0	0
45102	1981 028A	440358504	1	6976.4	0.0211	69.33	45.11	296.08	184	3000	0	0	0
45145	1980 089A	440358504	1	7103.7	0.0219	69.33	329.94	0.18	190	3000	0	0	0
45167	1981 089A	440358504	1	6769.4	0.0011	69.33	40.96	302.47	333	3000	0	0	0
45246	1981 072A	440358504	1	6689.7	0.0007	69.33	132.47	263.77	155	3000	0	0	0
45316	1982 115E	440303702	3	6707.6	0.0152	62.82	315.84	58.28	219	1100	0.0315	0	0
45378	1980 085A	441858304	1	26558	0.7022	62.92	87.8	123.6	182	1250	0.5	0	0
45524	1983 070A	441858304	1	26301.5	0.734	62.93	165.82	318.12	163	1250	0	0	0
45552	1982 038A	440358504	1	6754.8	0.0015	69.33	276.37	307.11	17	3000	0	0	0
45559	1983 038A	441858304	1	26518.7	0.7315	62.94	79.51	319.95	34	1250	0	0	0
45688	1982 088A	440358404	1	6701.4	0.0016	79.93	124.63	346.08	223	3000	0	0	0
45730	1981 108A	441858304	1	26563.3	0.7099	62.87	218.66	324.38	126	1250	0.5	0	0
45733	1984 011F	460250207	3	6689.5	0.0004	27.67	156.37	5.23	354	2200	0.0079	0	0
45736	1984 011E	460250207	3	6663.6	0.0002	28.16	135.79	323.34	40	2200	0.003	0	0
45947	1983 020B	440304503	3	7102.6	0.0702	51.5	90.54	248.48	306	55	0.0834	0	0
46138	1983 044A	440358404	1	7104.9	0.0215	79.93	331.39	232.32	139	3000	0	0	0
46240	1985 039A	440358604	1	6617.5	0.0094	64.88	359.26	51.7	317	6700	0	0	0
46324	1979 017A	460558204	4	6906	0.0033	97.65	182.21	96.14	301	850	1	0.1	10000
46362	1982 055A	440358404	3	7372.4	0.0013	65.84	349.15	67.51	21	650	0.2083	0	0
46394	1985 094B	440358104	3	7790	0.0007	82.62	341.08	95.56	52	220	0.2344	0	0
46430	1985 121F	440306602	3	6875.5	0.04836	71	250	72	12	9000	0.004	0	0
46432	1983 022A	460552304	3	7192.3	0.001	98.75	32.3	190.24	58	1000	0.0118	0	0
46487	1984 083A	440358504	1	6799.6	0.0013	69.33	246.84	296.2	96	3000	0	0	0
46683	1986 069A	460290004	1	6872.3	0.0407	14.3	39.27	12.59	9	930	0	0	0
46683	1986 069B	460201902	1	6798.6	0.0291	22.78	19.47	39.05	360	1455	0	0	0
46752	1986 019C	510500102	3	7193.3	0.0027	98.72	30.15	43.64	326	1400	1	0	0
46770	1981 058A	441858304	1	26553.7	0.6599	62.84	287.49	291.95	190	1250	0	0	0
46787	1985 082A	440358504	1	6807.2	0.0075	69.33	333.86	49.98	285	3000	0	0	0
46829	1987 004A	440358604	1	6762.2	0.0044	72.82	255.47	167.44	281	6300	0	0	0
47002	1987 059A	440358604	1	6580.8	0.0083	67.16	98.11	65.26	230	6700	0	0	0
47053	1987 078C	511600102	3	24767.9	0.7333	6.87	175.44	181.96	190	1200	0.8365	0	0

Breakup Epoch (MJD)	COSPAR ID	Class Number	Breakup Type	Semi-major Axis (km)	Eccentricity	Inclination (deg)	Right Ascension of Node (deg)	Argument of Perigee (deg)	True Anomaly (deg)	Object Mass (kg)	Breakup Mass Fraction	Impactor Mass (kg)	Impactor Velocity (km/s)
47059	1986 059A	440358504	1	6755	0.009	69.33	119.66	290.19	325	3000	0	0	0
47119	1985 030A	440358504	1	6775.7	0.0009	69.33	285.3	237.68	216	3000	0	0	0
47146	1987 020A	440353204	3	7878.6	0.0025	73.61	183.86	194.54	2	1500	0.4898	0	0
47165	1985 042E	440304503	3	7211.5	0.0025	66.5	198.74	264.79	184	55	0.1987	0	0
47191	1987 108A	440358604	1	6629.3	0.0023	82.58	253.48	125.54	64	6300	0	0	0
47218	1988 007A	440358604	1	6565.3	0.0067	64.88	263.87	57.14	18	6700	0	0	0
47291	1978 100D	440306202	3	8069.5	0.002	82.55	353.47	74.28	134	1360	0.2813	0	0
47736	1989 054A	440358604	1	6556.3	0.0055	67.14	88.57	63.45	354	6700	0	0	0
47772	1989 056A	440358604	1	6683.2	0.0101	50.56	242.21	58.58	62	6700	0	0	0
48173	1990 081D	70501602	3	7265	0.0013	98.94	311.3	141.78	137	1000	0.1741	0	0
48230	1990 087A	440358604	1	6614.9	0.007	64.75	346.52	147.19	331	6700	0	0	0
48231	1990 105A	460558204	1	7167.4	0.0081	98.86	3.43	6.38	166	855	0	0	0
48296	1983 127H	441304503	3	15952.4	0.5781	52.14	131.15	316.97	187	55	0.1614	0	0
48320	1991 009J	440301202	3	7970.6	0.0159	74.03	163.4	241.5	75	1435	0.3727	0	0
48377	1975 052B	460501903	3	7473.4	0.0015	99.96	336.9	103.67	327	900	0.9286	0	0
48596	1991 071A	440358604	1	6597.9	0.006	64.79	36.1	138.81	337	6700	0	0	0
48619	1985 118L	441304503	3	16143.4	0.565	65.43	37.16	243.88	283	55	1	0	0
48673	1968 081E	466106002	3	41835.7	0.0085	11.9	22.27	75.71	246	1500	1	0	0
48805	1989 101E	441304503	3	20353.4	0.6704	46.95	305.19	319.33	57	55	0.6233	0	0
48871	1984 106F	440304503	3	7217.3	0.0011	66.54	352.31	50.64	181	55	0.5431	0	0
48974	1989 004E	440804503	3	15253	0.5693	46.48	264.9	354.82	44	55	0.6233	0	0
48983	1992 093B	440306602	3	7226.7	0.0015	71.02	226.79	83.72	348	9000	0.0545	0	0
49000	1989 052F	441304503	3	21874.5	0.6976	46.56	212.03	47.85	225	55	0.6233	0	0
49037	1992 091A	440358604	1	6610.9	0.0043	64.9	91.81	107.46	7	6700	0	0	0
49075	1993 016B	440306602	3	7223.1	0.0003	71.01	260.31	75.22	8	9000	0.0042	0	0
49101	1992 021C	511600202	3	23535.5	0.719	4.02	109.38	161.43	182	1800	1	0	0
49107	1993 028A	440358604	1	6606.9	0.0055	70.35	56.77	82.07	350	6700	0	0	0
49196	1993 045A	440358604	1	6625.5	0.01094	67.1	133.42	69.17	27	6700	0	0	0
49281	1983 075A	440552504	3	6947.4	0.0027	98.01	317.36	328.95	23	1800	0.0241	0	0
49342	1993 057A	440358604	1	6602.2	0.0075	64.92	208.49	69.53	22	6500	0	0	0
49392	1967 066G	466106002	3	39840.5	0.0001	11.7	120	40	123	1500	1	0	0
49393	1994 004B	460305902	3	6610.4	0.0033	67	45.8	135.08	113	2860	0.0214	0	0

Breakup Epoch (MJD)	COSPAR ID	Class Number	Breakup Type	Semi-major Axis (km)	Eccentricity	Inclination (deg)	Right Ascension of Node (deg)	Argument of Perigee (deg)	True Anomaly (deg)	Object Mass (kg)	Breakup Mass Fraction	Impactor Mass (kg)	Impactor Velocity (km/s)
49474	1991 015C	511600202	3	20927.7	0.6824	7.1	139.15	177.67	160	1250	0.3831	0	0
49484	1991 010D	441304503	3	17393	0.620365	46.6	113.38	158.22	212	55	0.6233	0	0
49667	1992 047H	441304503	3	16135.5	0.574974	64.8	65.2	316.78	182	55	0.6233	0	0
49717	1994 085B	440804802	3	8418	0.019007	64.8	165.56	291.24	180	1000	0.3827	0	0
49807	1994 056B	241702902	3	18543	0.649032	28.6	18.41	357.51	212	3000	0.1596	0	0
49848	1994 069E	441804503	3	24188	0.729907	46.9	206.51	58.25	283	55	0.6233	0	0
50012	1994 038F	441804503	3	23983	0.7224	46.64	247.3	12	12	55	0.6233	0	0
50066	1990 102E	440804503	3	13015.5	0.4969	46.5	205.6	99.2	97	55	0.6233	0	0
50132	1996 010D	441804502	3	24750.5	0.732611	48.7	281.45	0.84	301	3400	1	0	0
50194	1991 003C	511600202	3	21960.5	0.698868	6.7	105.65	131.22	160	1760	0.3831	0	0
50238	1994 029B	460304302	1	7080.5	0.016595	82	206.4	277.95	52.65	97	1	0	0
50419	1987 079G	441304503	3	16105.5	0.583186	64.9	300.78	181.31	257	55	1	0	0
50590	1987 109E	441304503	3	18020.5	0.628867	46.6	255.04	347.64	65	55	1	0	0
50628	1995 028A	440358504	1	6645.5	0.008652	65	350.26	234.55	164	3000	0.0882	0	0
50710	1997 024A	440358604	1	6633	0.004523	65	2.29	113.84	33.7	6500	0	0	0
50782	1987 062A	440352404	3	6997	0.002144	82.5	102.47	130.76	95	1900	0.05	0	0
50810	1997 086D	441804502	3	24510.5	0.728769	51.4	91.4	1.51	180	3400	1	0	0
50862	1987 068B	440306202	3	7328	0.001365	82.6	229.54	329.88	90.01	1360	0.7493	0	0
50864	1988 109C	511600202	3	24533	0.722292	7.3	24.29	247.18	57.8	1200	0.3831	0	0
50868	1998 011B	240202902	3	7440.5	0.109872	30	298.49	187.95	1	3000	0.1596	0	0
50891	1990 110H	441304503	3	16135.5	0.572495	65.1	308.17	217.25	349	55	1	0	0

Breakup Type:

1 = High Intensity Explosion
2 = Catastrophic Collision
3 = Low Intensity Explosion
4 = Non-catastrophic Collision